PSDF

Power Systems Development Facility

Technical Progress Report
Gasification Test Run GCT4

March 7, 2001 -
March 30, 2001

DOE Cooperative Agreement Number
DE-FC21-90MC25140

SOUTHERN COMPANY

Energy to Serve Your World®

POWER SYSTEMS DEVELOPMENT FACILITY

TECHNICAL PROGRESS REPORT
GASIFICATION TEST RUN GCT4

MARCH 7 – MARCH 30, 2001

DOE Cooperative Agreement Number
DE-FC21-90MC25140

Prepared by:
Southern Company Services, Inc.
Power Systems Development Facility
P.O. Box 1069
Wilsonville, AL 35186
Tel: 205-670-5840
Fax: 205-670-5843
http://psdf.southernco.com

November 2002

POWER SYSTEMS DEVELOPMENT FACILITY

DISCLAIMER

Available to the public from the National Technical Information Service, U.S. Department of Commerce, 5285 Port Royal Road, Springfield, VA 22161. Phone orders accepted at (703) 487-4650.

ACKNOWLEDGEMENT

The authors wish to acknowledge the contributions and support provided by various project managers: Jim Longanbach (DOE), Neville Holt (EPRI), Cheryl Chartier (KBR), Zal Sanjana (Westinghouse), and Vann Bush (SRI). Also, the enterprising solutions to problems and the untiring endeavors of many personnel at the site during commissioning of the transport reactor train in gasification mode of operation are greatly appreciated. The project was sponsored by the U.S. Department of Energy National Energy Technology Laboratory under contract DE-FC21-90MC25140.

CONTENTS

Section Page

Listing of Tables

Listing of Figures

1.0 EXECUTIVE SUMMARY

1.1 SUMMARY

This report discusses test campaign GCT4 of the Kellogg Brown & Root, Inc. (KBR) transport reactor train with a Siemens Westinghouse Power Corporation (Siemens Westinghouse) particle filter system at the Power Systems Development Facility (PSDF) located in Wilsonville, Alabama. The transport reactor is an advanced circulating fluidized-bed reactor designed to operate as either a combustor or a gasifier using one of two possible particulate control devices (PCDs). The transport reactor was operated as a pressurized gasifier during GCT4.

GCT4 was planned as a 250-hour test run to continue characterization of the transport reactor using a blend of several Powder River Basin (PRB) coals and Bucyrus limestone from Ohio. The primary test objectives were:

- *Operational Stability* – Characterize reactor loop and PCD operations with short-term tests by varying coal-feed rate, air/coal ratio, riser velocity, solids-circulation rate, system pressure, and air distribution.

Secondary objectives included the following:

- *Reactor Operations* – Study the devolatilization and tar cracking effects from transient conditions during transition from start-up burner to coal. Evaluate the effect of process operations on heat release, heat transfer, and accelerated fuel particle heat-up rates. Study the effect of changes in reactor conditions on transient temperature profiles, pressure balance, and product gas composition.

- *Effects of Reactor Conditions on Synthesis Gas Composition* – Evaluate the effect of air distribution, steam/coal ratio, solids-circulation rate, and reactor temperature on CO/CO_2 ratio, synthesis gas Lower Heating Value (LHV), carbon conversion, and cold and hot gas efficiencies.

- *Research Triangle Institute (RTI) Direct Sulfur Recovery Process (DSRP) Testing* – Provide syngas in support of the DSRP commissioning.

- *Loop Seal Operations* – Optimize loop seal operations and investigate increases to previously achieved maximum solids-circulation rate.

Test run GCT4 was started on March 7, 2001, and completed on March 30, 2001. This test run provided additional data necessary to analyze reactor operations and to identify necessary modifications to improve equipment and process performance. The reactor temperature was varied between 1,675 and 1,825°F at pressures from 160 to 240 psig. In GCT4, 312 hours of solid circulation and 242 hours of coal feed were attained.

1.2 PSDF ACCOMPLISHMENTS

The PSDF has achieved over 4,985 hours of operation on coal feed and about 6,470 hours of solids circulation in combustion mode, and 1,291 hours of solid circulation and 876 hours of coal feed in gasification mode of operation. The major accomplishments in GCT1 through GCT4 are summarized below. Combustion related accomplishments are reported in the TC05 technical progress report.

1.2.1 Transport Reactor Train

The major accomplishments and observations in GCT1 through GCT4 include:

Commercial

- With subbituminous coal, more than 95-percent carbon conversion and 110-Btu/scf nitrogen-corrected syngas heating value can be attained. The nitrogen-corrected syngas characteristics were sufficient to support existing pressurized syngas burners.

- Transport reactor generated syngas can be combusted without propane enrichment. The thermal oxidizer (atmospheric syngas burner) operated well using syngas with different heating values and was run for short periods of time without propane addition while maintaining an exit temperature near 2,000°F.

Process

- In GCT1, the reactor was operated using two bituminous coals and a PRB coal with different sorbents. Gasifier operations were stable, but carbon conversions were low due to disengager and cyclone inefficiencies.

- During GCT2, the longest continuous run of 184 hours in gasification mode of operation was achieved with PRB coal. Reactor operations were smooth without any incident of oxygen breakthrough, temperature excursions, deposits, clinkers, or any other operational problem. The reactor loop was run consistently at about 50 percent of the design circulation rate. For the most part, the cyclone dipleg operated well with high solids flow due to the inefficiency of the disengager. However, there were brief cyclone dipleg upsets.

- In GCT3, stable gasification reactor operation was achieved at a range of coal-feed rates and solids-circulation rates, with reactor pressures ranging as high as 240 psig on PRB coal. The modification of the Y-type cyclone dipleg to a loop seal performed well, needing little attention and promoting much higher solids-circulation rates and higher coal-feed rates that resulted in lower relative solids loading to the PCD and higher char retention in the reactor. The level in the disengager standpipe reached its highest levels, attaining heights beyond expectations without difficulties. The coal-feed rate was the highest to date in this run, with much higher carbon conversions achieved. The high coal-feed rate produced the highest syngas heating value to date. Tar generation was also lower and could be completely eliminated by varying reactor operating parameters.

It was also demonstrated that coal feed can safely be restarted after more than 30 minutes of down time without lighting the reactor start-up burner.

- In GCT4, stable gasification reactor operation was achieved at a range of coal-feed rates, solids-circulation rates, and reactor pressures ranging as high as 240 psig on PRB coal. The coal-feed rate was increased further, exceeding 5,500 pph. The reactor experienced some of the highest circulation rates (more than double the design rate) and riser densities ever observed in the transport reactor. These characteristics improved the temperature distribution in both the mixing zone and the riser and likely resulted in higher coal particle heat-up rates. Lower coal-feed rates of about 2,500 pph were also tested due to grinding problems in the coal mill. Carbon conversions as high as 98 percent were achieved.

- Limestone calcination of 90 percent was achieved in the transport gasifier. The CO_2 partial pressures near the top of the riser ranged from 20 to 23 psia.

- The overall mass balance was excellent with less than +5 percent error.

- With PRB, the corrected fuel gas heating values ranged from 95 to 120 Btu/scf, depending on the coal-feed rate. In the test range, the solids-circulation rates, gas and solids residence times, and reactor temperatures do not show much effect on the fuel gas heating values. The observed increase in raw syngas heating value at higher coal-feed rates is mainly due to the reduced effect of added nitrogen (dilution and relatively less energy consumption for heatup).

- For PRB coal, the corrected cold gas efficiency (syngas latent heat to coal latent heat) remained between 50 and 70 percent. The corrected hot gas efficiency (syngas latent + sensible heat to coal latent heat) was between 80 and 95 percent and the remaining coal latent heat was mainly present in the ash/char stream from the process.

- Due to the low sulfur content of the PRB coal (0.25 to 0.35 weight percent) and equilibrium constraints, up to 70 percent of sulfur removal was achieved with sorbent and alkaline minerals in the coal ash.

- RTI began commissioning the DSRP. Simulated regenerated off-gas was prepared using liquid SO_2. The syngas and tail gas were successfully sampled and analyzed. The DSRP reaction was conducted with controlled flow of syngas from the transport reactor with conversions as high as 80 percent achieved.

- The mean particle size (mmd) of the PCD fines varied from 15 to 20 μm and the carbon content varied from 25 to 55 percent. The average higher heating value of PCD fines was about 5,800 Btu/lb at about 40-percent carbon content.

Equipment

- The PCD operates extremely well, with a low and stable DP when little or no tar is present in the gas, at the conditions tested in GCT4 (solids-circulation rates, loading, gas-flow rates, temperature, and pressure). The fines removal system also performed well.

- Since the high carbon conversion in the transport gasifier significantly reduced the amount of remaining char, the sulfator did not receive enough char to maintain a high temperature. Thus, the sulfator required additional heating from its start-up burner and fuel oil injection system. The sulfator performed well during the first portion of GCT4, maintaining a uniform temperature throughout the bed. The sulfator did experience bed stratification during the latter part of the run, making it difficult to heat the bottom of the bed.

- The coal feeder demonstrated a modest improvement during GCT4. As in GCT3, the coal feeder again experienced difficulties early in the run. The feeder became plugged when a vent filter bag fell into the surge bin. Once the bag was removed and the system cleaned out, the coal feeder ran for over 150 hours with no interruption.

- The coal-flow rate control loop was tested and tuned.

- The char/ash removal system (FD0510) operated well without any line plugging during gasification.

- The gas coolers upstream and downstream of the PCD operated well without fouling.

- Nonintrusive density measurements based on nuclear sensing were added to the coal feed line. This, coupled with pressurized conveying gas velocity measurements, enhanced the ability to measure instantaneous coal-feed rates. On-line calibration techniques are being developed to improve accuracy. This was the first-of-a-kind application of nuclear sensing technology to measure coal rates in small-bore pipes.

- Nuclear density gauge-based coal-feed rate measurements were quite informative in characterizing observed gasifier operation (temperature profiles, gas composition, etc.). This was due to the feed rate measurement sensitivity to changes induced by coal feeder cycle (feed vessel level and pressure swings) and particle size (grind, segregation). A controls algorithm to maintain mass-flow rate of coal by varying feeder speed was successfully implemented.

1.2.2 PCD

The most outstanding aspects of PCD operation for GCT4 are summarized below.

1. The PCD operated successfully for 242 on-coal hours. Although the baseline pressure drop generally increased throughout the run, operation of the filter vessel was reliable. In addition, the fines removal system operated without major problems, although it required

constant maintenance and engineering attention. During steady-state operations, stable PCD inlet temperature and solids loading were maintained. As seen in GCT3, the reactor loop seal modifications were successful in stabilizing solids carryover to the PCD.

2. All metal filter elements were used during GCT4 and consisted of new and previously exposed Pall iron aluminide filter elements. Ceramic filter elements were not used because of previous failures of ceramics and because of the potential for thermal transients in the PCD which can damage them. There were no filter element failures during GCT4.

3. SRI solids sampling at the PCD outlet showed no char leakage through the filter vessel. All samples taken indicated a solids concentration below the detectable limit of 0.1 ppmw. The one exception was a sample taken during a startup period that showed an outlet solids concentration of 38.6 ppmw, but this was assumed to be tar as no char was visible on the sample filter. PCD inlet samples were also taken which affirmed an overall decrease in the total amount of solids carryover.

4. Because of the effects of the loop seal modification on PCD char characteristics, which could negatively affect filter performance, a study on solids injection into the PCD was undertaken. An SRI laboratory examination was conducted in support of the solids injection project, and selection of additive materials was based on the SRI findings. Several different additives were injected into the PCD in an attempt to modify filter cake properties. Baseline pressure drop and pressure drop rise before and after injections were compared. Although one additive, a particular brand of diatomaceous earth, showed some potential for improving filter cake properties and thus reducing pressure drop, the observed improvement was quite small and field results were not repeatable.

5. On inspection, a large amount of char bridging was found, mostly on the bottom plenum. The bridging covered approximately one quarter of the filtering surface. Because previous run inspections indicated that the bottom plenum has not been cleaned as well as the top, using the same back-pulse pressures, a higher bottom plenum back-pulse pressure was at times employed during GCT4 to achieve the same cleaning effect as on the top plenum. However, the intermittent use of higher bottom plenum back-pulse pressures did not prevent char bridging. Char bridging was also found after GCT3, and because of this recurrence, eliminating char bridging is a priority for PCD operation.

6. Also found during inspection was a thick, strongly adhering residual cake on the filter elements. This cake was thicker than residual cakes previously seen—almost 10 times thicker than the residual cake found after GCT3—and it is likely that tar deposition on the filter surfaces contributed largely to the residual cake characteristics. The run included numerous startups and hot restarts, which necessitated reactor operation below 1,600°F (the temperature below which excessive tar formation is believed to occur).

7. Baseline pressure drop during GCT4, ranging from about 80 to 200 inH_2O, was higher than that seen in GCT2 or GCT3. This high baseline was largely attributable to char bridging, a thick residual char cake, and changes in char characteristics resulting from reactor loop seal modifications.

1.3 FUTURE PLANS

A 1,000-hour test campaign (TC06) is planned to start in July 2001. After completing TC06, the transport reactor will be modified by adding a lower mixing zone (LMZ) to enable operations as an oxygen-blown gasifier. A 500-hour air-blown test campaign (TC07) will begin in December 2001 to commission the LMZ and test a bituminous coal. A 500-hour test campaign (TC08) in oxygen-blown mode is scheduled for May 2002.

2.0 INTRODUCTION

This report provides an account of the GCT4 test campaign with the Kellogg Brown & Root, Inc. (KRB) transport reactor and the Siemens Westinghouse filter vessel at the PSDF located in Wilsonville, Alabama, 40 miles southeast of Birmingham. The PSDF is sponsored by the U. S. Department of Energy (DOE) and is an engineering-scale demonstration of two advanced coal-fired power systems. In addition to DOE, Southern Company Services, Inc., (SCS), Electric Power Research Institute (EPRI), and Peabody Holding Company are cofunders. Other cofunding participants supplying services or equipment currently include KBR and Siemens Westinghouse. SCS is responsible for constructing, commissioning, and operating the PSDF.

2.1 THE POWER SYSTEMS DEVELOPMENT FACILITY

SCS entered into an agreement with DOE/National Energy Technology Laboratory (NETL) for the design, construction, and operation of a hot gas clean-up test facility for pressurized gasification and combustion. The purpose of the PSDF is to provide a flexible test facility that can be used to develop advanced power system components, and assess the integration and control issues of these advanced power systems. The facility was designed as a resource for rigorous, long-term testing and performance assessment of hot stream clean-up devices and other components in an integrated environment.

The PSDF now consists of the following modules for systems and component testing that includes:

- A transport reactor module.
- A hot gas clean-up module.
- A compressor/turbine module.

The transport reactor module includes KBR transport reactor technology for pressurized combustion and gasification to provide either an oxidizing or reducing gas for parametric testing of hot particulate control devices. The filter system tested to date at the PSDF is the particulate control device (PCD) supplied by Siemens Westinghouse.

2.2 TRANSPORT REACTOR SYSTEM DESCRIPTION

The transport reactor is an advanced circulating fluidized-bed reactor operating as either a combustor or as a gasifier, using a hot gas clean-up filter technology (particulate control devices or PCDs) at a component size readily scaleable to commercial systems. The transport reactor train operating in gasification mode is shown schematically in Figure 2.2-1. A taglist of all major equipment in the process train and associated balance-of-plant is provided in Tables 2.2-1 and -2.

The transport reactor consists of a mixing zone, a riser, a disengager, a cyclone, a standpipe, a loop seal, a solids cooler, and J-legs. The fuel, sorbent, and air are mixed together in the mixing zone along with the solids from the standpipe and solids cooler J-legs. The mixing zone, located below the riser, has a slightly larger diameter compared to the riser. Provision is made to inject air at several different points along the riser to control the formation of NO_x during the combustion mode of operation. The gas and solids move up the riser together, make two turns, and enter the disengager. The disengager removes larger particles by gravity separation. The gas and remaining solids then move to the cyclone, which removes most of the particles not collected by the disengager. The gas then exits the transport reactor and goes to the primary gas cooler and the PCD for final particulate clean-up. The solids collected by the disengager and cyclone are recycled back to the reactor mixing zone through the standpipe and a J-leg. In the combustion mode of operation, the solids cooler (not shown) controls the reactor temperature by generating steam and provides solids surge volume. A part of the solids stream from the standpipe flows through the solids cooler. The solids from the solids cooler then return to the bottom of the reactor mixing zone through another J-leg. The solids cooler is not used in gasification. The nominal transport reactor operating temperatures are 1,800 and 1,600°F for gasification and combustion modes, respectively. The reactor system is designed to have a maximum operation pressure of 294 psig with a thermal capacity of about 21 MBtu/hr for combustion mode and 41 MBtu/hr for gasification mode.

For startup purposes, a burner (BR0201) is provided at the reactor mixing zone. Liquefied propane gas (LPG) is used as start-up fuel. The fuel and sorbent are separately fed into the transport reactor through lockhoppers. Coal is ground to a nominal average particle diameter between 250 and 400 μm. Sorbent is ground to a nominal average particle diameter of 10 to 30 μm. Limestone or dolomitic sorbents are fed into the reactor for sulfur capture. The gas leaves the transport reactor cyclone and goes to the primary gas cooler, which cools the gas prior to entering the Siemens Westinghouse PCD barrier filter. The PCD uses ceramic or metal elements to filter out dust from the reactor. The filters remove almost all the dust from the gas stream to prevent erosion of a downstream gas turbine in a commercial plant. The operating temperature of the PCD is controlled both by the reactor temperature and by an upstream gas cooler. For test purposes, the gas from the transport reactor can flow through the gas cooler from 0 to 100 percent. The PCD gas temperature can range from 700 to 1,600°F. The filter elements are back-pulsed by high-pressure nitrogen or air in a desired time interval or at a given maximum pressure difference across the elements. There is a secondary gas cooler located after the filter vessel to cool the gas before discharging to the stack or thermal oxidizer (atmospheric syngas combustor). In a commercial process the gas from the PCD would be sent to a gas turbine in a combined cycle package. The flue gas or fuel gas is sampled for on-line analysis after traveling through the secondary gas cooler.

After exiting the secondary gas cooler the gas is then let down to about 2 psig through a pressure control valve. In gasification the fuel gas is then sent to the thermal oxidizer to burn the gas and oxidize all reduced sulfur compounds (H_2S, COS, and CS_2) and reduced nitrogen compounds (NH_3 and HCN). The thermal oxidizer uses propane as a supplemental fuel. In combustion, the thermal oxidizer can be bypassed and fired on propane to make startup steam. The gas from the thermal oxidizer goes to the baghouse and then to the stack.

The transport reactor produces both fine ash collected by the PCD and coarse ash extracted from the transport reactor standpipe. The two solid streams are cooled using screw coolers, reduced in pressure in lock hoppers, and then combined together. The combustion solids are suitable for commercial use or landfill as produced. In gasification, any fuel sulfur captured by sorbent should be present as calcium sulfide (CaS). The gasification solids are processed in the sulfator to oxidize the CaS to calcium sulfate ($CaSO_4$) and burn any residual carbon on the ash. The waste solids are then suitable for commercial use or disposal. Neither the sulfator nor the thermal oxidizer would be part of a commercial process. In a commercial process, the gasification solids could be burned in an atmospheric or pressurized fluidized bed combustor to recover the solids heat value.

Table 2.2-1

Major Equipment in the Transport Reactor Train

TAG NAME	DESCRIPTION
BR0201	Reactor Start-Up Burner
BR0401	Thermal Oxidizer
BR0602	Sulfator Startup/PCD Preheat Burner
CO0201	Main Air Compressor
CO0401	Recycle Gas Booster Compressor
CO0601	Sulfator Air Compressor
CY0201	Primary Cyclone in the Reactor Loop
CY0207	Disengager in the Reactor Loop
CY0601	Sulfator Cyclone
DR0402	Steam Drum
DY0201	Feeder System Air Dryer
FD0206	Spent Solids Screw Cooler
FD0210	Coal Feeder System
FD0220	Sorbent Feeder System
FD0502	Fines Screw Cooler
FD0510	Spent Solids Transporter System
FD0520	Fines Transporter System
FD0530	Spent Solids Feeder System
FD0602	Sulfator Solids Screw Cooler
FD0610	Sulfator Sorbent Feeder System
FL0301	PCD — Siemens Westinghouse
FL0302	PCD — Combustion Power
FL0401	Compressor Intake Filter
HX0202	Primary Gas Cooler
HX0203	Combustor Heat Exchanger
HX0204	Transport Air Cooler
HX0402	Secondary Gas Cooler
HX0405	Compressor Feed Cooler
HX0601	Sulfator Heat Recovery Exchanger
ME0540	Heat Transfer Fluid System
RX0201	Transport Reactor
SI0602	Spent Solids Silo
SU0601	Sulfator

Table 2.2-2 (Page 1 of 3)

Major Equipment in the Balance-of-Plant

TAG NAME	DESCRIPTION
BO2920	Auxiliary Boiler
BO2921	Auxiliary Boiler – Superheater
CL2100	Cooling Tower
CO2201A-D	Service Air Compressor A-D
CO2202	Air-Cooled Service Air Compressor
CO2203	High-Pressure Air Compressor
CO2601A-C	Reciprocating N_2 Compressor A-C
CR0104	Coal and Sorbent Crusher
CV0100	Crushed Feed Conveyor
CV0101	Crushed Material Conveyor
DP2301	Baghouse Bypass Damper
DP2303	Inlet Damper on Dilution Air Blower
DP2304	Outlet Damper on Dilution Air Blower
DY2201A-D	Service Air Dryer A-D
DY2202	Air-Cooled Service Air Compressor Air Dryer
DY2203	High-Pressure Air Compressor Air Dryer
FD0104	MWK Coal Transport System
FD0111	MWK Coal Mill Feeder
FD0113	Sorbent Mill Feeder
FD0140	Coke Breeze and Bed Material Transport System
FD0154	MWK Limestone Transport System
FD0810	Ash Unloading System
FD0820	Baghouse Ash Transport System
FL0700	Baghouse
FN0700	Dilution Air Blower
HO0100	Reclaim Hopper
HO0105	Crushed Material Surge Hopper
HO0252	Coal Surge Hopper
HO0253	Sorbent Surge Hopper
HT2101	MWK Equipment Cooling Water Head Tank
HT2103	SCS Equipment Cooling Water Head Tank
HT0399	60-Ton Bridge Crane
HX2002	MWK Steam Condenser
HX2003	MWK Feed Water Heater

Table 2.2-2 (Page 2 of 3)

Major Equipment in the Balance-of-Plant

TAG NAME	DESCRIPTION
HX2004	MWK Subcooler
HX2103A	SCS Cooling Water Heat Exchanger
HX2103C	MWK Cooling Water Heat Exchanger
LF0300	Propane Vaporizer
MC3001-3017	MCCs for Various Equipment
ME0700	MWK Stack
ME0701	Flare
ME0814	Dry Ash Unloader for MWK Train
ML0111	Coal Mill for MWK Train
ML0113	Sorbent Mill for Both Trains
PG2600	Nitrogen Plant
PU2000A-B	MWK Feed Water Pump A-B
PU2100A-B	Raw Water Pump A-B
PU2101A-B	Service Water Pump A-B
PU2102A-B	Cooling Tower Make-Up Pump A-B
PU2103A-D	Circulating Water Pump A-D
PU2107	SCS Cooling Water Make-Up Pump
PU2109A-B	SCS Cooling Water Pump A-B
PU2111A-B	MWK Cooling Water Pump A-B
PU2300	Propane Pump
PU2301	Diesel Rolling Stock Pump
PU2302	Diesel Generator Transfer Pump
PU2303	Diesel Tank Sump Pump
PU2400	Fire Protection Jockey Pump
PU2401	Diesel Fire Water Pump #1
PU2402	Diesel Fire Water Pump #2
PU2504A-B	Waste Water Sump Pump A-B
PU2507	Coal and Limestone Storage Sump Pump
PU2700A-B	Demineralizer Forwarding Pump A-B
PU2920A-B	Auxiliary Boiler Feed Water Pump A-B
SB3001	125-V DC Station Battery
SB3002	UPS
SC0700	Baghouse Screw Conveyor
SG3000-3005	4160-V, 480-V Switchgear Buses

Table 2.2-2 (Page 3 of 3)

Major Equipment in the Balance-of-Plant

TAG NAME	DESCRIPTION
SI0101	MWK Crushed Coal Storage Silo
SI0103	Crushed Sorbent Storage Silo
SI0111	MWK Pulverized Coal Storage Silo
SI0113	MWK Limestone Silo
SI0114	FW Limestone Silo
SI0810	Ash Silo
ST2601	N_2 Storage Tube Bank
TK2000	MWK Condensate Storage Tank
TK2001	FW Condensate Tank
TK2100	Raw Water Storage Tank
TK2300A-D	Propane Storage Tank A-D
TK2301	Diesel Storage Tank
TK2401	Fire Water Tank
XF3000A	230/4.16-kV Main Power Transformer
XF3001B-5B	4160/480-V Station Service Transformer No. 1-5
XF3001G	480/120-V Miscellaneous Transformer
XF3010G	120/208 Distribution Transformer
XF3012G	UPS Isolation Transformer
VS2203	High-Pressure Air Receiver

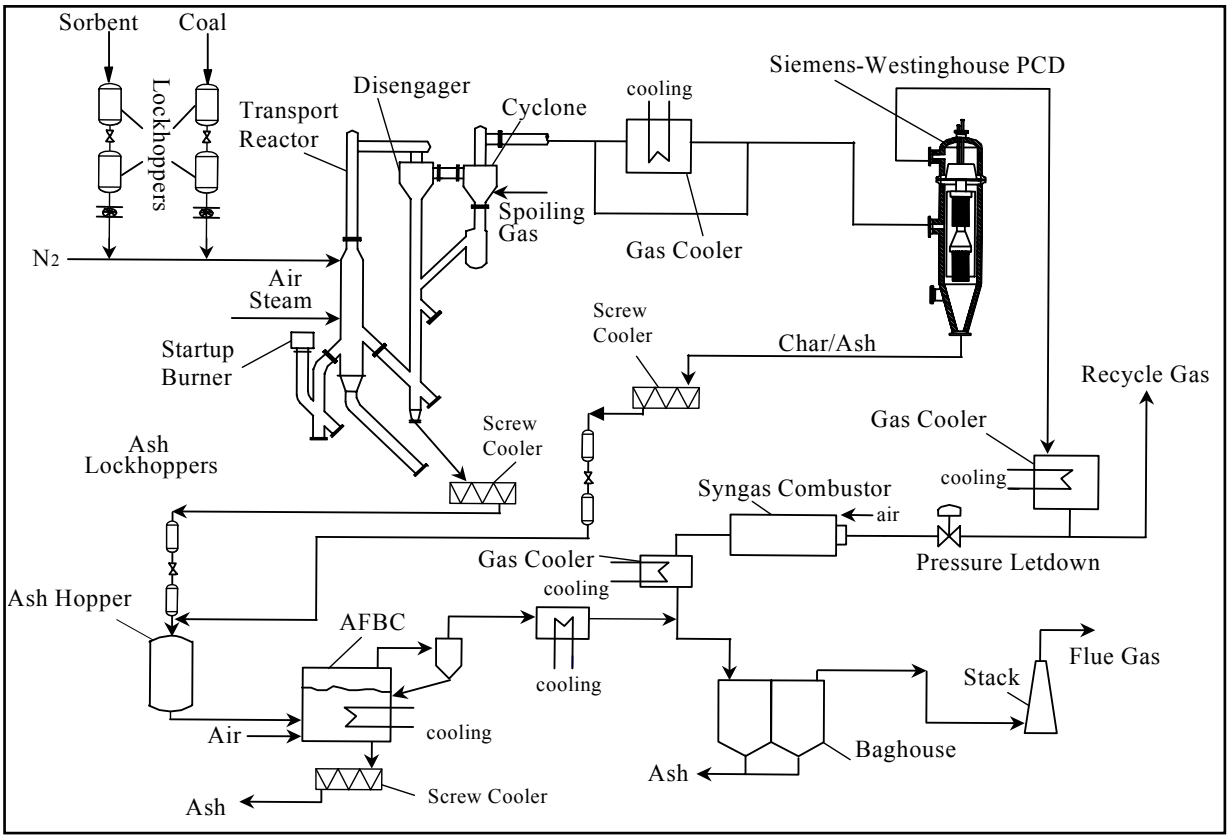

Figure 2.2-1 Flow Diagram of the Transport Reactor Train

2.3 SIEMENS WESTINGHOUSE PARTICULATE CONTROL DEVICE

Different PCDs will be evaluated on the transport reactor train. The first PCD that was commissioned in 1996 and has been used in all of the testing to date was the filter system designed by Siemens Westinghouse. The dirty gas enters the PCD below the tubesheet, flows through the filter elements, and the ash collects on the outside of the filter. The clean gas passes from the plenum/filter element assembly through the plenum pipe to the outlet pipe. As the ash collects on the outside surface of the filter elements, the pressure drop across the filter system gradually increases. The filter cake is periodically dislodged by injecting a high-pressure gas pulse to the clean side of the filter elements. The cake then falls to the discharge hopper.

Until the first gasification run in late 1999, the transport reactor had been operated only in the combustion mode. Initially, high-pressure air was used as the pulse gas for the PCD; however, the pulse gas was changed to nitrogen early in 1997. The pulse gas was routed individually to the two-plenum/filter element assemblies via injection tubes mounted on the top head of the PCD vessel. The pulse duration was typically 0.1 to 0.5 seconds.

A sketch of the Siemens Westinghouse PCD is shown in Figure 2.3-1.

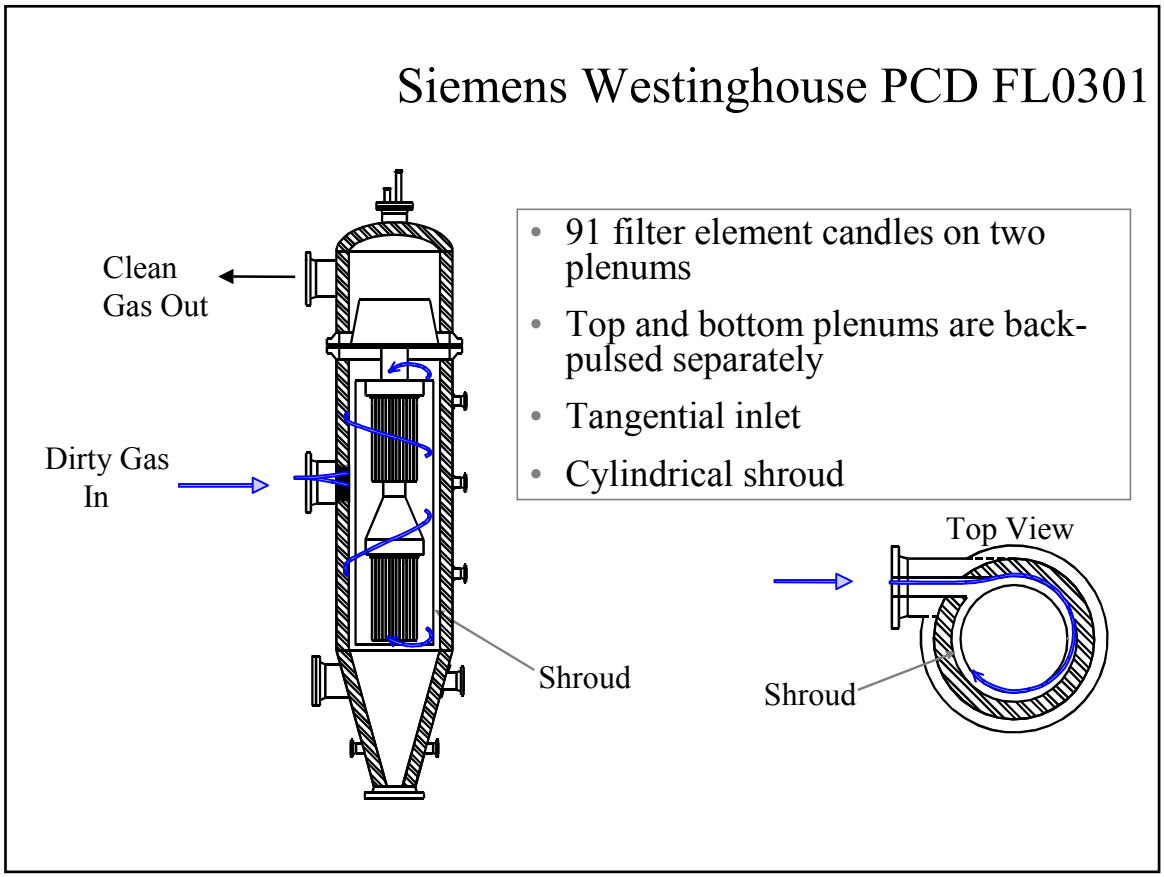

Figure 2.3-1 Siemens Westinghouse PCD

2.4 OPERATION STATUS

Commissioning activities began in September 1995 and proceeded in parallel with construction activities. Design and construction of the transport reactor and associated equipment was completed in early summer of 1996. All separate components and subsystems were fully operational by midsummer and commissioning work was focused on integration issues for the entire transport reactor train. The first coal fire in combustion mode of operation was achieved on August 18, 1996. A series of characterization tests was initiated to develop an understanding of reactor system operations. Test runs CCT1, CCT2, and CCT3 were completed by December 1996. Solids carryover from the reactor to the PCD was found to be excessive during these test runs. A number of startup and design problems associated with various equipment were successfully addressed.

During 1997, three additional sets of characterization test runs (CCT4, CCT5, and CCT6) and one major test campaign (TC01) were undertaken. TC01 focused on exposing the PCD filter elements to process gas for 1,000 hours at temperatures from 1,350 to 1,400°F and achieving stable reactor operations. An Alabama bituminous coal from the Calumet mine in the Mary Lee seam and Plum Run dolomite were used in these test runs.

Two test campaigns (TC02 and TC03) were successfully completed during 1998. TC02 was planned for reactor parametric testing to better quantify the effect of different variables on reactor and filter element operation. Test run TC02 was started on April 5, 1998, and completed on May 11, 1998. Based on TC02 observations, TC03 was planned for additional reactor parametric testing to better quantify the effect of different variables on reactor and PCD operation and to evaluate operation with an Eastern Kentucky bituminous coal and a Gregg Mine limestone from Florida. The third major test campaign, TC03, was performed from May 31, 1998, to August 10, 1998. Stable operations were demonstrated using the Eastern Kentucky coal and Plum Run dolomite, Bucyrus limestone, and Longview limestone during TC03. There were, however, circulation problems using the Eastern Kentucky coal and Florida Gregg Mine limestone because of deposits resulting from excessive fines (segregated) in the Eastern Kentucky feed. One additional test run, TC04, was started on October 14, 1998, but was prematurely ended due to a temperature excursion in the PCD during the initial heat-up of the transport reactor system.

The final combustion test campaign was started on January 10, 1999, in combustion mode of operation and completed May 2, 1999. During TC05 steady-state operations with a variety of fuel and sorbent feed materials were demonstrated (including petroleum coke with two different sorbents) and reactor parametric testing with different feed combinations was performed. Overall, TC05 was a successful test run with 10 different feed combinations tested.

Conversion of the transport reactor train to gasification mode of operation was performed from May to September 1999. The first gasification test run, GCT1, was planned as a 250-hour test run to commission the transport reactor train in gasification mode of operation and to characterize the limits of operational parameter variations. GCT1 was started on September 9, 1999, with the first part completed on September 15, 1999 (GCT1A). The

second part of GCT1 was started on December 7, 1999, and completed on December 15, 1999 (GCT1B-D). This test run provided the data necessary for preliminary analysis of reactor operations and for identification of necessary modifications to improve equipment and process performance. Five different feed combinations of coal and sorbent were tested to gain a better understanding of the reactor solids collection system efficiency.

GCT2, planned as a 250-hour characterization test run, was started on April 10, 2000, and completed on April 27, 2000. Additional data was taken to analyze effect of different operating conditions on reactor performance and operability. A blend of several PRB coals was used with Longview limestone from Alabama. In the outage following GCT2, the transport reactor underwent a major modification to improve the operation and performance of the reactor solids collection system. The most fundamental change was the addition of the loop seal underneath the primary cyclone.

GCT3 was planned as a 250-hour characterization test with the primary objective to commission the loop seal. A hot solids-circulation test (GCT3A) was started on December 8, 2000, and completed December 15, 2000. After a 1-month outage to address maintenance issues with the main air compressor, GCT3 was continued. The second part of GCT3 (GCT3B) was started on January 20, 2001, and completed on February 1, 2001. During GCT3B a blend of several PRB coals was used with Bucyrus limestone from Ohio. The loop seal performed well, needing little attention and promoting much higher solids-circulation rates and higher coal-feed rates that resulted in lower relative solids loading to the PCD and higher char retention in the reactor.

GCT4, planned as a 250-hour characterization test run, was started on March 7, 2001, and completed on March 30, 2001. A blend of several PRB coals with Bucyrus limestone from Ohio was used. More experience was gained with the loop seal operations and additional data was collected to better understand reactor performance. Also during GCT4, RTI began commissioning the DSRP. Figure 2.4-1 is a summary of operating test hours achieved with the transport reactor at the PSDF.

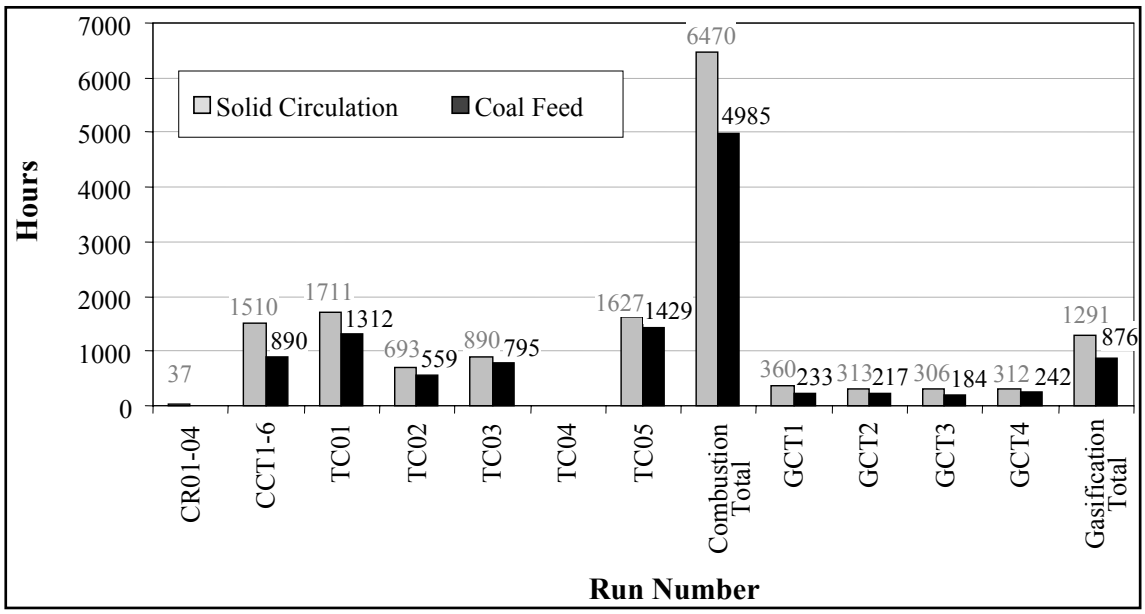

Figure 2.4-1 Operating Hours Summary for the Transport Reactor Train

3.0 PARTICLE FILTER SYSTEM

3.1 GCT4 RUN OVERVIEW

GCT4 was the fourth gasification run for the Kellogg Brown & Root, Inc. (KBR) transport reactor train at the PSDF and the second run since major modifications to the reactor cyclone dipleg seal were completed. As seen in GCT3, the modifications improved circulation and gasification, producing char with higher drag and also decreasing inlet solids concentration to the particulate control device (PCD). During the outage in which the reactor modifications were made, the FD0210 coal feeder motor was replaced with a larger motor, which allowed higher coal-feed rates. The higher coal-feed rates resulted in an increase in the total gas flow into the PCD, further reducing PCD inlet solids concentration. Because the coal-feed rate was increased, the reduced solids loading concentration resulted in little decrease in the absolute amount of solids entering the filter system. The change in char characteristics with no significant reduction in solids loading contributed to a higher PCD pressure drop rate and baseline experienced in GCT3 than seen in GCT2; therefore, high pressure drop was expected for GCT4.

Indeed, controlling PCD pressure drop was a concern during GCT4, and increasing system pressure was at times necessary to maintain control. Baseline pressure drop, generally increasing throughout the run, ranged from about 80 to 200 inH_2O during GCT4 with a backpulse frequency at times less than 5 minutes. Baseline pressure drops in previous gasification runs were significantly lower (except for runs GCT1A and GCT1B). In GCT2, baseline pressure drop was about 50 to 80 inH_2O; in GCT3, the range was 50 to 120 inH_2O. Rapidly rising pressure drop rates were seen frequently, particularly during startup periods.

In addition to high PCD pressure drop, a major concern with the PCD operation was the char deposition found on the filters during the GCT4 inspection and the implications of such deposition on long-term operation. A significant amount of char bridging occurred, mostly on the bottom plenum, covering roughly one-quarter of the PCD filtering surface. Also, the residual char cake was much thicker than the residual cake seen in previous run inspections (almost 10 times thicker than the residual cake from GCT3), and this crusty char cake was found to be quite difficult to remove.

Apparently, excessive tar formation during the numerous startups and low-temperature operation contributed to the filter system problems. During this run a PCD outlet sample taken during one startup period indicated a solids concentration of 38.6 ppmw, which was assumed to be tar as no char was visible on the sample filter. Also, tar condensation on the filter surfaces is believed to have formed a sticky surface, promoting the formation of a thick residual char cake as well as char bridging. The indications of excessive tar formation and the apparent negative effects thereof make the elimination of tar a priority for long-term, stable operation of the particle filter system.

Despite the often unsteady system conditions and the above mentioned concerns, operation of the filter system was stable and successful. There were no filter failures and all outlet samples taken during GCT4, with the exception of the above mentioned sample indicating tar, showed outlet loading concentrations below the detectable limit of 0.1 ppmw. The run provided the opportunity to test changing operational conditions such as increased back-pulse pressure on the

bottom plenum as well as to continue testing Pall iron aluminide (Fe_3Al) metallic filters and alternative Siemens Westinghouse fail-safes. An experiment with solids injection into the PCD was also conducted during the run to determine the effects of various additives on filtering performance.

Information about GCT4 is compiled in the sections listed below.

- GCT4 Run Report, Section 3.2 — This section describes the major events affecting PCD operation during the run, including a run summary. As noted in this section, controlling PCD pressure drop was the main concern with the filter system.

- GCT4 Inspection Report, Section 3.3 — The post-run conditions of various filter system components are reported in this section, including evaluations of char deposition, filters and filter element fixtures, gaskets, and fail-safes. The most remarkable aspects of the inspection were the char bridging and the crusty residual char cake (which was much thicker than the residual char cakes seen in previous run inspections). Notable also were the various colors and "pitting" of the filter surfaces seen following filter cleaning.

- GCT4 Char Characteristics and PCD Performance, Section 3.4 — Char chemistry and properties important to the understanding of hot-gas filtration in this gasification application are discussed in this section as well as inlet and outlet particulate sampling.

- Fines Handling System, Section 3.5 — Operation and inspection of the char removal system are included in this section. Crucial to successful system operation, the fines handling system operated with no major problems during GCT4.

- PCD Solids Injection, Section 3.6 — Several solid additives were injected into the PCD inlet during GCT4 to quantify the effects on filtration performance. This section describes the Southern Research Institute (SRI) study conducted in support of this experiment and the operational aspects and results of the solids injections.

3.2 GCT4 RUN REPORT

3.2.1 Introduction

The GCT4 test run was characterized by stable filter system operation but higher baseline pressure drop in the PCD than had been observed in GCT2 or GCT3. During this run the filter system was subjected to a variety of unusual operating conditions, such as repeated startups, increased back-pulse pressure, and solids injection into the PCD.

Although the filter system operated successfully up to the scheduled shutdown, high baseline pressure drop in the PCD was a concern during GCT4. This high pressure drop was believed to be caused by several factors, including increased char cake drag resulting from improved gasification and circulation in the transport reactor. Another factor was tar deposition on filter surfaces, attributable to excessive tar formation during startups and low-temperature reactor operation. The significant char bridging on the filter surfaces also increased pressure drop.

Run statistics for GCT4 are shown in Table 3.2-1 and the filter element layout is shown in Figure 3.2-1.

3.2.2 Test Objectives

Primary objectives for the filter system during GCT4 were:

- Maintain stable baseline and peak pressure drop in the PCD. During GCT3, the first gasification run after the transport reactor dipleg seal modifications, solids entering the PCD consisted of char particles that produced filter cakes with higher drag than had been seen in gasification runs before the changes. Therefore, PCD pressure drop was higher in GCT3 than in GCT2, and relatively high pressure drop was expected in GCT4.

- Test effects of varying back-pulse parameters. As seen from inspections after previous gasification runs, the bottom plenum of filter elements had not been cleaned by back-pulsing as thoroughly as the top plenum when using the same back-pulse pressure on both plenums. In the outage between GCT3 and GCT4 back-pulse pressure control was modified so that the back-pulse pressure could be set to automatically change with system pressure and back-pulse pressure on each plenum controlled independently. During the run a higher back-pulse pressure was used at times on the bottom plenum than on the top plenum in an attempt to improve filter cleaning.

- Continue to test metal filters. Because of previous failures of ceramic filters (most recently the filter breakage that occurred during the GCT3 sand circulation run) and because of the potential for thermal transients in the PCD, which can damage ceramics, all 90 filters used in GCT4 were metal. All of these filters were Pall iron aluminide (Fe_3Al) sintered metal, 37 of which were new and 53 which had been used in GCT3. As in GCT3, the filters were supported by metal brackets to reduce vibration. The GCT3 inspection revealed some char bridging on the brackets used on the 1-meter candle level, and it was thought that the brackets provided an origination point for char bridging.

Therefore, in GCT4 these brackets were not used except on the 2-meter filters, but the bottom-level brackets were attached to all filters.

- Test the effects of solids injection into the PCD. Because transport reactor modifications resulted in PCD solids loading with char particles that produce filter cakes with higher drag, the addition of several materials to the PCD inlet solids was tested in GCT4 in an attempt to decrease drag and thereby decrease pressure drop. In support of this effort, SRI had previously performed laboratory experiments to demonstrate effects of various additives on dustcake drag. Based on these experiments, four materials were chosen and injected into the PCD during GCT4. The solids injection testing is discussed in further detail in Section 3.6.

3.2.3 Observations/Events – March 7, 2001, Through March 30, 2001

Figures 3.2-2 through -13 show operating data trends corresponding to the events listed below.

A. Back-pulsing began on March 7, 2001, at 00:58 with the pressure set point at 250 psi above system pressure and the timer set on 30 minutes. At 01:30 the system was pressurized to 60 psig. The main air compressor was started at 16:45 and the start-up burner was lit at 18:00. At 23:42, system pressure was increased to 70 psig, and after 1 hour system pressure was increased to 80 psig.

B. On March 8, 2001, at 02:17 back-pulse pressure was increased to 400 psi above system pressure and the timer was decreased to 5 minutes. Coal feed was started, but it tripped at 02:54 and then was back on-line at 03:29. At 03:34, system pressure was increased to 90 psig and was incrementally increased to 130 psig over the next hour. At 05:02, system pressure was increased to 180 psig and to 200 psig at 06:18. At 09:33, system pressure was increased to 215 psig to lower PCD pressure drop.

C. At 12:00 on March 8, 2001, coal-feed rate and system pressure were decreased in preparation for a shutdown to repair a system leak at the flare header. System pressure was reduced to 60 psig. At 12:45, the coal feeder tripped when the FD0210 lock vessel spheri valve failed to close; coal feed resumed at 12:55.

D. At 14:23 on March 8, 2001, a coal feeder trip occurred due to a trip of shut-off valve XV107 on the coal feed line. At 14:35, the coal feeder tripped, again due to XV107 closing, and the main air compressor tripped. At 15:03, the back-pulse timer was increased to 10 minutes.

E. On March 8, 2001, at 16:46 the back-pulse timer was decreased to 5 minutes in anticipation of lighting the start-up burner. The main air compressor was started.

F. At 17:48 on March 8, 2001, the back-pulse timer was increased to 10 minutes when the start-up burner failed to light. Depressurizing the system began so that the start-up burner ignitor could be replaced. Back-pulse pressure was decreased to 250 psi above system pressure. Following three 10-minute cycles, the back-pulse sequence was stopped. At 18:05 the main air compressor stopped.

G. At 19:37 on March 8, 2001, the system was slowly pressurized to 60 psig. The main air compressor was started. Back-pulsing began at 19:55 with pressure set to 250 psi above system pressure and the timer set at 10 minutes. The start-up burner was lit at 20:05. At 22:13 the system pressure was increased to 70 psig, and at 23:55 system pressure was slowly increased to 110 psig.

H. On March 9, 2001, at 00:02 back-pulse pressure was increased to 400 psi above system pressure and the timer was decreased to 5 minutes. Coal feed started and system pressure was incrementally increased, reaching 230 psig at 03:00.

I. On March 9, 2001, at 9:45 back-pulse pressure on the bottom plenum was increased to 500 psi above system pressure, leaving the top plenum back-pulse pressure set at 400 psi above system pressure. At 11:30 the bottom plenum back-pulse pressure was increased to 600 psi above system pressure.

J. At 13:15 on March 9, 2001, system pressure was increased to 240 psig to lower PCD pressure drop because back-pulsing was being triggered more frequently than 3 minutes, which is the back-pulse logic limit.

K. At 17:00 on March 9, 2001, air- and coal-feed rates were reduced because back-pulsing was being triggered every 3 minutes with the trigger point set at 275 inH_2O. Back-pulse pressure was decreased because of a nitrogen compressor trip.

L. At 22:06 on March 9, 2001, the coal feeder tripped after about 2 hours of difficulty with coal feeding, but coal feed was quickly resumed. At 23:03 system pressure was slowly reduced to 180 psig to help coal feeding; at 23:55 the system pressure was increased to 235 psig.

M. On March 10, 2001, at 01:46 the coal feeder tripped and coal feed was discontinued. At 04:15 the system pressure was reduced to 80 psig.

N. At 06:00 on March 10, 2001, the start-up burner was lit after several attempts. At 09:00 the back-pulse timer was increased to 10 minutes.

O. At 12:09 on March 10, 2001, the back-pulse timer was decreased to 5 minutes. At 12:18, coal feed resumed and a slow increase in system pressure was begun at 12:26. At 15:00, system pressure reached 240 psig and was held steady. The back-pulse timer was increased to 10 minutes at 19:30.

P. On March 10, 2001, at 22:45 the coal feeder tripped and coal feed was very unsteady for the next hour. At 23:25, system pressure was decreased to 184 psig to improve coal feeding. System pressure was then increased and stabilized at 235 psig on March 11, 2001, at 00:35.

Q. On March 11, 2001, at 02:14 back-pulse pressure on the bottom plenum was decreased to 400 psi above system pressure.

R. At 09:15 on March 11, 2001, air flow was reduced and coal feed stopped for 10 minutes following the outbreak of a coal mill fire.

S. At 14:35 on March 11, 2001, air- and coal-feed rates were reduced because of difficulty feeding coal. At 17:11, the back-pulse timer was increased to 15 minutes.

T. On March 11, 2001, at 23:30 multiple coal-feed trips occurred due to high conveying line pressure. A bag and cage from the FD0210 baghouse were later found plugging the line.

U. On March 12, 2001, at 07:50 coal feed ended so the coal conveying line could be cleared. System pressure was reduced to 60 psig. The back-pulse timer was increased to 30 minutes, and back-pulse pressure was decreased to 250 psi above system pressure. At 20:43, the main air compressor was shut off.

V. On March 16, 2001, at 20:00 the system was depressurized and at 21:55 the back-pulse sequence was stopped.

W. On March 19, 2001, at 07:35 back-pulsing started with back-pulse pressure set to 250 psi above system pressure and the timer set to 30 minutes. Pressurizing the system up to 60 psig was begun at 08:45. Lighting the start-up burner was delayed until the MWK coal mill became functional at 14:00 on March 20, 2001.

X. On March 20, 2001, at 15:05 the main air compressor was started. At 15:22, after several unsuccessful attempts were made to light the start-up burner, the decision was made to replace the start-up burner flame rod and ignitor. At 16:43 the main air compressor was shut off, the system was depressurized, and back-pulsing was discontinued.

Y. At 18:40 on March 20, 2001, the system was pressurized to 60 psig and back-pulsing resumed with the timer set to 30 minutes and back-pulse pressure set at 250 psi above system pressure. At 22:32 system pressure was increased to 70 psig and was slowly increased to 83 psig over the next 5 hours.

Z. On March 21, 2001, at 02:00 coal feeding began. Back-pulse pressure was increased to 400 psi above system pressure and the timer was decreased to 5 minutes. At 03:30 system pressure was increased incrementally. On March 21, 2001, at 05:08 system pressure reached 200 psig and back-pulse pressure for the bottom plenum was increased to 600 psi above system pressure. System pressure reached 230 psig at 06:30.

AA. On March 21, 2001, at 07:25 CO detectors indicated a system leak (primary cyclone flange). In preparation for a shutdown to repair the leak the system was slowly depressurized and was depressurized completely at 10:10. At 08:15 coal feed ceased. At 09:01 bottom plenum back-pulse pressure was decreased to 400 psi above system pressure. At 09:35 the main air compressor was shut off.

BB. At 10:45 on March 21, 2001, after maintenance tightened the primary cyclone flange, the system was pressurized to 110 psig, but was depressurized at 11:24 because the leak continued.

CC. At 19:50 on March 21, 2001, system pressure was increased to 270 psig for a pressure check. No leaking was detected. At 21:03 system pressure was decreased to 60 psig and the start-up burner was lit at 21:32. At 23:37 back-pulse pressure was set to 250 psi above system pressure and the timer was set to 30 minutes.

DD. On March 22, 2001, at 02:00 system pressure was increased to 85 psig. At 02:40 coal-feed began, back-pulse frequency was increased to 5 minutes, and back-pulse pressure was increased to 400 psi above system pressure. At 3:20 system pressure was increased steadily, reaching 240 psig at 06:00.

EE. At 05:20 on March 22, 2001, bottom plenum back-pulse pressure was increased to 600 psi above system pressure.

FF. On March 22, 2001, at 06:20 the system was depressurized because leaking was found again at the flange. Back-pulsing was stopped at 09:25.

GG. On March 22, 2001, at 17:54 the system was pressurized up to 260 psig for pressure test with back-pulsing pressure set at 315 psig and back-pulse timer set at 10 minutes. At 07:20, after no leaking was detected, the system pressure was decreased to 60 psig and back-pulsing continued with the pressure set to 250 psi above system pressure and the timer set to 10 minutes. The start-up burner was lit at 20:30 and at 22:25 system pressure was increased to 80 psig. At 00:05 on March 23, 2001, system pressure was decreased to 75 psig. To decrease the risk of oxygen breakthrough in the PCD, a few hundred pounds of coal was fed to consume any excess oxygen in the reactor to keep the start-up burner lit. At 00:35 back-pulse pressure was increased to 400 psi above system pressure.

HH. Because leaking around the flange was again found, the system pressure was reduced to 60 psig on March 23, 2001, at 03:50. At 04:15 back-pulse pressure was decreased to 250 psi above system pressure and the timer was increased to 30 minutes.

II. On March 23, 2001, at 18:05 pressure testing began with the system pressurized up to 300 psig, back-pulse pressure set at 250 psi above system pressure, and back-pulse timer set at 30 minutes. System pressure was decreased at 19:45 to 60 psig. The main air compressor was started at 20:50 and at 21:00 the start-up burner was lit. System pressure was increased to 80 psig at 22:30 and at 23:12 the back-pulse timer was decreased to 5 minutes.

JJ. At 02:10 on March 23, 2001, coal feeding began and system pressure was increased to 240 psig.

KK. At 13:16 on March 24, 2001, the bottom plenum back-pulse pressure was increased to 600 psig above system pressure.

LL. At 11:10 on March 25, 2001, the system pressure was decreased to 100 psig because of difficulty feeding coal. At 13:05 pressure was increased up to 230 psig. At 07:15 on March 26, 2001, the back-pulse timer was increased to 20 minutes.

MM. On March 26, 2001, at 09:45 coal-feed was increased and the back-pulse timer was decreased to 15 minutes. The timer was again decreased to 12 minutes at 11:45. Coal feeding difficulty resumed and continued through the next day.

NN. On March 26, 2001, at 12:00 a temperature excursion occurred in the PCD in which candle temperatures increased about 100°F and inlet gas temperature increased 200°F in 1 minute.

OO. On March 26, 2001, at 12:45 system pressure was decreased to 180 psig because of difficulty feeding coal. At 13:36 pressure was increased up to 240 psig. At 16:08 system pressure was decreased to 210 psig, again because of coal feed problems. At 16:36 pressure was increased to 220 psig. System pressure was also reduced at 21:05 to 204 psig because of coal feeding difficulty.

PP. At 22:42 on March 26, 2001, system pressure was increased to 220 psig and was held at this pressure until it was increased to 240 psig on March 29, 2001, at 16:30.

QQ. On March 27, 2001, at 16:40 the coal-feed rate was reduced to conserve coal. The reactor temperature decreased.

RR. On March 28, 2001, at 00:10 the back-pulse timer was increased to 20 minutes.

SS. On March 28, 2001, at 07:43 the coal-feed rate was reduced.

TT. On March 29, 2001, at 18:00 the coal-feed rate was increased.

UU. On March 30, 2001, at 07:41 the back-pulse sequence was disabled for a dirty shutdown. Coal feed ended with a coal feeder trip at 08:17, and the main air compressor was shut off.

3.2.4 Run Summary and Analysis

GCT4 began on March 7, 2001, as the PCD back-pulsing sequence was initiated and the system was pressurized. System pressure was slowly increased, back-pulse pressure and frequency were increased, and coal feed was begun on March 8, 2001, at 02:18 when reactor temperatures were about 1,000°F. As coal feed was established the PCD face velocity quickly rose to about 7.5 ft/minute, largely due to the low system pressure required during the transition from start-up burner to coal feed. High pressure-drop rate was also seen, triggering back-pulsing before the 5-minute set point was reached, and the baseline pressure drop reached about 175 inH_2O before stabilizing. This high face velocity and pressure-drop rate were typical for each startup during the run. As system pressure was slowly increased and system operations stabilized over the next few hours, a face velocity as low as 3 ft/minute was achieved and maintained, and back-pulsing frequency reached the 5-minute set point without being triggered. At 12:45 on March 8, 2001, coal feed stopped for about 10 minutes after a coal feeder trip; when coal feed resumed, face velocity and pressure drop steadily increased until the system was shut down at 14:23 to repair a system leak.

After repairs were made to stop the leak, system start-up began and coal feed resumed on March 9, 2001, at 00:02. From about 05:15 to 13:30 on March 9, 2001, the coal feeder speed was the highest of the run. During this period, at 13:15, PCD pressure drop exceeded the trigger point of 275 inH_2O before the 3-minute back-pulse limit set by control logic, so system pressure was increased to decrease face velocity and the coal-feed rate was reduced. However, baseline pressure drop continued to increase, rising rapidly from 150 to 200 inH_2O, so coal and air rates were reduced. Reactor temperatures were fairly low, close to 1,600°F, and PCD cone thermocouples indicated a high solids carryover at that time. Fairly stable pressure drop was eventually achieved and maintained until a coal feeder trip at 22:06. Over the next few hours, coal feed was attempted but could not be maintained, and coal feed ended on March 10, 2001, at 01:46. It is possible that char bridging was present as early as this period of coal feed, as 1 of the 7 filter surface thermocouples on the bottom plenum began reading about 15 to 25 degrees higher than the other 6 thermocouples at around 08:00 on March 9, 2001. This indicated that the area surrounding this thermocouple, which was installed on B53, was probably covered by char at that point and, as found in the post-run inspection, this area was surrounded by char bridging.

Coal feed resumed at 12:18 on March 10, 2001, and this period of coal feed, marked by unstable coal feeder operation that included multiple trips, ended on March 12, 2001, at 07:20 so that repairs could be made to the coal feed line. During the first hour and a half of this startup, as reactor temperatures were rising from about 975 to 1,600°F, PCD inlet and outlet samples were taken by SRI. These samples showed an inlet solids loading of 59,500 ppmw, about three times the concentration found from the other samples taken during the run, and the outlet loading was found to be 38.6 ppmw, most likely due to tar as no char was visible on the sampling filter. Apparently, excessive tar formation, high solids carryover, and high face velocity contributed greatly to the high pressure-drop rate seen during startups.

On March 21, 2001, at 02:00 coal feed began again. During this startup, baseline pressure drop approached 250 inH_2O. Reactor temperatures were often below 1,600°F during this 6-hour period of coal feed. The system was shut down for repairs after a system leak was found. Another short period of coal feed was begun on March 22, 2001, at 02:40, but was also ended because of continued system leaking.

The next period of coal feed lasted from March 24, 2001, at 02:10 to 08:17 on March 30, 2001. During this time, several coal feeder trips caused periods of low-temperature reactor operation and rapid increases in baseline pressure drop. In general, most of the baseline pressure drop was recovered after stable reactor operation was achieved. However, after a coal feeder trip on March 26, 2001, at 12:06 baseline pressure drop, normalized for constant face velocity and temperature, showed a marked increase that was not overcome during the run. PCD operation was stable, however, largely due to the relatively low coal-feed rate during the last days of the run.

Overall, PCD operation was stable during the run, although long-term successful operation under the given conditions would not have been certain. Normalized pressure drop (that is, pressure drop corrected for a constant face velocity and temperature), which peaked early in the run, generally trended upward over the duration of the run. During the first short periods of

stable operation, normalized baseline pressure drop was about 120 inH_2O; near the end of the run the stable normalized baseline was about 170 to 180 inH_2O. The numerous startups and coal feeder trips accompanied by low-temperature reactor operation likely caused excessive tar formation that had a negative as well as cumulative effect on filtration performance. A typical startup as seen on March 21, 2001, can be seen in Figure 3.2-14. This figure illustrates the rapid rise in PCD pressure drop during coal feed establishment that corresponded to reactor operation below 1,600°F and high solids loading as indicated by the FD0502 screw cooler outlet temperature. Once system pressure was increased and reactor operations stabilized the baseline pressure drop decreased accordingly.

The following factors are thought to have significantly contributed to the unusually high and increasing PCD pressure drop:

- Thick residual cake. As discussed in Section 3.4, the residual cake was much thicker than that from previous runs. Because 53 of the filters used in GCT4 were left installed after exposure in GCT3, the run began with the GCT3 residual cake intact on these filters. The unusually thick residual cake appeared to have been agglomerated by tar.

- Char bridging. As mentioned above, the char bridging seemed to originate early in the run and likely grew throughout the run. In additional to the thermocouple on B53 that began deviating from the other bottom plenum filter surface thermocouples, other filter surface thermocouples began reading higher temperatures than the majority of thermocouples, indicating growth of the char bridging. As the char bridging covers the filter surfaces it impedes flow, increasing face velocity and, therefore, increasing pressure drop

- Higher particle drag. Table 3.2-2 shows the inlet solids concentration as measured by SRI and the measured gas flow at the corresponding times during GCT2 and GCT4. This table shows that the solids loading on March 9, 2001, and on March 27, 2001, was comparable to the solids loading in GCT2. (The periods during which the samples were taken on the March 28, 2001, and March 29, 2001, were some of the lowest coal-feed rates of the run. The March 26, 2001, sample period was a time of inconsistent coal-feed rate.) Even with a lower solids concentration there was not a significant reduction in the amount of solids entering the PCD for much of the run. As discussed in Section 3.4, the char produced after the reactor loop seal modifications is finer and has other characteristics that cause a higher drag than previously seen. This higher drag, coupled with a high solids loading during much of the run, likely contributed significantly to the high baseline-pressure drop.

Table 3.2-1

GCT4 Statistics and Steady-State PCD Operating Parameters
March 7, 2001, Through March 30, 2001

Start Time	3/7/01, 00:58 (Back-pulsing Began)
End Time	3/30/01, 08:17
Coal Type	Powder River Basin
Hours on Coal	242
Sorbent Type	Limestone
Number of Filter Elements	90
Filter Element Layout	Layout 19 (Figure 3.2-1)
Filtration Area	261.3 ft^2
Pulse Valve Open Time	0.2 sec
Pulse Timer Setpoint	5 to 25 min
Pulse DP Trigger	250 to 275 inH_2O
Pulse Pressure, Top Plenum	400 psi Above System Pressure
Pulse Pressure, Bottom Plenum	400 to 600 psi Above System Pressure
Inlet Gas Temperature	700 to 900^oF
Face Velocity	3 to 4 ft/min
Inlet Loading Concentration	10,000 to 59,500 ppmw*
Outlet Loading Concentration	Below Detectable Limit of 0.1 ppmw**
Baseline Pressure Drop	100 to 200 inH_2O

*During startup.
**38.6 ppmw during startup, no detectable char.

Table 3.2-2

PCD Inlet Solids Loading in GCT2 and GCT4

Sample Time	Inlet Concentration (ppmw)	Gas-Flow Rate (lb/hr)	Mass Loading (lb/hr)
GCT2			
4/17/00 09:55	34,000	24,772	842
4/19/00 10:00	31,100	21,607	672
4/20/00 13:35	31,000	22,653	702
4/21/00 08:21	28,300	21,628	612
4/22/00 10:10	25,700	18,264	469
4/24/00 12:35	29,600	21,506	637
4/25/00 10:07	30,900	21,204	655
GCT4			
3/09/01 09:00	23,300	25,258	589
3/26/01 09:45	14,800	23,563	349
3/27/01 12:15	19,800	25,621	507
3/28/01 09:50	10,500	20,111	211
3/29/01 12:20	12,600	20,397	257

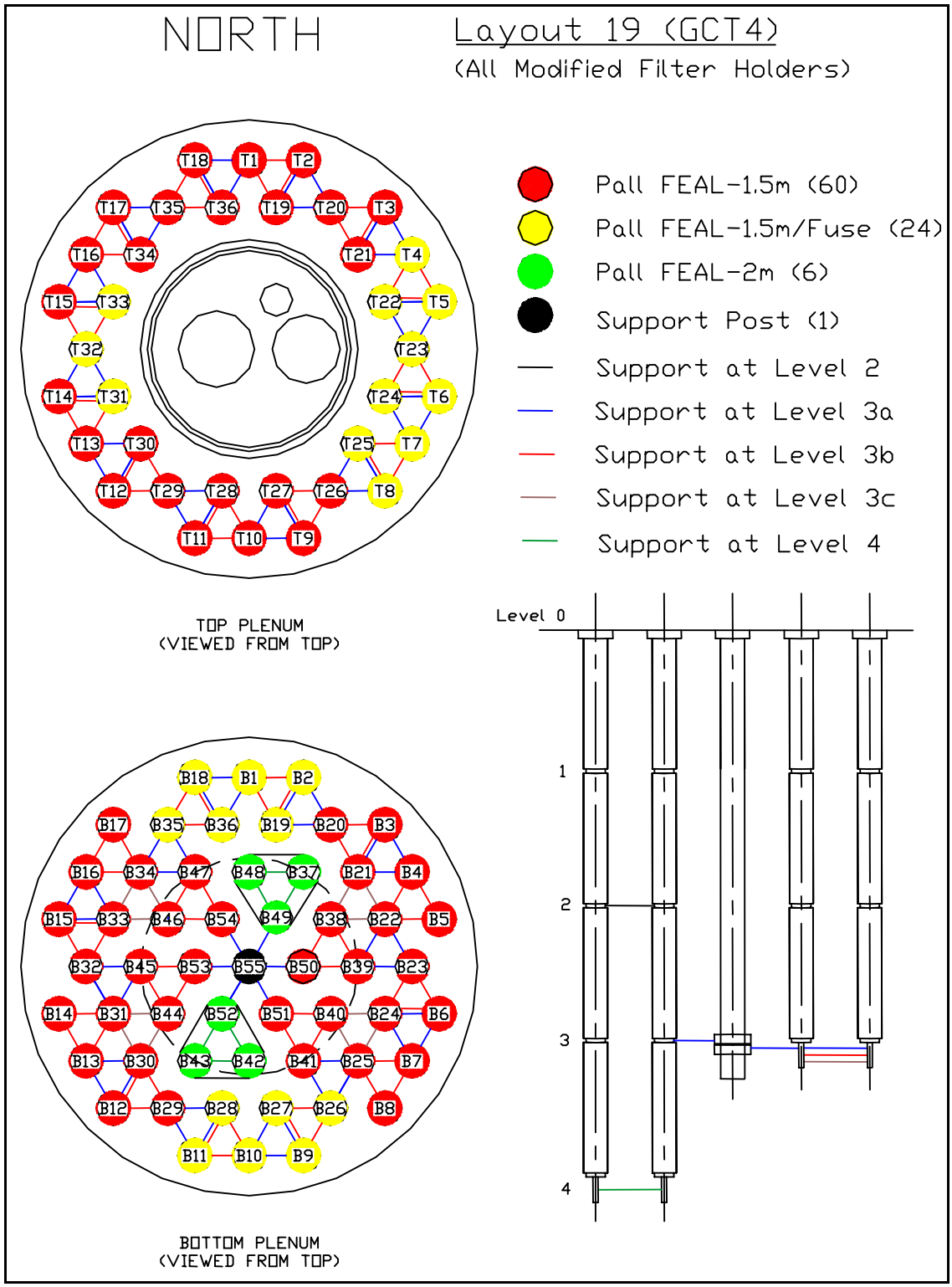

Figure 3.2-1 Filter Element Layout for GCT4

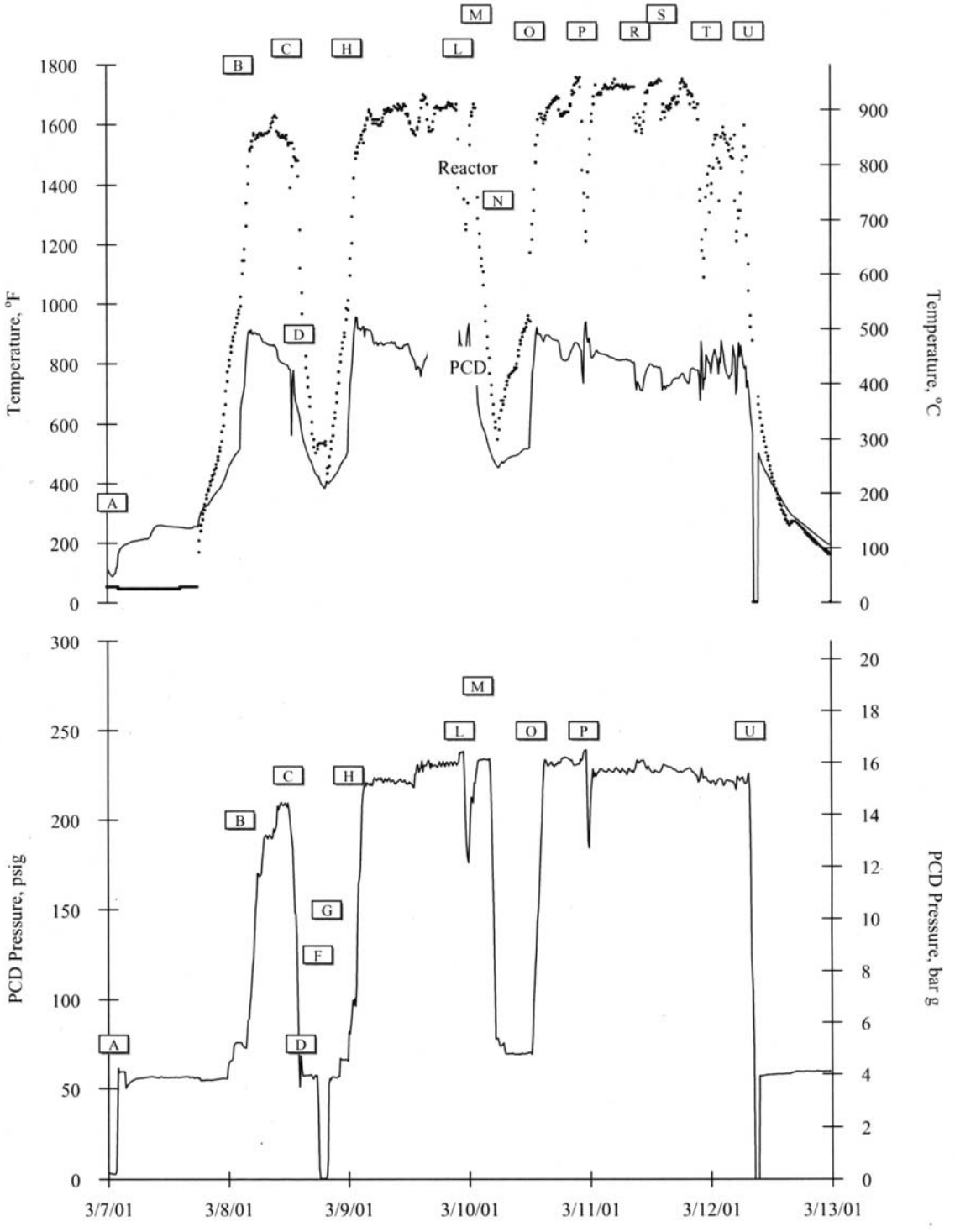

Figure 3.2-2 Reactor and PCD Temperatures and PCD Pressure, March 7, 2001, Through March 13, 2001

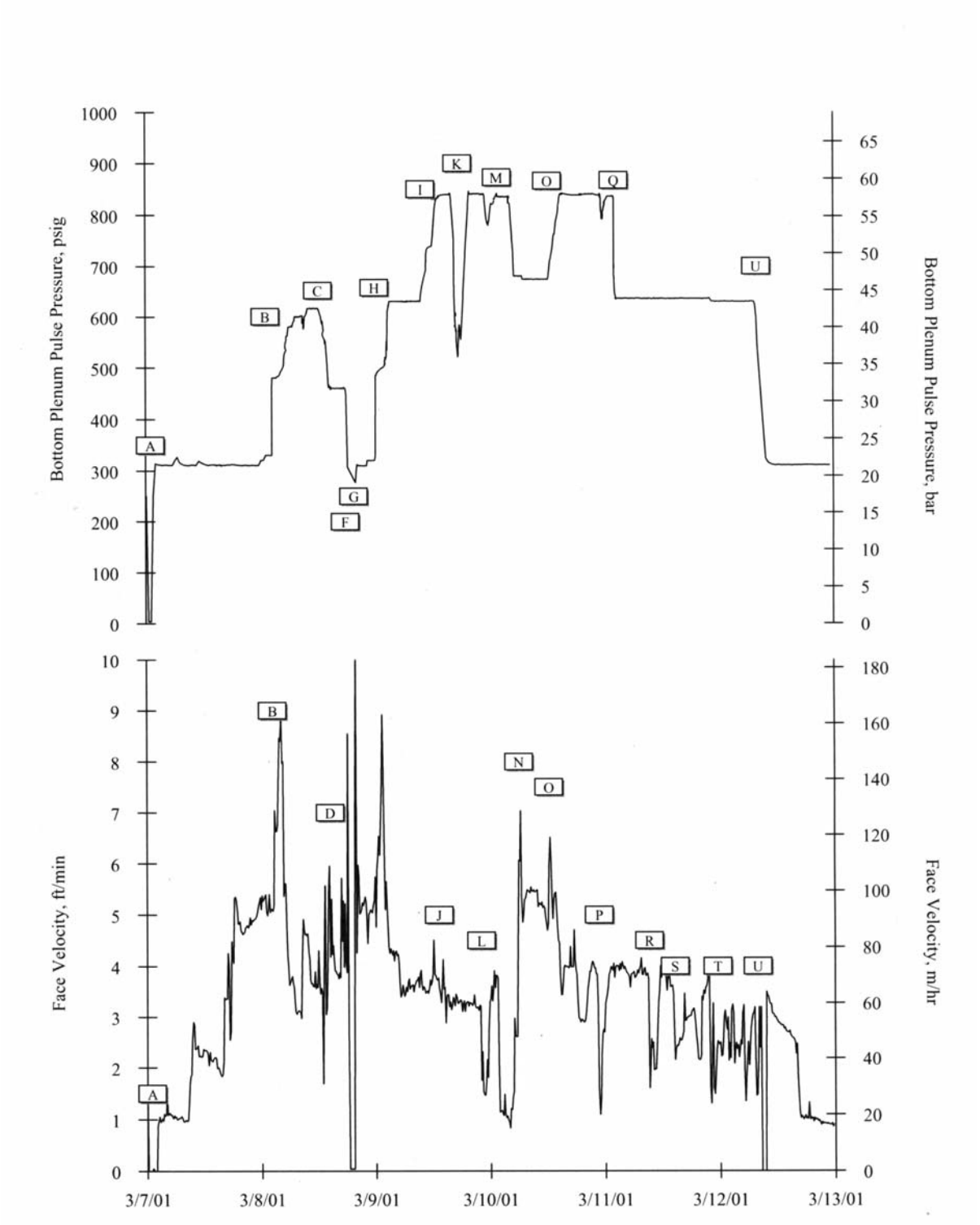

Figure 3.2-3 PCD Pulse Pressure and Face Velocity, March 7, 2001, Through March 13, 2001

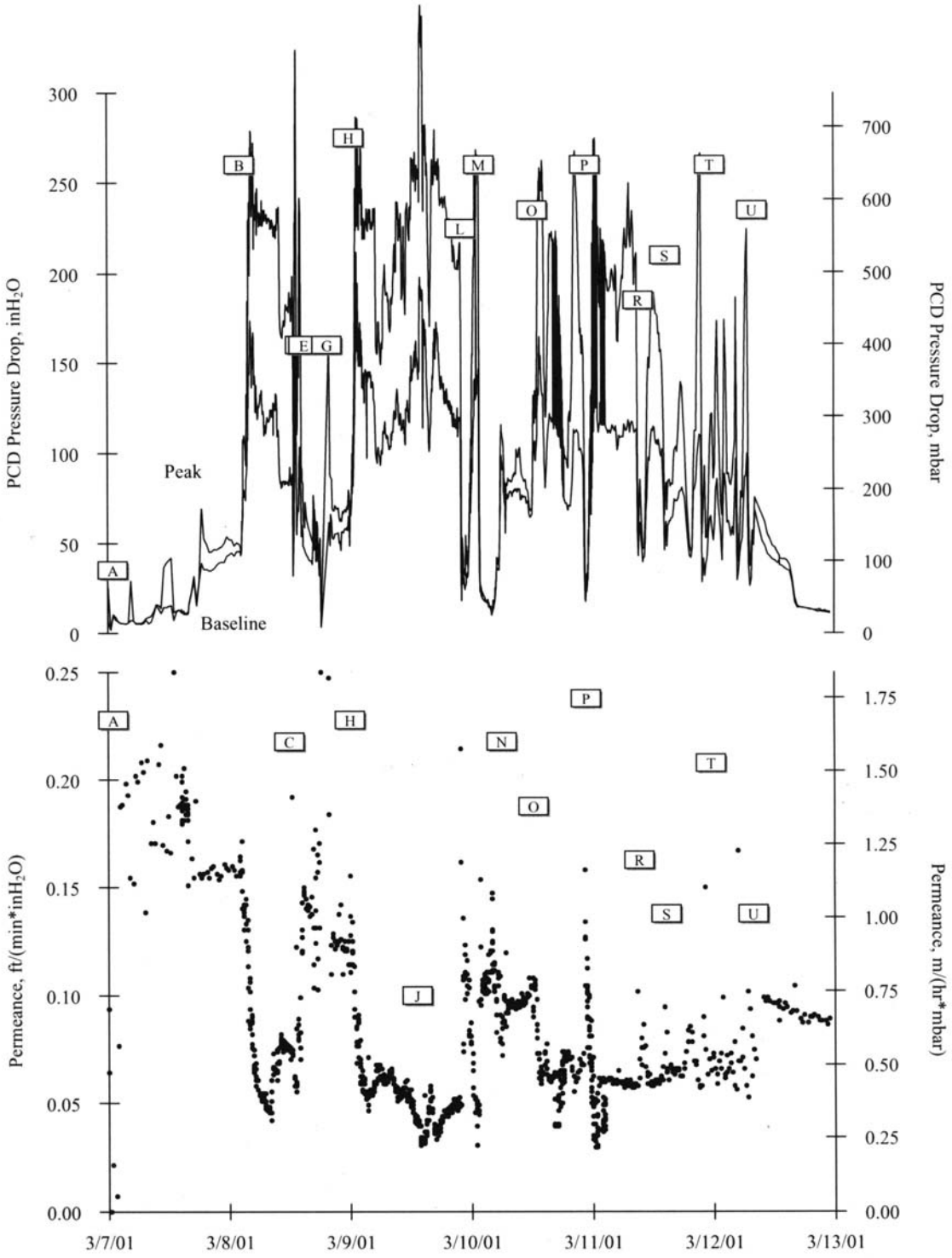

Figure 3.2-4 PCD Pressure Drop and Permeance, March 7, 2001, Through March 13, 2001

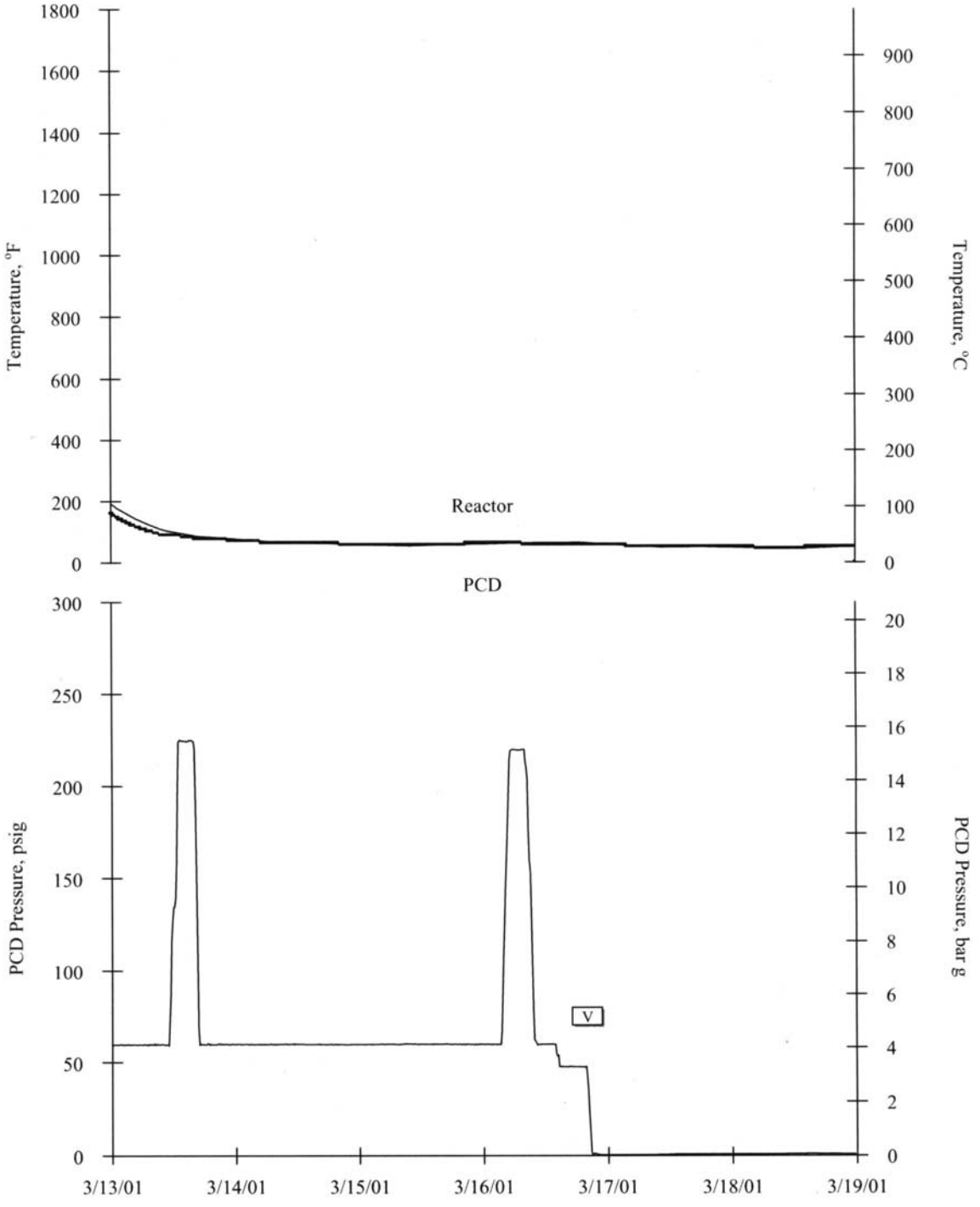

Figure 3.2-5 Reactor and PCD Temperatures and PCD Pressure, March 13, 2001, Through March 19, 2001

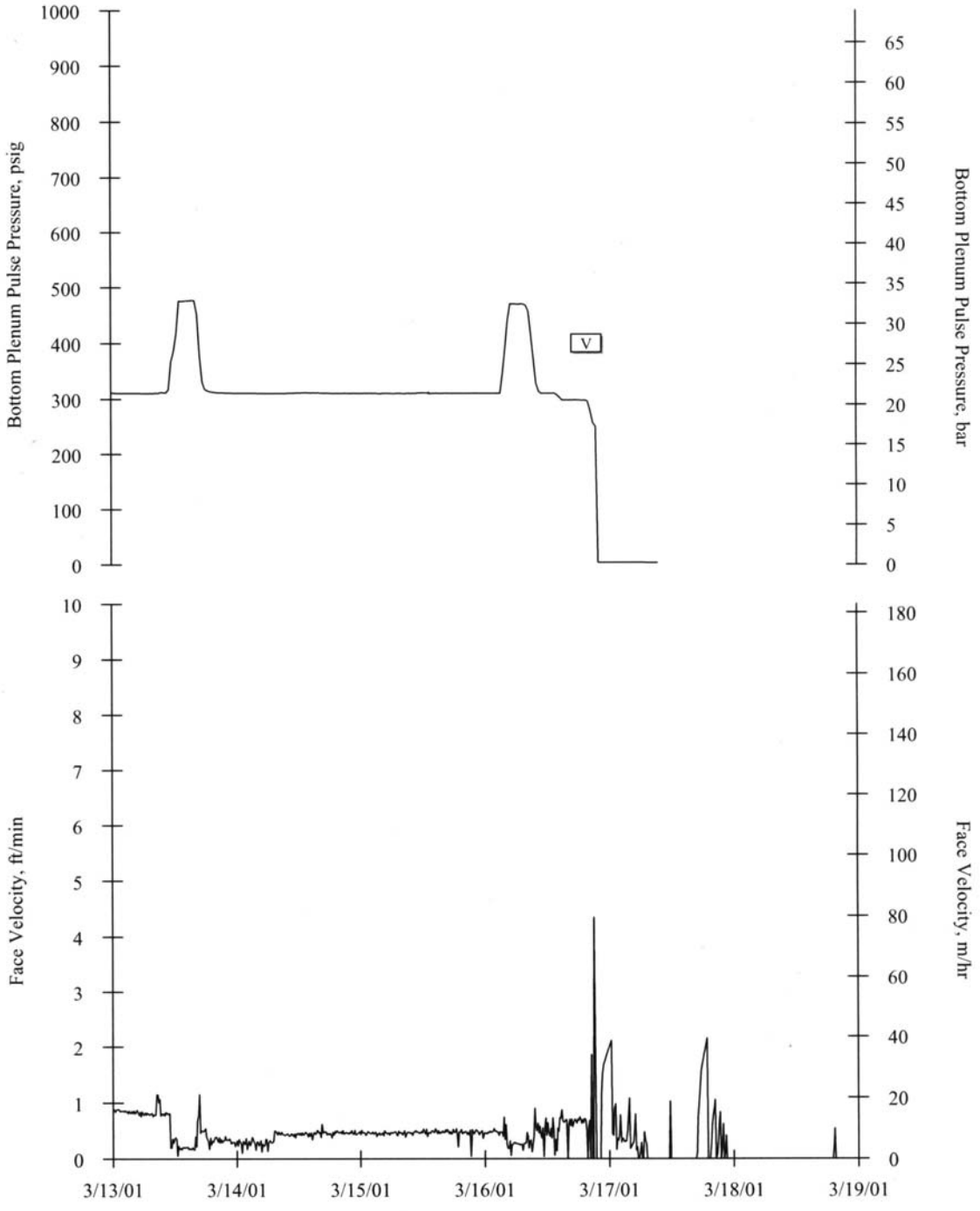

Figure 3.2-6 PCD Pulse Pressure and Face Velocity, March 13, 2001, Through March 19, 2001

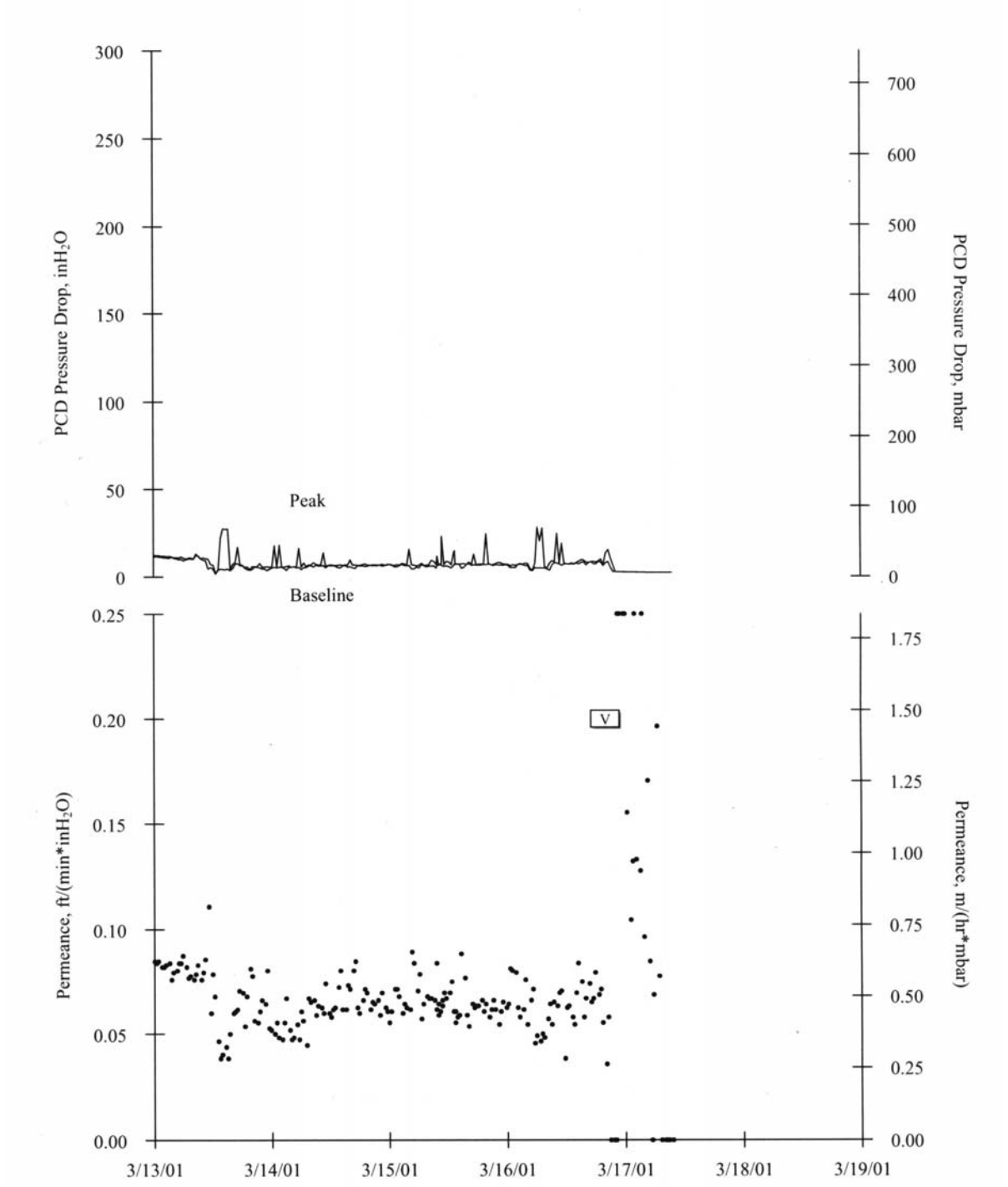

Figure 3.2-7 PCD Pressure Drop and Permeance, March 13, 2001, Through March 19, 2001

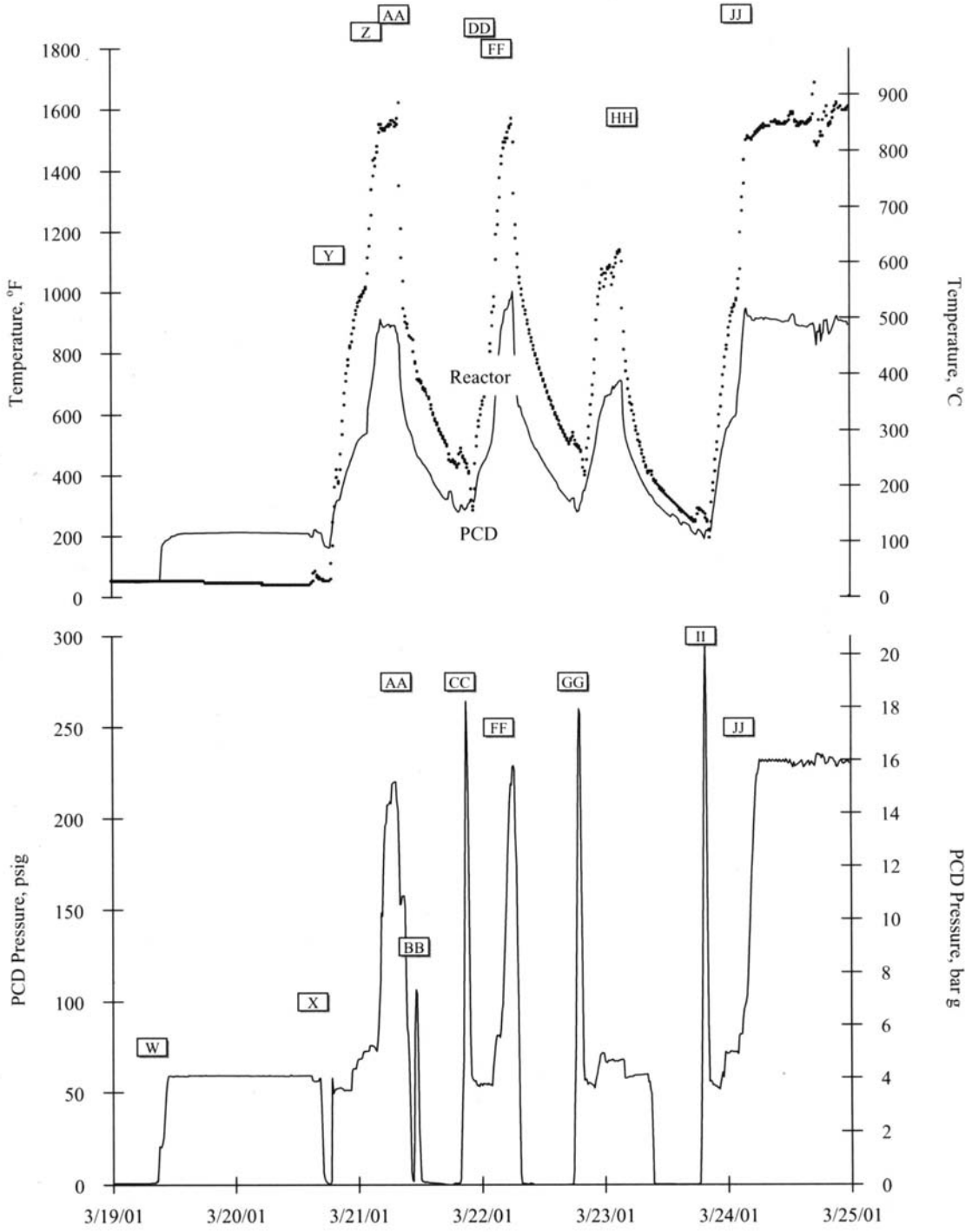

Figure 3.2-8 Reactor and PCD Temperatures and PCD Pressure, March 19, 2001, Through March 25, 2001

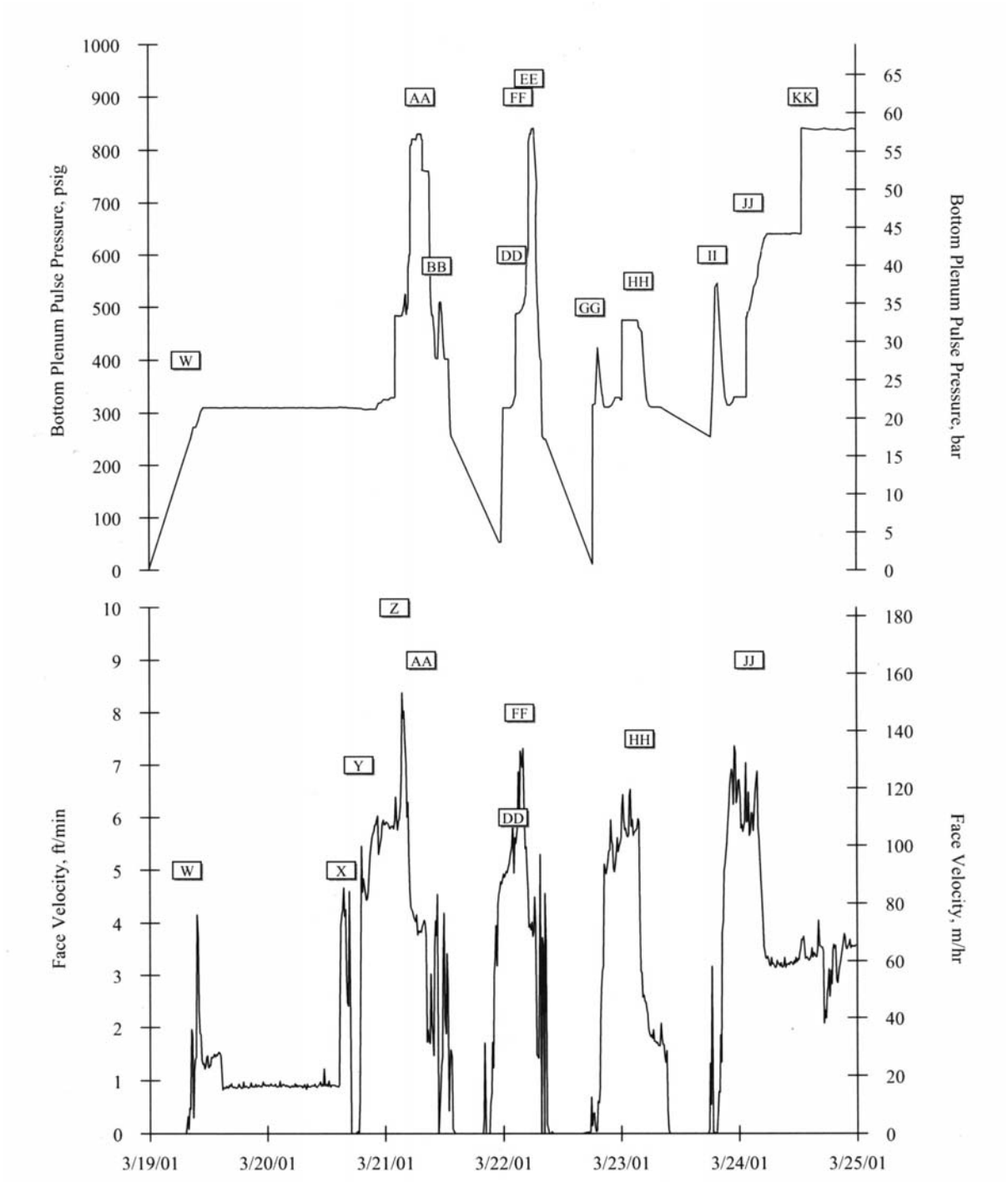

Figure 3.2-9 PCD Pulse Pressure and Face Velocity, March 19, 2001, Through March 25, 2001

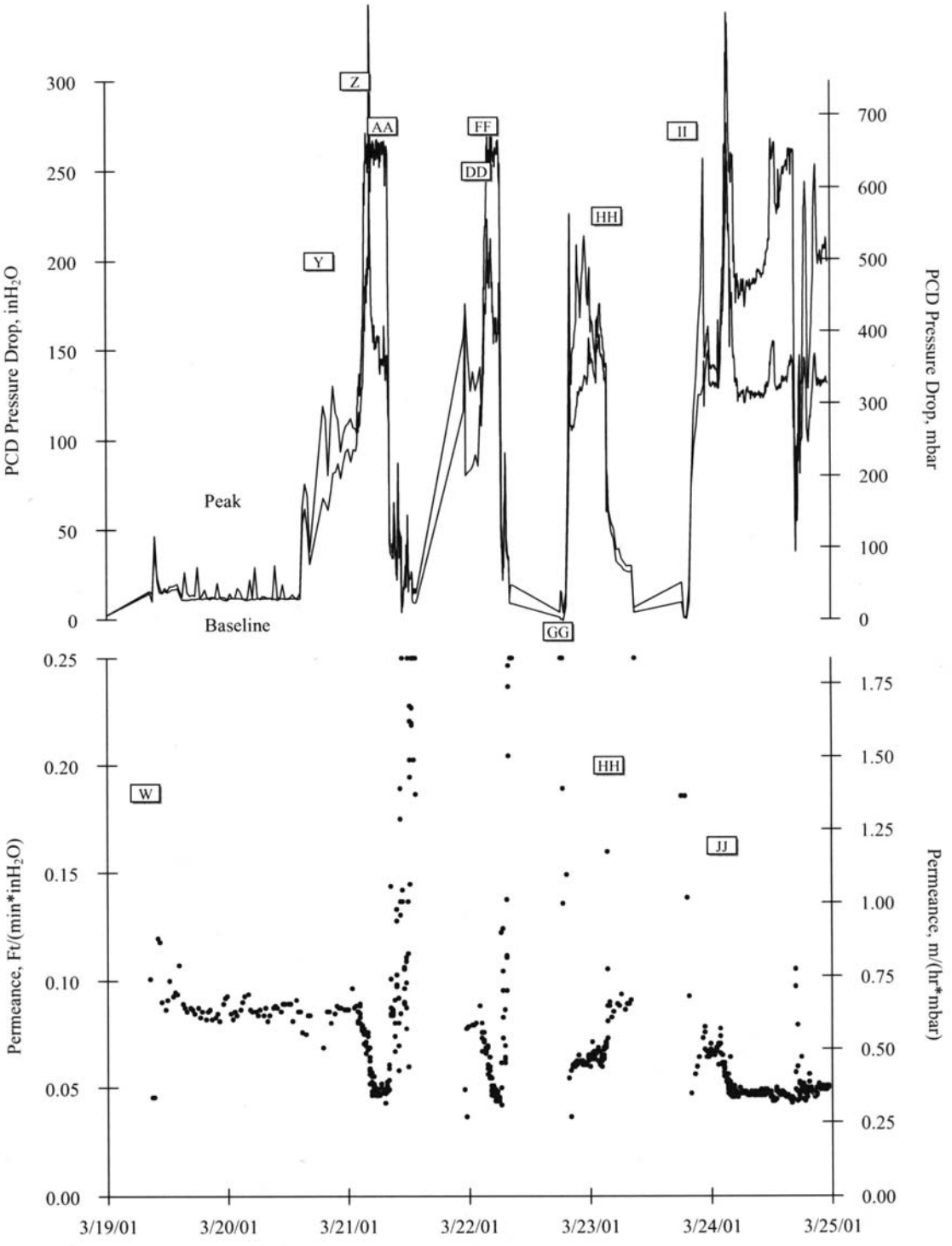

Figure 3.2-10 PCD Pressure Drop and Permeance, March 19, 2001, Through March 25, 2001

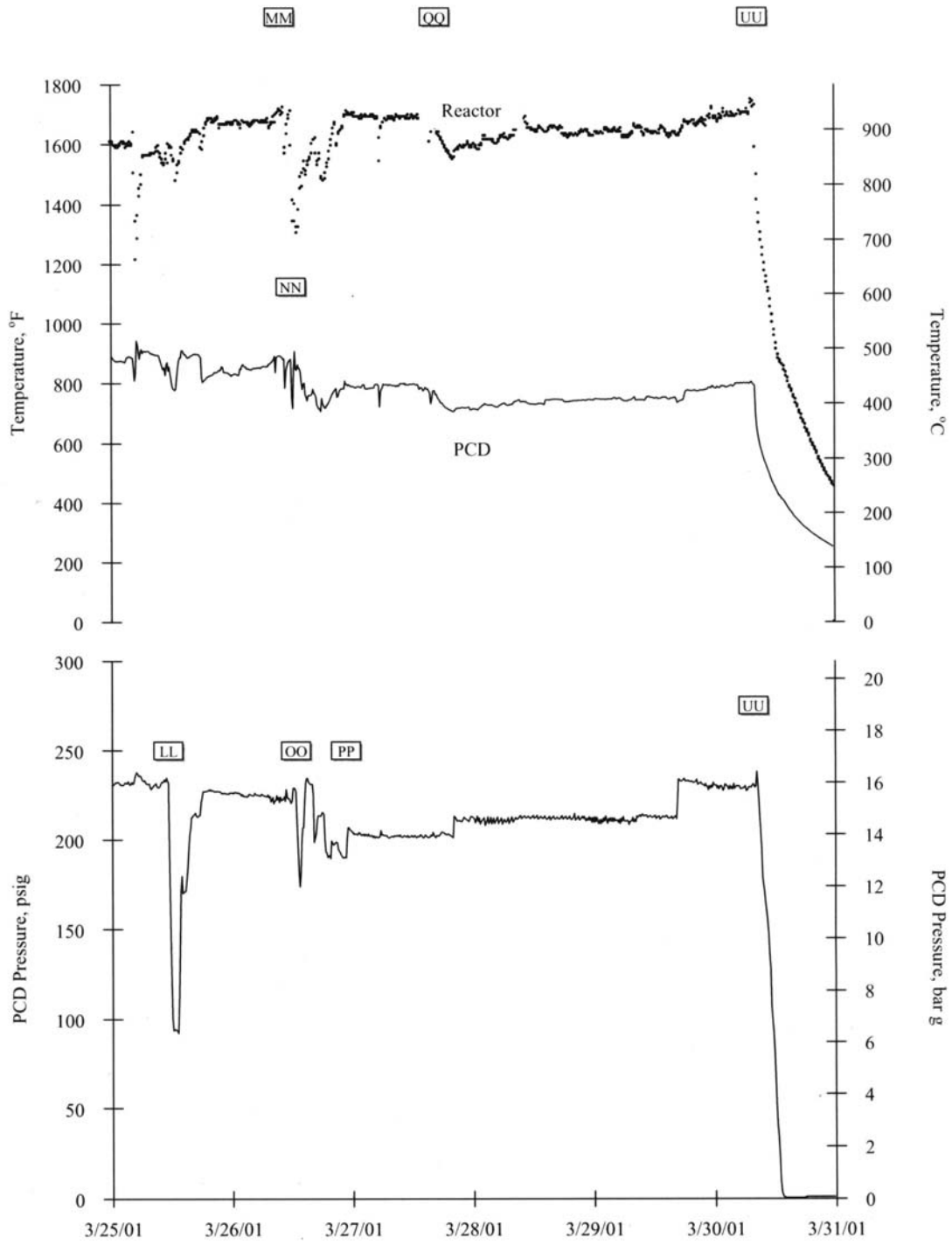

Figure 3.2-11 Reactor and PCD Temperatures and PCD Pressure, March 25, 2001, Through March 30, 2001

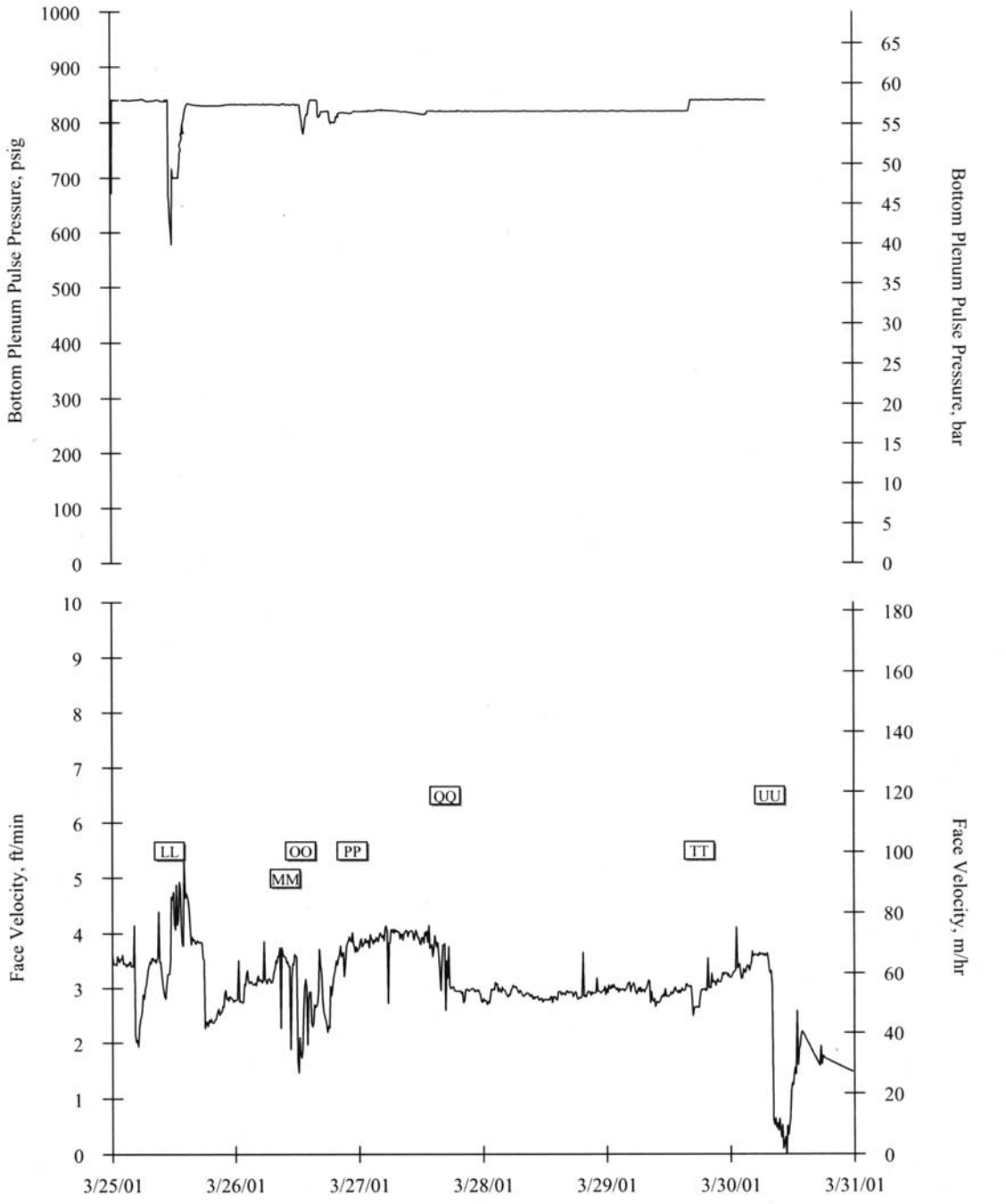

Figure 3.2-12 PCD Pulse Pressure and Face Velocity, March 25, 2001, Through March 30, 2001

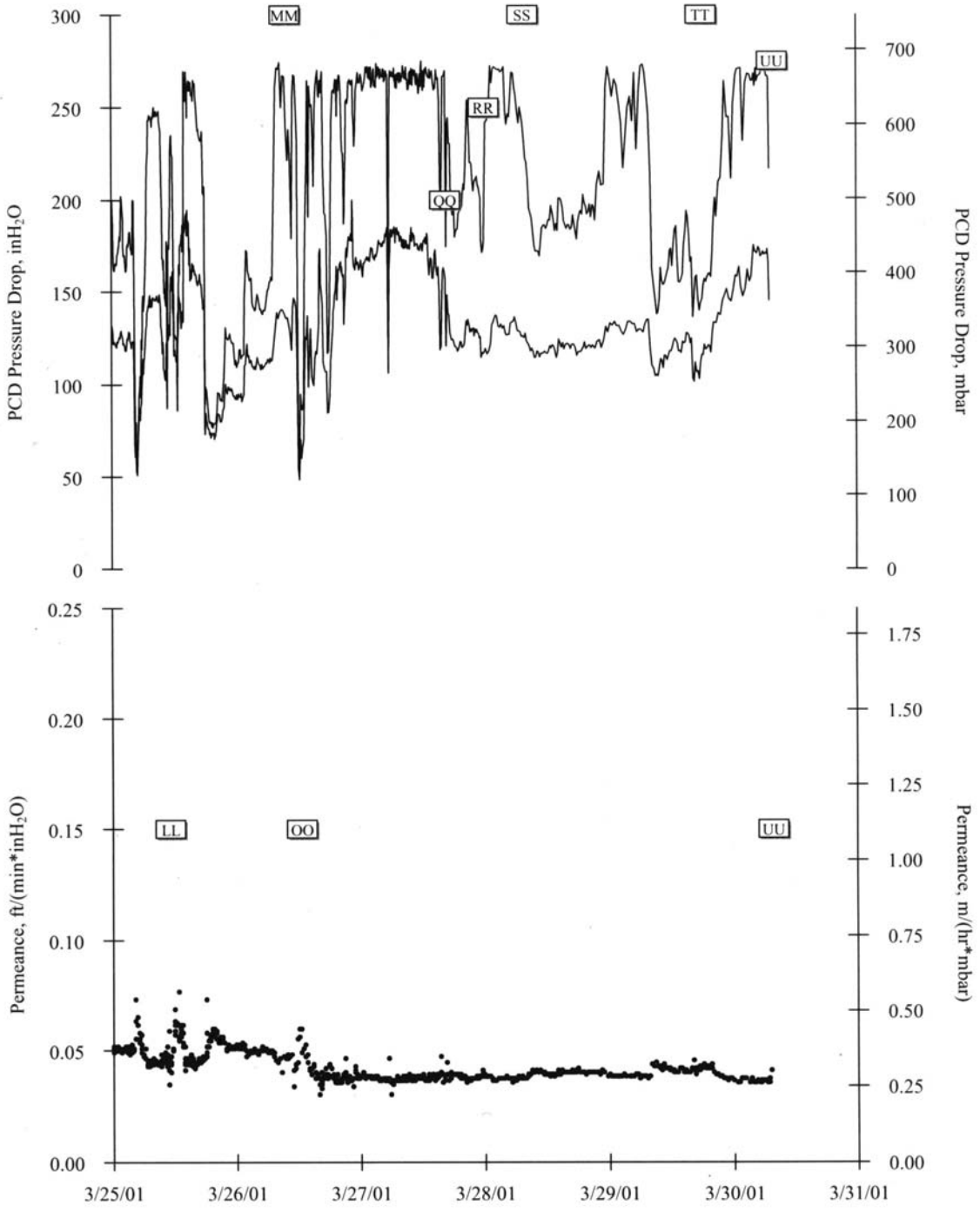

Figure 3.2-13 PCD Pressure Drop and Permeance, March 25, 2001, Through March 30, 2001

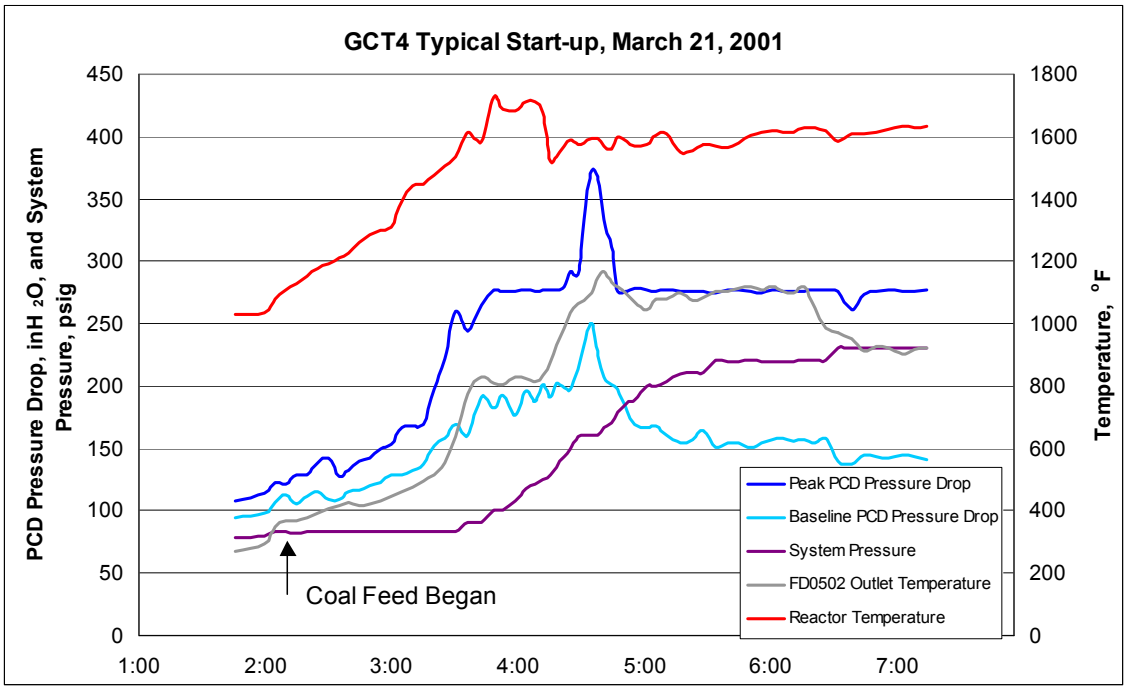

Figure 3.2.14 Typical GCT4 Startup

3.3 GCT4 INSPECTION REPORT

3.3.1 Introduction

The GCT4 run consisted of 242 on-coal hours. Outlet particulate sampling during the run indicated no detectable char leakage through the filter vessel and the fines handling system operated without critical problems. The scheduled shutdown was a "dirty" shutdown in that the back-pulsing sequence was disabled before coal feed ceased, leaving the transient char cake intact for examination during the run inspection.

Inspection of char deposition and all major components of the PCD were completed following GCT4. Some outstanding features of the run inspection are: 1) significant char bridging (see Figure 3.3-1); 2) thick, crusty, strongly adhering residual char cake; 3) discoloration and pits on filter surfaces; and 4) tar flakes on filter holders and other filter element fixtures.

3.3.2 Char Deposition

The major portion of char bridging occurred on the bottom plenum as depicted in Figures 3.3-2 and -3. Char build-up was seen on virtually all surfaces of the PCD internals (see Figures 3.3-3 and -4). Evidence of tar condensation in the PCD was found on the filter holders and other fixtures, and the char bridging that occurred was likely facilitated by this condensation. Tar condensing on the filter surfaces could form a sticky coating to which char would adhere. Mid-level filter support brackets were not used during GCT4, as they were thought to have provided an origination point for char bridging in GCT3. However, char bridging did occur even in the absence of these mid-level brackets.

Significant amounts of char were not seen on the clean-side tube sheet and filter surfaces, but some char was visible on the clean side of all top-plenum filters that were not removed after GCT3. Two PCD outlet particulate samples taken during the GCT3 sand circulation run indicated outlet concentrations of about 16 ppmw; this particulate leakage was the result of the ceramic filter failure during the sand circulation run. It is likely that the char seen on the clean-side filters during the GCT4 inspection leaked into the clean gas area and was blown onto the clean-side filter surfaces during back-pulsing of the top plenum during the sand circulation run.

Because of the dirty shutdown, both the residual and the transient filter char cakes were available for study. The residual cake was unusual in its thickness, hardness, and strong adherence to the filter surfaces. About 0.1 inches thick, the residual cake was about 10 times thicker than the residual cake from GCT3. Microscopic examination revealed the presence of pores about 0.1 mm wide that spanned the thickness of the residual cake. The open area for gas flow through the pores was estimated to be 11 percent.

The transient cake was the first one seen from a gasification run, as no other dirty shutdowns had been possible. However, during shutdown the coal feeder tripped, and operational data show an inconsistent pressure-drop rate in the PCD, indicating that the final transient cake formation did not occur during steady-state conditions. In addition, physical and chemical analysis of this transient cake suggests that it is not representative of the transient cakes formed

during the run. (Refer to Section 3.4 for detailed information on both the transient and residual char cakes.)

3.3.3 Filter Elements

Because of previous failures of ceramic filters, plus the likelihood of thermal transients occurring in the PCD that damage the ceramics, only metallic filters were used in GCT4. All 90 filters used were Pall iron aluminide (Fe_3Al) and included 53 tested in GCT3 and 37 new filters. There were no filter failures during GCT4; however, after cleaning the filters, distinctly different colors and pitting on filter surfaces were apparent, giving rise to the concern that the filters had possibly corroded. (Refer to Section 3.3.4 for more details on this subject.)

Notwithstanding the possibility that corrosion had occurred, it was decided to continue to test Pall Fe_3Al filters in future runs. Therefore, it was necessary to remove the thick, crusty residual cake to restore low-flow resistance to the filters. Section 3.3.4 describes the cleaning methods used and results of the cleaning. There were 73 cleaned filters reinstalled to be tested in the next gasification run (TC06).

3.3.4 Filter Element Cleaning and Inspection

Two filter elements were removed following the GCT4 run to investigate various methods of cleaning and to determine whether the flow resistance could be restored to virgin conditions. One of these filter elements, element 21080 removed from plenum location B-17, was used in both GCT3 and GCT4, and the other, element 22368 removed from B-8, was used only in GCT4. Pressure drop (ΔP) versus face velocity was determined for these two filter elements (see Figure 3.3-5). All flow tests discussed in this section were conducted using air at ambient temperature and pressure. At a face velocity of 3 ft/min, the pressure drops for the as-removed elements were approximately 40 inH_2O for element 21080 and 25 inH_2O for element 22368. Loose char was then blown off the outer surfaces of these elements (using compressed air) and the flow tests were repeated. For the same face velocity of 3 ft/min, ΔP was reduced to about 22 inH_2O for both of the elements. The outer surfaces of the elements were then vacuumed and compressed air was blown through the filter media (from inside to outside). Little change in the pressure drop was observed and no flow test results are shown for this test condition. Next, the elements were wire-brushed and retested. For the same face velocity of 3 ft/min, pressure drop was reduced to about 18 inH_2O for element 21080 and about 6 inH_2O for element 22368.

To restore the original flow resistance, other methods of cleaning were considered, including scraping with a putty knife, sandblasting, and high-pressure water washing (these methods were also tested on a section of virgin element). Both scraping and sandblasting damaged the surface, but water washing did not. Therefore, the two removed elements were water washed using a pressure washer on the outer surfaces. Water was also fed into the inside of the elements through the flanged end to help prevent char from being forced into the filter media pores. Immediately after washing, the elements were dried by first blowing instrument air (-40°F-dewpoint) through them and then placing them in front of a radiant heater. The elements were then flow-tested again (results are shown in Figure 3.3-5). At a face velocity of 3 ft/min, pressure drops were about 3 inH_2O for both elements, nearly the same as for virgin elements.

The outer surfaces of the two cleaned elements were examined and some pitting was found. Low-powered microscopic examination was required to determine if pitting was present, as there were small areas of remaining char on the element surfaces that could not be distinguished from pitting with unaided visual observation. A sample region of pitting from element 21080 is shown in Figure 3.3-6, which shows several pits approximately 0.008 in. across surrounded by what appears to be remaining char particles. This region is typical of several seen on the surface of this element; however, most of the surface had no pitting.

For several reasons, based on the flow test results and observations discussed above, the decision was made to remove and clean all elements. One reason for cleaning all the elements was the possibility of achieving a long, continuous run with stable PCD operation during TC06 would be greater if the elements were clean at startup rather than covered with the GCT4 residual char cake. Also, since coke breeze feed would be used during the TC06 start-up in an effort to reduce tar formation, beginning the run with clean elements would provide a much easier evaluation of this change. Finally, due to the pitting and possible corrosion seen on the first elements cleaned, the elements should be inspected to determine their suitability for continued operation.

All elements except two were cleaned using the high-pressure water-washing method. The two not cleaned by this method are discussed in the following paragraph. Inspection of the cleaned elements revealed an interesting array of colors, including blue-gray, green-gray, red-brown, and yellow-green, with varying degrees of darker mottling. A photograph of typical elements is shown in Figure 3.3-7. Inspection using a low-powered microscopy showed pitting on a substantial number of the elements; the amount of pitting varied from element to element. A correlation between pitting and one of the many variables that affect the elements, variables such as operational history, initial color (blue or gray), plenum location, bridging, and type of fail-safe, was not found. The sizes and shapes of most pits were similar to those seen in Figure 3.3-6, although some difference was noted. A pit observed in element 27060 from plenum location B-35 is shown in Figure 3.3-8. The area surrounding this pit was discolored but did not have any of the residual char particles as discussed above. Figure 3.3-9, showing element 21646 from plenum location B-51, is an example of an area where pits appeared to have grown together. The frequency of pits in this element was greater than in any other element. This photograph also shows areas of residual char, a feature observed on several elements. It is uncertain whether these areas are precursors to pitting.

Element 28072 from plenum location B-6 (used in both GCT3 and 4) and element 22366 from plenum location B-7 (used only in GCT4) were sent to Southern Metals Processing for chemical cleaning to determine whether this cleaning method was a viable option for the future. These two elements were flow-tested before and after cleaning, and the results are shown in the plot in Figure 3.3-10. At a face velocity of 3 ft/min, pressure drops measured before cleaning were ~44 inH_2O for element 28072 and ~21 inH_2O for element 22366. After cleaning, pressure drops measured at the same face velocity were ~4 inH_2O for element 28072 and ~3 inH_2O for element 22366. Although these results indicated that the flow was restored sufficiently for reinstallation, the outer surfaces were too blackened for inspection. Therefore, these two elements were pressure washed with water and then inspected. A small amount of surface rust was seen near the flanged end of both elements. This rust was seen on the inside and outside of

element 22366 and on the outside only of element 28072. Some pitting similar to that seen on the other elements was also on element 22366, and the pitting on element 28072 was more severe in frequency and size than any other element except element 21646.

Metallurgists from Pall, Southern Company Services, Inc. (SCS), and Oak Ridge National Laboratory (ORNL) came to the PSDF to examine the filter elements, assess the damage due to pitting, and determine their suitability for reinstallation for the next gasification run (TC06). Although no conclusive explanation was given for the color variations seen, they are considered by Pall to be normal and not an indication of corrosion or degradation. The cause of the pitting is not certain either, but the metallurgist from Pall contended that it is due to a manufacturing abnormality and not likely to worsen with continued operation. Microscopic examination of four virgin Pall Fe_3Al elements and one virgin Pall Hastelloy X element to be installed in TC06 revealed some pitting, which may support the suggestion that pitting is a result of a manufacturing process. Examples of the pits seen in virgin elements are shown in Figures 3.3-11 and -12. While these pits appeared similar to those seen in elements exposed during GCT4, there were differences. On the virgin elements, the frequency of pits is less than on exposed elements. Also, on the virgin elements there was no discoloration of the area around the pits, as seen in Figure 3.3-8, nor were there any areas where several pits appeared to have run together, as shown in Figure 3.3-9. Examination and analysis of selected sections of the exposed elements will continue at Pall, SCS, and ORNL and an updated explanation will be included in the TC06 run report.

Operating exposure will continue on 77 Fe_3Al filter elements from GCT4 and on 2 elements from GCT3. The two most severely pitted elements, 21646 and 28072, were not reinstalled. The main reasons for continuing use of these 79 elements are 1) to determine if the pits continue to appear and 2) because there were not enough new metal elements in inventory to totally replace the used elements. The option of replacing these elements with ceramic elements was not exercised because of the probability of thermal transients during TC06 and the resulting risk of catastrophic failure of ceramic elements. To track changes in the pitting, five of the exposed Fe_3Al elements were microscopically photographed and documented. In addition, four new Fe_3Al filter elements were installed for comparison purposes.

3.3.5 Filter Element Fixtures

The filter holder design used in the previous two gasification runs was also used in GCT4. All fail-safe holders were installed with a torque of 120 in.-lb on each of four bolts and all filter holder bolts were torqued to 100 in.-lb. During inspection the average remaining torque on fail-safe holder nuts was about 65 in.-lb in position B8 and 56 in.-lb in position B17. The remaining torque measurements on filter holders from B8, B17, and B35 were all less than 40 in.-lb, with the exception of one nut from B17 that had a remaining torque less than 60 in.-lb.

As in GCT2 and GCT3, a thin coating of tar was seen on many of the fixtures, including the fail-safe and filter holders. This shiny residue could be easily removed in flakes by wiping the coated surface.

3.3.6 Filter Element Gaskets

The gasket arrangement and types used in GCT2 and GCT3 proved to function adequately, so they were also used in GCT4. This arrangement consists of a Siemens Westinghouse lapped-construction primary gasket at the plenum-to-fail-safe connection; a top donut gasket between fail-safe and fail-safe holder; and two bottom donuts—one located at fail-safe holder-to-filter, and one at filter holder-to-filter. Filter socks were installed on all filters underneath the filter holder-to-filter donut.

Upon inspection, all the fail-safe holder-to-filter gaskets appeared clean. Several primary gaskets and top donuts were removed during inspection, as well as during the TC06 installation, and all these gaskets appeared clean.

3.3.7 Fail-safes

Ten Siemens Westinghouse prototype fail-safes containing metal fiber were evaluated in FL0301 during GCT4. They were previously exposed during GCT2 and GCT3, and have now accumulated about 642 hours of on-coal exposure time under test conditions. The metal fiber is designed to allow free flow of clean gas, but to plug completely when the gas contains particles. The 10 fail-safes tested contain fibers in various forms and are made from several different materials. Following GCT4, one of the fiber fail-safes was removed, weighed, and flow tested. The weight change compared to the pretest value was negligible. The flow coefficient was about 10 percent lower than the value measured after GCT2 (that is, at the same density and ΔP across the fail-safe, the flow rate would be 90 percent of the previous value, or at the same flow rate the ΔP would be $(1/0.90)^2$ of the previous value). The flow test results were consistent with results for two other fiber fail-safes that were weighed and tested following GCT3. Flow coefficients for those two fail-safes were 7 and 9 percent lower than the post-GCT2 values. Since none of the fail-safes had a significant change in weight, the increased flow resistance is thought to be due to settling of the fibers. Testing on all 10 fiber fail-safes will continue during TC06.

3.3.8 PCD Vessel and Plenum Assemblies

Following disassembly of the PCD the liner and shroud were visually inspected through the lower man-way. The liner sections had not visibly degraded. The cone liner had not shifted upward significantly since last inspected, but because the cone thermocouples are close to the bottom edges of the liner holes and further movement of the cone liner could damage them, liner movement will continue to be monitored closely in the future. In a previous inspection the shroud was found to have shifted, and during the GCT4 inspection the bottom of the shroud was found to be in contact with the liner in an approximate 60-degree-wide range. Figure 3.3-13 illustrates the current shroud position.

The bottom of the cone was filled with char that covered the cone thermocouples, TI3001 and TI3002. Operations personnel later removed this char. Since the char removal system was operated for over 7 hours after coal feed ceased it is possible that this remaining char was from the bridged char and filter cakes that fell in the time between shutdown and the PCD disassembly.

3.3.9 Auxiliary Equipment

There were 14 thermocouples used in GCT4 which were installed prior to GCT3 to monitor filter surface temperatures and detect temperature excursions in the PCD. Although they functioned properly during GCT4 they were replaced by new thermocouples for the next run because of potential wear damage.

The liner of the FL0301 pulse pipe A, removed following the GCT3 sand circulation, had rolled inward at the top, partly obstructing the gas path. The liner is a thin sheet metal tube inside the main pulse pipe. Its purpose is to reduce the thermal stress on the main pipe when the back-pulse gas is injected. The liner longitudinal weld seam had corroded away at the top, allowing the pulse gas to get behind the liner and roll it in. Material for a new liner could not be immediately obtained so one of the FL0352 pulse pipes whose design was identical to the FL0301 pulse pipes, except for the length, was removed and shortened to the correct length. The modified pipe from FL0352 was used during GCT3 and GCT4.

Corrosion had been a problem in the low-temperature upper section of the main pulse pipes, so in 1998 the original high-strength stainless pipe material was replaced with a corrosion-resistant stainless material. Following GCT4, this same modification was made on the pipe that was removed from FL0352. Since the replacement material for the upper part of the main pipe has resisted corrosion well, Siemens Westinghouse suggested changing the material for the top section of the liner to this same corrosion-resistant material, and the current high-strength material for the hot lower section. This change may be implemented at a later time if liner corrosion continues to be a problem.

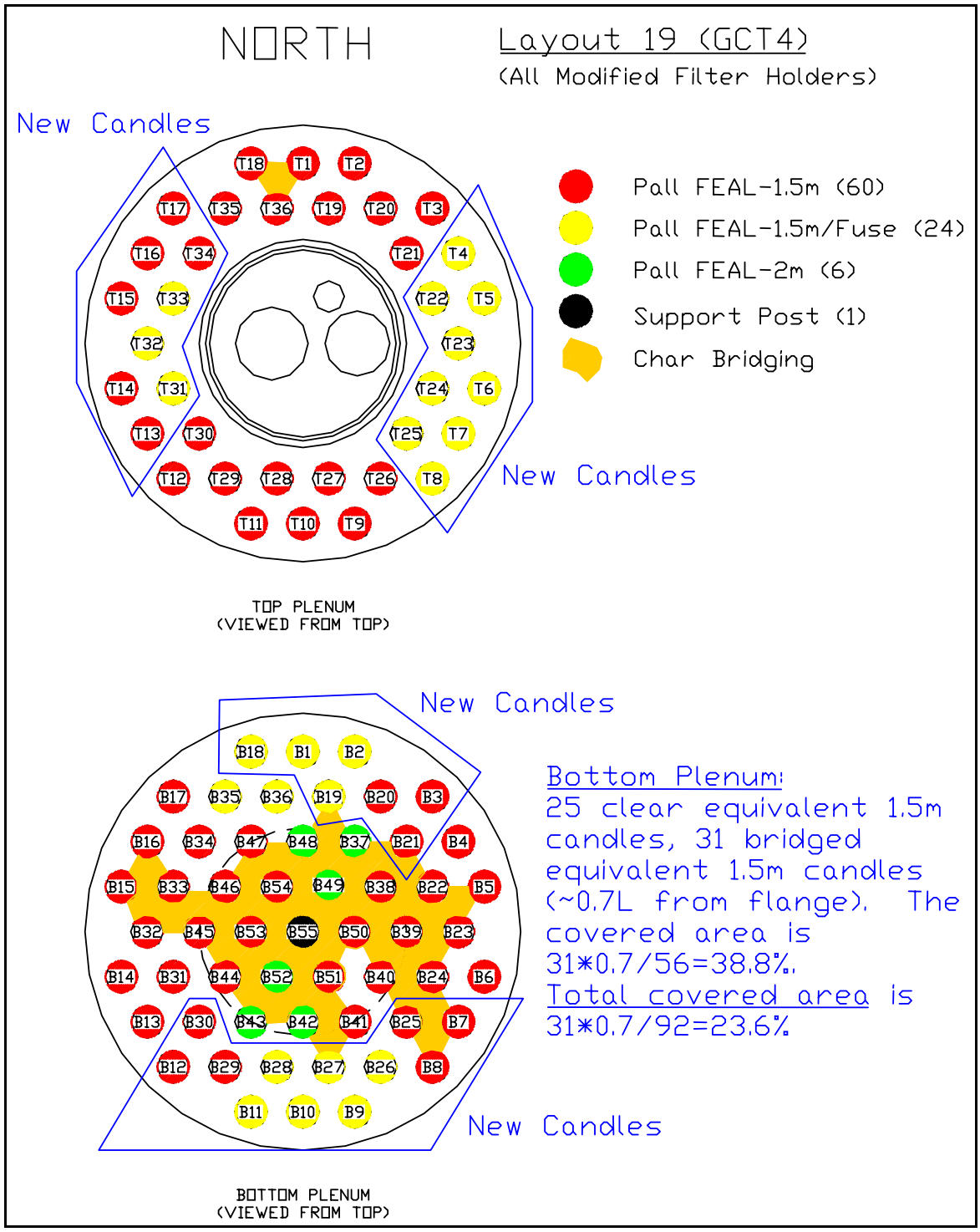

Figure 3.3-1 Filter Element Layout Showing Char Bridging

Figure 3.3-2 Char Bridging on FL0301 Bottom Plenum

Figure 3.3-3 Char Build-up on FL0301 Top Plenum Surfaces

Figure 3.3-4 Char Build-up on Bottom Plenum Support Brackets

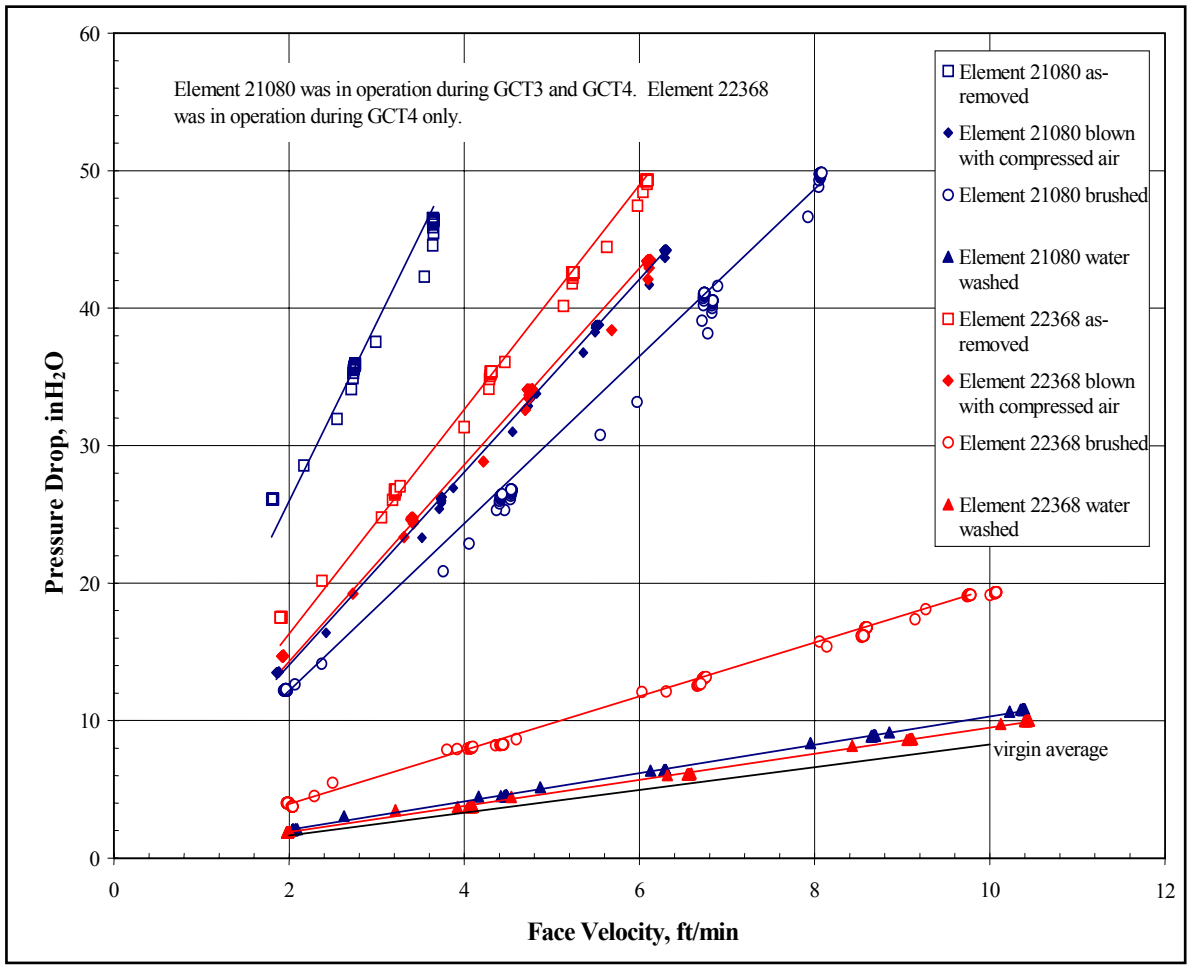

Figure 3.3-5 Pressure Drop Vs. Face Velocity for Pall Fe_3Al Elements 21080 and 22368 Removed After GCT4

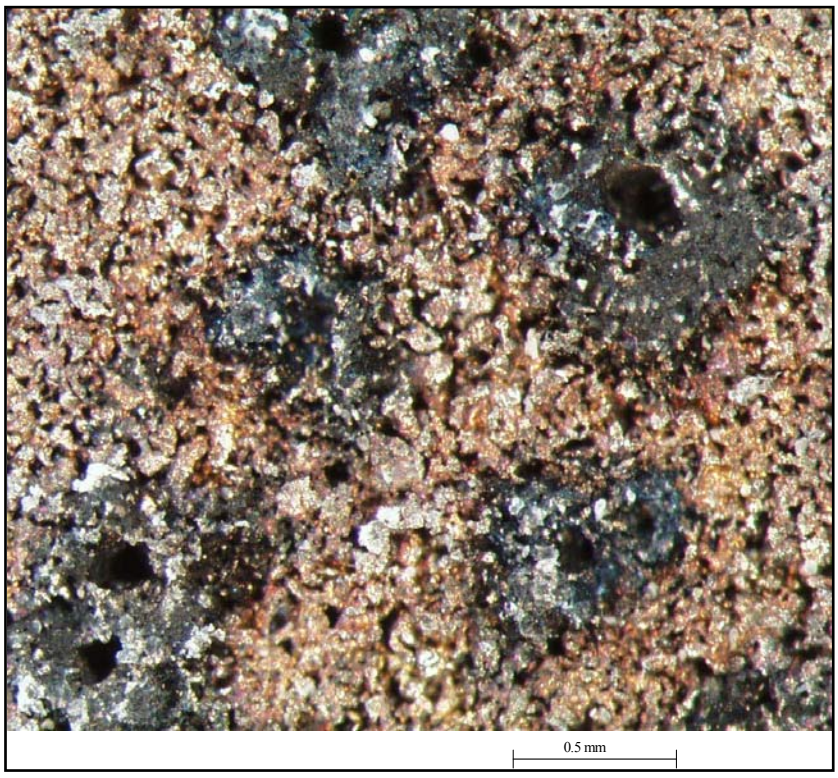

Figure 3.3-6 Pitting on the Outside Surface of Pall Fe_3Al Element 21080 Removed From Plenum Location B-17 After GCT-4

Figure 3.3-7 Typical Pall Fe_3Al Elements Removed From GCT4 After Cleaning by Pressure Washing

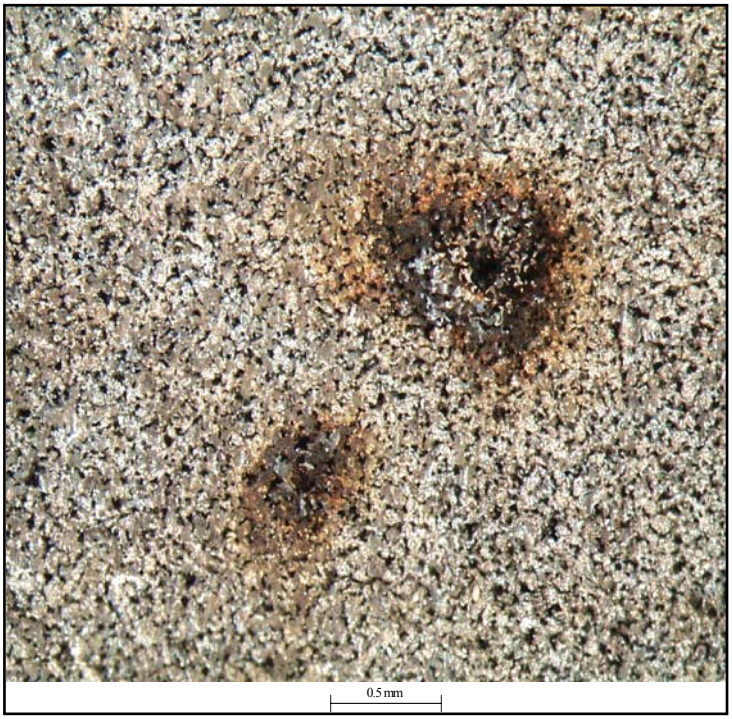

Figure 3.3-8 Pitting on the Outside Surface of Pall Fe_3Al Element 27060 Removed From Plenum Location B-35 After GCT4

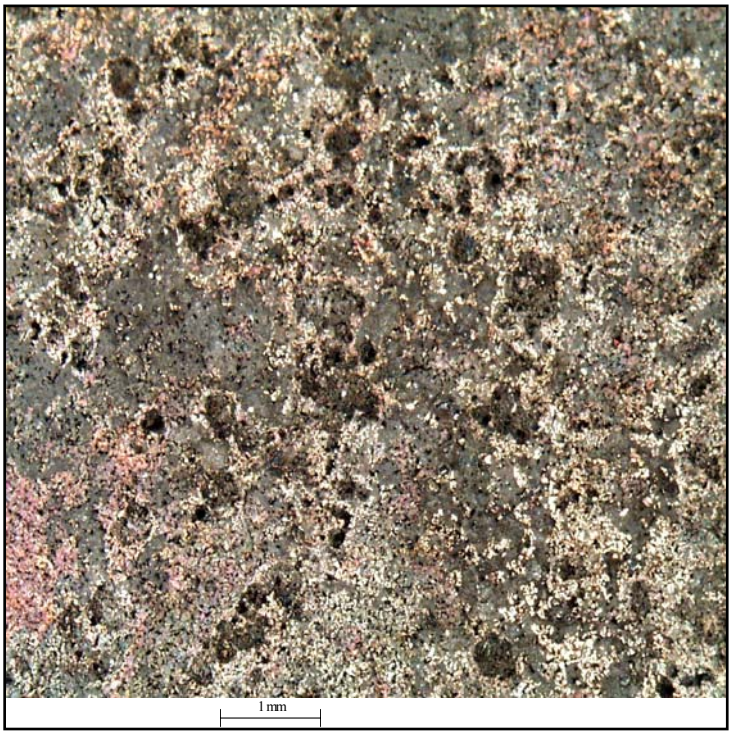

Figure 3.3-9 Pitting on the Outside Surface of Pall Fe_3Al Element 21646 Removed From Plenum Location B-51 After GCT4

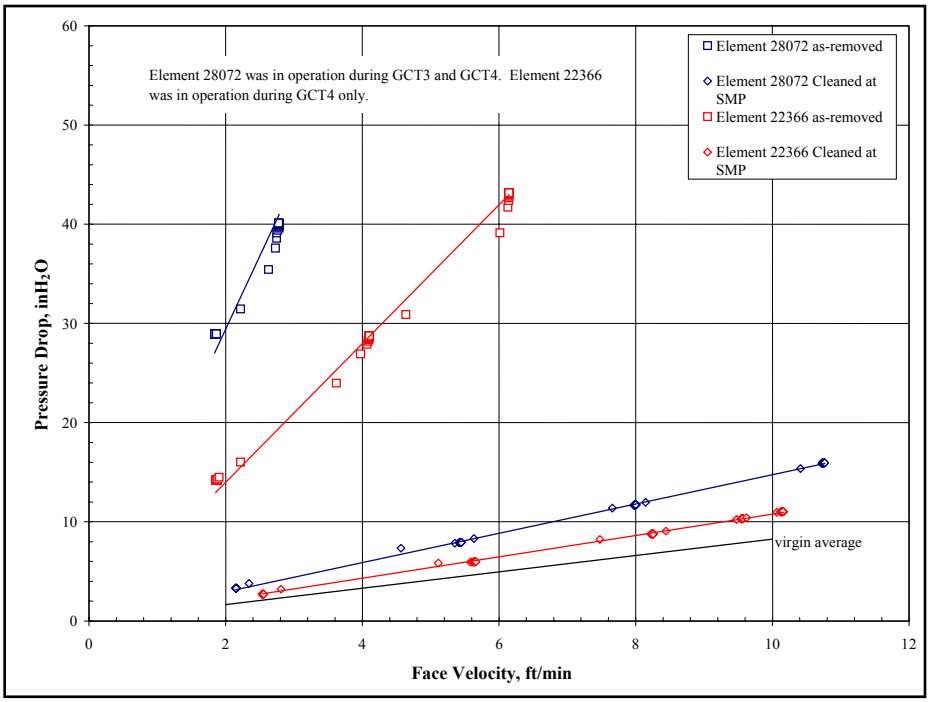

Figure 3.3-10 Pressure Drop Vs. Face Velocity for Pall Fe_3Al Elements 28072 and 22366 Removed After GCT4

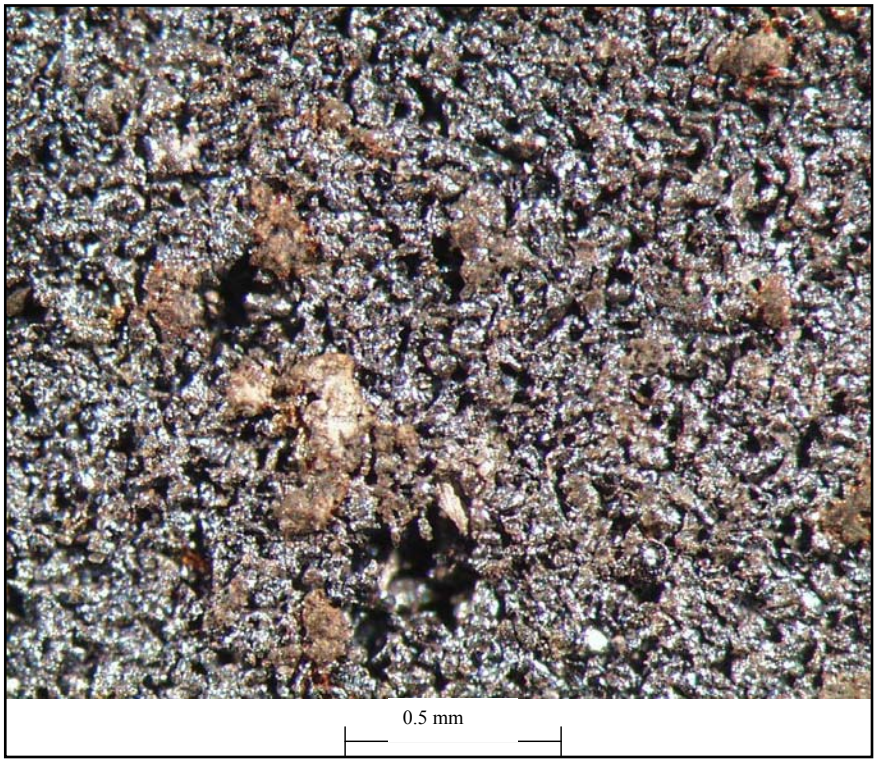

Figure 3.3-11 Pitting on the Outside Surface of Virgin Pall Fe_3Al Element 22362

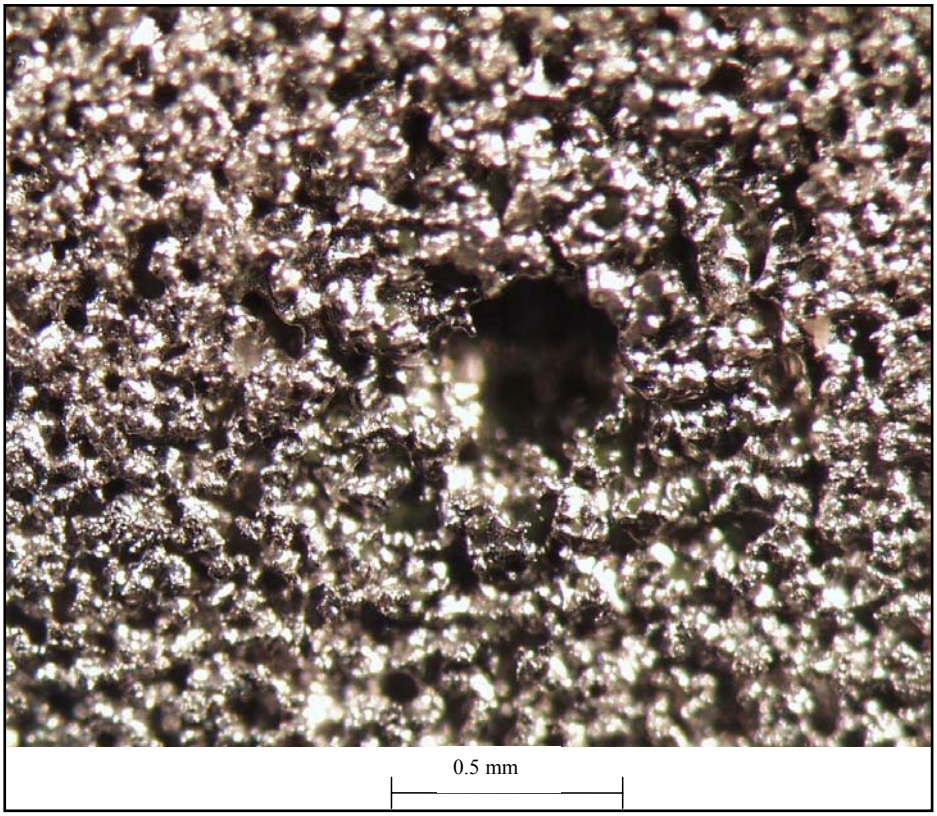

Figure 3.3-12 Pitting on the Outside Surface of Virgin Pall Hastelloy X Element PSDF Number 1337

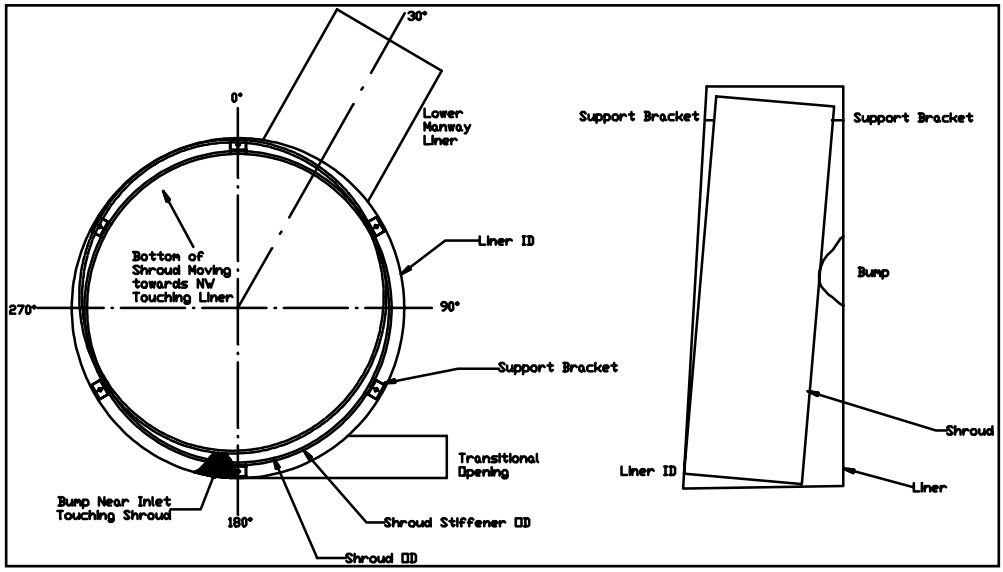

Figure 3.3-13 FL0301 Shroud Movement

3.4 GCT3 – GCT4 CHAR CHARACTERISTICS/PCD PERFORMANCE

This section describes the characteristics of the gasification char produced during GCT3 and GCT4 and the relationship between the char characteristics and PCD performance. As in previous tests, in situ char samples and dustcake samples from GCT3 and GCT4 were thoroughly characterized in an effort to better understand the effects of the char characteristics on filter pressure drop and cleanability. In situ char samples were collected at the PCD inlet and PCD outlet throughout GCT3 and GCT4. Samples of residual dustcakes and bridged deposits that were trapped between the filter elements were also collected after both GCT3 and GCT4. Characterization of the in situ char samples and dustcake samples included chemical analysis; particle-size analysis; laboratory drag measurements; and measurements of the true-particle density, bulk density, uncompacted bulk porosity, and specific-surface area. As in GCT2, drag measurements were made on the GCT3 and GCT4 char samples using the resuspended ash permeability tester (RAPTOR). The design and operation of the RAPTOR system has been described in previous reports. For the measurements discussed in this section, the RAPTOR system was modified to include various combinations of cyclones between the fluidized-bed dust generator and the dustcake collection section. The modified system made it possible to obtain data on drag as a function of particle size, thereby allowing a more accurate simulation of hot-gas filter performance. These drag measurements were used to better understand the relative contribution of the dustcake to the total PCD pressure drop and to gain insight into the effect of particle size on drag.

3.4.1 In situ Sampling

As in previous test campaigns, in situ particulate sampling runs were performed on a regular basis at the PCD inlet and PCD outlet throughout GCT3 and GCT4. The system and procedures used for the in situ particulate sampling have been described in previous reports. During GCT3, seven particulate sampling runs were performed at the PCD inlet and eight at the PCD outlet. During GCT4, six particulate sampling runs were performed at the PCD inlet and seven at the PCD outlet. As in GCT2, all of the GCT3 and GCT4 samples were obtained during gasification of Powder River Basin (PRB) coal with the addition of Ohio (Bucyrus) limestone for in-bed sulfur capture.

3.4.1.1 PCD Inlet Particle Mass Concentrations

Table 3.4-1 provides a summary of the particulate loadings measured in the process gas stream during GCT3 and GCT4. Excluding startup and sand-circulation periods, all of the GCT3 and GCT4 mass loadings varied from 10,500 to 28,700 ppmw with a mean value of 18,400 ppmw and a standard deviation of 6,000 ppmw (coefficient of variation of 0.3). These values may be compared to the mass loadings obtained in GCT2, which varied from 25,700 to 34,000 ppmw, with a mean value of 31,100 ppmw and a standard deviation of 2,600 ppmw (coefficient of variation of 0.08). Thus, the mean mass loading measured during GCT3 and GCT 4 was only about 59 percent of the mean mass loading measured during GCT2. The lower mass loadings obtained during GCT3 and GCT4 were produced with even higher coal-feed rates than those used in GCT2. Therefore, it is clear that the modifications made to the transport reactor cyclone/disengager system resulted in improved retention of char within the transport reactor

loop and significantly reduced the particulate carryover to the PCD. The reduction in the total particulate mass entering the PCD was roughly 40 percent on average.

3.4.1.2 PCD Outlet Particle Mass Concentrations

Also shown in Table 3.4-1 are the particle concentrations, measured at the outlet of the PCD, along with the PCD collection efficiency calculated from the corresponding inlet and outlet mass measurements. Except for the initial period of sand circulation at the beginning of GCT3, the PCD operated with very low outlet loadings, consistent with an absence of significant leaks. (The high loading obtained during the sand-circulation period was caused by a broken filter element, which was replaced prior to the testing with coal feed.) The measured outlet char loading during all tests with coal feed was less than 0.10 ppmw, with an average collection efficiency exceeding 99.999 percent. These measurements were at the lower limit of resolution on the sampling system. As noted in the table, higher outlet loadings were measured on two runs (0.26 ppmw on GCT3OMT-3 and 38.6 ppmw on GCT4OMT-2), but these samples were contaminated with a brown or black substance believed to be tar.

3.4.1.3 Tar Contamination

The inlet sample GCT4IMT-2 and the outlet sample GCT4OMT-2 were collected during a transition from propane to coal fire. During this period, there was apparently a large carryover of poorly gasified coal that produced an unusually high inlet loading (59,500 ppmw). The outlet sample collected during this time period (GCT4OMT-2) was contaminated with a black substance and the surface of the outlet sampler was coated with a black glaze. The deposition patterns on the sampler suggest that this material had impacted on the sampler surface in the form of liquid droplets. Thermogravimetric analysis of the black glaze showed that it lost only 30 to 35 percent of its weight when heated in nitrogen up to a temperature of 1,000°C, but it was completely burned away when heated in air up to 400°C. This result suggests that much of the tar that was originally present in the black glaze was cracked to carbon.

As discussed later in this report, evidence of partially cracked tar has also been found in the form of sticky residual dustcakes as well as condensed tar components found in the gas analysis system. The tar is apparently formed when coal is introduced into the transport reactor system while the temperatures in the system are too low to completely break down the tar components. It is generally believed that temperatures in excess of 1,600°F must be achieved in the transport reactor system to avoid tar formation. Since the propane start-up burner is only capable of producing temperatures of up to around 900 to 1,000°F, tar formation is unavoidable during the transition from propane to coal feed. Similarly, tar production can be expected whenever coal is reintroduced into the transport reactor system after a temporary loss of coal feed with a concomitant drop in transport reactor temperatures below the level required for tar cracking.

3.4.1.4 Syngas Moisture Content

As in previous tests, measurements of the syngas moisture content were made in conjunction with the outlet particulate sampling runs. The water vapor content of the syngas was determined by collecting the condensate from the syngas in an ice-bath condenser and

calculating the vapor concentration from the volume of gas sampled and the volume of condensate collected. The values determined for individual runs are included in Table 3.4-1.

3.4.2 PCD Dustcakes and Consolidated Deposits

Following each test program, samples were collected of the dustcakes and deposits remaining in the PCD. At the end of GCT3, the PCD was back-pulsed extensively during shutdown, resulting in a very thin residual dustcake on the filter elements. While there was no transient dustcake remaining on the elements after GCT3, there was one area that contained a bridged deposit that was trapped between filter elements. Samples of the bridged deposit and of the residual dustcake were taken and measurements were made of the residual dustcake thickness and areal loading.

To allow characterization of both the residual and transient dustcakes formed during GCT4, a dirty shutdown of the PCD was attempted at the end of that run. Unfortunately, the coal feeder tripped midway through the last filtration cycle, resulting in an unusually slow rate-of-pressure drop increase during the last filtration cycle. As discussed later in this report, the properties of the transient dustcake produced during this problematic shutdown differ considerably from the properties of the GCT4 in situ samples and hopper samples. Analytical results and physical properties, which are discussed in detail later in this report, suggest that this particular transient dustcake sample may not be representative of the transient dustcake that was being collected during normal operations. Nevertheless, samples of the transient dustcake were collected from various elements and the thickness and areal loading of the transient cake were estimated using procedures documented in previous reports. Residual dustcake samples were taken from several elements and the areal loadings of the residual dustcakes were determined by removing and weighing all of the residual dustcake on the elements. As in GCT3, samples were also taken of bridged deposits that were trapped between filter elements. (As mentioned in the section on PCD operations and inspection, the bridging was much more extensive after GCT4 than after GCT3.)

To determine any differences between the residual and transient cakes and the bridged material, all samples were thoroughly characterized to evaluate their physical properties, chemistry, and potential contribution to PCD pressure drop. The section below describes dustcake drag measured in the laboratory compared to the dustcake drag estimated from PCD pressure drop.

Residual Dustcake Observations

The GCT3 residual dustcake was extremely thin, making it difficult to obtain accurate measurements of dustcake thickness and areal loading. Nevertheless, multipoint measurements of dustcake thickness were made on four selected filter elements; the areal loadings of dustcake on these elements were determined by scraping off all of the dustcake within a known area of the element surface. Based on these measurements, the residual dustcake thickness was estimated to be about 0.02 in. and the residual dustcake areal loading was estimated to be about 0.04 lb/ft^2. Dustcake porosity determined from these values of thickness and areal loading was 83 percent. This value of dustcake porosity was in reasonable agreement with the dustcake porosity determined from RAPTOR tests on the GCT3 residual char (83 percent measured on the filter element versus 81 percent determined by RAPTOR). It had a slightly gummy feeling

and was tightly adhered to the elements, but once removed the GCT3 residual dustcake was fluffy with no lumps or flakes.

The GCT4 residual dustcake was considerably thicker than the GCT3 residual dustcake and was crusty. The GCT4 residual dustcake thickness was estimated to be 0.1 in. and the areal loading was estimated to be 0.2 lb/ft^2. Dustcake porosity determined from these values of thickness and areal loading was 83 percent, the same value determined for the GCT3 residual dustcake.

As mentioned above, the GCT3 residual dustcake was fluffy after removal, whereas when the GCT4 dustcake was removed from the elements it came off in flakes that could be handled without breaking. After air blowing the flakes, the pore structure shown in Figure 3.4-1 was observed. The pores or holes through the residual dustcake flake are approximately 0.2 mm in diameter. These holes were apparently formed during back-pulsing and give the appearance that the dustcake was somewhat fluid or wet at the time. Figure 3.4-2 is a SEM photo of the char particles in the solid portion (between the 0.2-mm pores) of the GCT4 residual dustcake at a magnification of 5,000x. The SEM indicates that the particles are significantly consolidated, which accounts for the high strength of the deposits. Presumably, the consolidating material is tar collected during the numerous coal restarts that occurred during GCT4.

After observing the substantial differences between the GCT3 and GCT4 dustcakes, the GCT2 samples were re-evaluated. Visual and microscopic inspection indicated that the GCT2 residual dustcake was also crusty and produced flakes that could be readily handled. However, the degree of consolidation was not as great as that observed for GCT4, and the pore structure was not well developed.

Listed below is a summary of dustcake thickness, areal loading, and porosity determined for GCT2, GCT3, and GCT4. Because of the pores and the consolidation, these porosity values should be used with caution. In the case of GCT2 and GCT4 the average and local values of porosity may be considerably different.

	Residual Dustcake			Transient
	GCT2	GCT3	GCT4	GCT4
Avg Thickness (in.)	0.05	0.02	0.1	0.3
Avg Areal Loading (lb/ft^2)	0.09	0.04	0.2	0.6
Avg Porosity (%)	84	83	83	83
RAPTOR Porosity (%)	81	81	84	84

3.4.3 Chemical Analysis of In situ Samples and Dustcakes

As in previous test runs, chemical analyses were performed on the in situ particulate samples and on the dustcake/bridging samples from GCT3 and GCT4. The samples were analyzed for carbon, hydrogen, nitrogen, sulfur, and ash; and ashes from the ignited samples were subjected to a standard ash mineral analysis. The standard ash mineral analysis included aluminum, calcium, iron, magnesium, phosphorous, potassium, silicon, sodium, and titanium. Only the results for aluminum, calcium, iron, magnesium, and silicon are reported here, since the

concentrations of the other elements were generally less than 0.5 wt percent in the original sample. The elemental analyses reported here are expressed as weight percent of the element in the original sample on an as-received basis.

Using the elemental analyses along with an analysis of CO_2 content, the chemical composition of each sample was calculated as follows:

- $CaCO_3$ content was calculated assuming that all of the CO_2 originated from $CaCO_3$.
- CaS content was calculated assuming that all of the sulfur was present as CaS.
- Any remaining Ca was assumed to take the form of CaO.
- All carbon not accounted for in $CaCO_3$ was assumed to be present as elemental carbon.
- All metals were assumed to be present as the oxides.

The justification for the assumptions used in these calculations are discussed in detail in the GCT2 report and are not duplicated here.

3.4.3.1 In situ Samples

Tables 3.4-2 and -3 provide the analytical results for the in situ particulate samples obtained during GCT3 and GCT4, and listed below is a summary of the average values of carbon, sulfur, calcium, magnesium, and silicon for each run.

	GCT2	GCT3	GCT4
Avg Carbon (Wt %)	39.7	40.6	40.4
Avg Sulfur (Wt %)	0.5	1.0	1.0
Avg Calcium (Wt %)	14.3	16.2	10.0
Avg Magnesium (Wt %)	2.0	2.8	1.8
Avg Silicon (Wt %)	8.3	7.6	9.0

Comparing these major elements, the most striking difference is in sulfur content, with the GCT3 and GCT4 char samples containing twice as much sulfur as the GCT2 char samples. There was no significant difference in coal sulfur content between GCT2 and GCT3/GCT4, and the difference in the calcium content of the char does not appear to be significant. Therefore, the higher sulfur content of the GCT3 and GCT4 char is almost certainly attributable to improved sorbent utilization. This assertion seems reasonable since the modifications made to the transport reactor loop between GCT2 and GCT3 would tend to improve the solids retention within the loop, resulting in longer solids residence times for sulfidation of the sorbent. Solids compositions that were calculated from the foregoing analytical results are summarized below.

	GCT2	GCT3	GCT4
Avg Elemental Carbon (Wt %)	35.7	N.D.	44.9
Avg $CaCO_3$ (Wt %)	13.7	N.D.	11.3
Avg Free Lime (CaO) (Wt %)	11.5	N.D.	6.2
Avg CaS (Wt %)	1.1	2.3	2.2
Avg Inerts (Wt %)	38.0	31.8	35.4

The designation "N.D." indicates that a component could not be determined because the sample size was insufficient for the CO_2 analysis. While this prevented the determination of elemental carbon, $CaCO_3$, and CaO in the GCT3 in situ samples it was still possible to determine CaS for these samples. As shown in the summary above, the GCT3 and GCT4 chars contain more CaS than does the GCT2 char, which again reflects the improved conversion of the $CaCO_3$ to CaS as a result of the increased residence time of the solids within the reactor loop.

It should be noted that the higher carbon content of the GCT4 sample does not contradict the assertion that the carbon conversion was higher in GCT4 than in GCT2. The average particulate loading exiting the transport reactor during GCT4 was only 18,000 ppmw, compared to 31,000 ppmw during GCT2. Therefore, the total mass flow of carbon from the reactor during GCT4 was only about 70 percent of the carbon mass flow during GCT2. Since the coal-feed rate was higher during GCT4 than during GCT2, it is clear that there was much better carbon conversion during GCT4.

3.4.3.2 Dustcake Samples

Following GCT3, one bulk residual dustcake sample was obtained by scraping the dustcakes from all of the accessible filter elements in the top and bottom plenums, and a bulk sample of the bridged material was obtained by removing the bridged material between certain elements in the bottom plenum. (The exact locations of the bridged material are described in the section on the GCT3 PCD inspection, Section 3.5.) Following GCT4, residual and transient dustcake samples were taken from individual filter elements and a bulk sample of the bridged deposit was also collected. (Again, the exact locations of the bridged deposits are described in the section on the GCT4 PCD inspection, Section 3.5.)

Tables 3.4-4 and -5 summarize the analytical results obtained on the residual dustcake samples and the samples of transient dustcake and bridged material removed during the post-GCT3 and the post-GCT4 PCD inspections. The information below compares the average values of the major elements in the residual dustcake samples and bridged deposits.

	Residual Dustcake			Bridged Deposits	
	GCT2	GCT3	GCT4	GCT3	GCT4
Avg Carbon (Wt %)	39.0	44.7	56.1	37.0	58.5
Avg Sulfur (Wt %)	0.7	1.1	1.0	0.8	1.0
Avg Calcium (Wt %)	11.8	13.5	9.3	16.8	11.1
Avg Magnesium (Wt %)	1.8	2.7	1.7	2.9	2.4
Avg Silicon (Wt %)	7.5	4.6	5.1	7.0	8.0
Calcium Utilization (%)	7.4	10.2	13.4	6.0	9.0

The calcium utilization values shown above were calculated as follows:

$$CalciumUtilization,\% = 100\% \bullet \frac{\frac{AvgSulfur, Wt\%}{32}}{\frac{AvgCalcium, Wt\%}{40}}$$

The term "calcium utilization" is used here instead of "sorbent utilization" because about half of the calcium comes from the coal. Since only about half of the calcium is derived from the sorbent, sorbent utilization values would be considerably higher than the calcium utilization values shown here. Assuming that half of the calcium originated from the sorbent, actual sorbent utilization is estimated to be 12 to 18 percent in the bridged deposits and 14 to 27 percent in the residual dustcakes. These sorbent utilizations are relatively low, as expected, because of the low-sulfur content of the PRB coal and the equilibrium limitations on H_2S removal.

In terms of the elemental analyses, the GCT3 residual dustcake appears to contain more sulfur and less calcium than the bridged material. The GCT4 residual dustcake contains the same amount of sulfur as the bridged deposit, but with less calcium. When the sulfur and calcium results are expressed in terms of calcium utilization as defined above, the differences in sulfur and calcium reflect a significant increase in the conversion of the calcium in the residual cake. For GCT3, this effect amounts to a 70-percent increase in calcium utilization. For GCT4, the addition sulfidation in the cake results in a 49-percent increase in calcium utilization. This increase in calcium utilization in the residual cake is not surprising since the residual cake was exposed to H_2S over a longer time period than was the bridged deposit.

The information following this paragraph summarizes the chemical compositions calculated from the analytical results of the residual dustcakes and bridged deposits. As noted previously, the designation "N.D." indicates that elemental carbon, $CaCO_3$, and CaO were not determined for the GCT3 residual dustcake and bridged deposits because no CO_2 analysis was done on these samples.

	Residual Dustcake			Bridged Deposit	
	GCT2	GCT3	GCT4	GCT3	GCT4
Avg Elemental Carbon (Wt %)	38.7	N.D.	54.7	N.D.	57.0
Avg $CaCO_3$ (Wt %)	2.0	N.D.	11.9	N.D.	12.7
Avg Free Lime (CaO) (Wt %)	14.2	N.D.	4.5	N.D.	6.8
Avg CaS (Wt %)	1.5	2.6	2.3	1.7	2.2
Avg Inerts (Wt %)	43.6	35.1	26.6	38.6	21.3

It is apparent from the compositions summarized above that the GCT4 residual dustcake and bridged deposit contain significantly more CaS and $CaCO_3$ and significantly less free lime (CaO) than does the GCT2 residual dustcake. As noted earlier, this difference is a reflection of the additional sulfidation that has occurred in the residual dustcake as a result of the prolonged exposure of the residual cake to syngas.

The analytical results for the GCT3 and GCT4 dustcake samples are compared to those of the in situ samples listed below.

	GCT3			GCT4		
	In situ	Residual	Bridging	In situ	Residual	Bridging
Avg Carbon (Wt %)	40.6	44.7	37.0	40.4	56.1	58.5
Avg Sulfur (Wt %)	1.0	1.1	0.8	1.0	1.0	1.0
Avg Calcium (Wt %)	16.2	13.5	16.8	10.0	9.3	11.1
Avg Magnesium (Wt %)	2.8	2.7	2.9	1.8	1.4	2.4
Avg Silicon (Wt %)	7.6	4.6	7.0	9.0	5.1	8.0

There appears to be a significant difference in calcium content between the GCT3 and GCT4 samples, as seen in the in situ samples (16 percent in GCT3 vs. 10 percent in GCT4), in the residual dustcake samples (13 percent in GCT3 vs. 9 percent in GCT4), and in the bridged deposits (17 percent in GCT3 vs. 11 percent in GCT4). This comparison suggests that the GCT3 samples contained more sorbent than the GCT4 samples.

Listed below is a comparison of the calculated chemical compositions for the GCT3 and GCT4 dustcake samples and the corresponding in situ samples. (Again, these compositions were calculated from the analytical data shown above, using the procedures and assumptions discussed previously.)

	GCT3			GCT4		
	In situ	Residual	Bridging	In situ	Residual	Bridging
Avg Elemental Carbon (Wt %)	N.D.	N.D.	N.D.	44.9	54.7	57.0
Avg $CaCO_3$ (Wt %)	N.D.	N.D.	N.D.	11.3	11.9	12.7
Avg Free Lime (CaO) (Wt %)	N.D.	N.D.	N.D.	6.2	4.5	6.8
Avg CaS (Wt %)	2.3	2.6	1.7	2.2	2.3	2.2
Avg Inerts (Wt %)	31.8	35.1	38.6	35.4	26.6	21.3

These results suggest that the GCT3 residual dustcake contains more CaS than the GCT3 in situ samples and bridged deposits (2.6 percent in the residual dustcake vs. 2.3 percent in the in situ sample and 1.7 percent in the bridged deposit). As suggested earlier, this difference can probably be explained in terms of the additional sulfidation of the calcium in the residual cake. In the case of the GCT4 samples this difference is less pronounced (2.3 percent in the residual cake vs. 2.2 percent in the in situ sample and in the bridged material). However, as indicated earlier, there is a significant difference in calcium utilization that supports the contention that there was significant additional sulfidation in the residual dustcakes in both GCT3 and GCT4.

3.4.4 Physical Properties of In situ Samples and Dustcakes

As in previous tests, the GCT3 and GCT4 in situ particulate samples and dustcake samples were subjected to the standard suite of physical measurements, including true-(skeletal) particle density, bulk density, uncompacted bulk porosity, specific-surface area, and particle-size analysis. The instruments and procedures used for making these measurements are described in previous reports.

3.4.4.1 In situ Particulate Samples

Physical properties of the in situ particulate samples from GCT3 and GCT4 are presented in detail in Table 3.4-6, and the information listed below compares the average in situ physical properties for GCT2, GCT3, and GCT4.

	GCT2	GCT3	GCT4
Avg Bulk Density (g/cc)	0.36	0.37	0.27
Avg Skeletal Particle Density (g/cc)	2.24	2.28	2.29
Avg Uncompacted Bulk Porosity (%)	83.9	84.0	88.0
Avg Specific-Surface Area (m^2/g)	93.4	128	197
Avg Mass Median Diameter (μm)	17.9	14.2	15.9

Based on the above comparison, the chars produced from GCT3 and GCT4 appear to be somewhat finer than the char produced in GCT2. This is, of course, an expected result of the increased cyclone collection efficiency and the improved carbon conversion in the transport reactor loop. The GCT3 and GCT4 chars also appear to have significantly higher specific-surface areas than the GCT2 char. This difference in surface area is not completely understood,

but it may be associated with the improved solids retention and enhanced carbon conversion (that is, better gasification) attained in the transport reactor. Again, it should be noted that all three of these chars were produced from the same Powder River Basin (PRB) coal and the same Ohio (Bucyrus) limestone.

Compared to PRB combustion ashes produced in the transport reactor system in earlier runs, it is now clear that the PRB gasification chars have relatively low bulk density, relatively high bulk porosity, and relatively high specific-surface area. As discussed in more detail later, the specific-surface area of the char is believed to be a significant contributing factor in the high flow resistance of this material, but differences in particle size and surface area alone do not completely explain the high drag of the gasification char. The role of these properties in determining dustcake drag will be discussed in more detail in the section on drag measurements (see Section 3.4.6). A more detailed comparison of the particle-size distributions of the GCT2, GCT3, and GCT4 chars will be presented later in this report (see Section 3.4.5).

3.4.4.2 Dustcake Samples

The physical properties of the residual and transient dustcake samples and bridged deposits from GCT3 and GCT4 are presented in detail in Table 3.4-7 and summarized below.

	Residual Dustcakes			Bridged Char	
	GCT2	GCT3	GCT4	GCT3	GCT4
Avg Bulk Density (g/cc)	0.43	0.36	0.34	0.37	0.34
Avg Skeletal Particle Density (g/cc)	2.15	2.37	1.91	2.40	2.21
Avg Uncompacted Bulk Porosity (%)	80.0	84.8	82.2	84.6	84.6
Avg Specific-Surface Area (m^2/g)	23.9	44.0	8.0	127	173
Avg Mass Median Diameter (μm)	7.4	4.3	8.4	12.0	12.7

The properties of the transient dustcake collected at the end of GCT4 are included in Table 3.4-7, but not included in the summary above because the transient cake was clearly not representative of normal operation (for example, specific-surface area = 28 to 37 m^2/g vs. 105 to 265 m^2/g for the in situ samples and 151 to 194 m^2/g for the bridged material). As discussed later in this report, the transient cake also had lower drag than the bridged material and hopper samples (in situ samples were not tested due to insufficient sample size). The relatively low drag, low surface area, and low carbon content of the transient cake sample, coupled with the low rate of ΔP increase during the last filtration cycle, suggest that the transient dustcake sample collected at the end of GCT4 was not representative of the transient dustcakes formed during normal operations.

In comparing all of the residual dustcakes from the three runs, it is the GCT3 residual dustcake that appears to be unusual in terms of the relatively small mean particle size (MMD of 4 μm vs. 7 to 8 μm for GCT2 and GCT4) and the relatively large specific-surface area (44 m^2/g vs. 8 to 24 m^2/g for GCT2 and GCT4). However, as mentioned previously, the GCT3 residual dustcake was the only one of the three that did not appear to undergo some degree of consolidation, presumably caused by collection of tar within the dustcake. This consolidation would prevent

the individual particles from being separated and sized correctly, resulting in a larger indicated particle size. Also, the tar would reduce the particle specific-surface area by coating and plugging the pore structure of the particles. This is not to suggest that no tar was present during GCT3. The fairly low surface area of the GCT3 residual dustcake compared to the in situ samples and bridged deposits suggest that some pore plugging occurred because of tar collection or due to reaction with other chemical components of the gas stream. However, it appears that this effect was much less with GCT3 than with other test programs.

The following information compares the average properties of the in situ samples, bridged deposits, and residual dustcakes from GCT3 and GCT4. From this comparison it is clear that the in situ samples and bridging material from GCT3 and GCT4 have much larger mean particle sizes (MMDs) than those of the residual dustcakes from these runs. In the past this difference in mean particle size has been blamed on inertial removal of large particles by the cyclonic action of the PCD system. (This was a demonstrated effect during combustion operation.) However, the data as compiled and shown on the previous page suggests that this explanation does not apply for char. In a comparison of the in situ samples to the bridged deposits, only a small amount of particle dropout is shown to have apparently occurred (that is, the mean particle size has been reduced from 14 to 16 compared to 12 to 13 μm). In the absence of significant dropout, alternative explanations for the finer size of the residual dustcakes could include fine particle enrichment with time or the possibility that a finer dust size was generated during initial startup with this material remaining in place throughout the run.

	GCT3			GCT4		
	In situ	Residual	Bridging	In situ	Residual	Bridging
Avg Bulk Density (g/cc)	0.37	0.36	0.37	0.27	0.34	0.34
Avg Particle Density (g/cc)	2.28	2.37	2.40	2.29	1.91	2.21
Avg Bulk Porosity (%)	83.8	84.8	84.6	88.2	82.2	84.6
Avg Surface Area (m^2/g)	128	44.0	127	197	8.0	173
Avg MMD (μm)	14.2	4.3	12.0	15.9	8.4	12.7

The similarity of the specific-surface area values between the in situ and bridged samples suggests that, although the bridging may have been caused by tar, the bridged deposit was not highly affected by the tar. If the bridged deposit had been subjected to extensive tar deposition it would have presumably been more agglomerated like the residual dustcake. Since this was not the case it may be inferred that the GCT4 bridging must have occurred near the end of the test program (probably on March 27, 2001, when there was an abrupt change in the baseline ΔP), after which there were no more episodes of tar formation and deposition.

3.4.5 Particle Size Analysis of In situ Samples and Dustcakes

The size distribution of the particles that make up the PCD dustcake is a critical factor in determining the drag properties of the dustcake. In addition, knowledge of the size distribution of particles leaving the transport reactor system can aid in understanding the operating characteristics of the system. As in previous tests, particle-size distribution measurements were made using a Leeds & Northrup Microtrac X-100 particle-size analyzer on the samples collected

in situ in the gas stream at the inlet of the PCD and on the bridged deposits and dustcake samples removed from the filter elements at the end of each test program.

The average particle size-distributions of the GCT3 and GCT4 in situ samples collected at the inlet of the PCD are shown in Figure 3.4-3. The distributions for these two gasification runs after modification of the transport reactor loop are almost identical. The average particle-size distribution of the GCT2 in situ samples is shown for comparison. This comparison shows that the changes made in the transport reactor loop resulted in a reduction in the mass concentration of particles over a wide range of particle sizes from a few microns up to the largest particle sizes detected. For the smaller particle sizes the reduction in mass concentration diminishes with decreasing particle size to a point where there is virtually no reduction at particle sizes below 1 μm. This result is consistent with more efficient particle collection in the disengager/cyclone system and improved carbon retention and gasification in the reactor loop.

Figure 3.4-4 compares the particle-size distributions of the various samples collected during and following GCT3. The distributions shown include samples from the inlet gas stream, PCD hopper, bridged deposit, and residual dustcake. The bridged deposits removed from the PCD are assumed to represent the transient dustcake. It is interesting that all of the distributions except for the residual dustcake are essentially identical. This suggests that little, if any, dropout or inertial collection is occurring in the PCD as was observed previously during combustion runs. As discussed in the previous section, the residual dustcake is much finer than the incoming dust for reasons that are not understood at this time.

The GCT4 particle-size distributions are shown in Figure 3.4-5. Although there is a little more scatter in the data, there is little real difference between the PCD inlet samples, the bridged deposit (transient dustcake), and the hopper samples. With the exception of the residual dustcakes, the GCT4 particle-size distributions are not significantly different from the particle-size distributions obtained for GCT3. As discussed previously, the apparent difference in the residual dustcakes is believed to be related to tar deposition in the cake, which makes it difficult to obtain accurate particle-size data. The GCT4 residual dustcake, which was bonded together with tar, was probably not sized correctly by the Microtrac particle-size analyzer because the particle dispersion techniques used with this instrument are probably not adequate to break apart particles that are bonded together with condensed tar. Consequently, the Microtrac instrument was probably measuring clumps of consolidated particles rather than individual particles in the residual dustcake sample. (These clumps have not been seen in samples since GCT4.)

Without the tar deposition there is no reason to believe that the residual dustcake from GCT4 would have been significantly different from the GCT3 residual dustcake. In future tests the transport reactor will be started on coke breeze in an effort to attain higher temperatures in the gasifier before coal is introduced. If this modification of the startup procedures is successful in eliminating tar formation in the reactor, the tar-related problems encountered with the particle size analysis should also be eliminated. Of course, it is also possible that the char produced from the coke may differ from the char produced from coal in terms of particle size and other characteristics.

3.4.6 Drag Characteristics of Dustcakes and Size-Segregated Hopper Samples

The normalized drag of a dust sample, *R*, provides a very valuable indication of the pressure drop, ΔP, that can be expected with a given areal loading of the dust, *AL*, at a given face velocity, *FV*, in accordance with the following simple relationship.

$$R = \frac{\Delta P}{AL \bullet FV}$$

Previous work has demonstrated a good correlation between PCD pressure drop and normalized drag measurements made using the resuspended ash permeability tester (RAPTOR), which has been described in previous reports. For the drag measurements discussed here, the RAPTOR apparatus was modified by adding various combinations of cyclones between the fluidized-bed dust feeder and the dust dispersion and collection sections. This modification made it possible to make drag measurements as a function of the mean particle size collected on the filter, thus providing valuable information on the effect of particle size on drag and on the ability of the modified RAPTOR system to accurately simulate the performance of the PCD. The drag measurements with the modified RAPTOR system were made on bulk residual dustcake samples from GCT2, GCT3, and GCT4; on bulk samples of the bridged material from GCT3 and GCT4; and on PCD hopper samples collected during all three runs.

Figure 3.4-6 shows the results of the modified RAPTOR measurements of drag vs. mass median particle diameter (MMD). These data were obtained on samples that were size classified using various combinations of cyclones in the modified RAPTOR system. The cyclones used in making these measurements were cyclone numbers 1, 2, and 3 from SRI's five-stage cascade cyclone sampling assembly. In order to obtain data with successively decreasing MMDs, drag measurements were made with no cyclones, with cyclone 1, with cyclone 2, and with cyclones 2 and 3 in series. The measurements of drag vs. MMD made on the redispersed samples of bridged deposits from GCT3 and GCT4 fell on the same trend line as the measurements made on the PCD hopper samples from these runs, so all of these data were grouped together for the regression analysis. As shown in the plot of drag versus MMD, the data for the GCT2 samples and for the GCT3 and GCT4 samples fell on two different straight lines in logarithmic space. These lines were of the form:

$$R_{RAPTOR} = 10^{[m \bullet \log(MMD) + b]}$$

in which R_{RAPTOR} is the drag measured using the modified RAPTOR apparatus in units of inWC/(lb/ft^2)/(ft/min); *MMD* is the mass median diameter of the dustcake collected in the RAPTOR apparatus in μm; *m* is the slope of the regression line; and *b* is the intercept of the regression line. The best-fit values of *m* and *b* and the coefficient of regression (r^2) for each straight-line fit are shown below.

	GCT2	GCT3/GCT4
m	-1.135	-0.982
b	2.740	2.997
r^2	0.91	0.90

The relatively high values of r^2 shown above indicate that the straight-line fits are reasonably good representations of the data and show a good correlation between drag and particle size for the hopper/bridged samples. These results clearly demonstrate that drag is a strong function of particle size and that there is a definite difference between the GCT2 char and the GCT3 and GCT4 char. At any given particle size the GCT3 and GCT4 char has significantly higher flow resistance than the GCT2 char. This result suggests that particle size is not the only significant factor affecting the drag. It seems intuitive that the surface roughness, or external surface area, of the particles could also have a strong influence on drag.

Measurements were made of the specific-surface area of the various size-classified samples collected in the RAPTOR apparatus to examine the effect of roughness/surface area on drag. The measurements of specific-surface area were made with a Micromeritics FlowSorb II surface-area analyzer that utilizes the Brunauer-Emmett-Teller (BET) nitrogen-adsorption technique. Unfortunately, the BET technique measures the total surface area and cannot distinguish between external surface area that affects drag and internal surface area that does not affect drag. Nevertheless, there is hope that these measurements might provide some insight into the role that surface area plays in determining the drag of the char.

Figure 3.4-7 shows how the BET specific-surface area varied with MMD of the RAPTOR filter catches. This plot shows that the GCT3 and GCT4 hopper samples and the GCT3 and GCT4 bridged deposits fall on two distinctly different lines (even though these two groups of samples fall on the same trend line-of-drag vs. MMD). At a given particle size the specific-surface areas of the GCT3 and GCT4 samples differ by as much as a factor of 2 (such as, from about 150 to about 300 m^2/g at an MMD of 10 μm), even though all of these samples fell on the same line-of-drag versus MMD. In other words, substantially different surface areas were measured on samples that have about the same MMD and drag. One way of explaining this result is to postulate that some of the measured surface area is in the form of internal pores that do not contribute to flow resistance. In fact, since all of the GCT3 and GCT4 hopper samples and bridged deposits have surface areas in excess of 150 m^2/g, and all of these samples fall on the same line-of-drag vs. MMD, it can be reasonably concluded that surface area in excess of 150 m^2/g does not affect drag. For these particular samples, most of the additional surface area beyond 150 m^2/g appears to be in the form of internal surface area that does not affect drag. Since the GCT2 samples fall on a different line-of-drag vs. MMD, and since the GCT2 samples all have surface areas of less than 70 m^2/g, it can be further inferred that the cutoff point for surface area that affects drag must be somewhere between 70 and 150 m^2/g with these particular samples.

As shown in the previous plot of surface area vs. MMD, the bridged deposits from both GCT3 and GCT4 have lower surface areas than the hopper samples from the same tests. This result suggests that some of the pores in the bridged deposits may have been blocked by tar

deposition, sulfidation, or some type of consolidation. Because of the Kelvin effect, tar vapors would tend to first condense in the smallest pores, which would not contribute to drag. This could explain why the surface area of the bridged deposits is decreased without a commensurate reduction in drag. Sulfidation could also result in the preferential closure of the smallest pores, but the chemical analyses discussed earlier show that the bridged deposits contain no more CaS than the in situ samples. Since the GCT3 and GCT4 bridged deposits were formed at relatively low temperatures (700 to 900°F), it seems unlikely that there was any type of consolidation that would require the formation of molten phases or eutectics. Therefore, tar deposition seems to be the most likely explanation for the lower surface areas of the bridged deposits.

The effect of tar deposition on surface area can be seen even more dramatically in the residual dustcake samples, as shown below.

	GCT2	GCT3	GCT4
Mean surface area of in situ samples (m^2/g)	93	128	197
Mean surface area of bridged material (m^2/g)	----	127	173
Mean surface area of residual dustcake (m^2/g)	24	44	13

The surface area values shown above suggest that the residual dustcakes were subjected to even greater degrees of pore closure by tar deposition. This result is consistent with the SEM photographs discussed previously that show that the char particles in the residual dustcakes were bonded together with tar.

Figure 3.4-6 shows that the GCT3 and GCT4 residual dustcakes have much lower measured drag values than do GCT3 and GCT4 hopper samples and bridged deposits. The drag data for the residual dustcakes are single-point measurements that were made using the residual dustcake samples without any cyclones to adjust the particle-size distribution reaching the RAPTOR filter. For these measurements, the cyclones were deemed to be unnecessary since the purpose of these measurements was to determine whether the drag of the bulk residual dustcake was similar to the drag of the hopper samples and the bridged deposits and the residual dustcake samples had MMDs that were smaller than or equal to the cutpoint of the number 1 cyclone anyway. As indicated in the plot shown in Figure 3.4-6, good agreement between the residual dustcake measurement and the size-segregated hopper measurement was achieved for GCT2, but not for GCT3 or GCT4 .

As mentioned previously, the residual dustcakes from GCT2 and from GCT4 contained flakes that presumably consisted of char particles that were "glued" together with tar and the average MMDs of these dustcakes was about 7 to 8 μm. The GCT3 residual dustcake did not contain these "glued-together" flakes and the MMD of the GCT3 residual dustcake was about 4 μm. As discussed previously in the section on particle-size analysis, this apparent difference in MMD was attributed to the inability of the dispersion techniques used with the Microtrac particle-size analyzer to break apart the agglomerates of tar-bonded char particles. If the residual dustcakes are held together tightly enough to prevent their complete dispersion in the Microtrac sample preparation procedures, it seems unlikely that they would be broken apart completely in the RAPTOR apparatus. Because of this incomplete dispersion, the dustcake formed in the

RAPTOR apparatus is probably comprised of particle agglomerates that are larger than the individual char particles. This effect probably explains why the porosity of the RAPTOR dustcake was 83 percent, while the porosity of agglomerated flakes taken from the residual dustcake ranged from 72 to 75 percent. Because of this large difference in porosity the RAPTOR dustcake would be expected to have a lower drag than one that was formed from the individual char particles and then glued together with tar. Therefore, the RAPTOR measurements on the residual dustcakes probably do not accurately reflect the true drag of the tar-bonded dustcake as it resided on the filter elements during the runs. The validity of this assertion will be tested later in the analysis of PCD pressure drop.

In the foregoing discussion the relationship between drag and particle size, the relationship between specific-surface area and particle size, and the effects of tar deposition on specific-surface area and drag have been examined. However, the relationship between drag and surface area has not been explicitly investigated. Efforts to develop correlations between specific-surface area and drag have failed to yield a simple, direct correlation between these parameters. Yet it seems reasonable that the flow resistance of a particle should be related to the surface area of the particle, or at least to a portion of the surface area. To investigate this possibility further, the particle surface area (SA_p) was calculated for all of the GCT2, GCT3, and GCT4 char samples using the following equation:

$$SA_p = BET \bullet \rho_{true} \bullet \frac{\pi}{6} \bullet (MMD)^3 \bullet 10^{-12}$$

in which SA_p is the surface area of the mass median particle in m^2; *BET* is the specific-surface area of the sample at the mass median particle size in m^2/g, ρ_{true} is the true particle density in g/cm^3; and *MMD* is the mass median particle diameter in μm. Using a typical value of true density of 2.2 g/cm^3, this equation simplifies to:

$$SA_p = 1.15x10^{-12} \bullet BET \bullet (MMD)^3$$

In Figure 3.4-8 the calculated values of SA_p are plotted against the drag values determined for the same samples. The regression fit shows that the drag-versus-SA_p provides a better correlation than the drag-versus-MMD regression presented earlier. For the GCT3/GCT4 data, the regression coefficient for the drag-versus-SA_p correlation is 0.93, compared to only 0.90 for the drag-versus-MMD correlation. This difference in regression coefficients represents a 30-percent reduction in the uncertainty of the correlation. One way of interpreting this result is that a better correlation with drag can be obtained by incorporating the BET surface area along with the MMD rather than using the MMD alone. This improvement was not achieved with the GCT2 data, presumably because there was little variation in the BET surface areas for these samples.

Even with the improved correlation obtained using the SA_p, there are still two distinctly different regression lines for GCT2 and for GCT3/GCT4. This result suggests that the combined effects of surface area and MMD still do not explain the substantial difference between the GCT2 and the GCT3/GCT4 data sets. The failure of the drag-SA_p correlation to collapse both sets of data onto one line may indicate that there are other factors affecting drag that are not being taken into account with this correlation. The quality of the correlation could

probably be improved substantially by using only the surface area that contributes to drag, as opposed to the total (BET) surface area. This is problematic because existing data are not adequate to define precisely the fraction of the surface area that influences drag. To address this shortcoming, efforts are underway to measure the distribution of surface area as a function of pore size, which is hoped to provide insight into the fraction of the surface area that is contained in pores large enough to affect drag. By subtracting the contribution of the smaller pores to the surface area, it may be possible to achieve a better correlation with drag and a better understanding of how surface area affects drag.

3.4.7 Analysis of PCD Pressure Drop

For the purposes of this discussion, it is convenient to consider the PCD pressure drop (ΔP) in two separate parts: (1) the transient ΔP, which is the pressure drop that accumulates during each filtration cycle; and (2) the baseline ΔP, which is the pressure drop that remains after the filter elements are back-pulsed. Transient ΔP is a function of the concentration and flow resistance (drag) of the dust reaching the filter elements, the gas flow, the length of the filtration cycle (time between back-pulses), and the total filter surface area. In addition to such factors as coal-feed rate and operating conditions, particle dropout in the filter vessel can also affect the particulate concentration reaching the filter elements and thereby influence the transient ΔP. According to conventional wisdom, baseline ΔP is not a function of the particulate concentration, or at least not a strong function. This assertion seems reasonable when the baseline ΔP is maintained at a stable value for prolonged periods of PCD operation, but it may be called into question when the baseline ΔP is increasing over time. In addition to the flow resistance of the residual dustcake, the baseline ΔP is also influenced by vessel losses and any irrecoverable changes that may occur in the flow resistance of the filter elements or fail-safes (for example, changes caused by backside blinding or fail-safe plugging). Based on flow tests that were performed on filter elements and fail-safes that were used in the various gasification runs, it can be assumed that backside blinding and fail-safe plugging were negligible during GCT2, GCT3, and GCT4.

In the following sections, the contributions of the transient and residual dustcakes to PCD ΔP are examined by comparing dustcake drag values calculated from the PCD ΔP to dustcake drag values measured by RAPTOR. This is a very valuable comparison because mismatches between these two methods of determining drag can indicate that other factors (for example, tar deposition) may be influencing the PCD ΔP.

3.4.7.1 Transient ΔP

Shown below is an analysis used to assess the portion of the PCD ΔP that was contributed by the transient dustcake accumulated during each filtration cycle. First, data from the PI system were used to determine the average rate of PCD ΔP rise (ΔP/Δt) during each of the in situ particulate sampling runs. The rate of increase in the dustcake areal loading during each sampling run [$\Delta (AL)/\Delta t$] was then calculated as follows:

$$\frac{\Delta(AL)}{\Delta t} = \frac{ML \bullet W}{1{,}000{,}000 \bullet 60 \bullet A}$$

in which $\Delta(AL)/\Delta t$ is the rate of increase in the dustcake areal loading in lb/ft^2/min; ML is the inlet particulate mass loading in ppmw; W is the process gas mass-flow rate in lb/hr; and the A is the total active surface area of the filter elements in ft^2. The values of $\Delta P/\Delta t$ and $\Delta(AL)/\Delta t$ determined for each sampling run may be used to calculate a corresponding value of PCD transient drag, R, using the same basic equation used in determining normalized drag from the RAPTOR data:

$$R = \frac{\Delta P}{AL \bullet FV} = \frac{\frac{\Delta P}{\Delta t}}{\frac{\Delta(AL)}{\Delta t} \bullet FV}$$

in which R is the PCD transient drag in inWC/(lb/ft^2)/(ft/min); $\Delta P/\Delta t$ is the average rate of pressure drop increase during the sampling run in inWC/min; $\Delta(AL)/\Delta t$ is the rate of increase in the dustcake areal loading in lb/ft^2/min; and FV is the average PCD face velocity in ft/min. To allow direct comparison of this PCD drag value with the RAPTOR drag measurements, the dustcake drag obtained in this manner must be adjusted to the RAPTOR conditions using the ratio of the syngas viscosity at process temperature to the viscosity of air at laboratory room temperature, according to the following equation:

$$R_{normalized} = R \bullet \frac{\mu_{air}}{\mu_{syngas}} = \frac{\Delta P}{AL \bullet FV} \bullet \frac{\mu_{air}}{\mu_{syngas}} = \frac{\frac{\Delta P}{\Delta t}}{\frac{\Delta(AL)}{\Delta t} \bullet FV} \bullet \frac{\mu_{air}}{\mu_{syngas}}$$

in which $R_{normalized}$ is the PCD transient drag normalized to the same gas viscosity as the RAPTOR measurements (air at room temperature); μ_{air} is the viscosity of air at room temperature (77°F) in poise; and μ_{syngas} is the viscosity of the syngas at the process gas temperature in poise.

The RAPTOR drag value for each particulate sampling run was taken from the plot of drag vs. MMD shown in Figure 3.4-6 and using the MMD values determined by Microtrac analysis for each sampling run. Since it was difficult to accurately interpolate values directly from the drag-versus-MMD plot, the drag data were obtained from the regression equations describing the best straight-line fits to the drag-versus-MMD data in logarithmic space. These equations are provided in the section on the laboratory drag measurements (see Section 3.4.6). Table 3.4-8 shows the laboratory drag values determined from the regression fits of the RAPTOR data and the PCD transient drag values determined from the rate of ΔP increase during the sampling runs. From the tabulated drag values, it is obvious that the data for runs GCT3IMT-2 and GCT4IMT-1 are outliers. Average values of drag determined by the two different approaches, excluding the outliers, are shown below. The drag values are in units of inWC/(lb/ft^2)/(ft/min) and are on the viscosity basis of air at 77°F.

	GCT2	GCT3	GCT4
Average drag from PCD ΔP rise	29	93	66
Average drag from RAPTOR data	21	70	70

This summary shows that there is fairly good overall agreement between the PCD calculations and the RAPTOR measurements. This agreement can also be seen by plotting the individual values of PCD drag and RAPTOR drag determined for each sampling run, as shown in Figure 3.4-9. The outliers mentioned above are the two data points that fall well below the perfect-agreement line on the plot. Ignoring these outliers, the plot clearly shows that the RAPTOR drag values track the PCD transient drag values reasonably well. This result suggests that the flow resistance of the char is high enough to account for all of the transient ΔP, and that the transient dustcake drag was not affected by tar deposition or other anomalies during the in situ particulate sampling runs.

3.4.7.2 Baseline ΔP

In order to facilitate the direct comparison of the baseline pressure drops during GCT2, GCT3, and GCT 4, the baseline ΔP data from all three runs were first normalized to the same temperature (850°F) and the same face velocity (3.5 ft/min). Figure 3.4-10 shows a plot of the normalized baseline ΔP as a function of time throughout all of the gasification runs. As shown in the plot, both GCT3 and GCT4 were characterized by increasing baseline pressure drop, with the normalized baseline ΔP achieving values as high as 150 inWC in GCT3 and values of over 200 inWC in GCT4. This behavior may be contrasted with the baseline pressure drop performance during GCT2 in which the normalized baseline ΔP increased initially and then stabilized at about 70 inWC. Unlike GCT2, a stable baseline ΔP was never achieved in GCT3 or GCT4.

As discussed previously, one of the possible explanations for the observed increase in PCD baseline ΔP is tar deposition within the residual dustcake. It is also possible that some of the observed increase in baseline ΔP could be caused by a reduction in the effective filtration area brought about as a result of bridged deposits. The deposition of tar on char particles could make the particles sticky, thereby contributing to the formation of the bridged deposits. The presence of agglomerated flakes in the GCT2 and GCT4 residual dustcakes suggests that these cakes may have been substantially affected by tar deposition. Although these flakes were not seen in the GCT3 residual dustcake, the presence of bridged deposits within the PCD after GCT3 suggests that tar could have also had some effect on the PCD pressure drop during GCT3. Also, it was observed during both GCT3 and GCT4 that the coal restarts (when tar was formed due to low gasification temperatures) were frequently followed by increases in baseline ΔP.

These effects complicate the analysis of PCD baseline ΔP and make it difficult to rationalize the baseline ΔP in terms of laboratory drag measurements. Nevertheless, comparison of residual dustcake drag values determined from the PCD baseline ΔP and from the RAPTOR measurements can bring about better understanding of the magnitude of the effect of tar deposition on the residual dustcake drag. Therefore, the remainder of this section will focus on attempts to quantify the contribution of the residual dustcake to the PCD baseline ΔP.

As shown in previous reports, the contribution of the residual dustcake to the baseline ΔP can be estimated by subtracting the contributions of the vessel losses and any irreversible increases in the filter element ΔP and the fail-safe ΔP. For GCT2, GCT3, and GCT4 vessel losses were estimated from the baseline ΔP recorded during the startups prior to the initiation of coal feed.

To put both the final baseline ΔP and the startup baseline ΔP on the same basis, the startup ΔPs were also normalized to a temperature of 850°F and to a face velocity of 3.5 ft/min. The changes in filter element and fail-safe ΔPs were assumed to be negligible for all of these runs, since there was no potential for backside blinding and flow tests performed on the used filter elements and fail-safes showed no irrecoverable change in ΔP.

After establishing the pressure drop attributable to the residual dustcake ($\Delta P_{residual}$) as discussed above, the residual dustcake drag ($R_{residual}$) can then be calculated using the same basic formula used in reducing the RAPTOR data and in calculating the transient dustcake drag:

$$R_{residual} = \frac{\Delta P_{residual}}{AL_{residual} \bullet FV}$$

in which $R_{residual}$ is the residual dustcake drag in inWC/(lb/ft^2)/(ft/min), $\Delta P_{residual}$ is the residual dustcake pressure drop in inWC, $AL_{residual}$ is the residual dustcake areal loading in lb/ft^2, and FV is the face velocity in ft/min. The values of FV recorded during GCT3 and GCT4 were adjusted to account for the fraction of the filter surface that was blocked by bridged deposits. Based on the observations of the bridging after GCT3 and GCT4, it was estimated that about 10 percent of the filter surface was blocked in GCT3 and about 30 percent of the filter surface was blocked in GCT4. Therefore, the face velocities recorded by PI were increased by 10 percent for GCT3 and by 30 percent for GCT4. (Of course, it is possible that the blockage of the filter surface was actually higher than 10 percent and 30 percent, since some of the bridged deposits may have fallen out after shutdown; the values of 10 percent and 30 percent are used here because there is no rational basis for specifying an alternative degree of blockage.)

To allow direct comparison of the PCD residual dustcake drag values with the RAPTOR drag measurements, the PCD residual dustcake drags were adjusted to laboratory conditions using the same viscosity correction technique applied in the transient drag analysis. The results of these calculations are summarized below.

	GCT2	GCT3	GCT4
1. Final baseline ΔP normalized to 850°F and 3.5 ft/min (inWC)	70	180	200
2. Vessel losses (startup ΔP normalized to same conditions) (inWC)	30	30	30
3. Residual dustcake ΔP (item 1 minus item 2) (inWC)	40	150	170
4. Residual dustcake areal loading (lb/ft^2)	0.09	0.04	0.2
5. Adjusted face velocity (ft/min)	3.5	3.9	4.6
6. PCD dustcake drag (item 3/item 4/item 5) (inWC/(lb/ft^2)/(ft/min))	130	960	185
7. PCD dustcake drag at room temp (item 5/1.74)	73	550	110

The PCD residual dustcake drag values calculated above may now be compared with the RAPTOR measurements made on the residual dustcake samples. However, as discussed previously, the residual dustcake samples were apparently agglomerated with tar. Since this

agglomeration prevented the complete dispersion of the residual dustcake samples for particle-size analysis, it is also very likely that the residual dustcake samples were not dispersed into their constituent char particles in the RAPTOR apparatus. Because of this effect, the RAPTOR measurements made on the residual dustcake samples are probably unrealistically low. It may be possible to obtain a better estimate of the true residual dustcake drag by using the drag-versus-MMD regression fit to the RAPTOR measurements made on the hopper samples and bridged deposits, while using the MMDs of the respective residual dustcake samples in the regression equation. Therefore, the comparisons provided here include both the RAPTOR measurements made on the residual dustcake samples and the RAPTOR drag values obtained from the hopper and bridging regression fits at the residual dustcake MMDs. The following information shows a comparison of all of these values.

$$\text{Normalized drag, } \frac{\text{inWC}}{(\text{lb}/\text{ft}^2)(\text{ft}/\text{min})}$$

	GCT2	GCT3	GCT4
Calculated From PCD Baseline ΔP	73	550	110
RAPTOR on Residual Dustcake	60	85	42
RAPTOR on Hopper/Bridged Samples	57	240	130

This comparison shows that the RAPTOR measurements on the samples collected from the residual dustcakes tend to underpredict the actual residual dustcake drag. However, much better agreement is achieved by using the drag values obtained from the regression fits on the hopper/bridging samples at the actual MMDs of the residual dustcake. This result suggests that the drag of the char alone may be sufficient to explain much of the PCD baseline ΔP, at least in the case of GCT2 and GCT4. This comparison also demonstrates that it may be dangerous to rely on RAPTOR measurements made on agglomerated samples that cannot be completely redispersed.

The very high drag value calculated for the PCD residual dustcake during GCT3 may be partially caused by a dustcake areal loading that is not representative. After both GCT2 and GCT3, the PCD was back-pulsed repeatedly to remove as much dust as possible. After GCT4, the PCD was not back-pulsed to preserve the dustcakes. As discussed earlier, the residual dustcake after GCT2 was crusty, while after GCT3 the residual layer was fluffy. It is possible that the back-pulsing after shutdown was more effective at the end of the GCT3 test program, resulting in an unrealistically low areal loading and an unrealistically high drag.

It could also be argued that some of the disagreement between the RAPTOR measurements and the actual residual dustcake drag could be attributed to a failure to accurately take into account the degree of bridging within the PCD during operation. If some of the bridged deposits fell out while removing the internals or during the system shutdown and cooling, the blockage of the filter surface area may have actually been more extensive than the 10 percent and 30 percent blockages used in this analysis. This would have the effect of increasing the effective face

velocities in GCT3 and GCT4, resulting in lower values of PCD residual dustcake drag for these runs. However, the effect of the bridging cannot completely explain the difference between the actual PCD and the RAPTOR measurements made on the residual dustcakes. In order to bring these values into agreement it would be necessary to have over 85-percent blockage of the surface area in GCT3 and over 70-percent blockage in GCT4, which seems unlikely. Therefore, it seems improbable that bridging can completely explain the discrepancy between the actual baseline ΔP and the RAPTOR measurements of residual dustcake drag.

3.4.8 Real-Time Particulate Monitor Evaluation

Protection of the combustion turbine located downstream of the PCD is of paramount importance. Accordingly, an instrument that could provide real-time particle concentration monitoring at the exit of the PCD is desirable to minimize turbine damage resulting from a filter failure or other high-mass emission event. During GCT3 and GCT4, the ongoing evaluation of real-time particulate monitors was continued with testing of the PCME DustAlert 90 emissions monitoring system. This instrument is manufactured by Pollution Control & Measurement (Europe) of Cambridgeshire, England.

The DustAlert 90 determines particle concentration by detecting the naturally occurring electrical charge on the suspended particles in the gas stream as they flow past the probe. This type of probe differs from the triboelectric probes that measure the charge generated when a particle impacts the surface of the probe. Triboelectric probes typically do not measure very small particles well because those particles tend to follow the gas flow streamlines around the probe and fail to impact. Since we are attempting to detect particle sizes and concentrations that are quite low, the PCME technique was considered to be a promising approach.

Previous tests of the PCME probe had not successfully demonstrated that it could detect particles at the low concentrations required for turbine protection. To enhance the detection capabilities of the probe, modifications were made to improve the electrical insulators and to increase the electrical sensitivity of the probe. The modified probe was installed prior to GCT3, but the insulators were fouled with tar during startup of the transport reactor. The fouling effectively shorted the probe signal to ground and no signal could be detected from the unit for the remainder of GCT3. Although there was a nitrogen purge system on the PCME that was intended to prevent insulator contamination, it was not adequate for the high-tar concentrations encountered. After completion of GCT3, the insulators were cleaned and the normal response of the probe returned.

Prior to GCT4, an improved purge system was installed on the PCME port to shield the insulators from the gas stream and to prevent tar contamination. The modified purge system worked as planned, and signal output from the PCME was maintained for the duration of GCT4. During normal operation, the PCME generally indicated a very low reading that appeared to be in the noise range of the instrument. This response was consistent with the actual mass concentration at the outlet of the PCD, which was determined by in situ batch measurements to be less that 0.1 ppmw. Thus, from observation of the instrument during normal operation, the lower limit of resolution appears to be above 0.1 ppmw. This result was

not surprising since this instrument was not expected to be able to detect such low concentrations.

Since the PCD outlet particulate concentration was too low to test the PCME under normal operating conditions, a brief period of comparative tests was conducted with dust injected into the PCD outlet stream. The dust injection system used for these tests has been described in previous reports. Although current operation is in gasification mode, combustion ash particles were used for the test because the behavior of the injection system with combustion ash has been thoroughly characterized. Figure 3.4-11 shows the output of the PCME over a 1.5-hour period with various injected dust concentrations. The vertical scale of the chart is zero to 100 percent of full-scale output (the PCME will not provide absolute concentration data unless it can be calibrated to known conditions). In the chart, the background reading with no dust injected (0 ppmw) can be compared to three injected concentrations. The three concentrations, 8, 12, and 30 ppmw, are estimated values taken from the calibration curve of the dust injection system. Additional testing planned for the following day, using the in situ batch sampling system to substantiate the injected concentrations, was cancelled due to problems with the coal feeder, and the test program was terminated before those data could be collected. Nevertheless, it is clear that the PCME responded to the injected dust in a definite and repeatable way.

In addition to the uncertainty as to the exact injected concentrations, there are several other caveats that must be considered in evaluation of these results. Since the instrument does not actually detect particles, but instead measures the charge on the particles, char particles may produce a different response than the combustion ash used in these tests. The dust injection system will be modified before the next test program to allow these tests to be repeated with char injection upstream of the PCME. Even then, all of the questions regarding the response of this measurement system will not be answered with injected char because char exiting the transport reactor may have a different charge-to-mass ratio than the particles blown out of the dust injection system. If elevated PCD outlet concentrations are encountered in the future, the batch sampling system will be used to calibrate the output of the PCME. In the meantime, the results presented here indicate that the PCME output should be monitored as an early warning of PCD leakage problems. (This was an initial test to see if the PCME would respond at all to particles. Subsequent tests have been done with char, and these results will be included in subsequent run reports.)

3.4.9 Conclusions

The GCT3 and GCT4 test programs successfully demonstrated that very low levels of particulate emissions (< 1 ppmw) can be achieved during operation of the PCD on gasification char. All of the outlet loadings were below the limit of resolution of the measurements (<0.1 ppmw) except for two measurements in which it appears that tar penetrated through the PCD as a vapor and was subsequently collected as tar droplets.

Inlet particulate loadings and particle-size distributions measured during GCT3 and GCT4 confirmed that the modifications made to the transport reactor loop had the expected effect on the mass concentration and size distribution of dust entering the PCD. On average, the particulate loading entering the PCD was reduced by about 40 percent compared to GCT2, even though the coal-feed rate was typically higher in GCT3 and GCT4 than it was in GCT2.

Contrary to the results obtained in GCT2, stable PCD operation at an acceptable baseline ΔP was not achieved in either GCT3 or GCT4. There were several episodes of significant baseline ΔP creep during both GCT3 and GCT4, which are believed to be associated with tar deposition and the formation of bridged deposits caused by sticky char particles.

Based on a comparison of RAPTOR drag measurements with transient drag values calculated from the rate of PCD ΔP rise, the drag of the char appears to be high enough to account for all of the observed ΔP rise during filtration. Tar deposition or other anomalies apparently did not have any significant effect on the PCD transient ΔP.

The residual dustcake drag measured by RAPTOR appears to be far too low to explain the observed baseline ΔP. Much better agreement with the baseline ΔP was obtained by using the MMDs of the residual dustcake samples in the regression fits of the drag-versus-MMD data for the hopper samples and bridged deposits. This result suggests that the RAPTOR apparatus may not accurately simulate the formation of residual cakes that are stuck together with tar.

Correlations of the drag with MMD and surface area demonstrate that these parameters are not sufficient to completely explain the char drag observed in all three gasification tests, even though these parameters can separately correlate the data from GCT2, GCT3, and GCT4. In an effort to investigate the other factors that may be contributing to the observed variation in drag, further studies are planned to investigate the distribution of surface area as a function of pore size. There is hope that from these studies a better understanding will be gained about the fraction of particle-surface area that contributes to drag, making it possible to develop more reliable correlations between char drag and physical properties.

A preliminary evaluation of the PCME real-time particulate monitor with injected combustion ash yielded promising results, but additional testing is needed to determine whether this instrument will reliably detect char particles from coal gasification.

Table 3.4–1

PCD Inlet and Outlet Particulate Measurements From GCT3 and GCT4

Test Date	PCD Inlet				PCD Outlet					PCD Collection Efficiency, %
	SRI Run No.	Start Time	End Time	Particle Loading, ppmw	SRI Run No.	Start Time	End Time	H_2O Vapor, Vol. %	Particle Loading, ppmw	
GCT-3										
12/15/00	1	09:35	10:35	1,700[1]	1	09:30	11:30	6.4	16.87	99.01
12/15/00	--	--	--	--	2	14:45	16:15	3.0	15.92	--
1/25/01	2	10:45	11:02	11,000	3	10:30	11:16	4.4	0.26[2]	--
1/26/01	3	09:30	09:39	25,900	4	08:50	10:20	5.6	< 0.1	> 99.9996
1/27/01	4	08:25	08:40	20,700	5	08:05	11:05	6.8	< 0.1	> 99.9995
1/29/01	5	10:30	10:45	19,300	6	10:22	11:25	8.1	< 0.1	> 99.9995
1/30/01	6	09:35	09:50	28,700	7	09:20	12:20	6.8	< 0.1	> 99.9997
1/31/01	7	09:27	09:37	15,500	8	09:15	12:15	9.2	< 0.1	> 99.9994
GCT-4										
3/09/01	1	09:00	09:15	23,300	1	09:30	11:30	4.9	< 0.1	> 99.9996
3/10/01	2	13:40	13:48	59,500[3]	2	12:45	13:50	9.4	38.6[4]	------
3/25/01	--	--	--	--	3	15:50	17:20	4.6	< 0.1	------
3/26/01	3	09:45	09:55	14,800	4	09:35	10:45	8.7	< 0.1	> 99.9993
3/27/01	4	12:15	12:25	19,800	5	09:10	12:40	8.0	< 0.1	> 99.9995
3/28/01	5	09:50	10:00	10,500	6	09:30	13:30	10.2	< 0.1	> 99.9990
3/29/01	6	12:20	12:35	12,600	7	10:55	13:55	10.3	< 0.1	> 99.9992

1. Sample collected during circulation of bed material, only, without any coal feed.
2. Sample contaminated with brown substance (possibly tar); no visible char on sampling filter.
3. Sampling performed during start of coal feed.
4. Sampling filter covered with black substance assumed to be tar.

Table 3.4-2

Analytical Results on In situ Particulate Samples From GCT-3
(Wt %)

Elemental Analysis (As-Received Basis)

Lab ID	SRI Run No.	Date	C	H	N	S	Al	Ca	Fe	Mg	Si
AB07661	GCT3IMT-2	01/25/01	42.59	0.57	0.36	1.31	3.84	15.14	2.09	2.70	7.47
AB07684	GCT3IMT-3	01/26/01	43.64	0.56	0.40	1.06	3.22	16.34	1.85	2.74	6.55
AB07835	GCT3IMT-4	01/27/01	41.16	0.55	0.33	0.96	3.05	17.38	1.84	2.92	6.50
AB07836	GCT3IMT-5	01/29/01	41.65	0.59	0.32	1.02	3.47	16.39	1.95	2.83	6.68
AB07837	GCT3IMT-6	01/30/01	50.36	0.64	0.41	1.04	3.40	12.76	1.72	2.13	6.54
AB07838	GCT3IMT-7	01/31/01	24.31	0.35	0.15	0.83	5.37	19.17	2.74	3.33	11.58
Average			40.62	0.54	0.33	1.04	3.72	16.20	2.03	2.78	7.55

Chemical Composition Calculated from Elemental Analysis*

Lab ID	SRI Run No.	Date	CO_2	$CaCO_3$	CaS	CaO	Al_2O_3	Fe_2O_3	MgO	SiO_2	Elem C**
AB07661	GCT3IMT-2	01/25/01	N.M.	N.D.	2.95	N.D.	7.25	2.99	4.51	16.01	N.D.
AB07684	GCT3IMT-3	01/26/01	N.M.	N.D.	2.39	N.D.	6.08	2.64	4.56	14.04	N.D.
AB07835	GCT3IMT-4	01/27/01	N.M.	N.D.	2.16	N.D.	5.76	2.63	4.87	13.92	N.D.
AB07836	GCT3IMT-5	01/29/01	N.M.	N.D.	2.30	N.D.	6.55	2.79	4.71	14.32	N.D.
AB07837	GCT3IMT-6	01/30/01	N.M.	N.D.	2.34	N.D.	6.42	2.46	3.55	14.01	N.D.
AB07838	GCT3IMT-7	01/31/01	N.M.	N.D.	1.87	N.D.	10.14	3.92	5.56	24.82	N.D.
Average			N.M.	N.D.	2.33	N.D.	7.03	2.90	4.63	16.19	N.D.

*Assumes that all CO_2 is present as $CaCO_3$, all sulfur is present as CaS, and remaining Ca is present as CaO.
** Assumes that all carbon not accounted for as $CaCO_3$ is in the form of elemental carbon.
N.M. = Not measured due to insufficient sample size.
N.D. = Not determined since CO_2 was not measured.

Table 3.4-3

Analytical Results on In situ Particulate Samples From GCT4
(Wt %)

Elemental Analysis (As-Received Basis)

Lab ID	SRI Run No.	Date	C	H	N	S	Al	Ca	Fe	Mg	Si
AB08051	GCT4IMT-1	03/09/01	52.87	0.61	0.01	1.87	3.44	12.05	1.86	2.12	5.38
AB08052	GCT4IMT-2	03/10/01	40.36	0.27	0.01	0.60	3.00	9.73	1.59	1.69	12.11
AB08233	GCT4IMT-3	03/26/01	35.12	0.37	0.01	N.M.	N.M.	N.M.	N.M.	N.M.	N.M.
AB08234	GCT4IMT-4	03/27/01	45.18	0.58	0.01	0.84	5.34	8.20	2.53	1.63	9.63
AB08235	GCT4IMT-5	03/28/01	34.79	0.40	0.01	N.M.	N.M.	N.M.	N.M.	N.M.	N.M.
AB08236	GCT4IMT-6	03/29/01	33.93	0.43	0.01	0.65	N.M.	N.M.	N.M.	N.M.	N.M.
Average			40.38	0.44	0.01	0.99	3.93	9.99	1.99	1.81	9.04

Chemical Composition Calculated from Elemental Analysis*

Lab ID	SRI Run No.	Date	CO_2	$CaCO_3$	CaS	CaO	Al_2O_3	Fe_2O_3	MgO	SiO_2	Elem C**
AB08051	GCT4IMT-1	03/09/01	5.41	12.30	4.22	6.70	6.50	2.65	3.53	11.53	51.39
AB08052	GCT4IMT-2	03/10/01	5.69	12.93	1.36	5.33	5.67	2.27	2.82	25.96	38.81
AB08233	GCT4IMT-3	03/26/01	N.M.	N.D.	N.D.	N.D.	N.D.	N.D.	N.D.	N.D.	N.D.
AB08234	GCT4IMT-4	03/27/01	2.63	5.98	1.90	6.66	10.08	3.61	2.71	20.65	44.46
AB08235	GCT4IMT-5	03/28/01	N.M.	N.D.	N.D.	N.D.	N.D.	N.D.	N.D.	N.D.	N.D.
AB08236	GCT4IMT-6	03/29/01	6.08	13.82	1.46	N.D.	N.D.	N.D.	N.D.	N.D.	N.D.
Average			4.95	11.26	2.23	6.23	7.42	2.84	3.02	19.38	44.89

*Assumes that all CO_2 is present as $CaCO_3$, all sulfur is present as CaS, and remaining calcium is present as CaO.
**Assumes that all carbon not accounted for as $CaCO_3$ is in the form of elemental carbon.
N.M. = Not measured due to insufficient sample size.
N.D. = Could not be determined since CO_2 was not measured.

Table 3.4-4

Analytical Results on Dustcake Samples From GCT3
(Wt %)

Elemental Analysis (As-Received Basis)

Lab ID	Description	Date	C	H	N	S	Al	Ca	Fe	Mg	Si
AB07857	Transient/bridging	02/06/01	36.96	0.54	0.25	0.77	3.86	16.76	2.16	2.89	6.99
AB07858	Residual dustcake	02/06/01	44.70	0.86	0.53	1.14	3.14	13.47	2.11	2.65	4.60
AB07859	FD0520 Hopper	02/02/01	34.14	0.49	0.25	0.71	3.90	16.58	2.14	2.84	9.42

Chemical Composition Calculated from Elemental Analysis*

Lab ID	Description	Date	CO_2	$CaCO_3$	CaS	CaO	Al_2O_3	Fe_2O_3	MgO	SiO_2	Elem C**
AB07857	Transient/bridging	02/06/01	N.M.	N.D.	1.73	N.D.	7.29	3.09	4.81	14.99	N.D.
AB07858	Residual dustcake	02/06/01	N.M.	N.D.	2.57	N.D.	5.93	3.01	4.41	9.86	N.D.
AB07859	FD0520 Hopper	02/02/01	N.M.	N.D.	1.60	N.D.	7.36	3.06	4.73	20.19	N.D.

*Assumes that all CO_2 is present as $CaCO_3$, all sulfur is present as CaS, and remaining calcium is present as CaO.
**Assumes that all carbon not accounted for as $CaCO_3$ is in the form of elemental carbon.
N.M. = Not measured due to insufficient sample size.
N.D. = Could not be determined since CO_2 was not measured.

Table 3.4–5

Analytical Results on Dustcake Samples From GCT4
(Wt %)

Elemental Analysis (As-Received Basis)

Lab ID	Description	Date	C	H	N	S	Al	Ca	Fe	Mg	Si
AB08248	Transient, Candle T-6	04/06/01	32.27	1.11	0.19	0.91	4.82	16.90	2.33	4.20	6.43
AB08249	Transient, Candle T-8	04/06/01	30.15	0.98	0.13	0.90	4.29	18.14	2.39	4.56	6.40
AB08250	Transient, Candle T-9	04/06/01	30.69	0.98	0.18	0.94	4.16	17.95	2.38	4.47	6.65
AB08251	Transient, Candle T-14	04/06/01	32.69	1.08	0.18	1.32	4.44	17.49	2.78	4.11	7.03
AB08252	Residual, Top Plenum	04/06/01	57.19	1.16	0.75	1.02	2.87	9.06	1.44	1.70	4.77
AB08253	Residual, Top Plenum	04/06/01	55.06	1.07	0.62	1.01	3.22	9.46	1.27	1.62	5.48
AB08254	Bridging, Top Plenum	04/06/01	73.21	4.70	1.42	0.99	3.62	10.93	2.16	2.30	7.85
AB08255	Bridging, Bottom Plenum	04/06/01	43.74	0.26	0.32	0.92	3.81	11.31	2.20	2.48	8.22

Chemical Composition Calculated from Elemental Analysis*

Lab ID	Description	Date	CO_2	$CaCO_3$	CaS	CaO	Al_2O_3	Fe_2O_3	MgO	SiO_2	Elem C**
AB08248	Transient, Candle T-6	04/06/01	4.81	10.93	2.05	15.95	9.11	3.33	7.00	13.78	30.96
AB08249	Transient, Candle T-8	04/06/01	4.78	10.86	2.03	17.73	8.10	3.42	7.59	13.71	28.85
AB08250	Transient, Candle T-9	04/06/01	4.76	10.82	2.12	17.42	7.86	3.39	7.45	14.26	29.39
AB08251	Transient, Candle T-14	04/06/01	4.74	10.77	2.97	16.14	8.39	3.97	6.85	15.06	31.40
AB08252	Residual, Top Plenum	04/06/01	5.07	11.52	2.30	4.43	5.42	2.06	2.84	10.22	55.81
AB08253	Residual, Top Plenum	04/06/01	5.40	12.27	2.28	4.60	6.09	1.82	2.70	11.75	53.59
AB08254	Bridging, Top Plenum	04/06/01	5.62	12.77	2.23	6.42	6.84	3.09	3.83	16.82	71.68
AB08255	Bridging, Bottom Plenum	04/06/01	5.55	12.61	2.08	7.16	7.20	3.15	4.14	17.62	42.23

* Assumes that all CO_2 is present as $CaCO_3$, all sulfur is present as CaS, and remaining calcium is present as CaO.
** Assumes that all carbon not accounted for as $CaCO_3$ is in the form of elemental carbon.

Table 3.4–6

Physical Properties of GCT3 and GCT4 In situ Samples

Lab ID	SRI Run No.	Date	Bulk Density, g/cm^3	True Density, g/cm^3	Uncompacted Bulk Porosity, %	BET Surface Area, m^2/g	Mass-Median Diameter, µm
GCT-3							
AB07834	GCT3IMT-1	12/15/00	0.89	2.61	65.9	2.2	22.0
AB07661	GCT3IMT-2	01/25/01	0.32	2.23	85.7	96.7	14.9
AB07684	GCT3IMT-3	01/26/01	0.39	2.26	82.7	118.0	13.8
AB07835	GCT3IMT-4	01/27/01	0.37	2.28	83.8	100.0	12.9
AB07836	GCT3IMT-5	01/29/01	0.41	2.22	81.5	81.6	13.0
AB07837	GCT3IMT-6	01/30/01	0.32	2.15	85.1	181.0	14.3
AB07838	GCT3IMT-7	01/31/01	0.38	2.54	85.0	188.0	16.1
GCT-3 Average[1]			0.37	2.28	84.0	127.6	14.2
GCT-4							
AB08051	GCT4IMT-1	03/09/01	0.31	2.25	86.2	132.0	16.9
AB08052	GCT4IMT-2	03/10/01	0.54	2.28	76.3	105.0	13.2
AB08233	GCT4IMT-3	03/26/01	0.22	2.28	90.4	265.0	16.4
AB08234	GCT4IMT-4	03/27/01	0.26	2.21	88.2	198.0	12.1
AB08235	GCT4IMT-5	03/28/01	0.27	2.35	88.5	204.0	15.9
AB08236	GCT4IMT-6	03/29/01	0.31	2.34	86.8	188.0	18.3
GCT-4 Average[2]			0.27	2.29	88.0	197.4	15.9

1. GCT3IMT-1 excluded from average since it was done with sand circulation only.
2. GCT4IMT-2 excluded from average due to high bulk density and low surface area.

Table 3.4–7

Physical Properties of GCT3 and GCT4 Dustcake Samples

Type of Sample	Plenum or Element	Date	Bulk Density, g/cc	Particle Density, g/cc	Uncompacted Bulk Porosity, %	Specific Surface Area, m^2/g	Mass-Median Diameter, μm
GCT-3							
Bridged Material	Various	02/06/01	0.37	2.40	84.6	127	12.0
Residual Dustcake	Various	02/06/01	0.36	2.37	84.8	44.0	4.3
GCT-4							
Bridged Material	Top	04/06/01	0.31	2.21	86.0	194	11.9
Bridged Material	Bottom	04/06/01	0.36	2.21	83.7	151	13.5
Residual Dustcake	Top	04/06/01	0.32	2.00	84.0	8.0	8.0
Residual Dustcake	B-8	04/10/01	0.35	1.82	80.8	N.M.	8.7
Residual Dustcake	Top	04/06/01	0.33	2.02	83.7	16.9	7.8
Residual Dustcake	B-17	04/10/01	0.30	1.81	83.4	N.M.	7.8
Transient Dustcake	T-6	04/06/01	0.31	2.36	86.9	36.8	11.8
Transient Dustcake	T-8	04/06/01	0.35	2.33	85.0	32.4	11.0
Transient Dustcake	T-9	04/06/01	0.34	2.35	85.5	27.7	11.9
Transient Dustcake	T-14	04/06/01	0.32	2.34	86.3	35.9	11.6

Table 3.4-8

Transient Drag Determined From PCD ΔP and From RAPTOR

Sampling Run No.	ΔP/Δt, inWC/min	Δ(AL)/Δt, lb/ft²/min	FV, ft/min	MMD, μm	Drag (R), inWC/(lb/ft²)/(ft/min)		
					PCD	PCD @ RT	RAPTOR
GCT-2							
GCT2IMT-1	14.16	0.0540	4.86	17.4	54	29	21
GCT2IMT-2	9.33	0.0340	3.84	17.6	72	39	21
GCT2IMT-3	8.27	0.0448	3.34	16.3	55	31	23
GCT2IMT-4	6.09	0.0376	3.16	15.8	51	29	24
GCT2IMT-5	3.40	0.0294	2.73	19.9	42	24	18
GCT2IMT-6	5.38	0.0396	3.10	19.3	44	24	19
GCT2IMT-7	6.20	0.0408	2.84	18.6	53	29	20
Average for GCT-2					**53**	**29**	**21**
GCT-3							
GCT3IMT-1	0.51	0.0012	3.36	22.0	126	95	68
GCT3IMT-2	9.49	0.0103	3.07	14.9	301	178	92
GCT3IMT-3	14.67	0.0405	3.13	13.8	116	69	98
GCT3IMT-4	10.97	0.0304	2.90	12.9	125	74	104
GCT3IMT-5	12.37	0.0292	3.06	13.0	138	82	103
GCT3IMT-6	19.92	0.0376	3.00	14.3	177	106	96
GCT3IMT-7	6.45	0.0229	3.07	16.1	92	55	87
Average for GCT-3 (1)					**129**	**80**	**70**
GCT-4							
GCT4IMT-1	21.96	0.0344	3.12	16.9	205	116	49
GCT4IMT-2	44.67	0.0873	4.71	13.2	109	60	65
GCT4IMT-3	5.82	0.0208	3.03	16.4	92	51	51
GCT4IMT-4	15.03	0.0305	3.27	12.1	151	88	71
GCT4IMT-5	3.79	0.0126	2.42	15.9	124	75	53
GCT4IMT-6	3.64	0.0153	2.47	18.3	96	58	45
Average for GCT-4 (2)					**114**	**66**	**70**

(1) Excluding run no. GCT3IMT-2.
(2) Excluding run no. GCT4IMT-1.

Figure 3.4–1 GCT4 Residual Dustcake at 30x Magnification

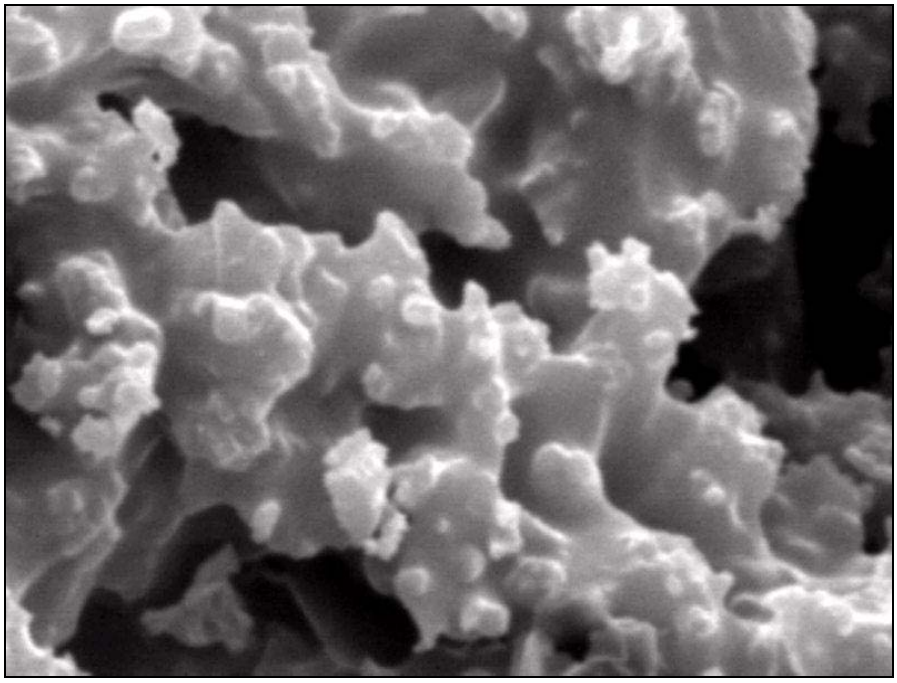

Figure 3.4–2 GCT4 Residual Dustcake at 5000x Magnification

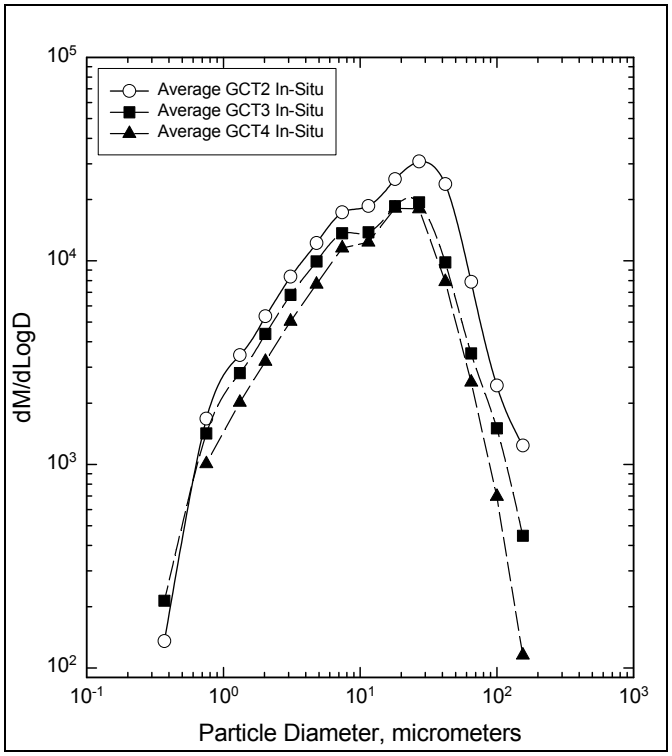

Figure 3.4–3 PCD Inlet Particle Size Distributions

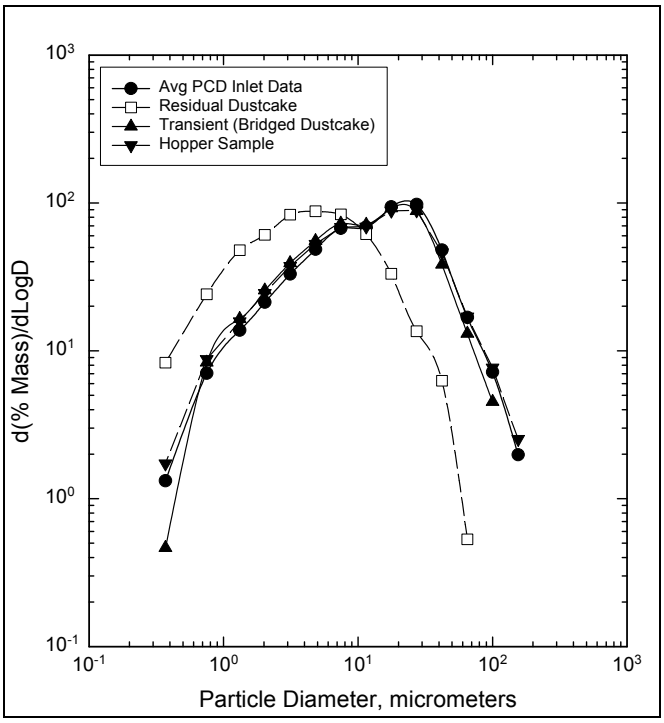

Figure 3.4–4 Particle Size Distributions for GCT3 Char

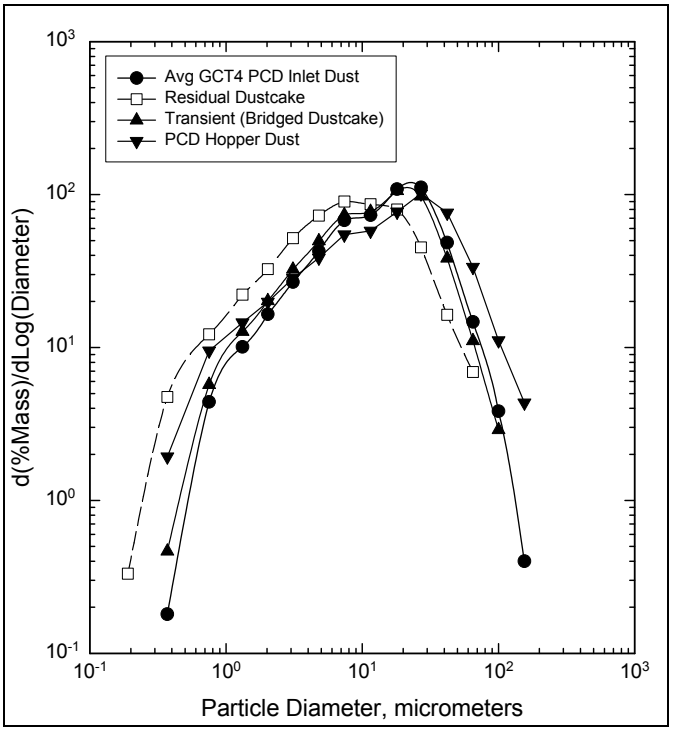

Figure 3.4–5 Particle Size Distributions for GCT4 Char

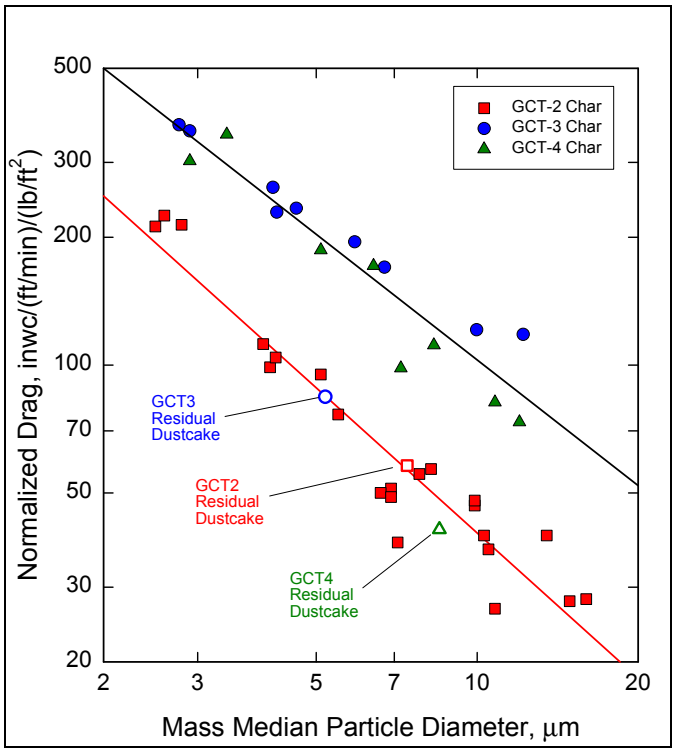

Figure 3.4–6 RAPTOR Drag Vs. Particle Size

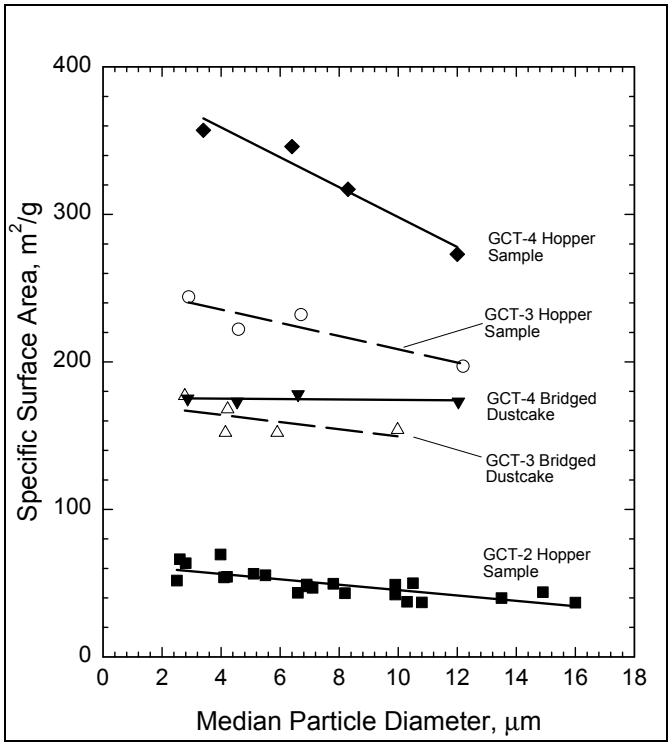

Figure 3.4–7 Specific-Surface Area of PSDF Char Vs. Particle Size

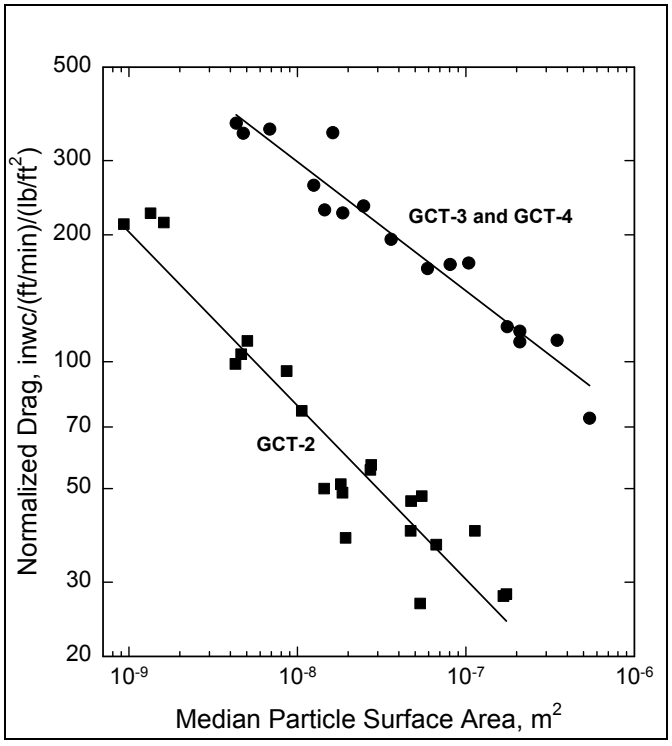

Figure 3.4–8 Normalized Drag Vs. Median Particle Surface Area

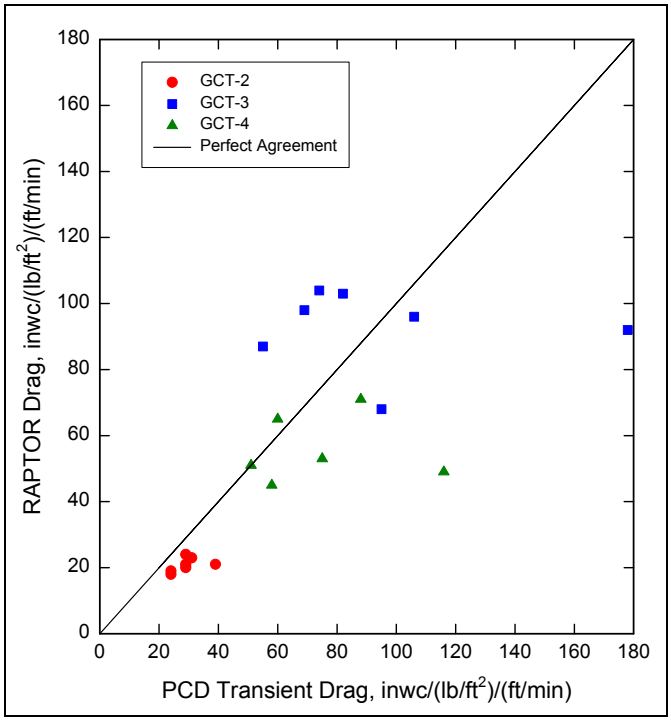

Figure 3.4–9 Comparison of Laboratory and Actual PCD Drag

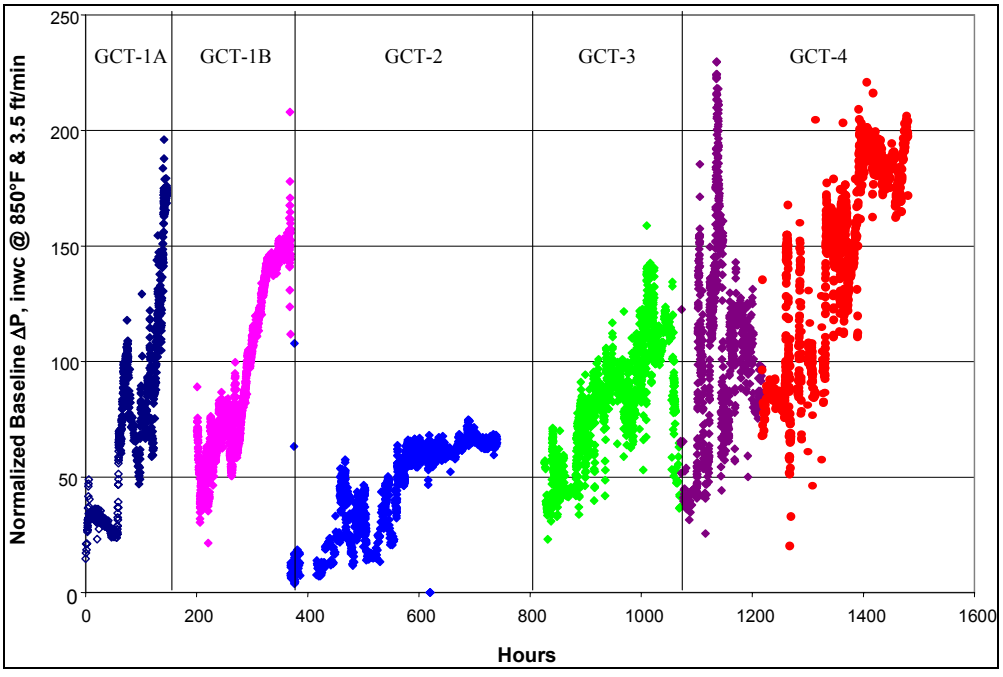

Figure 3.4–10 Normalized PCD Baseline dP During GCT Tests

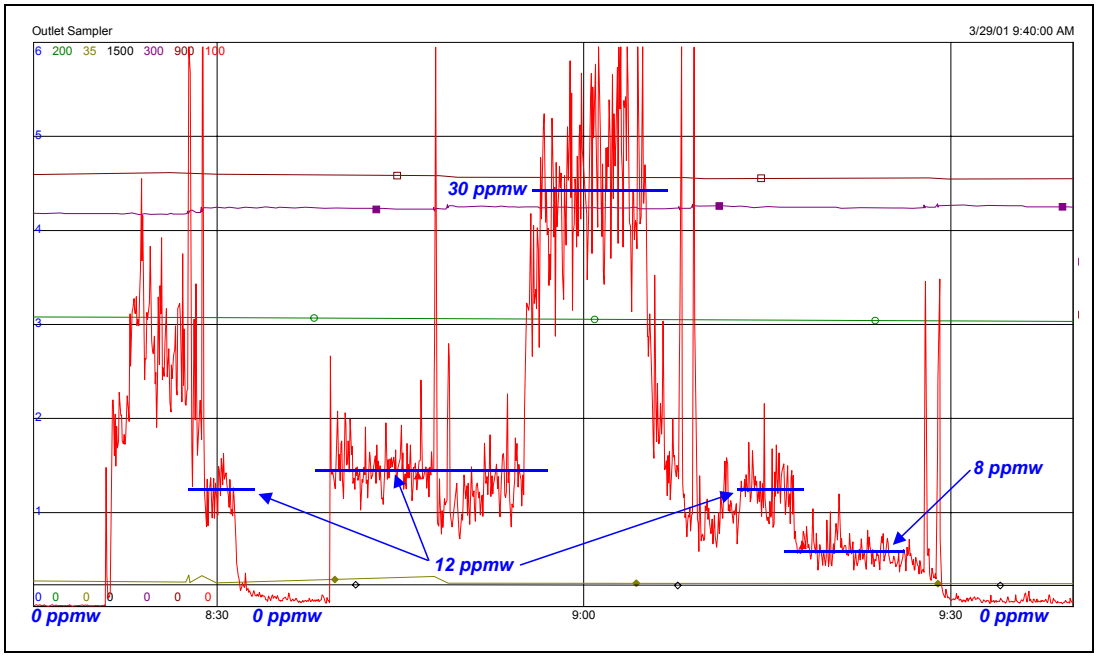

Figure 3.4–11 PCME Real-Time Particulate Monitor Output During Duct Injection

3.5 FINES HANDLING SYSTEM

The fines handling system operated with no major problems during GCT4. While the system was pressurized before and after coal feed, the fines handling system was cycled to prevent solids buildup. At these times the screw cooler was usually set to 50-percent operating capacity and FD0520 cycling frequency was 5 to 30 minutes. During coal feed the screw cooler (FD0502) was usually operated at 95-percent capacity and the lock-hopper vessel (FD0520) was cycled every 1.5 to 3 minutes.

As in previous runs, there was some leaking from the screw cooler FD0502 seal. During the run a leak between the follower and flange required maintenance personnel to tighten the follower to stop the leak. Also, the bearing on the nondrive side of the cooler required tightening and the bellows were adjusted. In the outage following GCT4, automatic seal pressure control was added to improve sealing FD0502 and other maintenance such as replacement of seal packing and a stuffing box was required.

Inspection of the FD0520 system revealed a groove cut out of the top ring plate where pressurizing nitrogen enters the plate and the nitrogen nozzle nipple was coated with char. The groove in the ring plate can be seen in Figure 3.5-1. Since inspection of all the Clyde systems in the transport reactor train revealed contamination of the shuttle valves by material associated with each system (that is, char was found on the FD0520 shuttle valves, coal was found on the coal feeder FD0210 shuttle valves, and limestone was found on the sorbent feeder FD0220 shuttle valves), it appeared that solid materials were leaking through the inflatable process-side seals in the Clyde systems. This leakage was probably the cause of the groove found on the FD0520 ring plate. The ring plate will be replaced prior to the next run. The spheri dome and the inflatable seals on FD0520 appeared clean and were reinstalled. Also, the instrument lines associated with the FD0520/FD0502 systems were inspected for char contamination and appeared clean.

Because a reliable solids level measurement in FD0520 was not available, the lock vessel sequence was controlled by a timer as it was in the previous gasification runs since the char removal cycling frequency was based on estimates of solids loading (at times cycling was more frequent than needed, causing excessive equipment wear). Because of the frequent changes in system conditions such as coal-feed rate, char removal system cycling times were changed often, requiring much attention from operations and engineering personnel.

Observations/Events — March 7, 2001, Through March, 30, 2001

A. On March 8, 2001, at 02:50 the dense-phase vessel of FD0520 plugged, tripping FD0502.

B. On March 9, 2001, at 15:38 a faulty high-level probe reading from FD0530 caused FD0520 to trip.

C. On March 9, 2001, at 16:56 a high-level probe reading from FD0530 again caused FD0520 to trip.

D. On March 9, 2001, at 18:25 the FD0530 level probe tripped FD0520 again.

E. On March 10, 2001, at 07:20 FD0502 was found to be leaking at the inlet end between the follower and flange. Maintenance personnel tightened the follower and stopped the leak.

F. On March 25, 2001, at 19:15 a small leak was found on FD0502.

G. On March 26, 2001, at 06:05 the FD0502 was briefly stopped so maintenance could tighten a set screw on the nondrive end.

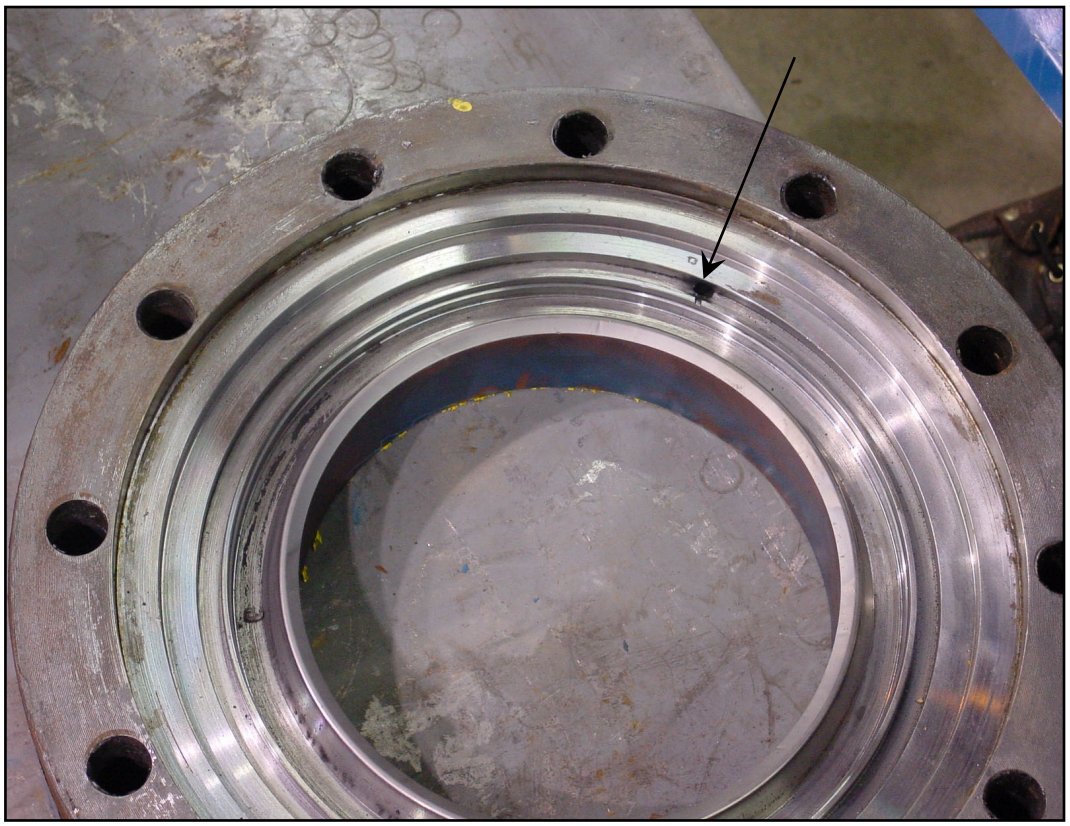

Figure 3.5-1 Groove in FD0520 Ring Plate

3.6 PARTICULATE DUSTCAKE ADDITIVES

Early transport reactor runs in gasification mode produced a char particulate with substantially higher flow resistance than the flyash produced in combustion mode. Although the drag of this particulate was not so high that the PCD could not be successfully operated, there were concerns for the future. Char samples produced at the Transport Reactor Development Unit (TRDU) at the University of North Dakota had much higher drag than the PSDF char from GCT1. The higher drag was consistent with a finer particle-size distribution and higher specific-surface area of the TRDU char. Since modifications to the PSDF transport reactor were planned that might produce dust characteristics similar to the TRDU, a study was undertaken to investigate ways to artificially reduce dustcake drag.

It had been widely speculated that mixing low-drag particles into a high-drag dustcake could potentially reduce PCD pressure drop (ΔP). In fact, particulate additive injection tests had been conducted at the TRDU, but the results were inconclusive. However, it seemed reasonable that mixing a high-drag char with a particulate (such as combustion ash) that had only one-fifth the drag might produce a lower drag dustcake.

There are a number of potential problems with this approach:

- It can be difficult to maintain a constant rate of additive injection and achieve uniform dispersion of the additive within the gas stream.
- The PCD tangential entry and inner cylindrical shroud may cause large additive particles to discharge directly to the lower cone section, avoiding candle filters altogether.
- The PCD char discharge system may not be able to handle the extra material.
- The increased areal loading of the dustcake could offset the effect of the decreased drag, resulting in little or no reduction in PCD pressure drop.
- To control the baseline pressure drop, it may be necessary to begin additive injection during startup and continue the additive injection without interruption.
- The costs of installing the additive injection equipment and purchasing and handling the additive may be prohibitive.

Despite all of the potential problems listed above, the threat of extremely high pressure drops and severe restrictions on PCD operations was enough to motivate a study of various low-drag additives. A laboratory study was conducted by Southern Research Institute to evaluate the usefulness of additives for reducing PCD ΔP. The results of this study were used to choose additives and conditions for further testing at the PSDF. The remainder of this section will describe the laboratory study, followed by the results of the PSDF trials.

3.6.1 Laboratory Additive Study

The laboratory study was conducted during the late summer and fall of 2000. The following section will describe the additives and char selected for use in the tests. Section 3.6.1.2 describes the experimental procedure and apparatus, which included extrapolation of existing techniques and the development of new measurement techniques to simulate the expected effect in the PCD. Section 3.6.1.3 presents results of the lab study.

3.6.1.1 Additive Selection

A number of additives were chosen for use in this study, all of which had inherently low drag, and, thus, were perceived to have the potential to reduce the drag of a mixture containing high-drag char. Most of the additives were chosen for their ready availability and low cost, but two more expensive additives were chosen for the unusual structures of their particles. The additives tested are shown in Table 3.6-1. The limestone, sand, ash, and low-drag char were on hand or readily available either at the PSDF or at nearby power plants. The limestone, sand, and PSDF ash were made up mainly of solid, nonspherical, particles. The Gaston and Miller plants flyash tends to be more spherical in nature due to the high temperature of combustion that occurs in pulverized-coal-fired boilers. The AZS-45 material was composed of hollow ceramic spheres that were injected into the PCD at the TRDU as a dustcake additive. Although the results at the TRDU were inconclusive, it was believed by some TRDU personnel at the time that the AZS-45 had a slight beneficial effect on PCD pressure drop. Celite is a product of World Minerals, Inc., and consists of skeletons of microscopic sea creatures. The Celite has a very complex structure (see Figure 3.6-1) that was thought to be particularly useful in producing an open dustcake structure that would lower drag.

The char that had been produced at the PSDF at this time did not have sufficiently high drag to be useful for this study. The drag of the PSDF char that was produced during GCT1 and GCT2 was only about twice the drag of the additives to be tested. Although some preliminary work was conducted with the PSDF char, most of the data were collected on char generated at the TRDU in November 1996. The TRDU test run (P050) was conducted on PRB coal with dolomite as the sorbent. The normalized drag of the TRDU char was three times higher than the drag of the PSDF char and over seven times higher than that of the additives.

3.6.1.2 Experimental Procedure

During the initial work conducted on dustcake additives, measurements were made on dustcakes that were created by combining the char and the additive in appropriate weight ratios and thoroughly mixing them by vigorous agitation. Hereafter, the dustcakes prepared in this manner are referred to as "mechanically created" dustcakes to differentiate them from the "flow-collected" dustcakes formed by collecting resuspended particles of char and additive. The effect of the additive on drag was measured with the compressed ash permeability tester (CAPTOR), considered to be the standard method of measuring drag at the time. The CAPTOR device determines the flow resistance of the powder mixture as a function of porosity by measuring the pressure drop across a compacted layer of the mixture as a function of air-flow rate through the layer. After initial experiments were conducted to determine the degree of mixing necessary, this

technique gave reproducible results. However, comparison of the CAPTOR results with another measurement technique produced a disturbing disagreement, as described below.

The effect of particle additives on drag was also measured using a new measurement technique under development at the time, the resuspended ash permeability tester (RAPTOR). Although this system is based on a technique that Schumacher has used for years, a number of improvements have been implemented. The major components of the system are shown in Figure 3.6-2. The dust to be measured is resuspended in air using a fluidized bed. The suspended dust enters the center tube of an annular distribution nozzle at the top of the dustcake collection chamber. The outer annulus of the nozzle has a separately controlled air stream for adjusting the flow patterns in the chamber to produce a uniform dustcake and avoid buildup on the walls. The dust is then collected on a sintered metal collection filter at constant face velocity. (Since the measurement is made at room temperature the velocity through the dustcake is corrected for the change in viscosity at high temperature to better simulate conditions in the PCD.) When sufficient dustcake is accumulated for an accurate thickness measurement the dustcake pressure drop is recorded and the sample collection is ended. A measurement jig is fitted to the lower section of the filter chamber and very accurate measurements of dustcake thickness are made at 16 locations over its surface. The sample is then removed from the filter and weighed to calculate areal loading and porosity.

The RAPTOR device has several advantages over the CAPTOR measurement. These are:

- The dust is suspended in air and collected under flowing conditions rather than spooned into the measurement cell. This may produce more realistic dustcakes.

- An estimate of the porosity of the dustcake is obtained along with the drag.

- The fluidized-bed dust generator will not evolve very large particles (>50 μm). This may make it a better simulation of the PCD, with its cyclonic separation resulting from the tangential inlet nozzle. As can be seen from Table 3.6-1, many of the additives tested contained large quantities of large particles that would probably drop out in the PCD vessel before reaching the filter elements.

The RAPTOR system also had disadvantages. In general, the RAPTOR requires a much larger quantity of sample than does the CAPTOR, and it is much more time consuming to operate. The main difficulty for this study was in determining the actual concentration of the additive in the collected dustcake. In the CAPTOR device, the additive and char were weighed and blended in specific concentrations before the test, so that the weight fractions of char and additive were well known. However, in the RAPTOR the two materials were mixed together in the fluidized-bed dust generator in a known ratio, but the two components were generally evolved into the air stream at different rates because of differences in density and particle-size distribution. Two different techniques were used to determine the actual additive content of the resulting dustcake. For the inert additives (sand, ash, AZS-45, and Celite), the sample was ignited and the loss-on-ignition (LOI) was used to determine the concentration of inert material that had been added to the high-LOI char. The LOI technique could not be used for the limestone, which has an LOI

value similar to that of the char. Since limestone and char are very different colors, visual colorimetry was used to approximate the concentration of limestone in the blend.

Figure 3.6-3 shows a comparison of RAPTOR and CAPTOR measurements of the effect of limestone addition on dustcake drag. This was one of the preliminary measurements made with PSDF char; hence the low drag for pure char. These measurements were made over the entire range of additive concentrations, from pure char (zero-percent limestone) to pure limestone dust (100 percent). Clearly, the two measurement techniques give different results for the same additive concentration. At some concentrations, the CAPTOR indicated that the effect of limestone addition was twice as great as did the RAPTOR.

The disagreement between RAPTOR and CAPTOR is believed to be primarily a function of the way that the dustcake is formed in the two devices. While the mechanically created dustcake of the CAPTOR may accurately simulate a homogeneous dust with a narrow particle-size distribution, the RAPTOR is believed to more accurately simulate a PCD dustcake that is made up of a nonhomogeneous mixture of particles of different sizes and densities. Figure 3.6-4 illustrates how the same mixture of large and small particles may build up under flowing conditions to produce a higher gas-flow resistance than is obtained with a mechanically created dustcake. Both samples shown in the figure have the same particle-size distribution, the same average dustcake porosity, and very different drag characteristics. When a dustcake is formed under flowing conditions the small particles will partially follow the gas flow stream lines until they impact in a void space between larger particles, as illustrated in Figure 3.6-4. As a result, the gas must flow through dustcake voids that are filled by small, high-drag particles.

When large and small particles are simply stirred together the small particles tend to be distributed uniformly over the surface of the large particles, as illustrated in the sketch. As a result, mechanically created dustcakes tend to have lower flow resistance than do flow-collected dustcakes of equivalent porosity. To match the drag of a flow-collected dustcake, the mechanically created dustcake must be compacted to a much lower porosity, much lower than the dustcake porosities typically measured at the PSDF. As a result of this effect, the RAPTOR measurements provide a much better simulation of actual PCD performance in terms of matching both the dustcake drag and porosity. For example, in the GCT2 test the PCD dustcake porosity was 84 percent and the dustcake porosity measured by RAPTOR was 82 percent. To match the PCD and RAPTOR drag it was necessary to compact the mechanically created (CAPTOR) dustcake to a porosity of 71 percent. This result confirms the structural differences between the mechanically created and the flow-collected dustcakes illustrated in Figure 3.6-4. Because of these differences it was clear that the RAPTOR apparatus was the most appropriate measurement system for the additive study, and all further work was conducted with this device.

Many of the additives tested had a substantial fraction of their mass contained in particles larger than 45 μm. These particles are believed to be removed by the cyclonic separation system integral to the PCD and, therefore, not be available to modify the PCD dustcake properties. In order to prevent these particles from confusing the experiment, both the additives and char were sieved to <45 μm before they were loaded into the fluidized-bed feeder on the RAPTOR system. Although most of the experiments were conducted with sieved dusts, the accuracy of

the assumption that the large-particle fraction would have no effect on the results was tested at the end of the test program.

3.6.1.3 Laboratory Results

The results of the RAPTOR tests conducted with additives and TRDU char are shown in Table 3.6-2 and graphically illustrated in Figures 3.6-5 through -9. The first line of data in the table contains the normalized drag value of the pure TRDU char, while a "100-percent additive" entry indicates the normalized drag of a pure additive. Extensive tests were performed on the first six samples listed in the table to evaluate the relationship between additive concentration and drag. The results for the last three additives were single-point measurements made after conclusion of the main lab study. Most of the following analysis applies primarily to the six samples that were thoroughly tested.

Figure 3.6-5 shows a plot of the normalized dustcake drag as a function of the amount of additive that appeared in the dustcake sample. For most of the additives the normalized drag of the blended sample approximated a linear relationship between the relative amounts of additive and char and the drags of the two pure materials. Since the fine sand was too coarse to evolve from the fluidized-bed it had no effect on the dustcake and is not shown. The Celite seemed to reduce dustcake drag more than the other materials, possibly because of its open structure. The flyash shown in the figure is combustion ash generated at the PSDF.

Columns two and three in Table 3.6-2 show, respectively, the mixture of char and additive that was added to the fluidized-bed dust generator and the fraction of additive that was found in the dustcake. Despite sieving out the particles larger than 45 μm, none of these materials evolved from the fluidized-bed as easily as the char. Therefore, extra additive material had to be used to achieve the desired dustcake concentration. A similar effect would likely occur in the PCD because of the cyclonic separation that occurs there.

Although it was useful in the lab to use sieved additives, in order to understand the full effect on plant operation the total amount of additive that must be injected into the duct must be considered. As used here, the "bulk-addition rate" includes the amount of material that was sieved out of the original additive samples and the fraction that was added to the fluidized-bed during the RAPTOR tests. Figure 3.6-6 shows a plot of the amount of additive that would be expected to be in the dustcake as a function of the bulk-addition rate. As the figure shows, no matter how much fine sand was added, there was none found in the dustcake. The other materials carried over to the dustcake in amounts that were dependent on their particle-size distribution (that is, finer particles carried over better).

Although the lab tests were conducted with very high concentrations of additives there is a practical limit on the amount of additive that can be added to a given PCD system. At the PSDF, the PCD hopper dust removal system was perceived to be the primary limitation on the amount of material that could be added to the PCD inlet-gas stream. Even if the injected additive does not reach the dustcake to modify drag it must still be removed from the PCD hopper. Based on the amount of char being removed from the hopper during GCT1, plus the known capacity of the dust removal system, it was estimated that a reasonable addition-rate limit was about 1 lb of additive per lb of char. The actual limit at any give time will vary depending

on the amount of char exiting the transport reactor, but this was a reasonable value with which to work. The addition-rate limit is represented by the vertical dashed line in Figure 3.6-6. When this limit is taken into account, it becomes obvious that some of these additives have severe limitations because of their large particle-size distributions.

When the data showing the effect of additives on dustcake normalized drag is plotted against the bulk addition rate, the results shown in Figure 3.6-7 are obtained. At the addition-rate limit, the effect of most additives on normalized drag is small. In this illustration the flyash had the largest effect on normalized drag, primarily because of the small size of the flyash and resulting high carryover rate. However, drawing a conclusion based only on normalized drag data can be very misleading, as discussed below.

The results discussed so far only consider the effect of the additives on the normalized drag, which describes their ability to modify the fundamental flow resistance property of the dustcake. However, another issue that is equally important to actual PCD pressure drop performance is dustcake areal loading. Since additional material is being added to the dustcake in the form of the additive, the dustcake areal loading will be increased by additive injection. Both normalized drag and areal loading have a directly proportional effect on PCD ΔP. While these additives produce a reduction in normalized drag, they will have the opposite effect on areal loading and, thus, tend to negate the beneficial effect on drag. Figure 3.6-8 shows the effect of the bulk-addition rate on the areal loading of the PCD dustcake. The flyash increases the areal loading the most because, as mentioned previously, it has a relatively fine particle-size distribution.

The combined effect of the increased areal loading and reduced normalized drag can be seen in the rightmost column of Table 3.6-2 and by the solid symbols and connecting lines in Figure 3.6-9. The net effect is that, for all but one additive, the increased areal loading completely negates the reduced normalized drag and results in no reduction in PCD ΔP. Celite was the one material that showed a net-positive effect, suggesting that the addition of Celite affects drag more than it affects areal loading.

As described previously, the laboratory tests represented by the solid symbols in Figure 3.6-9 were done on samples of additives that were sieved to less than 45 μm. This was done with the assumption that the large particles would escape neither the laboratory fluidized-bed nor the PCD cyclonic action and, thus, would not affect dustcake properties. To test this assumption, one sample of each additive and char mixture was made using the bulk additive at the maximum injection rate of 1 lb/lb char. When this mixture was loaded into the fluidized-bed and evaluated with the RAPTOR, the data shown in Table 3.6-3 and by the open symbols in Figure 3.6-9 were obtained. As expected, the large fraction did not carry over as readily as did the sieved material. Once again, these data indicate that only Celite would be expected to have a net-positive benefit to PCD pressure drop. In fact, the bulk Celite produced a result that was three times greater than was obtained with the sieved additive, suggesting that the large (>45-μm) Celite particles were carried over to the dustcake at a higher rate than expected. This is not surprising, considering the open structure and low bulk density of the Celite. The aerodynamic particle size of the Celite is considerably smaller than its physical size, and the larger particles may be even more effective at modifying dustcake structure and changing flow resistance.

Three additional single-point measurements are shown in Table 3.6-2 that were not included in any of the figures discussed thus far. Two samples of flyash that were obtained from pulverized coal-fired (pc-fired) boilers in the Alabama Power Company plant system were tested at the maximum-injection rate. The flyash particles from the pc-fired boilers were finer and more spherical than the larger, angular particles found in the other additives that were tested. A test was also conducted using GCT2 char as the additive. Relative to the TRDU char, the GCT2 char had a fairly low drag but was similar to the TRDU char in particle size and density. In none of these tests with the pc flyash and the GCT2 char did the net effect of the additive reduce PCD ΔP.

3.6.2 Field Evaluation of PCD Solids Injection

Because of the expected increase in PCD pressure drop resulting from more thoroughly gasified char, modifying char cake properties was explored as a possibility for counteracting this pressure drop increase. As discussed in the laboratory additive study, Section 3.6.1, additives were shown to decrease char cake drag, but the added solids loading tended to cause an overall increase in pressure drop in most laboratory testing. In an effort to assess the effects of solids injection into the PCD under gasification operating conditions, several solids injection tests were conducted during GCT4. The results of the SRI laboratory study were used in developing a plan and selecting materials for the PCD solids injection experiments. Based on the SRI study, four materials were selected to test. Piping modifications were made so that the existing transport reactor sorbent feeder could alternately feed into the reactor and the PCD.

3.6.2.1 Materials Tested

According to the SRI study, one material, Celite, a particular brand of calcined diatomite, promised to have a beneficial albeit small effect on PCD pressure drop (dP), while the other materials tested were not expected to have an effect on filtration operation. Although the Celite diatomite is quite expensive (~$0.35/lb at the time of this testing) and not likely to be a viable option in a commercial power plant, it was decided to test this material since it was the most likely to show whether or not solids injection can in fact reduce PCD pressure drop significantly. Three other materials were chosen based on their availability and economic feasibility, and they were not likely to negatively affect PCD pressure drop according to the SRI study. These three materials included limestone, fine sand known as sand flour, and combustion ash from a nearby pulverized-coal boiler plant.

The objective of the solids injection test was to assess the effect on PCD pressure drop of each particular material using approximately the same volumetric flow rate for each material since the sorbent feeder is a constant volume feeder. The mass-flow rate of each material was to be approximately 50 to 100 percent of the solids loading from the reactor, as this ratio was expected to show a noticeable change in PCD pressure drop, at least for Celite addition. For an expected solids loading of about 300 lb/hr from the reactor, this would increase the solids entering the PCD to approximately 450 to 600 lb/hr, which would not exceed the maximum-removal rate of the fines handling system. The available instruments to determine mass-flow rates are the weigh cells on the sorbent feeder and on the fines removal vessel FD0530. Although these weigh cells are not precise, they give estimates of the solids-flow rates.

For the first portion of the solids injection testing each of the four materials was to be tested for 1 to 3 hours to assess short-term results. Then, the most promising of those materials was to be tested for a period of 24 hours to determine any long-term results. As particles above 45 μm were not expected to reach the filters due to the cyclonic action in the PCD, the materials used had an average particle size of less than 45 μm. The median particle diameter (D_{50}), standard deviation (μm), Sauter mean diameter ($d_{ps,v}$), bulk density, and true density of each material, as reported by the on-site SRI chemistry laboratory, are shown in Table 3.6-4. Due to an operational error, larger size sand with a median particle diameter of 145 μm was used in the place of sand flour. The cost of each material at the time of testing is also included in this table.

3.6.2.2 Material Injection Assembly

Solids injection testing was made possible with minimal system modifications in which the existing transport reactor sorbent feeder FD0220 could be used to feed solids into the PCD inlet duct. This feeder was used since it is capable of feeding very fine materials and is rated for operation above 240 psig, the system pressure normally used during gasification runs. Using this feeder required the loss of sorbent feed into the reactor during PCD solids injection testing.

The hardware required for PCD solids injection included a "Y" assembly added to the sorbent feed line between the feeder and the transport reactor connecting the sorbent feeder to a new PCD sorbent feed line that was constructed of 1-inch carbon steel Schedule 160 piping. A thermocouple was installed on the sorbent line entering the PCD duct that was interlocked with a shut-off valve next to FD0220 so that, in case of a high temperature reading indicating reverse flow, the feed line would be closed automatically. Other safety precautions, such as a requirement to have one branch of the "Y" assembly isolated at all times and nitrogen purge flows on both ends of the assembly, were implemented prior to the solids injections testing.

The 1-inch solids injection line entered the PCD inlet duct at a preexisting nozzle. This nozzle is approximately 60 feet from the PCD vessel, and at this point unclean gas from the transport reactor travels downward about 10 feet before turning upward toward the PCD. The injection nozzle was chosen because of its location at a curve in the pipe that allows solids injection in the existing flow direction so that the injection solids would not impinge on the inner duct surface.

3.6.2.3 Solids Injection Results

The solids injection testing consisted of nine injection periods, including two limestone tests, five Celite tests, one sand test, and one ash test. Table 3.6-5 shows the field tests, including material amounts and test durations. For each injection period the PCD dP rate and dP baseline, which have been normalized for a constant temperature of 800°F and a constant face velocity of 3.5 ft/min, have been plotted, as have the changes in coal feeder speed and air-flow rate. These plots can be seen in Figures 3.6-10 through -12.

The first solids injection test used limestone, and this testing initially corresponded to a reduction in dP, although this reduction also corresponded to a significant reduction in air-flow

rate. As the test ended, dP increased but began increasing before solids injection ended. Limestone was retested, but once again system conditions changed during the testing. The pressure-drop rate and baseline decreased as the injection period began, although this trend started before injection. As the injection period concluded, dP baseline increased about 4 inH_2O, and this trend began before the injection stopped.

During the first Celite injection, the material would not convey adequately due to its flow characteristics. Therefore, limestone was added to Celite in the feeder surge bin in approximately a one-to-one weight ratio (about three times more Celite by volume), and this mixture could be conveyed to the PCD. At the beginning of this injection period on March 26, 2001, the air-flow rate dropped, so the reduction in dP could not be solely attributed to the additive. The beginning of the second Celite/limestone test on March 26, 2001, corresponded to a modest reduction in dP baseline as normalized baseline decreased from about 144 to 141 inH_2O and the dP increased after injection ended. This small reduction could not be directly attributed to changing operating conditions, and might have been caused by the additive. However, this apparent positive effect could not be reproduced in three subsequent Celite tests during which consistent solids feed was not achieved. The last Celite injection was intended to be a 24-hour test, but due to a blockage caused by a foreign object in the conveying line this test had to be ended after only about 6 hours.

The other materials, sand and ash, were both tested on March 27. As mentioned above, large sand was inadvertently used in the place of sand flour. Therefore, it is unlikely that any of this material reached the filter surfaces. The coal feeder tripped early in the ash injection test, and the coal-feed rate was unsteady throughout the testing period. There was no apparent effect on PCD dP from either material.

There were many areas of uncertainty associated with the solids injection testing including the following:

- Changing system conditions. Although the testing periods were anticipated as stable operating periods, system conditions changed often. During GCT4, the air flow rate, rarely constant, was manually controlled and was changed to maintain a constant temperature in the reactor. The coal feeder speed set point generally remained constant, although at times the speed changed due to various operational problems. Even with a constant coal feeder speed, the coal-flow rate is not constant, and this inconsistent coal-flow rate can cause fluctuations in the reactor temperature, which were met with changes in the air flow rate. Many other factors that could affect PCD dP, such as steam-flow rate and reactor velocity, changed during the testing.

- Solids injection rates. The amount of solids that were injected is not certain for any period because there is not an accurate solids flow measurement available for this system. Also, even with the same sorbent feeder speed, the solids-flow rate can vary and may not be consistent during a given period.

- Effect of loss of reactor sorbent. Since the reactor sorbent is inert and is carried over to the PCD, the addition of reactor sorbent affects solids loading. However, the extent

of this effect has not been quantified. Also, some chemical effects of the reactor sorbent are not certain but could affect PCD dP.

- Mixing of limestone with Celite. For the Celite injection tests, limestone was added to the Celite in the feeder surge bin. About 150 lb of each material was added alternately so that some mixing would occur. However, the extent of mixing could not be determined, and during these tests there may have been some periods of time when Celite was not being introduced to the PCD. Also, the extent of material segregation due to density differences is unknown.

- PCD pressure drop changes. Because PCD dP changes often (sometimes due to undetermined causes) the effect of solids injection may not be noticeable. Char bridging, found upon inspection, decreases filter area and would affect dP.

- Injection test durations. Since there was no on-line solids-flow rate measurement available, the test durations were estimated using weigh cell measurements and sorbent feed-line pressure changes.

3.6.2.4 Solids Injection Summary

During GCT4, limestone, Celite, sand, and combustion ash were injected into the PCD to determine if these materials could improve char cake qualities to the extent of appreciably reducing PCD pressure-drop rate and baseline. Nine injection tests were performed, including five Celite injections. During the first two celite injections a small reduction in pressure drop was observed. However, in the last three tests there was no noticeable reduction in pressure drop, possibly due to inconsistent sorbent feeder operation. There was no noticeable effect of the addition of the three other materials. The field results were consistent with the SRI lab study.

There were many areas of uncertainty associated with this solids injection experiment. Most importantly, process conditions were not constant, particularly the coal-feed and air-flow rates. Also, because of the frequent fluctuations in PCD dP that normally occur, small changes in dP are negligible. Solids injection testing would be more meaningful if performed during a steady test campaign. Also, accurate solids-flow measurements would be helpful in determining solids-injection rates as well as actual coal-feed rates.

3.6.3 Conclusions From Dustcake Additive Study

Based on both the laboratory and field results, none of the additives evaluated here would be expected to produce a substantial reduction in PCD ΔP. These results suggest that the addition of nonporous materials (flyash, pulverized limestone, etc.) increases dustcake areal loading as much or more than normalized drag is reduced. Consequently, these types of materials have no beneficial effect on PCD ΔP.

Unlike the other additives tested, Celite appeared to have a positive effect, probably because of its open structure. The open structure of the Celite allows it to modify the dustcake structure in

a beneficial way, and the open structure also results in a beneficial ratio of aerodynamic and physical particle sizes that allows the Celite to be carried over into the dustcake in larger particle sizes and concentrations. There could be other materials with these types of characteristics that may be even better than Celite, but none have been identified at this time.

Unfortunately, Celite is quite expensive compared to the other alternatives tested. Considering the relatively small benefit of the Celite in terms of ΔP reduction (20-percent reduction, at most), the cost of this material would probably be considered to be prohibitive in most situations. There could also be an issue of availability with this material.

Despite the above, there are situations where additives, even those that do not directly reduce dustcake pressure drop, might be effectively used. If collection of a sticky char in the PCD is resulting in an increasing residual dustcake thickness and creeping baseline pressure drop, it is possible that adding a particulate additive to the char dustcake could improve cleanability and help prevent further increases. The same might be true for consolidation problems like those encountered at the PSDF during combustion of petroleum coke with dolomite as a sorbent. In these cases, an inert additive could simply act as a buffer that would prevent the sticky or reactive particles from coming into contact with one another. By separating the particles that would otherwise tend to consolidate, the additive would provide low-cohesivity sites for the dustcake to fracture during cleaning. While this approach could be an effective means of bringing a creeping baseline ΔP under control, it seems unlikely that it could successfully reduce the baseline ΔP after it has already increased.

This study focused on attempting to reduce PCD ΔP, without significant hardware modifications, by adding a low-drag material to the existing char entering the PCD. A better approach may be to reduce the inlet char concentration by increasing the collection efficiency of the upstream cyclone. Figure 3.6-13 shows how normalized drag, areal loading, and PCD pressure drop change with char particle-size distribution. These data were generated with the RAPTOR device with the size-classification modifications described in Section 3.4. The data indicate that using a cyclone to reduce the median-particle size and particle loading to the dustcake reduces the areal loading much more than normalized drag is increased. Therefore, in theory, the more large particles that can be removed from the PCD inlet stream the lower the pressure drop will be. In actual practice, however, particles tend to become more cohesive as size is reduced, and it is likely that baseline creep problems will be encountered at median-particle sizes below about 5 μm and may be with larger sizes. However, with the very low char concentrations that would result with a very small median-size distribution, high additive levels could be used to prevent stickiness. The use of additives to prevent stickiness with very low char loadings might be a useful approach to maintaining low PCD ΔP with high-drag chars.

Table 3.6-1

Additives Evaluated in Drag Reduction Tests

Additive Name	Description	Percent of Additive $< 45\mu m$
Celite	Commercial Diatomaceous Earth	6
Limestone	Pulverized Sorbent From KBR Transport Reactor	41
AZS-45	FCC Support Media Tested at TRDU	24
Sand Flour	Very-Fine Pulverized Sand	32
Fine Sand	Transport Reactor Start-up Bed Material	1
PSDF Ash	TC05 Combustion Ash From Kellogg PCD	91
Gaston Ash	PRB Flyash From PC Boiler at Plant Gaston	70
Miller Ash	PRB Flyash From PC Boiler at Plant Miller	79
PSDF Char	Lower Drag Char From KBR Transport Reactor	85

Table 3.6-2

Drag Results for Blended Samples With TRDU Char

Material	% Mass Additive In		Normalized Drag (1)	Fractional Change In		
	Bed	Sample		Normalized Drag	Areal Loading	PCD ΔP
Pure TRDU Char	--	--	145.9	1.00	1.00	1.00
Celite	20	6.5	126.7	0.868	1.07	0.93
	50	24.2	77.1	0.528	1.32	0.70
	75	53.1	27.3	0.187	2.13	0.40
	100	100	10.4	--	--	--
Limestone	50	33	105.2	0.721	1.49	1.08
	75	63	63.4	0.435	2.70	1.17
	100	100	25.6	--	--	--
AZS-45	25	6.8	151.9	1.041	1.07	1.12
	50	19.7	132.2	0.906	1.25	1.13
	75	49	89.0	0.610	1.96	1.20
	100	100	14.6	--	--	--
Sand Flour	50	29.9	105.6	0.724	1.43	1.03
	75	60.2	67.1	0.460	2.51	1.16
	100	100	37.4	--	--	--
Fine Sand	50	0	149.4	1.00	1.00	1.00
PSDF Combustion Ash	25	21.5	124.0	0.850	1.27	1.08
	50	36.9	90.3	0.619	1.58	0.98
	75	60.5	60.3	0.413	2.53	1.05
	100	100	21.9	--	--	--
Flyash (Plant Gaston)	50	31.5	114	0.781	1.46	1.14
	100	100	21.8	--	--	--
Flyash (Plant Miller)	50	26	131.7	0.903	1.35	1.22
	100	100	29.4	--	--	--
PSDF Char	50	N.D.	146.9	1.007	2.00	2.01
	100	100	49.7	--	--	--

1. Units of: inWC/(ft/min)/(lb/ft^2)

Table 3.6-3

Results of Bulk Additive Drag Tests

Material	Additive Size	% Mass Additive In		Normalized Dustcake Drag *	Fractional Change In		
		Bed	Sample		Areal Loading	Normalized Drag	PCD Drag
Celite	< 45 μm	50	24.2	77.1	1.32	0.53	0.70
	Bulk	50	3.2	111	1.03	0.76	0.79
Limestone	< 45 μm	50	33	105.2	1.49	0.72	1.08
	Bulk	50	25	119.8	1.33	0.82	1.10
AZS-45	< 45 μm	50	19.7	132.2	1.25	0.91	1.13
	Bulk	50	8.8	155.4	1.10	1.07	1.17
Sand Flour	< 45 μm	50	29.9	105.6	1.43	0.72	1.03
	Bulk	50	26.8	124.2	1.37	0.85	1.16
PSDF Ash	< 45 μm	50	36.9	90.3	1.58	0.62	0.98
	Bulk	50	23.8	109.6	1.31	0.75	0.99

* - Units of inWC/(ft/min)/(lb/ft^2)

Table 3.6-4

Physical Characteristics and Cost of Solids Injection Test Materials

	D_{50} (μm)	σ_m (μm)	$d_{ps,v}$ (μm)	Bulk Density (g/cm^3)	True Density (g/cm^3)	Cost ($/lb)
Limestone	19.80	22.40	10.12	0.98	2.74	0.0023
Celite Diatomite	28.64	19.47	25.41	0.27	2.27	0.3477
Sand Flour	16.45	15.81	9.48	0.78	2.65	0.1270
Sand	145.01	55.63	163.96	1.47	2.64	0.0800
Ash, PC Boiler	15.12	27.42	5.69	0.96	2.58	--

Table 3.6-5

Solids Injection Test Periods

Field Test	Amount Fed	Start Time	End Time	Duration
Limestone Test 1	1,080 lb Limestone	3/24/01 - 23:49	3/25/01 - 03:00	3 hr, 11 min
Celite Test 1	220 lb Celite/ Limestone Mixture	3/25/01 - 22:56	3/26/01 - 00:34	1 hr, 38 min
Celite Test 2	520 lb Celite/ Limestone Mixture	3/26/01 - 03:00	3/26/01 - 06:00	3 hr, 0 min
Limestone Test 2	1,000 lb Limestone	3/26/01 - 23:45	3/27/01 - 02:03	2 hr, 18 min
Sand Test	1,200 lb Sand	3/27/01 - 02:34	3/27/01 - 04:34	2 hr, 0 min
Ash Test	1,500 lb Ash	3/27/01 - 05:16	3/27/01 - 09:35	4 hr, 19 min
Celite Test 3	380 lb Celite/ Limestone Mixture	3/27/01 - 10:21	3/27/01 - 11:27	1 hr, 6 min
Celite Test 4	370 lb Celite/ Limestone Mixture	3/27/01 - 14:10	3/27/01 - 16:52	2 hr, 42 min
Celite Test 5	1,230 lb Celite/ Limestone Mixture	3/27/01 - 18:10	3/28/01 - 00:00	5 hr, 50 min

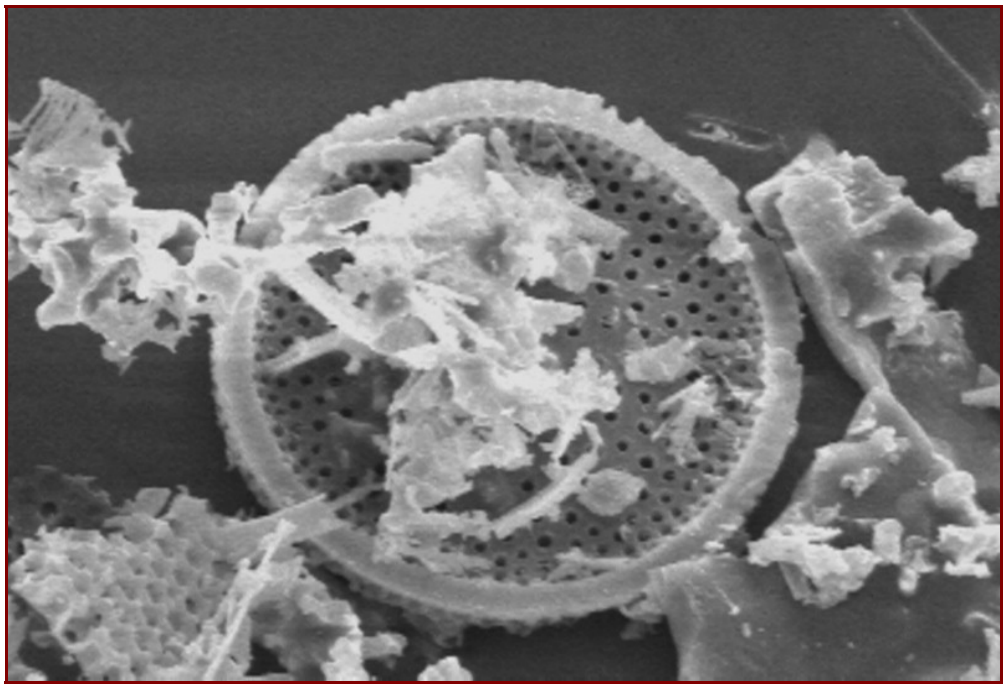

Figure 3.6-1 SEM Photo of Celite at 1,250x Magnification

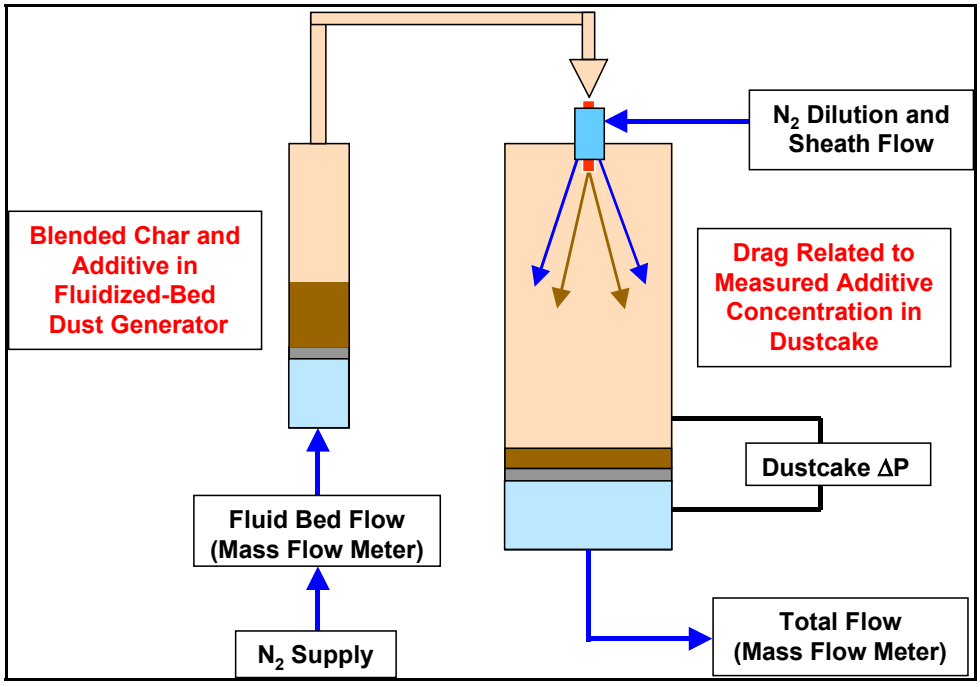

Figure 3.6-2 Resuspended Ash Permeability Tester (RAPTOR)

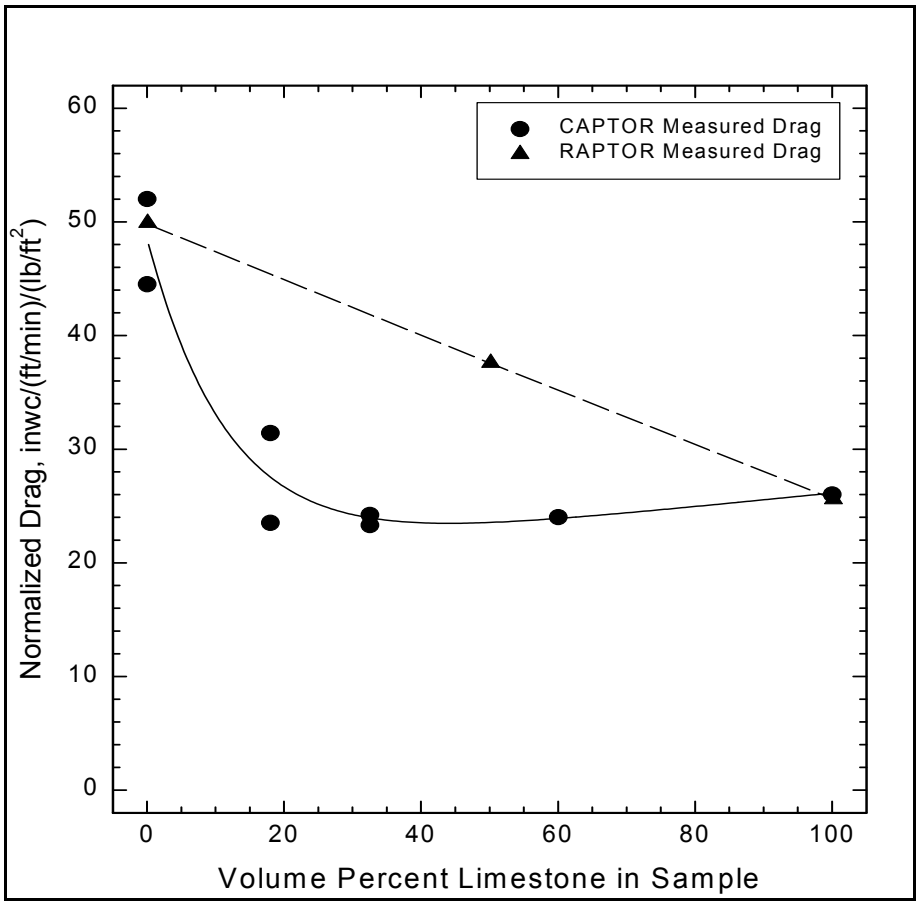

Figure 3.6-3 Comparison of RAPTOR and CAPTOR Additive Results

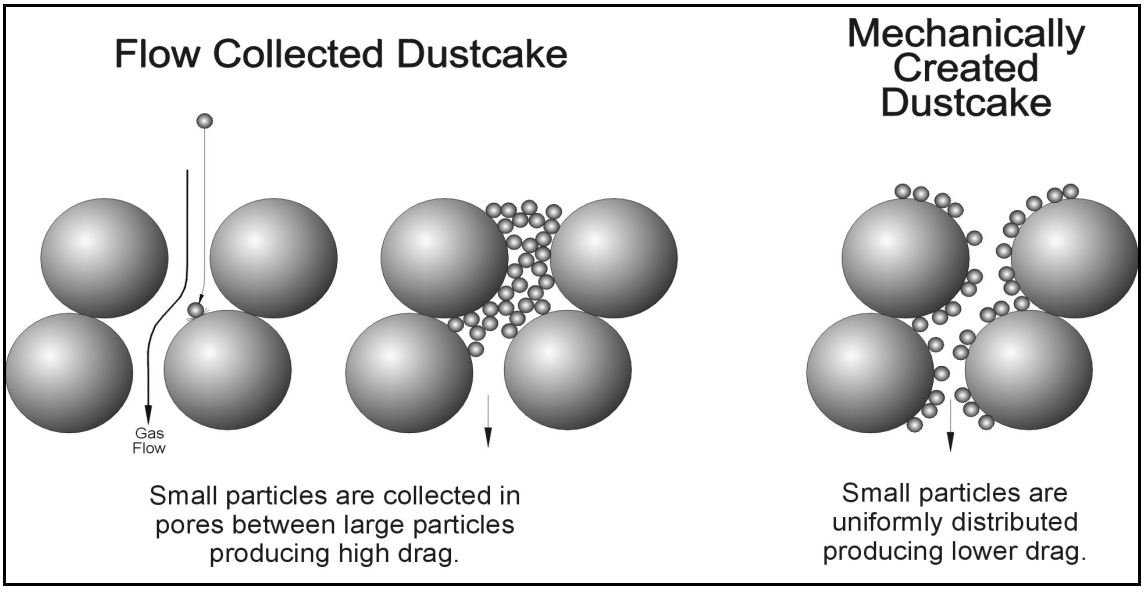

Figure 3.6-4 Structural Differences for Different Dustcake Creation Methods

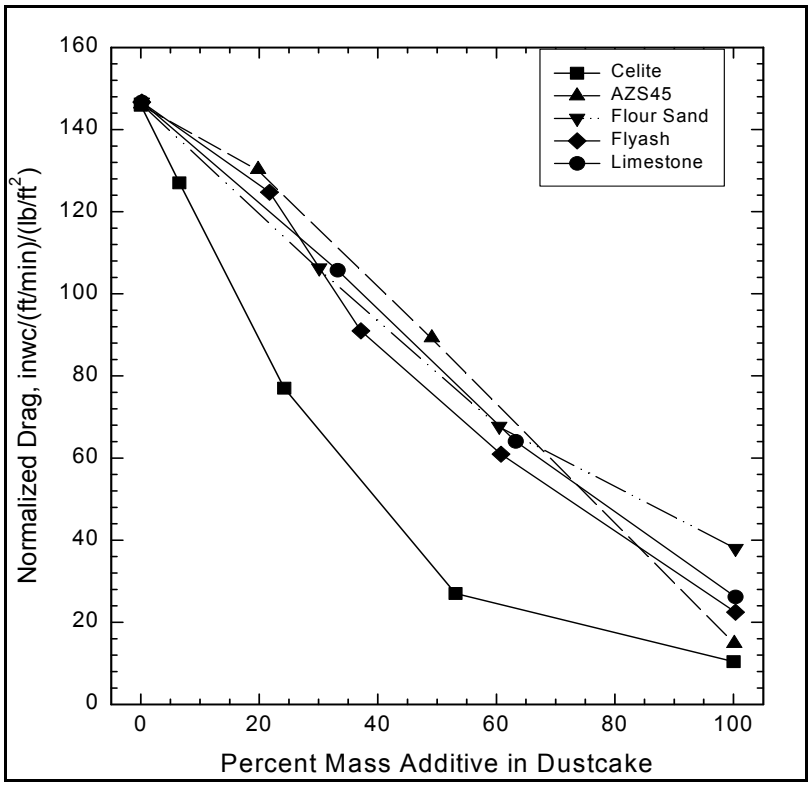

Figure 3.6-5 Effect of Additive Dustcake Concentration on Drag

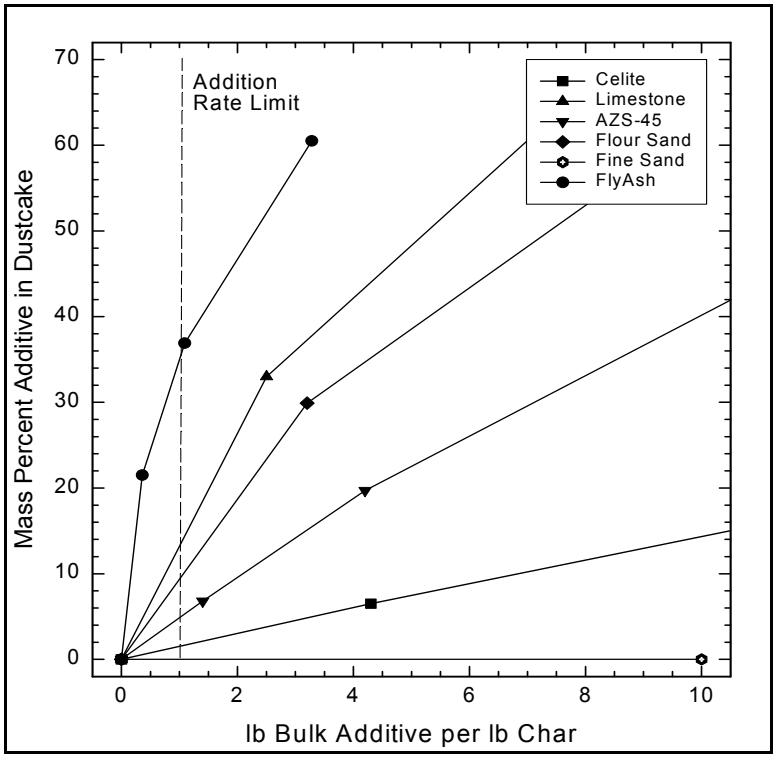

Figure 3.6-6 Additive Carryover Rates

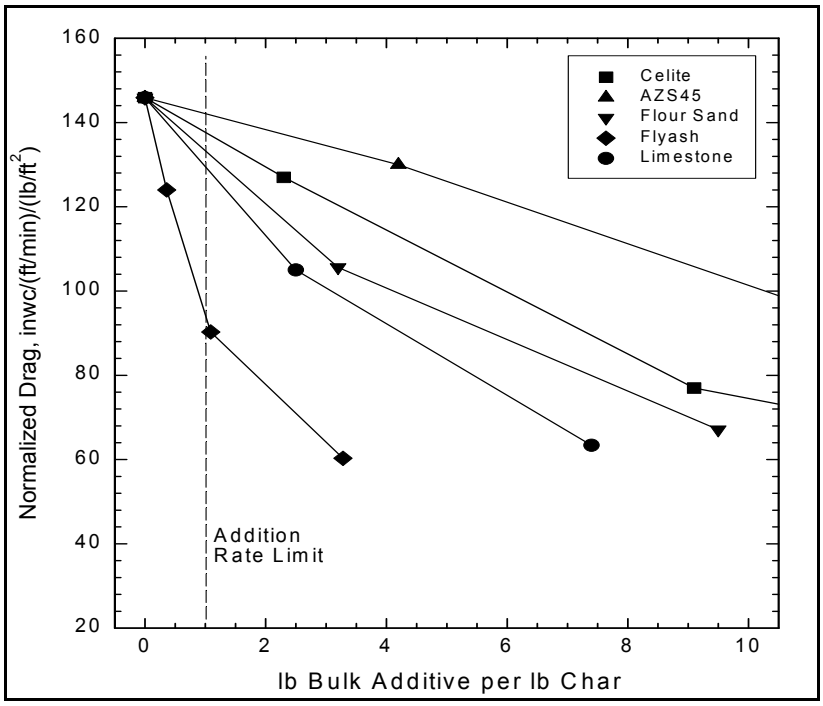

Figure 3.6-7 Effect of Bulk-Additive-Injection Rate on Dustcake Drag

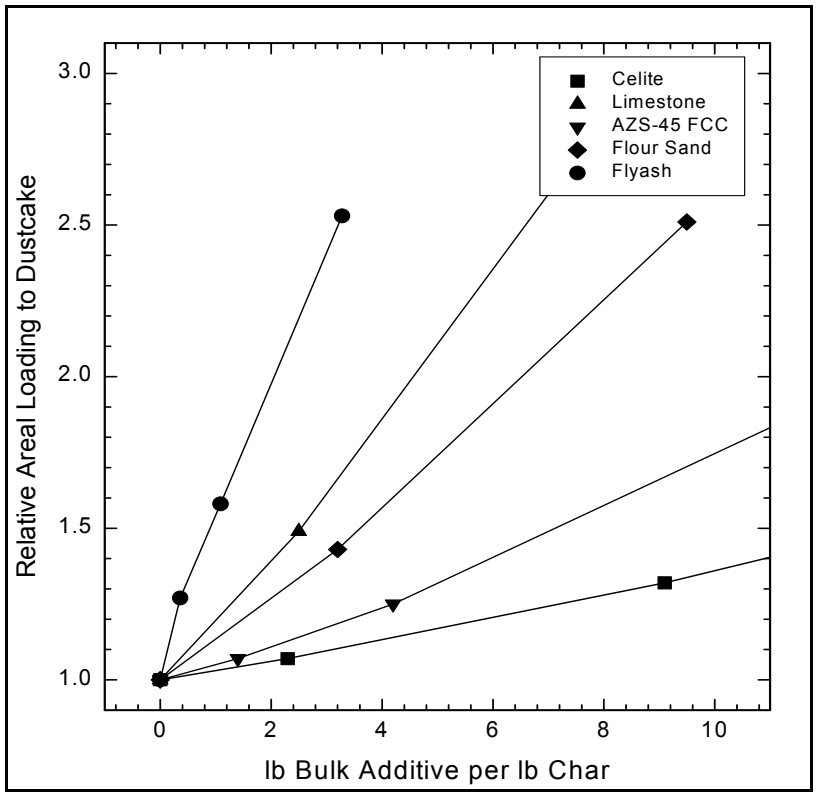

Figure 3.6-8 Effect of Bulk-Additive Rate on Dustcake Areal Loading

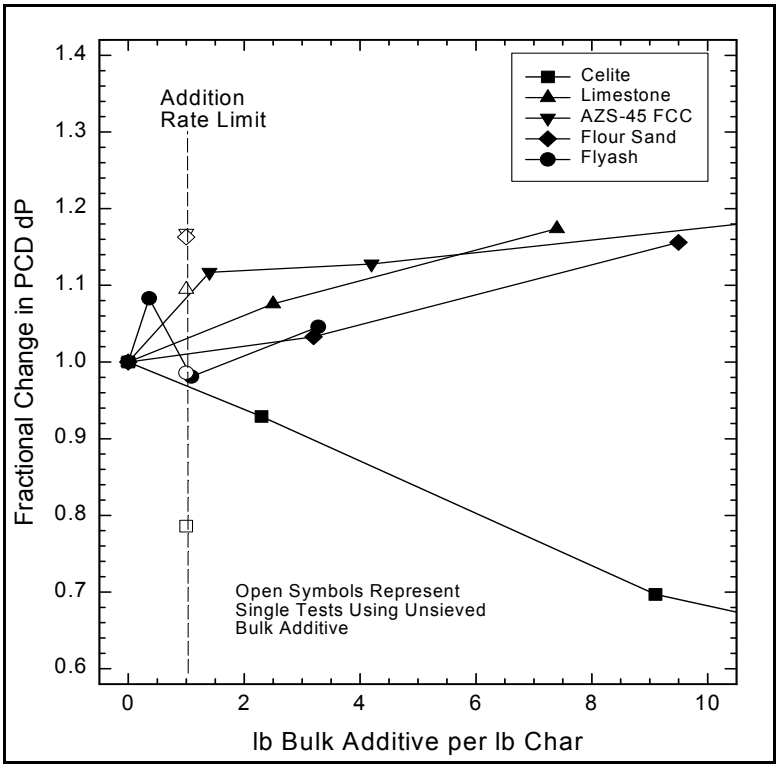

Figure 3.6-9 Effect of Bulk-Additive Rate on Dustcake Pressure Drop

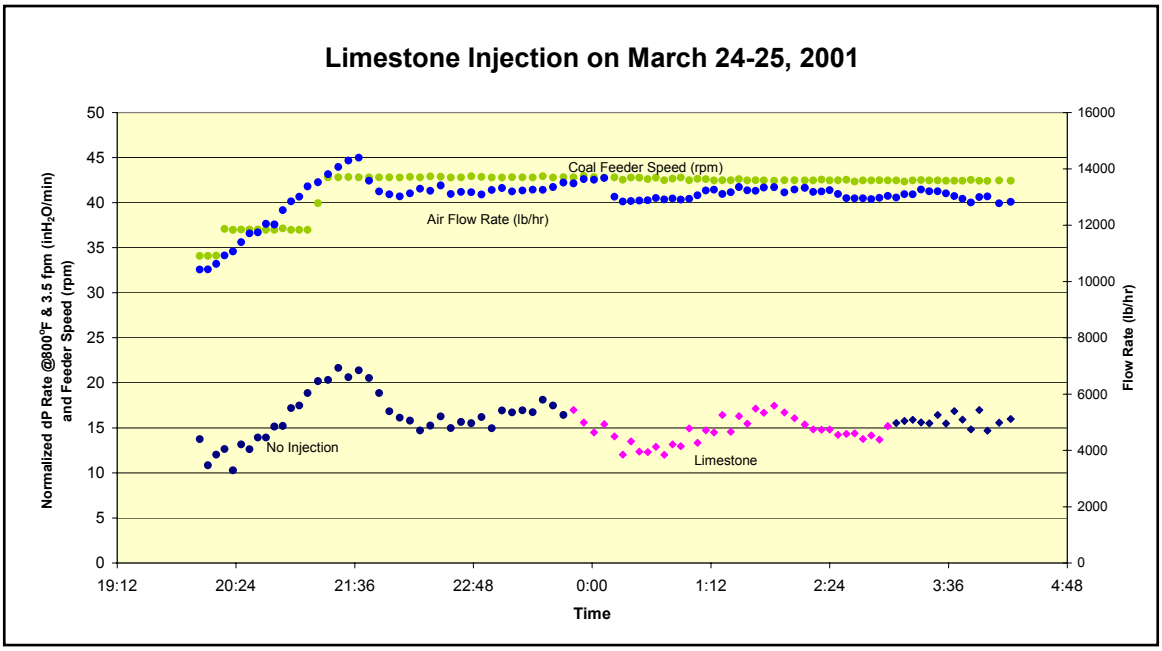

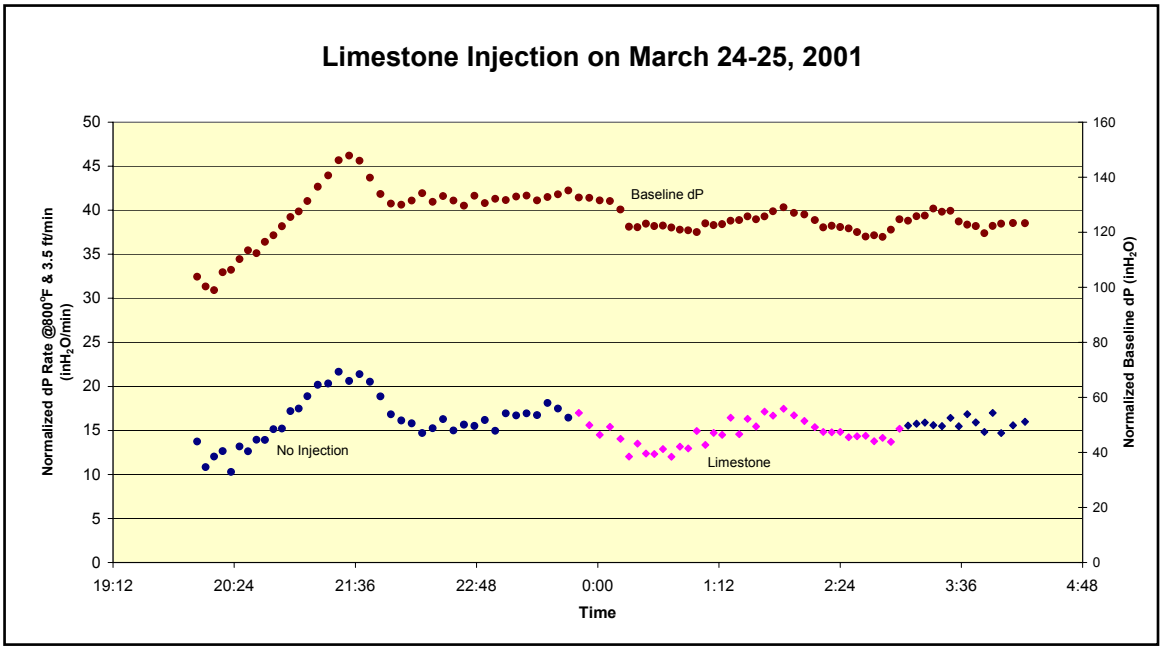

Figure 3.6-10 Limestone Injection on March 24 to 25, 2001

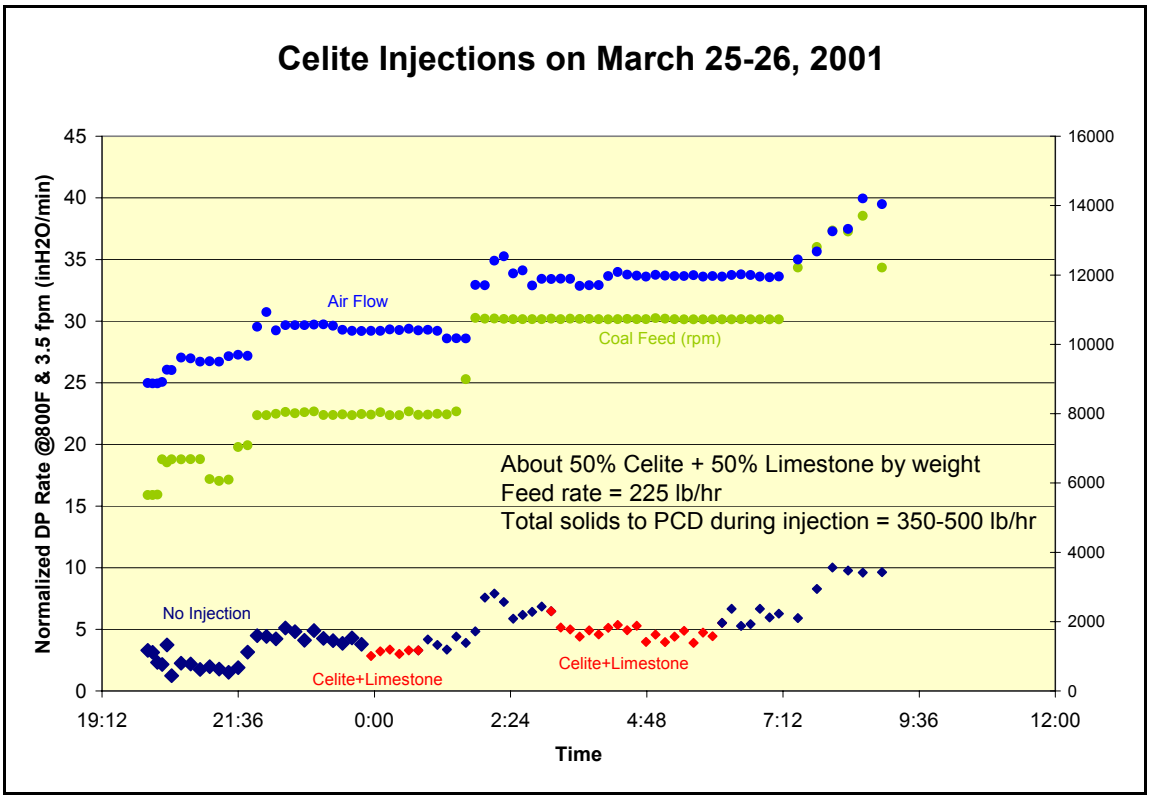

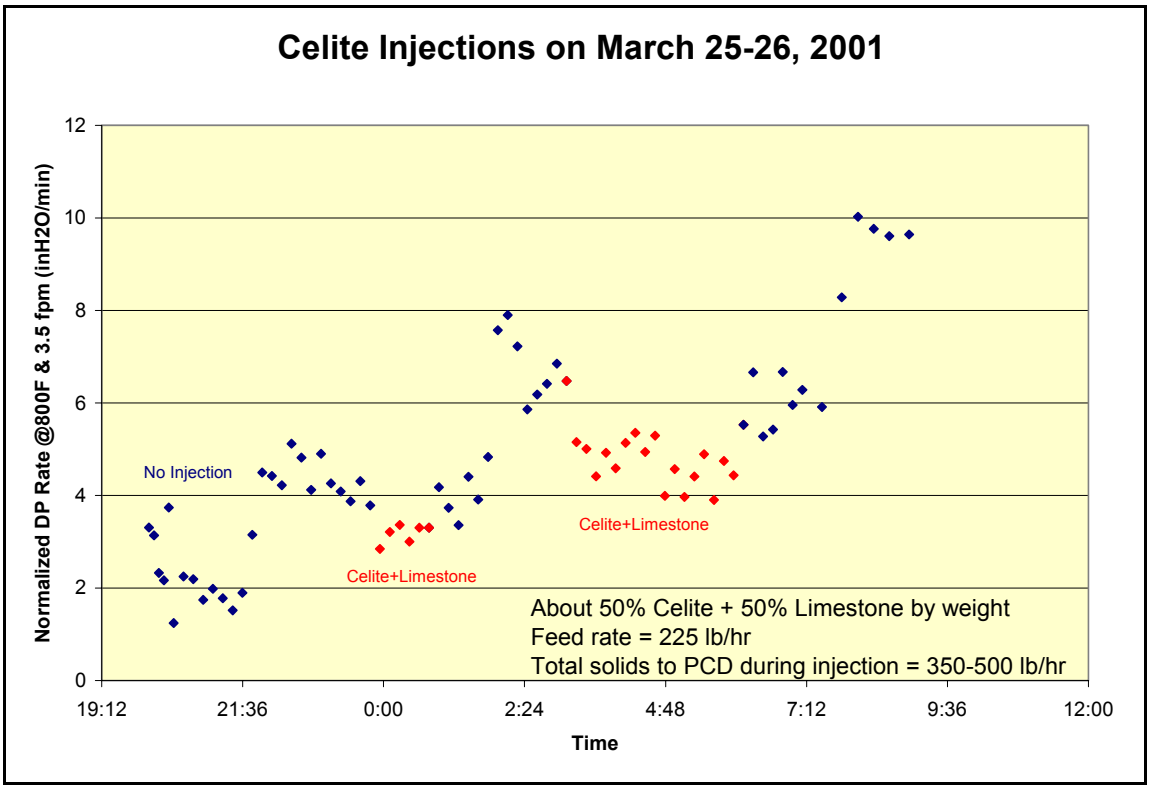

Figure 3.6-11 Celite Injections on March 25 to 26, 2001

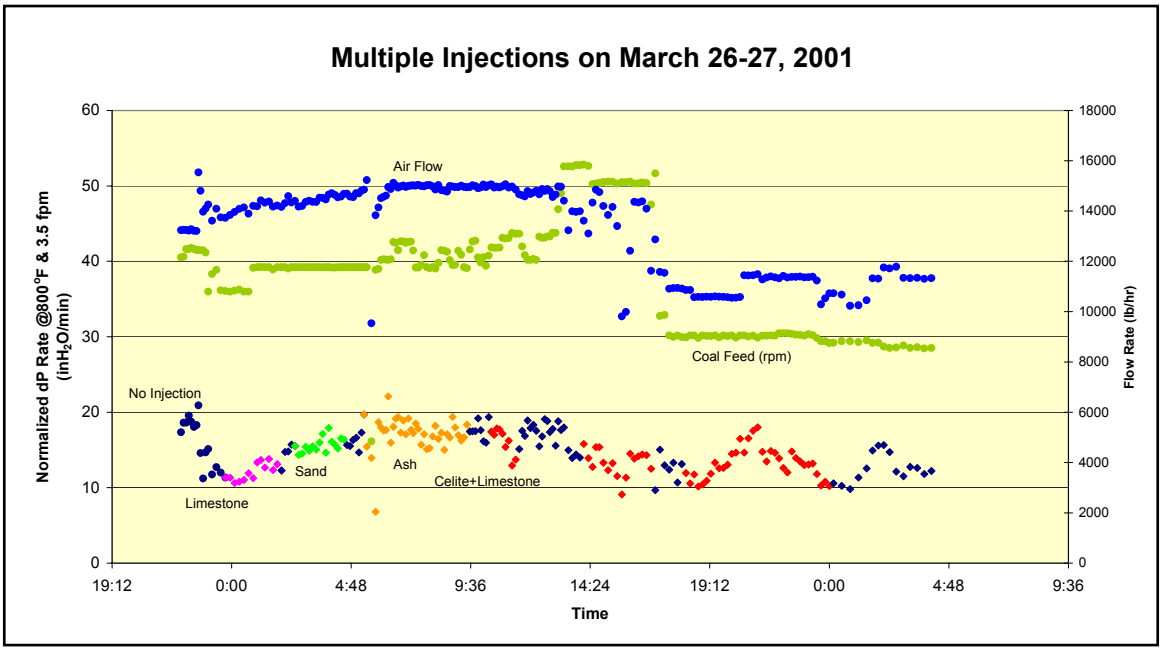

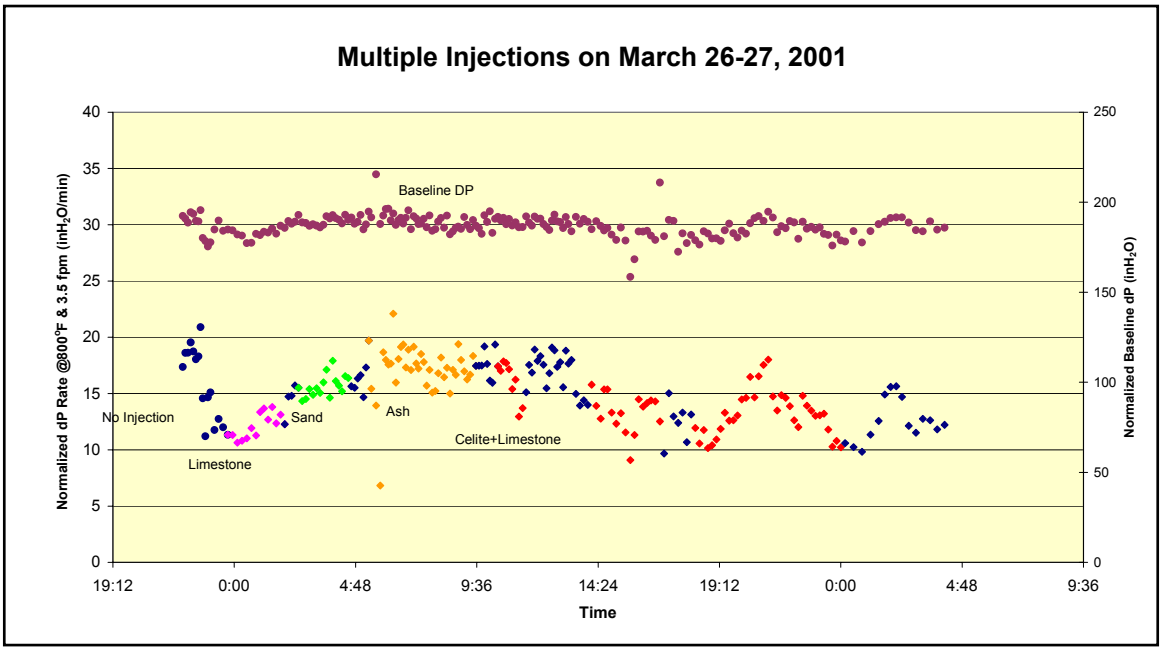

Figure 3.6-12 Multiple Injections on March 26 to 27, 2001

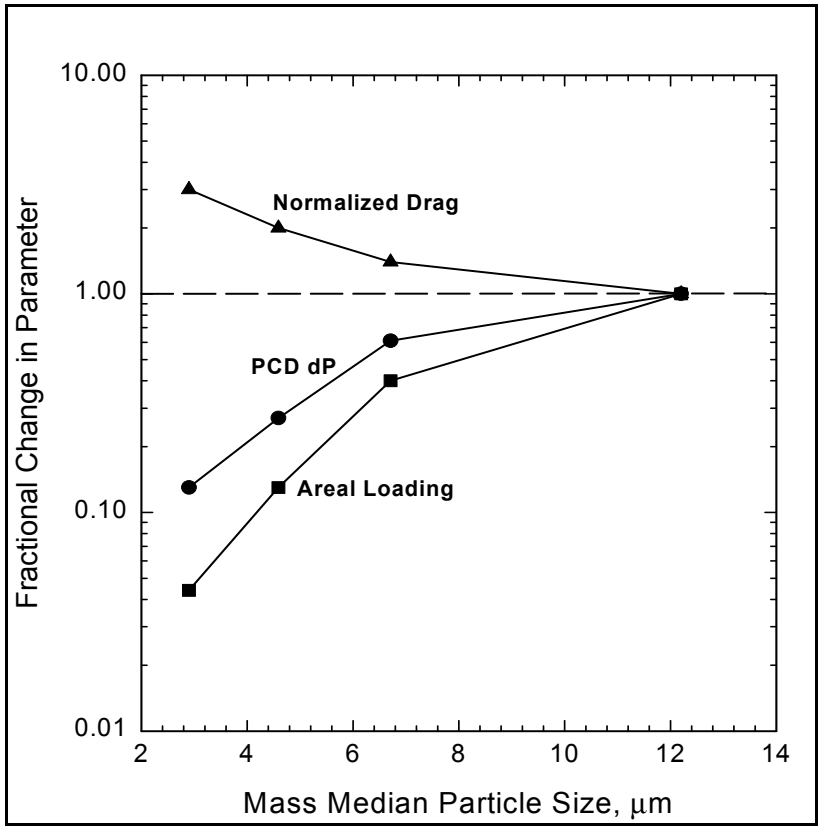

Figure 3.6-13 Effect of Char-Size Distribution on PCD Pressure Drop

4.0 TRANSPORT REACTOR

4.1 GCT4 RUN SUMMARY

After reactor pressure tests were completed in the first week of March the GCT4 test run began on March 7, 2001, with the startup of the main air compressor and lighting of the reactor start-up burner to increase reactor temperatures. After completion of the PCD warm-up, the reactor temperatures were increased on March 7 using the reactor start-up burner. When the reactor temperatures reached 1,200°F, coal feed was initiated on March 8. Between March 8 and March 30, 2001, 242 hours on coal were achieved with 518 tons of PRB coal gasified. The limestone for the run was Ohio Bucyrus. Various other materials were added to test pressure drop for the PCD.

The primary objective of test run GCT04 was:

- Operational Stability – Characterize reactor loop and PCD operations with short-term tests by varying coal-feed rate, air/coal ratio, riser velocity, solids-circulation rate, system pressure, and air distribution.

Secondary objectives included the following:

- Reactor Operations – Study the devolatilization and tar cracking effects from transient conditions during transition from start-up burner to coal. Evaluate the effect of process operations on heat release, heat transfer, and accelerated fuel particle heatup rates. Study the effect of changes in reactor conditions on transient temperature profiles, pressure balance, and product gas composition.

- Effects of Reactor Conditions on Synthesis Gas Composition – Evaluate the effect of air distribution, steam/coal ratio, solids-circulation rate, and reactor temperature on CO/CO_2 ratio, synthesis gas Lower Heating Value (LHV), carbon conversion, and cold and hot gas efficiencies.

- Research Triangle Institute (RTI) Direct Sulfur Recovery Process (DSRP) Testing – Provide syngas in support of the DSRP commissioning.

- Loop Seal Operations – Optimize loop seal operations and investigate increases to previously achieved maximum solids circulation rate.

Activities during the outage preceding and during test run GCT4 included about 28 equipment revisions. Those affecting the process the most were the installation and modifications listed below:

- Density measurement on the coal feed line was added, which combined with the conveying velocity enhanced the ability to measure coal flow. Simple flow control loop was configured utilizing this flow measurement.

- A pipe from the limestone feeder to the PCD inlet was added to test the effect of various materials on the PCD pressure drop.

- The pipes on the feeders from the coal mill pulverized silos were modified to allow for emptying the silos. Long radius elbows were replaced with crosses to provide a method to blow out the conveying line should plugging occur.

- Main reactor interlock was modified to switch reactor air to nitrogen when FD0210 motor stops based on additional PLC output.

- Since another filter bag fell from the coal feeder baghouse into the coal feeder surge bin, a mesh below the filter bags was added to catch falling bags.

Prior to startup the gas analyzers could not be put into service due to a high differential pressure in the flare line caused by sand in the flare seal drum. A bleed on a double block was inadvertently left open causing the sand to flow into the flare header line and, eventually, the flare seal drum. After completing all other startup activities, coal feed was started at 03:27 on March 8, 2001. Approximately 11 hours later the reactor was tripped off-line when the coal feed isolation valve tripped close due to a PLC configuration problem. After revisions to the PLC program coal feed was resumed at 00:03 on March 9. At 01:44 on March 10 the coal feeder tripped due to a malfunction with the coal feeder lock vessel valve. The malfunction was caused by material accumulation in the shuttle valves. After cleaning the shuttle valves, coal feed was resumed at 12:16 on March 10. The coal feeder tripped again on March 12 due to a high coal conveying line pressure. When problems persisted as attempts were made to restart the coal feeder, it was decided to shut the system down at 07:22. Debris caused by problems with the coal mill baghouse as well as a coal surge bin filter that was accumulated in the coal feeder elbow was cleaned out. A 9-day outage was taken to repair a bent sweeper arm in the KBR coal mill. Due to problems with the FW mill, it was not operated for the rest of the run. A screen was placed below the bags in the coal feeder surge bin to prevent further interruptions from fallen bags.

Coal feed resumed at 23:45 on March 20. Six hours later a leak on the flange above the primary cyclone was detected. Coal feed was stopped at 08:18 on March 21 to tighten the flange at pressure but it was not successful. The reactor was depressurized and the flange gasket was replaced. The reactor was successfully pressure tested to 275 psig before starting again. Coal feed resumed at 02:40 on March 22. Within 5 hours the flange leak returned. Again, coal feed was stopped and the reactor was depressurized. The flange was tightened more and the reactor was pressure checked at 275 psig without leaks. (Maintenance believes that the flange is over torque so they are going to tighten only enough to hold pressure.) Coal feed was started at 02:02 on March 24. At 05:05 several flange leaks were found and hot bolted. For the remainder of the run there were multiple problems with the coal feeder lock vessel due to solids retention in the lock vessel. The run was terminated at 08:18 on March 30, 2001, because of problems with the KBR coal mill.

During the run, the nonintrusive density measurements on the coal feed line, coupled with pressurized conveying gas velocity measurements, enhanced the ability to measure instantaneous coal-feed rates. Online calibration techniques were being developed to improve accuracy. The controls algorithm to maintain mass-flow rate of coal by varying feeder speed was successfully tested.

Also during the run, syngas was successfully delivered to the RTI DSRP. RTI successfully sampled and analyzed the syngas and tail gas and conducted the DSRP.

Post run inspections revealed that the riser refractory is showing more wear since starting gasification. The disengager roof was in excellent condition and the cyclone roof also appears to be in good condition. However, the sulfator refractory that was previously replaced is showing significant wear and cracks.

The run was broken down into the following steady-state test periods:

	Comments
GCT4-1	First steady state period
GCT4-2	Increased pressure and temperature
GCT4-3	Increased air flow
GCT4-4	Higher temperature, high air flow
GCT4-5	Reduced air flow, reduced coal feed
GCT4-6	Reduced pressure, increased air flow, increased FV289 steam
GCT4-7	High temperatures, increased coal feed, increased standpipe level
GCT4-8	Reduced coal feed, high standpipe level, reduced air flow
GCT4-9	Low standpipe level, high coal feed, reduced FV289 steam
GCT4-10	Reduced air flow, increased standpipe level
GCT4-11	Slightly increased air flow
GCT4-12	Reduced pressure, higher standpipe level
GCT4-13	Increased pressure, reduced coal feed, reduced air flow
GCT4-14	Increased air flow, increased coal feed
GCT4-15	Increased air flow, increased coal feed
GCT4-16	Increased steam flow, increased air flow, increased coal feed
GCT4-17	Higher temperatures, increased steam, increased air flow
GCT4-18	Reduced pressure, increased standpipe level
GCT4-19	Increased air flow, increased coal feed
GCT4-20	Increased air flow, decreased standpipe level
GCT4-21	Increased coal feed
GCT4-22	Reduced air flow, reduced coal feed
GCT4-23	Increased standpipe level
GCT4-24	High standpipe level, reduced coal feed
GCT4-25	Long steady-state run at low coal-feed rate
GCT4-26	Increased air flow, high standpipe level
GCT4-27	Increased coal feed
GCT4-28	Low temperature
GCT4-29	Lowered coal feed, FD0510 off

GCT4-30	Lowered coal feed, FD0510 on
GCT4-31	Increased air flow
GCT4-32	Increased pressure, higher standpipe level
GCT4-33	Increased coal feed, higher temperatures
GCT4-34	Increased coal feed, decreased standpipe level

Table 4.1-1

GCT4 Planned Operating Conditions for Transport Reactor

Start-up Bed Material	Sand (~ 120 μm)
Fuel Type	Powder River Basin
Fuel Particle Size (mmd)	250 to 400 μm
Average Fuel-Feed Rate (pph)	4,000 to 6,000
Sorbent Type	Ohio Bucyrus Limestone
Sorbent Particle Size (mmd)	10 to 30 μm
Sorbent Feed Rate	As required for 90-%+ sulfur capture and tar formation reduction
Reactor Temperature (°F)	1,750 to 1,825
Reactor Pressure (psig)	160 to 240
Riser Gas Velocity (fps)	min to 50
Solids Circulation Rate (pph)	100,000 to 400,000 (slip ratio = 2)
Primary Gas Cooler Bypass	0%
PCD Temperature (°F)	700 to 900
Total Gas Flow Rate (pph)	18,000 to 26,000
Air/coal Ratio	As needed to control reactor temperature
Primary Air Split ($1^{st}/2^{nd}$ Levels)	50/50 to 90/10
Steam/Coal Ratio	0.2 to 0.5
Sulfator Operating Temperature (°F)	1,500 to 1,600
Planned Duration of Coal Feed	Nominally 250 hours

Table 4.1-2

PRB Coal Analyses As Fed

	Weight Percent
Moisture	19.5
Ash	5.6
Sulfur	0.3
C	57.8
H	4.0
N	0.7
O	12.0
Vol	35.0
Fix C	41.0
Heating Value	9,550(Btu/lb)

Table 4.1-3

Sorbent (Bucyrus Limestone From Ohio) Analyses

	Weight Percent
$CaCO_3$	77.6
$MgCO_3$	16.5
Inerts	5.9

Table 4.1-4
(Page 1 of 2)

Operating Periods

	Start	End	MZ temp °F	Rsr Temp °F	Pres (psig)	Coal-Feed Rate (lb/hr)	Air Flow (lb/hr)	Air/Coal	Air/C	Steam Flow (lb/hr)	Steam/ Coal
GCT4-1	3/8/01 07:15	3/8/01 08:45	1,630	1,650	200	5,158	14,299	2.77	5.04	0	0
GCT4-2	3/9/01 18:15	3/9/01 20:15	1,767	1,741	240	4,489	12,925	2.88	5.23	94	0.01
GCT4-3	3/10/01 16:00	3/10/01 17:00	1,760	1757	240	4,799	15,730	3.28	5.96	23	0.00
GCT4-4	3/10/01 17:00	3/10/01 18:00	1,785	1,782	240	4,800	15,760	3.28	5.97	12	0.00
GCT4-5	3/10/01 18:30	3/10/01 20:00	1,728	1,709	240	3,582	11,431	3.19	5.80	6	0.00
GCT4-6	3/11/01 01:45	3/11/01 05:00	1,796	1,776	236	5,405	16,130	2.98	5.43	746	0.14
GCT4-7	3/11/01 05:30	3/11/01 08:15	1,797	1,776	236	5,552	15,892	2.86	5.20	972	0.18
GCT4-8	3/11/01 16:45	3/11/01 17:45	1,744	1,713	236	3,943	12,205	3.10	5.63	1,075	0.27
GCT4-9	3/24/01 22:30	3/25/01 00:30	1,714	1,684	240	5,383	13,231	2.46	4.47	6	0.00
GCT4-10	3/25/01 00:30	3/25/01 01:30	1,700	1,671	240	5,371	13,050	2.43	4.42	6	0.00
GCT4-11	3/25/01 01:30	3/25/01 03:30	1,706	1,681	240	5,367	13,148	2.45	4.45	7	0.00
GCT4-12	3/25/01 15:45	3/25/01 17:30	1,726	1,718	224	5,217	13,884	2.66	4.84	82	0.01
GCT4-13	3/25/01 18:45	3/25/01 20:00	1,730	1,711	232	2,090	8,884	4.25	7.73	40	0.02
GCT4-14	3/25/01 20:30	3/25/01 21:30	1,744	1,725	232	2,491	9,573	3.84	6.99	33	0.01
GCT4-15	3/25/01 22:00	3/26/01 00:45	1,749	1,728	232	3,284	10,490	3.19	5.81	23	0.01
GCT4-16	3/26/01 02:45	3/26/01 07:15	1,750	1,736	232	4,352	11,924	2.74	4.98	242	0.06
GCT4-17	3/26/01 09:00	3/26/01 10:30	1,774	1,762	232	4,970	13,576	2.73	4.97	384	0.08
GCT4-18	3/26/01 23:30	3/27/01 00:30	1,755	1,761	220	4,948	13,926	2.81	5.12	461	0.09
GCT4-19	3/27/01 01:00	3/27/01 05:15	1,753	1,759	220	5,182	14,444	2.79	5.07	485	0.09
GCT4-20	3/27/01 08:00	3/27/01 09:30	1,755	1,740	220	5,246	14,942	2.85	5.18	472	0.09
GCT4-21	3/27/01 10:30	3/27/01 11:30	1,756	1,743	220	5,384	14,936	2.77	5.04	434	0.08
GCT4-22	3/27/01 18:30	3/27/01 19:30	1,645	1,618	220	4,345	10,590	2.44	4.43	446	0.10
GCT4-23	3/28/01 05:30	3/28/01 08:30	1,679	1,659	220	4,108	11,242	2.74	4.98	454	0.11
GCT4-24	3/28/01 08:45	3/28/01 10:00	1,713	1,692	220	3,671	11,064	3.01	5.48	401	0.11
GCT4-25	3/28/01 12:30	3/28/01 16:00	1,707	1,679	220	3,659	10,880	2.97	5.41	509	0.14

Table 4.1-4
(Page 2 of 2)

Operating Periods

	Start	End	MZ temp °F	Rsr Temp °F	Pres (psig)	Coal-Feed Rate (lb/hr)	Air Flow (lb/hr)	Air/Coal	Air/C	Steam Flow (lb/hr)	Steam/ Coal
GCT4-26	3/28/01 19:15	3/28/01 22:30	1,683	1,668	220	3,670	11,090	3.02	5.49	446	0.12
GCT4-27	3/29/01 00:15	3/29/01 04:00	1,687	1,678	220	3,944	11,474	2.91	5.29	451	0.11
GCT4-28	3/29/01 06:00	3/29/01 08:00	1,675	1,663	220	3,965	11,283	2.85	5.17	381	0.10
GCT4-29	3/29/01 10:30	3/29/01 12:20	1,690	1,680	220	3,771	11,006	2.92	5.31	382	0.10
GCT4-30	3/29/01 12:20	3/29/01 14:45	1,695	1,683	220	3,766	11,318	3.01	5.46	394	0.10
GCT4-31	3/29/01 15:00	3/29/01 16:30	1,679	1,668	220	3,787	11,558	3.05	5.55	443	0.12
GCT4-32	3/29/01 17:00	3/29/01 18:00	1,683	1,676	240	3,800	11,330	2.98	5.42	220	0.06
GCT4-33	3/29/01 18:30	3/29/01 20:00	1,724	1,724	240	4,337	12,894	2.97	5.41	188	0.04
GCT4-34	3/29/01 20:45	3/29/01 22:00	1,729	1,721	240	4,645	13,376	2.88	5.24	183	0.04

4.2 REACTOR TEMPERATURE PROFILES

Section 4.2 describes the temperature profiles in runs GCT2 through GCT4. The temperature profiles were plotted for similar operating conditions for a low and high solids-circulation steady state operating period in each test run. In GCT2 the solids collection system limited the solids-circulation rate, so there is only a low solids circulation plot for GCT2. The high solids-circulation rates in GCT3 and GCT4 were about 3 times higher than the low solids-circulation rates, respectively.

Figure 4.2-1 provides the temperature profiles for low solids-circulation rates during GCT2 through GCT4. The plots are similar in that all show a general increase in temperatures, with height into the upper mixing zone and then a decrease in temperatures as the solids and gas mixture move up through the riser. The increases and decreases in temperature in the mixing zone are also similar with the magnitudes being slightly higher for GCT2. These increases and decreases are due to the entry locations of the air, steam, nitrogen, coal feed, and sorbent feed. Figure 4.2-2 provides the temperature profiles for low and high solids-circulation rates during GCT3 and GCT4. Again, the profiles are similar in that all show a general increase in temperatures with height into the upper mixing zone and then a decrease in temperatures as the solids and gas mixture move up through the riser. However, the temperature decrease in the riser is higher for the low solids-circulation operating period in both GCT3 and GCT4. The temperature decrease in the riser also appears to be higher in GCT3 than in GCT4 for both solids-circulation rates. This effect is likely due to modifications that were made to the installation of the riser thermocouples in the outage before GCT4.

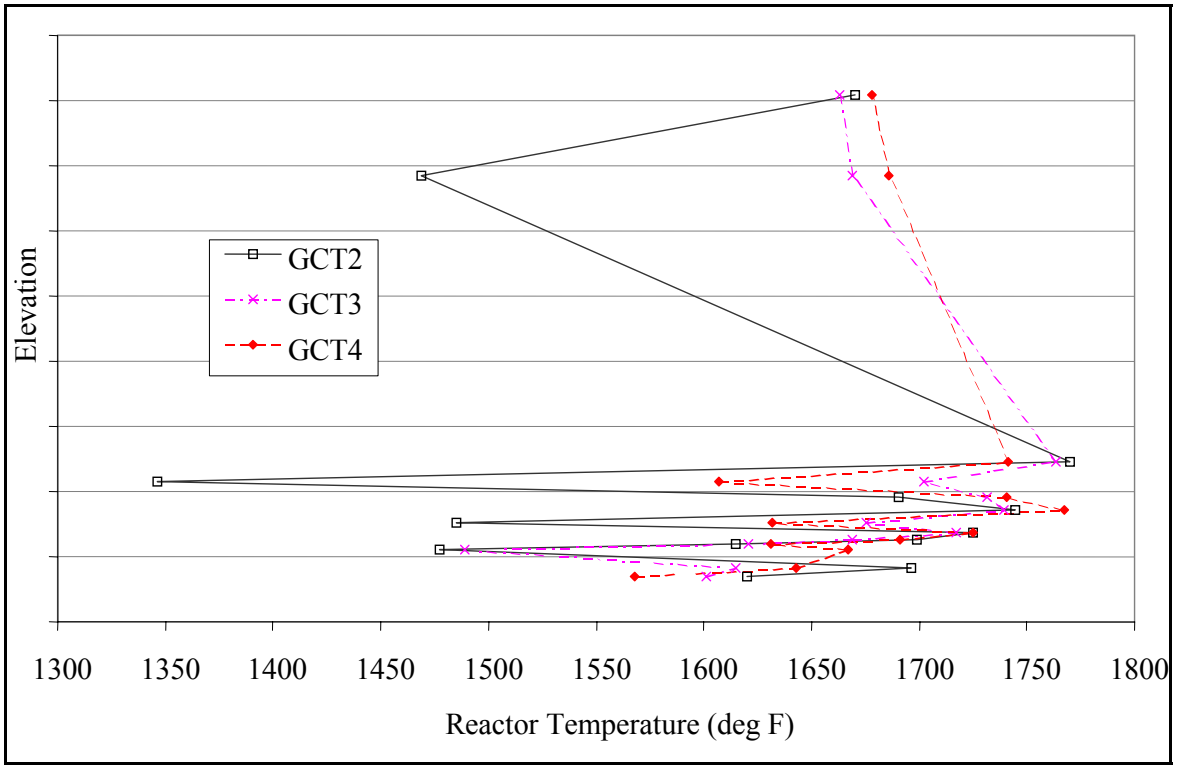

Figure 4.2-1 Temperature Profiles for Low Solids-Circulation Rates During GCT2 Through GCT4

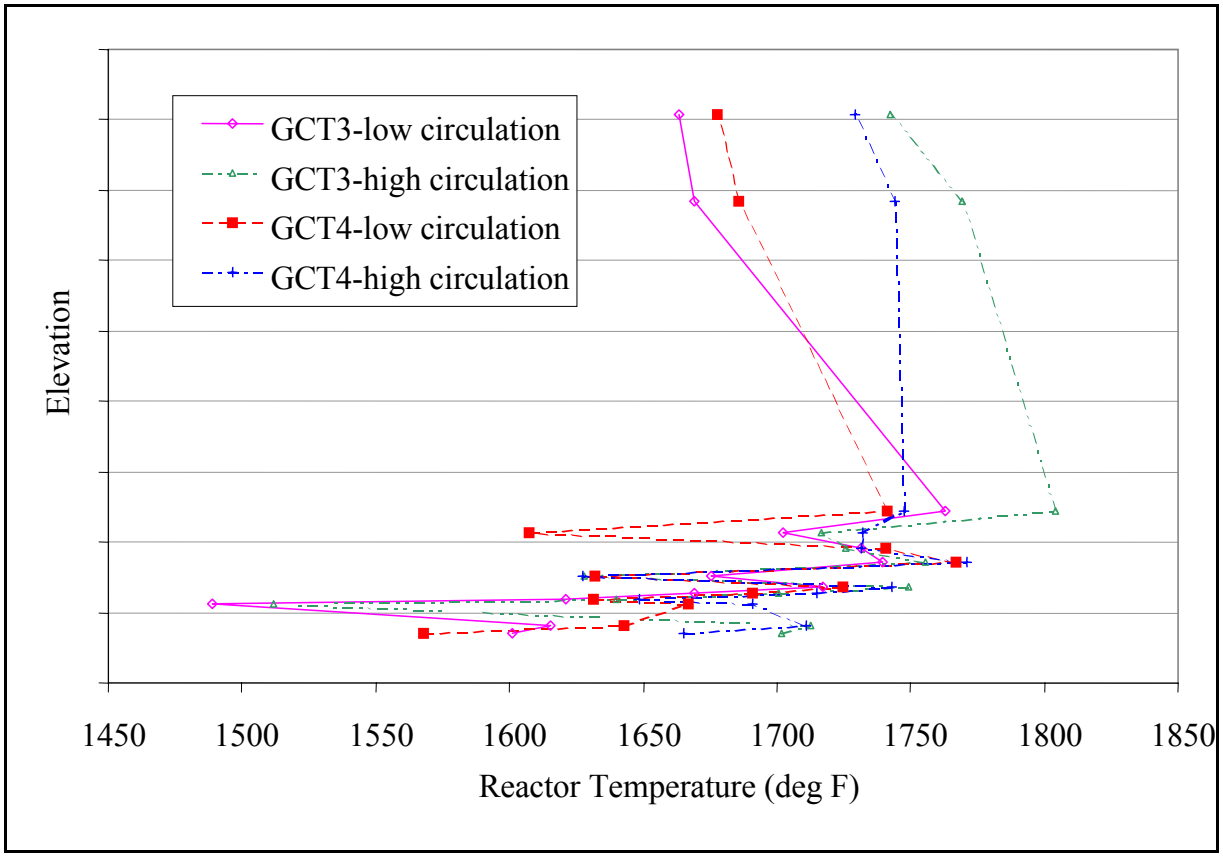

Figure 4.2-2 Temperature Profiles for Low and High Solids-Circulation Rates During GCT3 and GCT4

4.3 GAS ANALYSIS

Synthesis gas and synthesis gas combustor outlet gas analyzers were continuously monitored during GCT4 and recorded by the plant information (PI) system. Several in situ grab samples of synthesis gas moisture content were measured during the PCD outlet loading sampling. The Research Triangle Institute (RTI) measured synthesis gas compositions during a portion of GCT4 and results were made available to the PSDF. This section will use gas analyzer data to show:

- Synthesis gas heating value.
- Synthesis gas molecular weight.
- Synthesis gas compositions, for CO, H_2, CO_2, H_2O, N_2, CH_4, $C_2H_6^+$, and total reduced sulfur (H_2S, COS, and CS_2).
- Sulfur removal and emissions.
- Equilibrium H_2S concentrations.

GCT4 coal feed began on March 8, 2001, and ended on March 30, 2001. The run consisted of two periods of operation; the first was March 8 to March 12, 2001, with eight steady periods of operation (GCT4-1 to -8) (see Table 4.1-4 for the steady periods of operations). The second period of operation was March 21 to March 30, 2001, with 26 periods of operation (GCT4-9 to -34). The only fuel used during GCT4 was Powder River Basin coal, a mixture of four different coals. The sorbent used was Ohio Bucyrus limestone.

Figure 4.3-1 shows the first 5 days of operation (GCT4-1 to -8) hourly averages for the mixing zone temperatures, PCD (FL0301) temperatures, and reactor pressures. The data for the operating periods are shown in Table 4.3-1. Operation on March 8 lasted only 10 hours before shutting down due to a coal feeder trip. The reactor mixing zone temperature stabilized at 1,650°F for 5 hours, but the pressure was in the process of being increased to full operating pressure. The PCD inlet temperature was gradually decreasing during operation on March 8.

The unit was then restarted on March 9 and operated for about 24 hours. This was the GCT4-2 operating period. The mixing zone temperature increased to 1,800°F after startup and was constant for about 6 hours. Temperature varied between 1,600 and 1,775°F for the afternoon of March 9, when the coal-feed system was unstable with pressure at either 220 or 240 psig. PCD temperature slowly decreased to 800°F at 14:00 and then was constant.

The unit was then restarted on March 10 at 12:00 and operated for about 2 days, including operating periods GCT4-3 to -8. The reactor temperature was maintained at 1,800°F for most of March 10 and 11, with a few drops in temperature due to coal trips at 22:45 on March 11 and at 22:00 on March 12. Unit pressure was maintained at 230 to 240 psig. PCD temperature slowly decreased from 900 to 800°F during the first 24 hours after startup on March 10, and

then leveled off at around 800°F. Testing stopped when coal feeder inspections revealed FD0210 vent filter bag material in the feeder system.

The first 5 days of operation (GCT4-1 to -8) hourly averages for the coal-feed rate and the air rate are shown in Figure 4.3-2. The coal-feed rate was calculated from a correlation that used the coal feeder speed and the FD0210 weight cell data (see Section 4.5). The air rate was obtained from FI205. During the first 5 days of operation the coal rate was intermittent due to operational problems with the coal feed system. The low excursions of the air rates are also a result of coal feeder trips. The decrease in air rate at 14:00 on March 11 was to conserve coal due to problems in the coal grinding system, which were corrected without taking the transport reactor off-line.

The hourly synthesis gas (FI465_COMP) and aeration instrument nitrogen (FI609) rates are shown in the plot in Figure 4.3-3. It is estimated that about 1,000 lb/hr from FI609 does not enter the process, but is used to seal valves, pressurized/depressurized feed and ash lock hopper systems, and in the seals for the screw coolers. Values shown in Figure 4.3-3 assume that 1,000 lb/hr of nitrogen from FI609 does not enter the transport reactor. The synthesis gas rate varied widely during the first 5 days of GCT4 operation. The March 10 synthesis gas rate varied from 18,500 to 27,500 lb/hr. Synthesis gas rates on March 10 were constant at around 25,000 lb/hr, until the coal trip at 22:00. The synthesis gas rates were at 28,000 or 17,000 in between the coal trips during the last 2 days of operation. The nitrogen rate was between 5,000 and 8,000 lb/hr during the first 5 days of operation.

The last 7 days of GCT4 operation (GCT4-9 to -34) hourly averages for the mixing zone temperatures, PCD (FL0301) temperatures, and reactor pressures are shown in Figure 4.3-4. The data for the operating periods are shown in Table 4.3-1. The unit was started up on March 24 and ran until March 30, with coal trips on March 25 and 26. The coal feed system seemed to operate better after the reactor pressure was lowered to 220 psig. On startup, the mixing zone temperature was increased to 1,625°F and held there for about 12 hours. The temperature was then raised to 1,700°F until the coal trip on March 25. In between the coal trips that occurred on March 25 and 26 the temperature was held constant at 1,750°F. The final 4 days of operation were free of coal trips. The temperature was held constant at 1,750°F for the first 15 hours of March 27. The coal and air rates were decreased at 17:00 on March 27 to conserve coal because one of the coal mills was down. Mixing zone temperature decreased to 1,600°F after the coal rate was decreased, then was gradually increased to 1,700°F for about a day. In the last 12 hours of operation the mixing zone temperature slowly increased to 1,800°F. The system pressure was at 240 psig until the coal trips on March 24, then set to 230 until the coal trip on March 26. From 00:00 on March 27 to 16:00 on March 29 the pressure was at 200 psig. For the last 12 hours of operation the system pressure was set at 240 psig. The PCD temperature started March 24 at 925°F, then was steady at 900°F until the coal trip on March 25. This was higher than the desired PCD temperature of 800°F. The PCD temperature was at 825°F between the coal trips that occurred on March 25 and 26. After the coal trips on March 26 the PCD temperature was at 800°F, and then decreased to 725°F after the coal-feed rate was decreased. After the coal-feed rate decrease the PCD temperature was constant at 750°F until the reactor pressure was increased on March 29 when the PCD temperature increased to 800°F.

The last 7 days of GCT4 operation (GCT4-9 to -34) hourly averages for the coal-feed rate and the air rate are shown in Figures 4.3-5. The coal-feed rate was calculated from a correlation that used the coal feeder speed and the FD0210 weight cell data (see Section 4.5). The air rate was obtained from FI205. The coal rate for March 24 to 26 was at 5,375 lb/hr when the coal feeder was not tripping. Every dip in the air rate and coal-feed rate during March 24 to 26 was due to a coal feed trip. There were no coal trips after March 26. The coal-feed rate was maintained at 5,100 to 5,500 lb/hr, until the coal-feed rate was decreased to about 4,000 lb/hr on March 27, to match the rate at which coal could be ground. The coal mill problems were solved and the coal-feed rate was increased up to 5,000 lb/hr on March 29 and held at 5,000 lb/hr until the end of the test. The air rates generally followed the coal rate. Air-to-coal ratios shown in Table 4.3-1 were from 2.4 to around 4.3 for the operating periods, but most were around 3.0.

The last 7 days of GCT4 operation (GCT4-9 to -34) hourly synthesis gas (FI465_COMP) and aeration instrument nitrogen (FI609) rates are found in the plot shown in Figure 4.3-6. It is estimated that about 1,000 lb/hr from FI609 does not enter the process, but is used to seal valves, pressurized/depressurized feed and ash lock hopper systems and in the seals for the screw coolers. Values shown in Figure 4.3-3 assume that 1,000 lb/hr of nitrogen from FI609 do not enter the transport reactor. The synthesis gas rate varied widely during the periods of frequent coal trips from March 24 to 26. In between coal trips the synthesis gas rate was from 22,000 to 24,000 lb/hr. The synthesis gas rate generally followed the air rate. The nitrogen rate was at 6,200 lb/hr from March 23 to March 26. At 00:00 on March 26 the nitrogen rate was decreased to 5,500 lb/hr, where it remained until the end of the run.

The plant gas analyzer system analyzed synthesis gas for the following gases during GCT4, using the associated analyzers listed below.

CO	AI425, AI434B, AI453G, AI464C
CO_2	AI434C, AI464D
CH_4	AI464E
C_2^+	AI464F
H_2	AI464G
H_2O	AI7510
N_2	AI464B

The AI464B-G analyzers use a gas chromatograph and typically have about a 6-minute delay. The other three CO analyzers (AI425, AI434B, and AI464C) and CO_2 analyzer (AI434C) are IR based and provide more real-time measurements. All analyzers (except for the H_2O analyzer) require that the gas sample is conditioned to remove water vapor, therefore all these analyzers report gas compositions on a dry basis. The gas analyzer conditioning system frequently plugged with tar and naphthalene during the run, which required the analyzer technicians to clean the gas analyzer conditioning systems. There was more gas analyzer plugging in GCT4 than in GCT2, probably due to the increased number of coal feed trips. The GC analyzers were not in operation from March 24 to the end of the run; therefore, there was very little H_2, N_2, CH_4, and $C_2H_6^+$ analyzer data obtained during this period.

RTI was onsite for the DSRP and obtained CO, CO_2, and H_2 data from 14:03 on March 26 to 23:17 on March 28. This data will be used for operating periods GCT4-18 to -26. DHL

Analytical Laboratory, Inc. (DHL) also took several grab samples during GCT4 and analyzed for several components, including CO, H_2, and CO_2.

The raw synthesis gas analyzer data was adjusted to produce the best estimate of the actual gas composition in three steps:

1. Choice of CO and CO_2 analyzers.

2. Normalization of dry gas compositions (force to 100-percent total).

3. Conversion of dry compositions to wet compositions.

With four CO analyzers there is a measure of self-consistency when all or several of the four analyzers read the same value. There is also the choice of which analyzer to use when problems with others arise due to solids plugging the gas sampling lines. The first 5 days of operation (GCT4-1 to -8) hourly averages for the four CO analyzers are shown in Figure 4.3-7. The CO analyzers (AI464C, AI434B, and AI53G) were reading zero during March 8. AI425 was reading zero during GCT4-1, so there is no CO data for GCT4-1. All analyzers were in operation after 09:00 on March 9 and generally agreed with each other. During the afternoon of March 10, CO analyzer AI464C (GC) drifted, but the other three CO analyzers generally agreed with each other. On the morning of March 11, AI434B and AI53G agreed with each other and AI425 was reading about 1.5 percent below AI434B and AI53G. During most of GCT4, CO analyzers AI425 and AI434B agreed very well with each other. During the early afternoon of March 11, all four analyzers again agreed with each other. At 20:00 on March 11 analyzers AI464C, AI434B, and AI53G all dropped to zero, so only the reading of AI425 was available.

The low-CO measurements are either periods when the gas analyzers were being calibrated or measurements during coal feeder trips. The CO compositions used in calculations were interpolated for times when the gas analyzers were being calibrated. Plant analyzer data for CO was available for operating periods GCT4-2 to -8.

Hourly averages data for the CO_2 analyzers for the first 5 days of operation (GCT4-1 to -8) are shown in Figure 4.3-8. Neither CO_2 analyzer was operating on March 8, so there is no CO_2 data for GCT4-1. From 09:00 to 16:00 on March 9, both CO_2 analyzers were working, but AI464D was reading higher than the AI434C. Data from AI464D was used for further analysis, since previous testing indicated that AI464D data was more consistent with previous results. From 16:00 on March 9, to March 11 there was good agreement between the two CO_2 analyzers. At 20:00, March 11, both analyzers dropped to zero. Data for CO_2 were only available for operating periods GCT4-2 to -8.

Hourly averages water analyzer data for the first 5 days of operation (GCT4-1 to -8) are provided in Figure 4.3-9, where they are compared with the in situ synthesis gas moisture measurement made during PCD outlet particulate sampling. The feed-steam rate is also shown in Figure 4.3-9. The first in situ moisture data was about 1 percent below the moisture analyzer data. The second in situ moisture data was taken during startup and was consistent with 1 hour of moisture analyzer data. The plant moisture analyzer data was consistent with the increase in steam rate early on March 11, but did not track the decrease in steam rate late on March 11.

Hourly averages gas analyzer data for the first 5 days of operation (GCT4-1 to -8) for H_2, CH_4, and C_2^+ for GCT4 are shown in Figure 4.3-10. None of the three analyzers gave results for March 8, so there were no H_2, CH_4, and C_2^+ data for GCT4-1. At 20:00 on March 12, all analyzers dropped to zero. All H_2 analyzer AI464G readings are low compared to GCT3 and preliminary TC06 H_2 data, and are certainly in error. This H_2 data will be used in further analyses, but further inconsistencies with other test run data will be noted. The CH_4 seemed to be giving reasonable results for the March 9 to 11 period. The GCT4 C_2^+ data were much higher than GCT2 and preliminary TC06 C_2^+ data. The C_2^+ data will be used for the rest of the analysis, but inconsistencies with past data will be noted.

The hourly averages of the sum of the dry gas analyses are shown in Figure 4.3-11 for the first 5 days of operation (GCT4-2 to -8). Despite the obvious inconsistencies with the H_2 concentrations, between 19:00 on March 9, and 08:00 on March 11, the sum of the dry gas analyses were between 97 and 100 percent.

The best estimates for the wet gas compositions are shown in Table 4.3-2 for the steady operating periods (GCT4-2 to -8) defined in Section 4.1. The gas compositions were normalized to add up to 100 percent. No estimate was made for GCT4-1.

Hourly averages for the CO analyzer (AI425) for the last 7 days of GCT4 operation (GCT4-9 to -34) are shown in Figure 4.3-12. The CO analyzers AI464C, AI434B, and AI53G were out of operation from March 24 to 31. The low-CO measurements are either periods when the gas analyzers were calibrated or during coal feeder trips. The CO compositions used in calculations were interpolated for times when the gas analyzers were being calibrated.

During the last 7 days of GCT4 operation (GCT4-9 to -34), neither CO_2 analyzer was operating, so there was no PSDF CO_2 data for operating periods GCT4-9 to -34. During this same time period the H_2, N_2, CH_4, and C_2^+ analyzers were not operating, so there was no PSDF H_2, N_2, CH_4, and C_2^+data for operating periods GCT4-9 to -34.

Hourly averages water analyzer data for the last 7 days of GCT4 operation (GCT4-9 to -34) are shown in Figure 4.3-13, where they are compared with the in situ synthesis gas moisture measurements made during PCD outlet particulate sampling. The feed-steam rate is also shown in Figure 4.3-13. The first in situ moisture measurement (on March 25) was about 1 percent lower than the moisture analyzer data. The next three in situ moisture measurements agreed well with the moisture analyzer data. The last in situ moisture measurement (on March 29) was about 1 percent higher than the moisture analyzer measurements. The moisture analyzer measurements were consistent with the increase in steam rate on March 26, but did not track the decrease in steam rate late on March 29.

RTI provided CO and CO_2 gas analyses for the period 14:03 on March 26, to 22:04 on March 28. The RTI CO data are shown in the plot in Figure 4.3-14 and compared with the PSDF CO analyzer AI425 as well as two gas grab samples analyses from DHL. Due to a data logging error, the second significant figure of the RTI data was lost for most of the RTI CO data. The CO data from all three sources show very good agreement. Note that the RTI data followed the hourly swings in CO analyzer AI425 data. Future calculations will use the PSDF CO analyzer AI425 data.

The RTI CO_2 data are shown in the plot in Figure 4.3-15 as compared with two gas grab samples analyses from DHL. Due to a data logging error, the second significant figure of the RTI data was lost for most of the RTI CO_2 data. The CO_2 data from DHL is about 1 percent below the RTI data. Future calculations will use the RTI CO_2 analyzer data.

The RTI H_2 data are shown in the plot in Figure 4.3-16 as compared with two gas grab samples analyses from DHL. The H_2 data from DHL are about 1 percent below the RTI data for one sample and 2.5 percent above the RTI data. Future calculations will use the RTI H_2 analyzer data.

Calculation of the lower heating value for the gas requires an estimate for CH_4 and C_2^+ for the period from March 24 to 31. These values were estimated from preliminary TC06 data for use in GCT4 calculations, since the gas analyzers operated very well for the entire 1,000-hour TC06 test. The dry gas composition for CH_4 was assumed to be 1.5 percent and the C_2^+ concentration was assumed to be zero percent. Since there were also no N_2 data for the period March 24 to 31, the N_2 gas concentration was determined by difference from 100 percent.

The best estimates of the gas compositions for the operating periods GCT4-18 to -26 are provided in Table 4.3-2. There was insufficient gas data to determine gas compositions for operating periods GCT4-9 to -17 and from GCT4-27 to -34.

For operating periods GCT4-2 to -8 and GCT4-18 to -26 the water-gas shift (WGS) equilibrium constant has been calculated from the gas data. The WGS was 0.20 to 0.31 for operating periods GCT4-2 to -8, with equilibrium temperatures (2,431 to 3,093°F) well above the maximum temperature in the transport reactor. These WGS equilibrium constants are inconsistent with GCT2 and preliminary TC06 data, which indicates that the WGS equilibrium temperature should be close to the mixing zone temperature.

The water-gas shift reaction and equilibrium constant are as follows:

$$CO + H_2O \leftrightarrow H_2 + CO_2 \quad (1)$$

$$Kp = \frac{(H_2)(CO_2)}{(H_2O)(CO)} \quad (2)$$

The WGS was 0.67 to 0.74 for operating periods GCT4-18 to -26, with equilibrium temperatures (1,663 to 1,729°F) close to the transport reactor mixing zone temperature as measured by TI360. This is consistent with previous results and preliminary TC06 data. The riser temperature at TI360 and the WGS equilibrium at TI360 are shown in Table 4.3-2 for all operating periods.

A comparison of the WGS equilibrium constant calculated from GCT4 data and those calculated using the mixing zone TI360 as the WGS equilibrium temperature are provided in Figure 4.3-17. Note the excellent agreement between the measured and calculated WGS equilibrium constant, using operating periods GCT4-18 to -26 data, and the poor agreement

between the measured and calculated WGS equilibrium using operating periods GCT4-2 to -8 data.

Also shown in Table 4.3-2 are the synthesis gas molecular weight and the synthesis gas CO/CO_2 ratios. All of the synthesis gas CO/CO_2 ratios are consistent with previous data. The lower heating value (LHV) for each gas composition was calculated and is provided in Table 4.3-2.

The LHV value was calculated using the formula:

$$\mathrm{LHV(Btu/SCF)} = \left\{ \begin{array}{l} 275\times(\mathrm{H_2\%}) + 322\times(\mathrm{CO\%}) + \\ 913\times(\mathrm{CH_4\%}) + 1641\times(\mathrm{C_2H_6^+\%}) \end{array} \right\} / 100 \qquad (3)$$

The C_2^+ was assumed to be C_2H_6. The LHV were from 83 to 92 Btu/SCF for the GCT4-2 to -8 data and 61 to 73 Btu/SCF for the GCT4-18 to -26 data. Again, the GCT4-2 to -8 LHV were inconsistent with LHV from GCT2, GCT3, and preliminary results from TC06.

The synthesis gas compositions and synthesis gas-flow rate can be checked by an oxygen balance around the synthesis gas combustor (SGC) since the synthesis gas combustor exit O_2 is measured by AIT8775. A synthesis gas combustor energy balance can be used to estimate the synthesis gas LHV for periods not measured by gas analyzers. The synthesis gas combustor energy balance and oxygen balance were calculated by using the following thermal oxidizer process tags:

- Primary air flow, FI8773.
- Secondary air flow, FFIC8772MEAS.
- Quench air flow, FI8771.
- Propane flow, FI8753.
- Oxygen concentration, AIT8775.

The measured and mass balance calculated O_2 values are shown in Figure 4.3-18 and Table 4.3-3. The measured and calculated O_2 concentrations agreed well with each other for GCT4-18 to -26 data. The agreement is consistent with GCT2 and preliminary TC06 results when there was more reliable N_2, H_2, CH_4, and C_2^+ gas analyzer data. It also shows confidence in the synthesis gas-flow rate and synthesis gas combustor-flow rate measurements. The agreement was poor for the GCT4-2 to -8, which places more doubt on the consistency of this data.

The synthesis gas combustor energy balance is done by calculating the synthesis gas combustor heat loss, so as to make the synthesis gas LHV calculated by the synthesis gas combustor energy balance agree with LHV calculated from the synthesis gas analyzer data. In GCT2, the synthesis gas combustor heat loss was usually between 1.5 and 4.0 x 10^6 Btu/hr to obtain agreement. In GCT3, the best fit was 1.0 x 10^6 Btu/hr. The best fit for the GCT4-18 to -26 data was 2.25 x 10^6 Btu/hr. A comparison between the measured LHV and the synthesis gas combustor energy

balance LHV is provided in Figure 4.3-19. A best fit of the LHV for GCT4-2 to -8 would require a SGC heat loss of about 7.0 x 10^6 Btu/hr.

Using a synthesis gas combustor heat loss of 2.25 x 10^6 Btu/hr, the LHV for all of the operating periods can be calculated. The LHV are shown in Table 4.3-3 and in the plot in Figures 4.3-20 and -21. Figure 4.3-20 shows a plot of the LHV as determined by gas analyzers for periods GCT4-2 to -8, and the LHV calculated by the synthesis gas combustor (SGC) energy balance for periods GCT4-1 to -8. As shown in Figure 4.3-19, the analyzer data in GCT4-2 to -8 are higher than the SGC energy balance calculations, probably because of the higher-than-normal analyzer C_2^+ concentrations. Since the SGC oxygen balance is not acceptable in GCT4-2 to -8, the SGC energy balances LHV are more believable than the gas analyzer LHV. The LHV value for operating period 1 (86 Btu/SCF) is much higher than the others in the GCT4 time periods. This operating period data were taken only about 4 hours after coal feed started and were not representative of long-term operation. The other four points (GCT4-2 to -8) for the SGC energy balance were in the range of 60 to 75 Btu/SCF, which is consistent with previous testing.

Figure 4.3-21 shows the plot of the LHV determined by gas analyzers for periods GCT4-18 to -26 and the LHV calculated by the SGC energy balance for periods GCT4-9 to -34. As shown in Figure 4.3-19, the analyzer data agree well with the SGC energy balance calculations. All but three of the operating periods LHV (GCT4-13, -14, and -15) were in the range of 60 to 75 Btu/SCF. These three low LHV from the SGC energy balance were a result of high SGC propane rates of 2,000 SCFH, while the more typical propane flows were 520 SCFH. The higher the SGC propane rate, the lower the SGC energy balance synthesis gas LHV. During these three periods the coal rate was quite low at 2,000 to 3,300 lb/hr (see Table 4.3-1) as opposed to the majority of the operating periods where the coal rate was above 5,000 lb/hr. The other operating periods where the LHV dipped below 64 Btu/SCF also had lower coal-feed rates.

Figure 4.3-22 is a plot of the LHV determined from the SGC energy balance and the coal-feed rate. The LHV clearly increases with coal rate. All of the data were taken at the same mixing zone temperatures. Again, the outliner point is GCT4-1. The lower LHV at the lower coal rates is caused by the increased dilution of the synthesis gas by the aeration and instrument nitrogen fed to the reactor. When the coal-feed rate is changed, the nitrogen rate is not changed, so at lower coal-feed rates there is a higher ratio of nitrogen to coal fed and, hence, more dilution of the synthesis gas by nitrogen. The nitrogen correction described in the next paragraph decreases the effect of the coal rate and nitrogen dilution.

The PSDF transport reactor adds more N_2 per lb synthesis gas than a commercial reactor because of the additional PSDF sampling purges, additional PSDF instrument purges, and the need to aerate the lower portion of the reactor. Instrument purges would be proportionally smaller in a commercial design due to the scale factor (number of instruments stay the same size as plant size increases). Any additional N_2 added to the riser requires additional fuel to bring the additional N_2 up to operating temperatures. This additional fuel then requires additional air, which then adds more N_2 from air to the reactor and further dilutes the synthesis gas. In a commercial reactor, aeration N_2 would only be used for startup. To determine a commercial synthesis LHV, the following components are deleted from the raw synthesis gas:

- Nitrogen that is added through FI609.
- Nitrogen that is added with the air required for burning coal required to heat FI609 nitrogen to reactor process temperature.
- Carbon dioxide from burning the coal required for heating FI609 nitrogen.
- Water vapor from burning the coal required for heating FI609 nitrogen.

The N_2 corrected LHV are listed in Table 4.3-3 and are shown in the plot in Figure 4.3-22. All the N_2 corrected LHV were between 93 and 118 Btu/SCF, except for GCT4-1, which was 174 Btu/SCF. The N_2 correction adds about 40 to 50 Btu/SCF to the raw LHV. This correction is an attempt to predict what the LHV of a commercial reactor would be if the aeration nitrogen-to-coal ratio were much lower. This correction does not correct for the lower reactor heat loss per pound of coal fed in a commercial reactor.

Since the transport reactor H_2S analyzer was not working during GCT4, the H_2S concentration and sulfur emissions from the transport reactor were not directly measured. The synthesis gas combustor SO_2 analyzer, AI534A, measures the total sulfur emissions from the transport reactor. The total sulfur emissions consists of H_2S, COS, and CS_2. The main sulfur species in coal gasification are considered to be H_2S and carbon oxysulfide (COS). There should also be a minor amount of carbon disulfide (CS_2). The Waltz Mills, KRW gasifier data indicate that the majority of the gaseous sulfur is present as H_2S, with the balance COS. KRW typically measured concentrations of 100 to 200 ppm COS for 0.6- to 1.0-percent sulfur fuels.

The sulfur emissions expressed as total reduced sulfur (TRS) from the transport reactor are provided in Table 4.3-3. Since the synthesis gas combustor exit gas-flow rate is about twice that of the synthesis gas rate, the synthesis gas total reduced sulfur concentration is about twice that of the measured synthesis gas combustor SO_2 concentration. The synthesis gas combustor SO_2 concentrations are provided in Table 4.3-3 and the maximum sulfur emissions possible in Table 4.3-3. The maximum sulfur emissions were calculated from the coal-feed rate, coal sulfur level, and the synthesis gas rate, assuming that all of the coal sulfur left the system with the synthesis gas (zero-percent sulfur removal). Coal-feed rate is discussed in Section 4.5 and coal sulfur levels in Section 4.4. The percent-sulfur removal and sulfur emissions in pounds sulfur dioxide, per MBtu coal fed, are shown in Table 4.3-3.

The SO_2 emissions for operating periods GCT4-1 to -8 are shown in the plot in Figure 4.3-23. For these operating periods the sulfur emissions varied from 0.17 to 0.45 lb sulfur dioxide per MBtu coal-fired (higher coal heating value used). The total reduced-sulfur removal varied from 28 to 71 percent. There appears to be two different levels of sulfur removal. Until March 10 the sulfur removals were 60 to 70 percent, then dropped to 28 to 36 percent on March 11. This is shown in Section 4.5 to be a function of the Ca/S level in the PCD solids.

The SO_2 emissions for operating periods GCT4-9 through -34 are shown in Figure 4.3-24. For these operating periods the sulfur emissions varied from 0.19 to 0.46 lb sulfur dioxide per MBtu

of coal fired (higher coal heating value used). The sulfur removal varied from 0 to 64 percent. Data from two operating periods (GCT4-13 and -14) are not in the plot because their sulfur removals were very low, essentially zero. These two operating periods had very low coal-feed rates and the coal feed correlation might have been in error for these two operating periods. There appears to be two different levels of sulfur removal. Before March 26 and after 21:00 on March 28 the SO_2 removals were 55 to 75 percent, while from 00:00 on March 26 to 21:00 on March 28 the sulfur removals were 30 to 42 percent. This is shown in Section 4.5 to be a function of the Ca/S level in the PCD solids.

The lower sulfur removals are consistent with results from GCT1 (40-percent sulfur removal with PRB coal) and KRW reactor results (40- to 50-percent sulfur removals with 0.6-percent sulfur coal), while the higher removals are consistent with GCT3 (50- to 80-percent sulfur removal with PRB coal). Since sulfur emissions are equilibrium controlled in gasification, sulfur emissions are a function of operating temperature, CO_2 partial pressure, and H_2O partial pressure. In commercial plants, the CO_2 and H_2O partial pressures should be different and will change the sulfur emissions.

The equilibrium H_2S concentration in coal gasification using limestone is governed by three reversible reactions:

$$CaCO_3 \leftrightarrow CaO + CO_2 \tag{4}$$

$$H_2S + CaO \leftrightarrow CaS + H_2O \tag{5}$$

$$H_2S + CaCO_3 \leftrightarrow CaS + H_2O + CO_2 \tag{6}$$

Reaction (4) is the limestone calcination reaction. At thermodynamic equilibrium, the CO_2 partial pressure should be a function of only the system temperature, as long as there are both $CaCO_3$ and CaO present according to the equilibrium constant:

$$K_1 = P^O_{CO_2} \tag{7}$$

where P^O_{CO2} is the partial pressure of CO_2. A plot of the partial pressure of CO_2 and temperature is shown in Figure 4.3-15 of the GCT1 report. At thermodynamic equilibrium, $CaCO_3$ and CaO coexist on the equilibrium curve, while above the curve only $CaCO_3$ exists, and below the curve only CaO exists. Typically, there are both $CaCO_3$ and CaO present in the PCD solids. This is because of kinetic limitations and the quick cooling down of the solids in the fuel gas from the reactor temperatures to PCD temperatures. This quick cool down tends to freeze reactions at higher equilibrium temperatures than would be indicated by the actual system-exit temperature.

The H_2S equilibrium is governed by reactions (8) and (9), with the associated equilibrium constants:

$$K_2 = \frac{P^O_{H_2O}}{P^O_{H_2S}} \tag{8}$$

$$K_3 = \frac{P^O_{H_2O} P^O_{CO_2}}{P^O_{H_2S}} \quad (9)$$

Equations (8) and (9) state that the equilibrium H_2S concentrations in the $CaCO_3$-CaO-CaS system is a function of the system temperature and the CO_2 and H_2O partial pressures. As the CO_2 and H_2O partial pressures increase, so would H_2S partial pressures. The equilibrium constants are all functions of temperature and can be determined using thermodynamic data with Aspen simulations.

The GCT4-25 H_2S equilibrium concentrations as a function of temperature are shown in Figure 4.3-25. The H_2S equilibrium curve was determined from Aspen simulations. The average partial pressure of CO_2 was 19 psia, which means that the CO_2 partial pressure crosses the CO_2 equilibrium partial pressure curve at 1,662°F. This means that at equilibrium for 19 psia CO_2 partial pressure, 1,662°F is the only temperature at which CaO and $CaCO_3$ can coexist. At equilibrium, calcium is only present as CaO or CaS above 1,662°F, and below 1,662°F all calcium is present as $CaCO_3$ or CaS. In Figure 4.3-25, the heavy vertical line divides the figure into a $CaCO_3$ region (left-hand side) and CaO region (right-hand side).

The temperature dictates which H_2S reaction will be used for sulfur removal, either Equation (5) or (6), since (5) contains CaO and (6) contains $CaCO_3$. Thermodynamic data for Equation (6) indicates that H_2S concentration decreases with temperature increase, while thermodynamic data for Equation (5) indicates that H_2S concentration increases with temperature increase. Both curves meet at the equilibrium temperature for $CaCO_3$ calcination (1,662°F, determined by the CO_2 partial pressure), which determines the minimum equilibrium H_2S concentration possible for the measured partial pressures of H_2O and CO_2. This minimum equilibrium concentration (205 ppm H_2S) should be independent of the amount of excess sorbent that is added to the system.

The measured TRS concentrations and the maximum coal TRS concentration (calculated from the coal sulfur, assuming that all coal sulfur is released as sulfur to the fuel gas) are shown as horizontal lines in Figure 4.3-25. The measured TRS and maximum coal TRS indicate 38-percent sulfur capture. This data indicates that if the entire coal sulfur was present as H_2S, the transport reactor achieved 66 percent of the theoretically possible H_2S removal.

The minimum thermodynamic H_2S concentrations are shown in Table 4.3-3 for the 16 operating periods where CO_2 and H_2O synthesis gas concentrations are available. The measured total reduced sulfur and minimum H_2S concentrations are compared in Figure 4.3-26. The data fall into three groups. Data from operating periods GCT4-2 to -5 are centered around the 45-degree line, indicating that they are close to the minimum thermodynamic equilibrium H_2S. These observations are consistent with observations from operation at Beijing Research Institute of Coal Chemistry in the early 1990's (Guohai Liu, personal communications).

The rest of the data is below the 45-degree line, indicating that the measured sulfur emissions are greater than the minimum equilibrium H_2S concentrations. Data from GCT4-6 to -8 had about the same equilibrium H_2S concentrations as the GCT4-18 to -26 data, but had a higher measured TRS concentrations. Measured TRS concentrations higher than equilibrium H_2S concentrations can be explained by either the presence of COS and CS_2 (counted in TRS) or that the H_2S reactions did not reach equilibrium.

Table 4.3-1

Operating Conditions

Operating Periods	Mixing Zone Temperature TI349 °F	Pressure PI287 psig	PCD Inlet Temperature TI458 °F	Coal Rate lb/hr	Air Rate lb/hr	Air to Coal Ratio	Synthesis Gas Rate lb/hr	Nitrogen Rate (Note) lb/hr
GCT4-1	1,630	200	864	5,158	14,299	2.77	19,729	7,123
GCT4-2	1,767	240	814	4,489	12,925	2.88	23,883	7,252
GCT4-3	1,760	240	885	4,799	15,730	3.28	27,298	6,984
GCT4-4	1,785	240	876	4,800	15,760	3.28	27,534	7,221
GCT4-5	1,728	240	811	3,582	11,431	3.19	21,817	7,147
GCT4-6	1,796	236	827	5,405	16,130	2.98	28,040	5,838
GCT4-7	1,797	236	810	5,552	15,892	2.86	27,649	5,733
GCT4-8	1,744	236	748	3,943	12,205	3.10	22,489	5,323
GCT4-9	1,714	240	895	5,383	13,231	2.46	24,218	6,551
GCT4-10	1,700	240	872	5,371	13,050	2.43	24,192	6,612
GCT4-11	1,706	240	875	5,367	13,148	2.45	24,068	6,536
GCT4-12	1,726	224	894	5,217	13,884	2.66	24,362	6,301
GCT4-13	1,730	232	820	2,090	8,884	4.25	17,093	6,333
GCT4-14	1,744	232	835	2,491	9,573	3.84	18,050	6,330
GCT4-15	1,749	232	833	3,284	10,490	3.19	19,662	6,472
GCT4-16	1,750	232	849	4,352	11,924	2.74	21,572	5,576
GCT4-17	1,774	232	886	4,970	13,576	2.73	23,458	5,363
GCT4-18	1,755	220	790	4,948	13,926	2.81	24,713	5,780
GCT4-19	1,753	220	786	5,182	14,444	2.79	25,607	5,795
GCT4-20	1,755	220	790	5,246	14,942	2.85	25,979	5,536
GCT4-21	1,756	220	795	5,384	14,936	2.77	25,767	5,316
GCT4-22	1,645	220	716	4,345	10,590	2.44	20,445	5,520
GCT4-23	1,679	220	729	4,108	11,242	2.74	20,990	5,537
GCT4-24	1,713	220	740	3,671	11,064	3.01	20,273	5,343
GCT4-25	1,707	220	735	3,659	10,880	2.97	20,357	5,529
GCT4-26	1,683	220	740	3,670	11,090	3.02	20,599	5,571
GCT4-27	1,687	220	745	3,944	11,474	2.91	21,055	5,471
GCT4-28	1,675	220	741	3,965	11,283	2.85	20,877	5,528
GCT4-29	1,690	220	751	3,771	11,006	2.92	20,164	5,197
GCT4-30	1,695	220	749	3,766	11,318	3.01	20,753	5,447
GCT4-31	1,679	220	748	3,787	11,558	3.05	21,321	5,501
GCT4-32	1,683	240	740	3,800	11,330	2.98	20,455	5,189
GCT4-33	1,724	240	774	4,337	12,894	2.97	22,496	5,300
GCT4-34	1,729	240	774	4,645	13,376	2.88	23,230	5,231

Note: Feed nitrogen was determined by subtracting 1,000 lb/hr from FI609 reading to account for nitrogen losses.

Table 4.3-2

Gas Compositions, Molecular Weight, and Heating Value

Operating Period	H_2O Mole %	CO Mole %	H_2 Mole %	CO_2 Mole %	CH_4 Mole %	$C_2H_6^+$ Mole %	N_2 Mole %	Total Mole %	Measured WGS K_p	Equilibrium Temp ^OF	Riser TI360 ^OF	Calculated WGS K_p @ TI360	Syngas MW lb./Mole	Syngas CO/CO_2 Ratio	Syngas LHV Btu/SCF
GCT4-1	7.2										1,603	0.81			
GCT4-2	6.3	10.9	1.3	10.3	1.5	1.8	67.8	100.0	0.20	3,093	1,686	0.71	28.5	1.1	83
GCT4-3	5.4	14.2	1.9	10.0	1.8	1.4	65.4	100.0	0.25	2,716	1,703	0.70	28.4	1.4	90
GCT4-4	5.4	14.0	1.9	9.9	1.7	1.5	65.6	100.0	0.25	2,720	1,726	0.67	28.4	1.4	90
GCT4-5	5.3	11.4	1.5	9.2	1.5	1.6	69.4	100.0	0.23	2,845	1,663	0.74	28.4	1.2	82
GCT4-6	9.6	11.8	2.1	13.0	1.5	1.9	60.2	100.0	0.24	2,735	1,762	0.64	28.4	0.9	88
GCT4-7	8.9	12.5	2.2	12.3	1.6	1.9	60.6	100.0	0.24	2,767	1,775	0.63	28.4	1.0	92
GCT4-8	9.9	10.1	2.5	12.2	1.4	2.2	61.7	100.0	0.31	2,431	1,699	0.70	28.2	0.8	88
GCT4-9	6.3	11.7									1,637	0.77			
GCT4-10	6.6	11.4									1,627	0.78			
GCT4-11	6.4	11.7									1,636	0.77			
GCT4-12	5.9	12.2									1,683	0.72			
GCT4-13	5.3	7.8									1,723	0.67			
GCT4-14	5.5	8.9									1,728	0.67			
GCT4-15	5.9	10.0									1,712	0.69			
GCT4-16	8.6	10.4									1,709	0.69			
GCT4-17	8.6	11.2									1,751	0.65			
GCT4-18	9.0	11.0	8.0	8.2	1.4	0.0	62.5	100.0	0.67	1,729	1,733	0.67	26.2	1.3	70
GCT4-19	9.0	11.1	8.2	8.2	1.4	0.0	62.2	100.0	0.67	1,727	1,733	0.66	26.1	1.4	71
GCT4-20	8.7	11.4	8.4	8.2	1.4	0.0	61.9	100.0	0.69	1,703	1,732	0.67	26.1	1.4	72
GCT4-21	8.7	11.5	8.5	8.2	1.4	0.0	61.7	100.0	0.69	1,705	1,736	0.66	26.1	1.4	73
GCT4-22	9.4	9.2	8.1	8.2	1.4	0.0	63.8	100.0	0.76	1,645	1,596	0.82	26.1	1.1	64
GCT4-23	9.0	9.2	7.5	8.2	1.4	0.0	64.7	100.0	0.74	1,660	1,639	0.77	26.3	1.1	63
GCT4-24	9.1	9.1	7.0	8.2	1.4	0.0	65.2	100.0	0.70	1,702	1,679	0.72	26.4	1.1	61
GCT4-25	9.4	8.9	7.3	8.2	1.4	0.0	64.8	100.0	0.72	1,682	1,666	0.74	26.3	1.1	61
GCT4-26	8.9	9.1	7.1	8.5	1.4	0.0	65.0	100.0	0.74	1,663	1,649	0.76	26.4	1.1	61
GCT4-27	8.6	9.7									1,658	0.75			
GCT4-28	8.5	9.7									1,641	0.76			
GCT4-29	8.9	9.0									1,660	0.74			
GCT4-30	9.0	9.2									1,662	0.74			
GCT4-31	9.3	9.2									1,648	0.76			
GCT4-32	8.4	10.1									1,648	0.76			
GCT4-33	8.1	11.2									1,704	0.69			
GCT4-34	8.0	11.8									1,702	0.70			

Notes:

1. For GCT4-18 to -26, H_2, and CO_2 were measured by RTI analyzers.
2. For GCT4-18 to -26, CH_4 was estimated from TCO6 data.
3. For GCT4-18 to -26, $C_2H_6^+$ values were estimated from TCO6 data.
4. For GCT4-18 to -26, N_2 was estimated by difference.

Table 4.3-3

Synthesis Gas Combustor Calculations

Operating Period	Calculated SGC Exit H_2O M %	AIT8775 SGC Exit O_2 M %	Measured SGC Exit O_2 M %	Calculated SGC Exit O_2 M %	Gas Analyzer LHV Btu/SCF	Energy Balance LHV Btu/SCF	N2 Corr. EB LHV Btu/SCF	Combustor SO_2 AI534A ppm	Syngas TRS SGC SO_2 Analyzer ppm	Syngas SO_2 Emissions lb. SO_2/ 10^6 Btu coal	Syngas TRS Coal Max. ppm	Syngas TRS Removal %	Thermo. Equlibrium H_2S ppm
GCT4-1						86	174	97	230	0.23	557	59	
GCT4-2	10.1	3.4	3.4	1.0	83	60	107	80	139	0.19	400	65	154
GCT4-3	8.4	5.0	5.0	3.8	90	74	118	72	149	0.22	389	62	131
GCT4-4	8.6	4.8	4.8	3.2	90	73	117	80	160	0.23	385	58	129
GCT4-5	9.3	3.6	3.6	1.4	82	61	115	61	107	0.17	363	71	122
GCT4-6	11.3	4.6	4.6	2.6	88	66	95	171	329	0.44	458	28	255
GCT4-7	11.0	4.7	4.7	2.6	92	71	101	180	353	0.45	485	27	232
GCT4-8	12.2	4.7	4.7	2.1	88	63	96	155	295	0.43	459	36	256
GCT4-9						72	118	76	163	0.19	573	72	
GCT4-10						72	118	93	201	0.23	573	65	
GCT4-11						72	117	95	204	0.23	575	64	
GCT4-12						73	115	93	204	0.24	526	61	
GCT4-13						46	98	151	349	0.00	300	0	
GCT4-14						53	107	145	323	0.00	339	0	
GCT4-15						58	109	110	239	0.37	417	43	
GCT4-16						68	108	147	312	0.40	504	38	
GCT4-17						69	103	177	373	0.45	538	31	
GCT4-18	10.8	6.1	6.1	5.5	70	69	103	158	333	0.43	507	34	196
GCT4-19	10.8	6.2	6.2	5.7	71	71	105	162	347	0.44	512	32	197
GCT4-20	10.5	6.2	6.2	5.9	72	74	106	161	355	0.45	511	31	190
GCT4-21	10.6	6.2	6.2	5.9	73	74	105	153	337	0.41	528	36	190
GCT4-22	11.1	5.8	5.8	5.8	64	70	112	151	320	0.39	538	41	204
GCT4-23	11.0	5.9	5.9	5.4	63	63	100	151	319	0.42	515	38	196
GCT4-24	11.1	6.0	6.0	5.3	61	59	94	150	326	0.46	478	32	198
GCT4-25	11.1	6.0	6.0	5.7	61	62	100	134	295	0.42	473	38	205
GCT4-26	10.7	6.0	6.0	5.8	61	62	101	105	231	0.33	486	53	197
GCT4-27						66	104	94	202	0.28	506	60	
GCT4-28						67	107	100	213	0.29	498	57	
GCT4-29						59	93	96	207	0.28	475	56	
GCT4-30						59	94	94	200	0.28	446	55	
GCT4-31						63	98	102	214	0.31	436	51	
GCT4-32						66	103	90	193	0.27	456	58	
GCT4-33						68	102	78	166	0.22	466	64	
GCT4-34						72	106	81	176	0.23	475	63	

Notes:

1. For GCT4-18 to -26, H_2 and CO_2 were measured by RTI analyzers.
2. For GCT4-18 to -26, CH_4 was estimated from TCO6 data.
3. For GCT4-18 to -26, C_2H_6+ values were estimated from TCO6 data.
4. GCT4-18 to -26, N_2 was estimated by difference.
5. Synthesis gas total reduced sulfur (TRS) estimated from synthesis gas combustor SO_2 analyzer data.

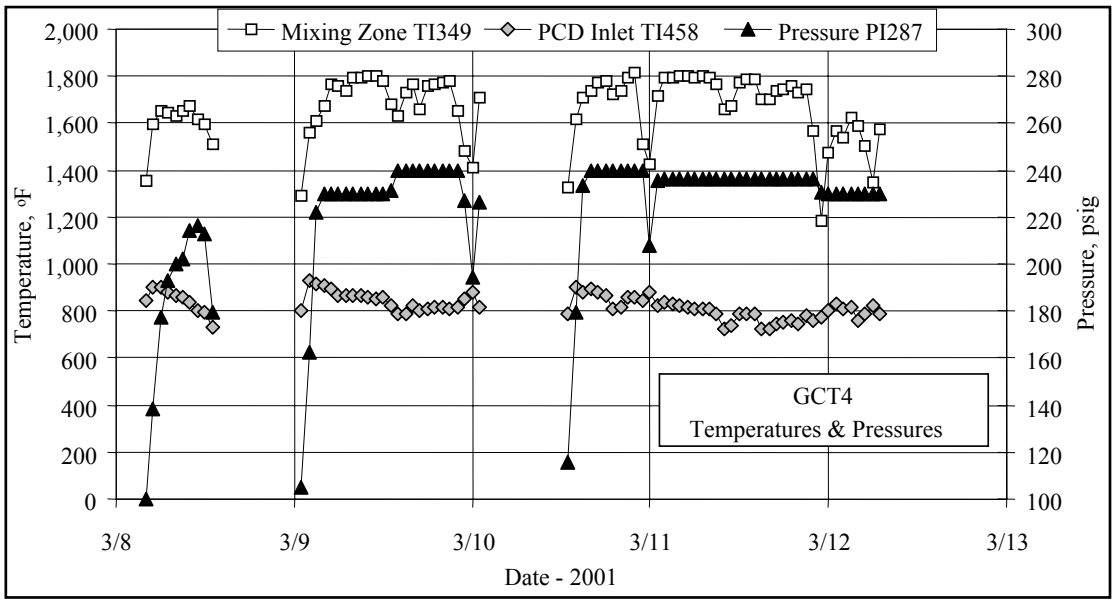

Figure 4.3-1 Temperatures and Pressures

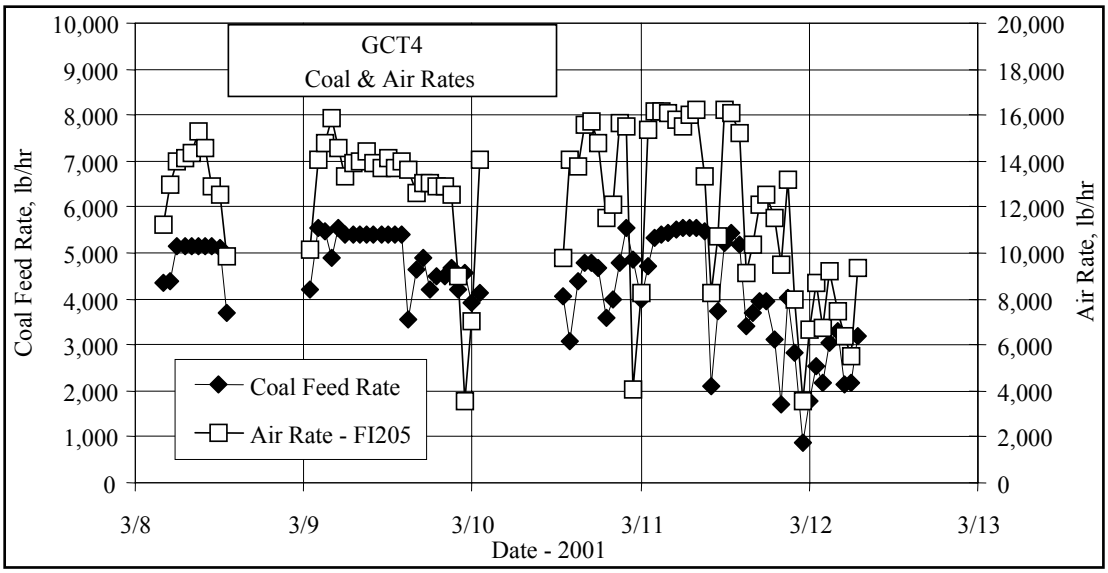

Figure 4.3-2 Coal and Air Rates

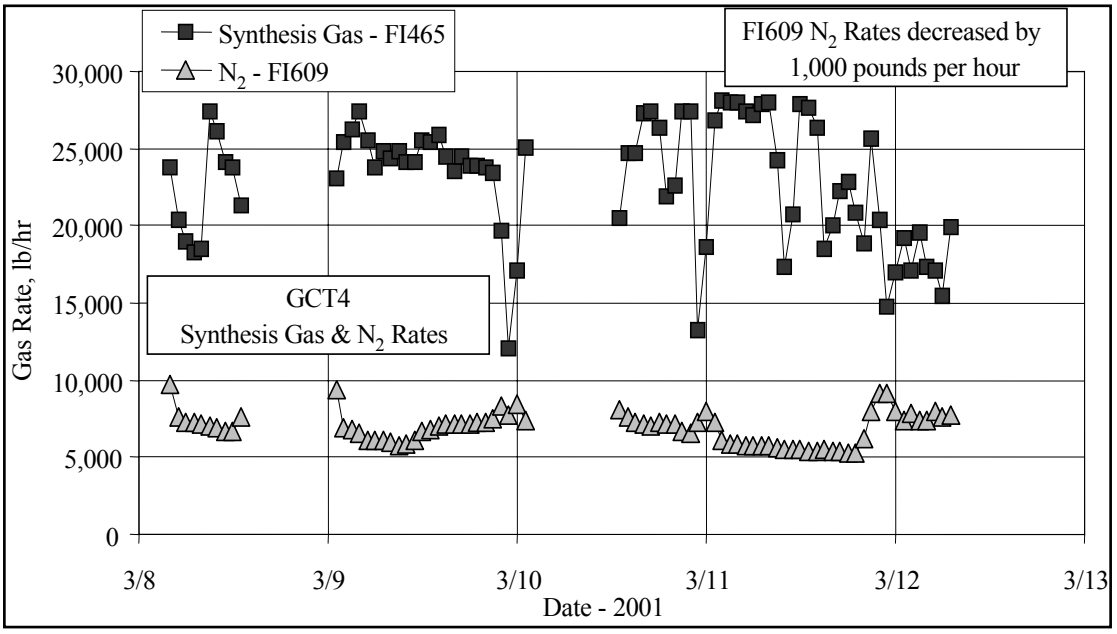

Figure 4.3-3 Synthesis Gas and Nitrogen Rates

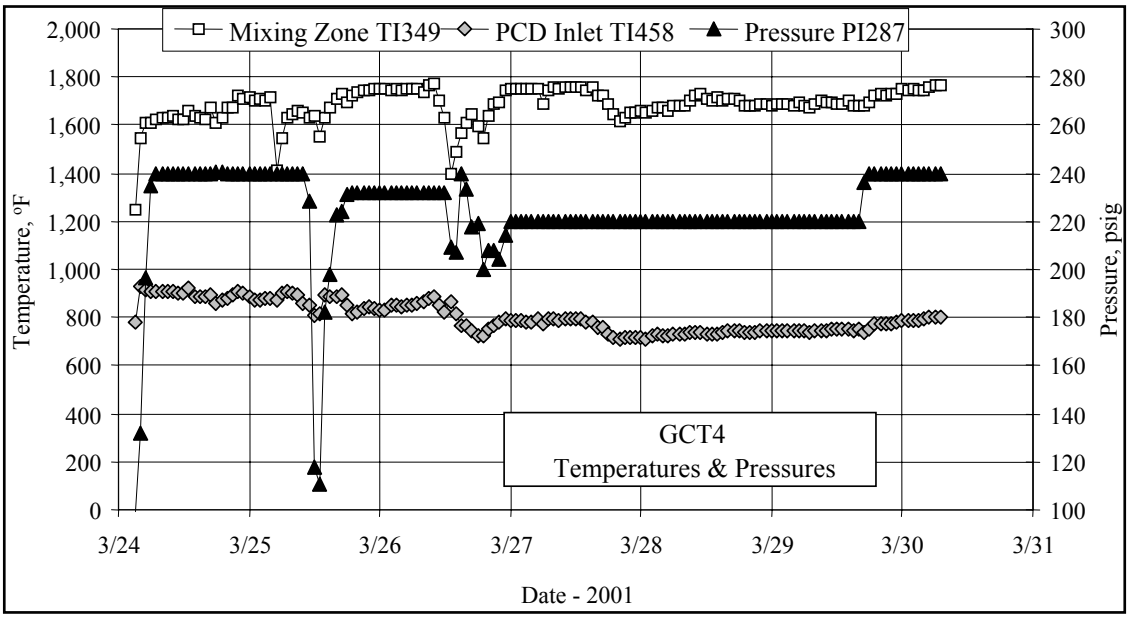

Figure 4.3-4 Temperatures and Pressures

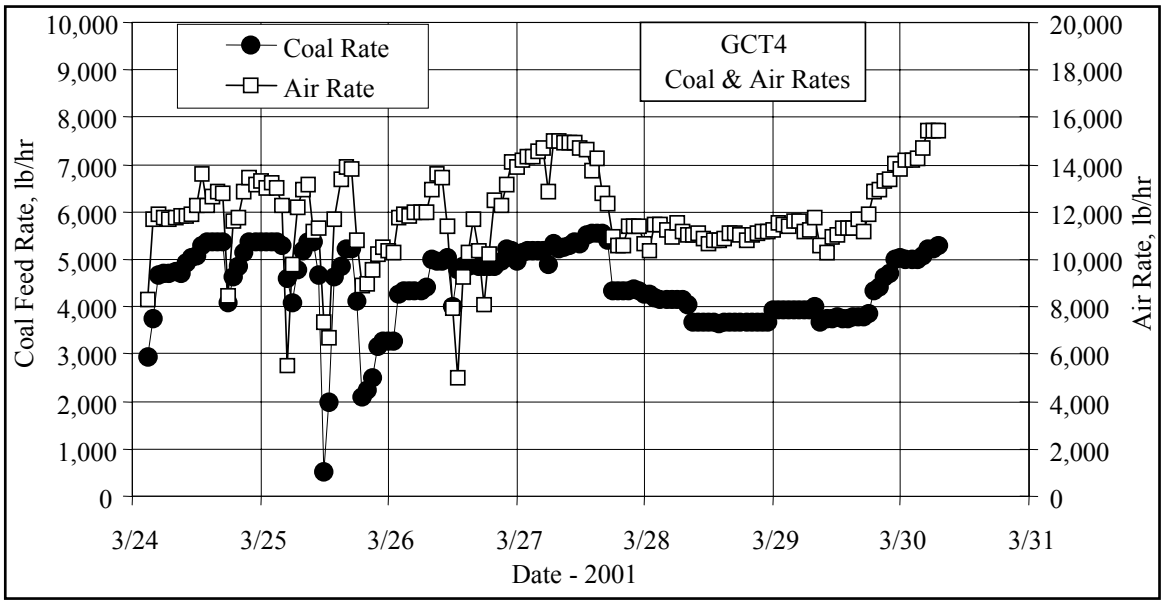

Figure 4.3-5 Coal and Air Rates

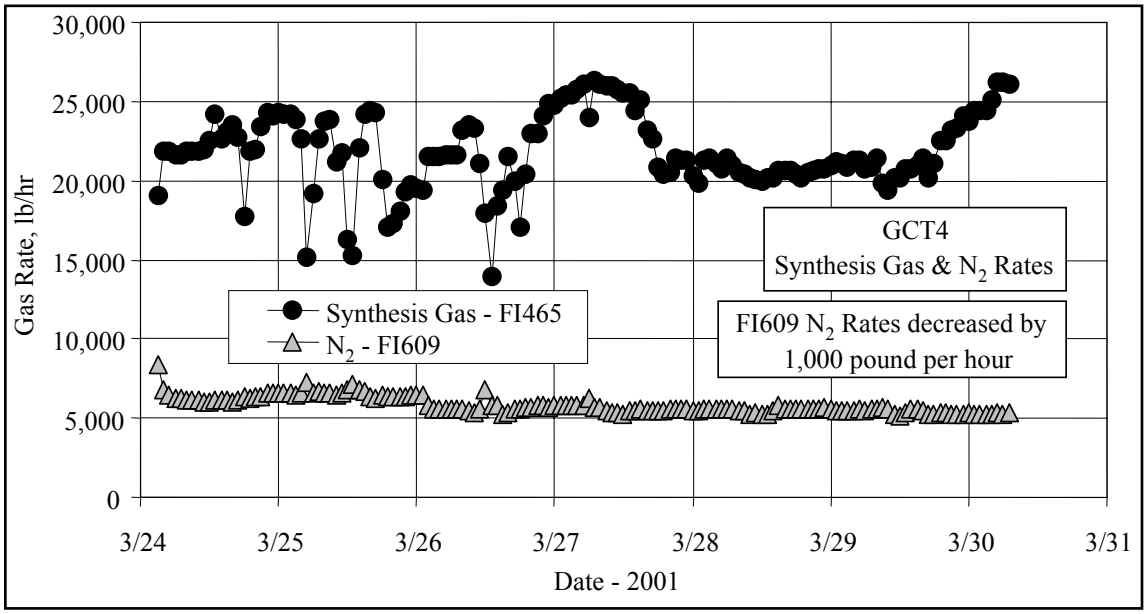

Figure 4.3-6 Synthesis Gas and Nitrogen Rates

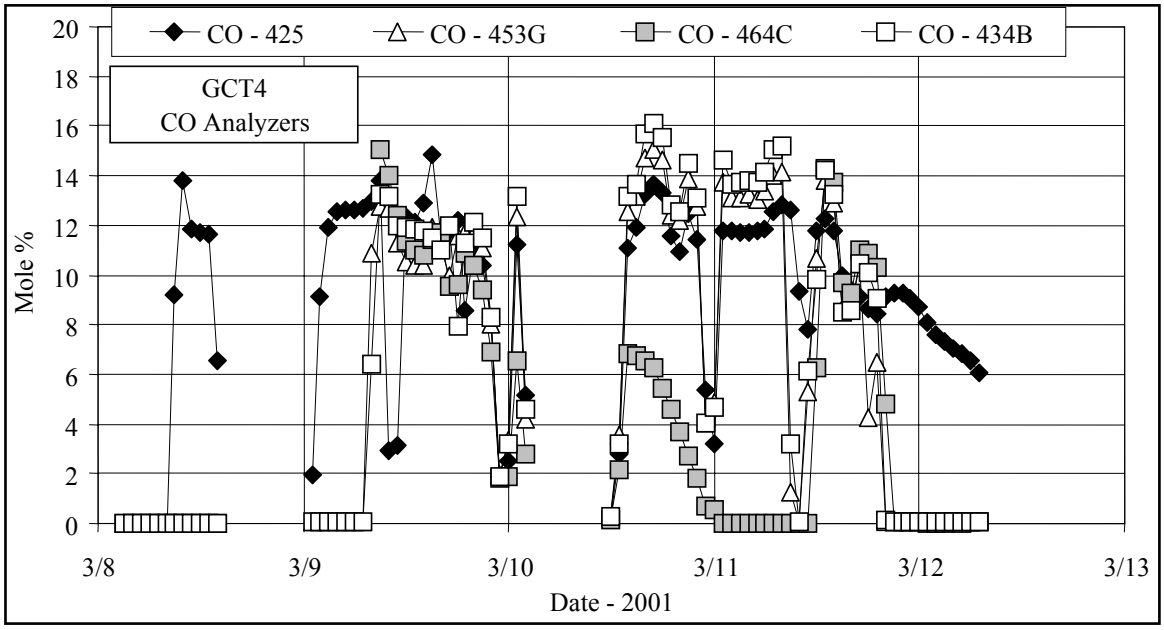

Figure 4.3-7 CO Analyzer Data

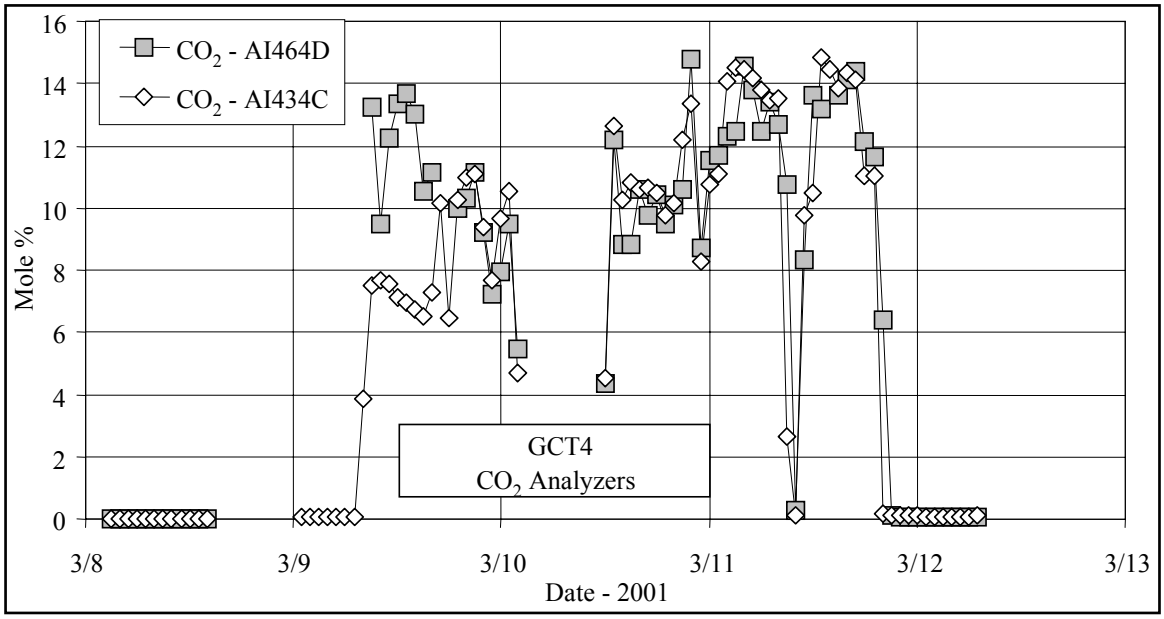

Figure 4.3-8 CO_2 Analyzer Data

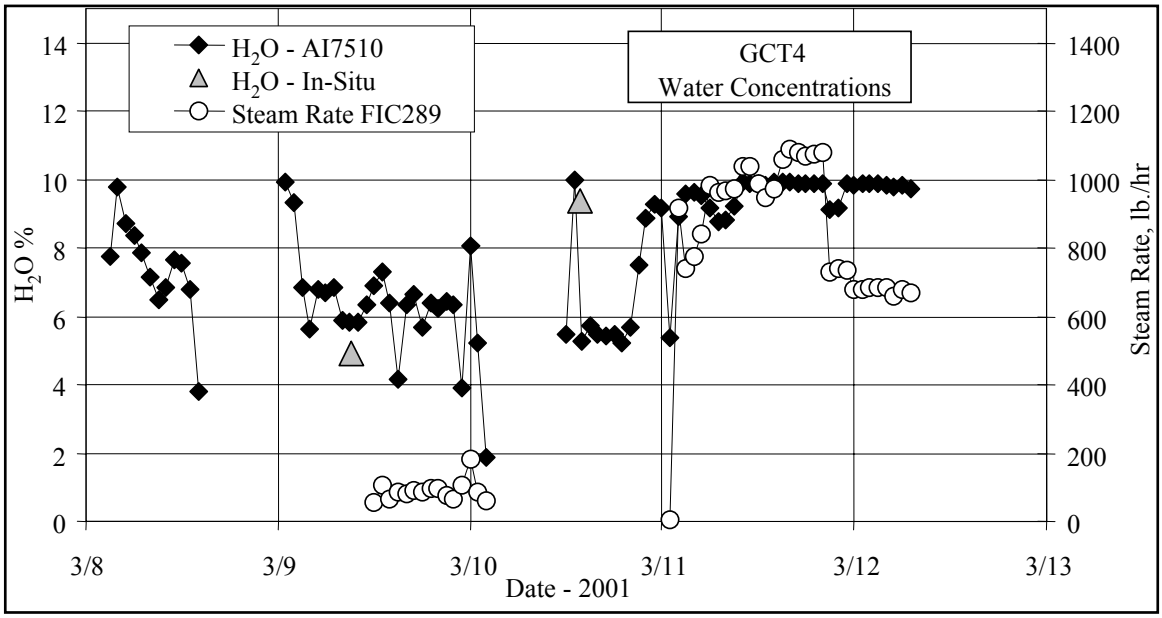

Figure 4.3-9 Analyzer H_2O Data

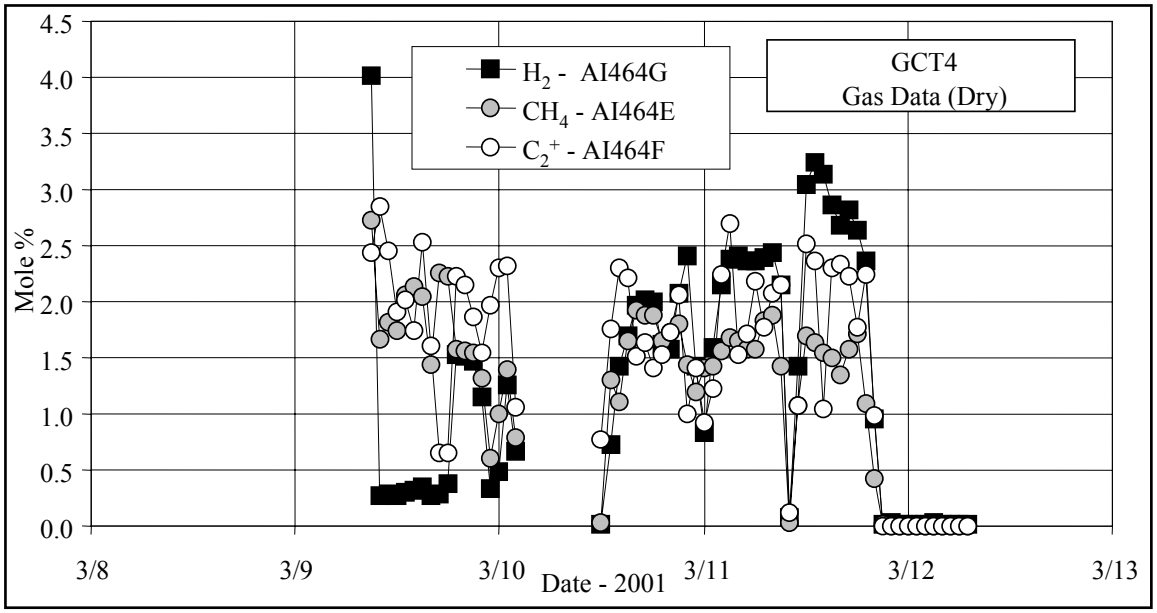

Figure 4.3-10 Analyzer H_2, CH_4, C_2^+ Data

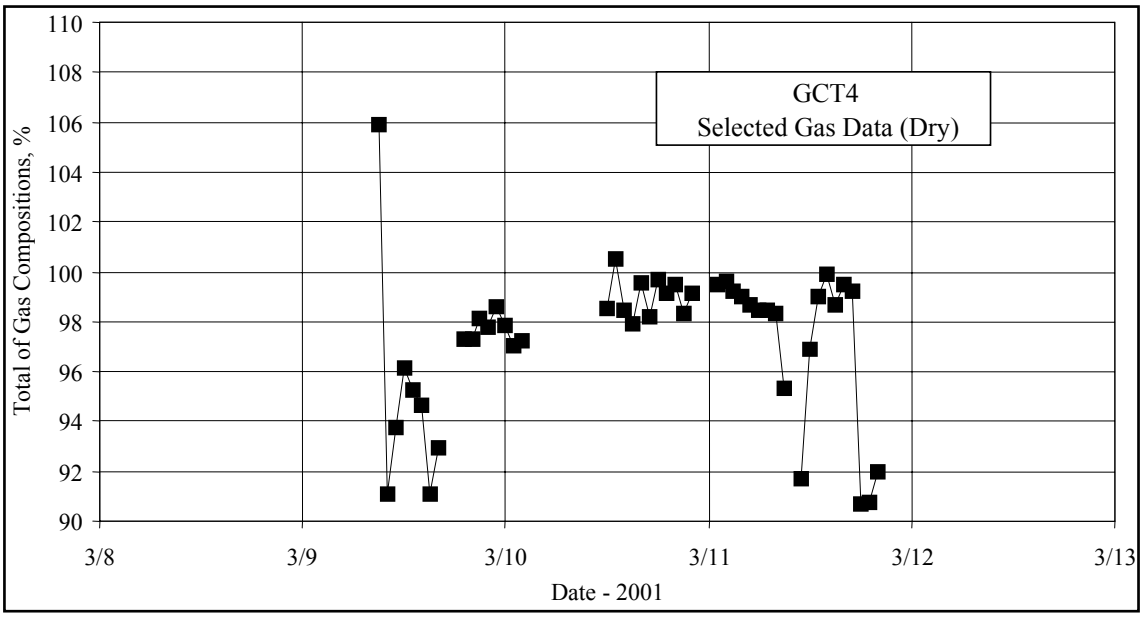

Figure 4.3-11 Sum of Selected Dry Analyzer Data

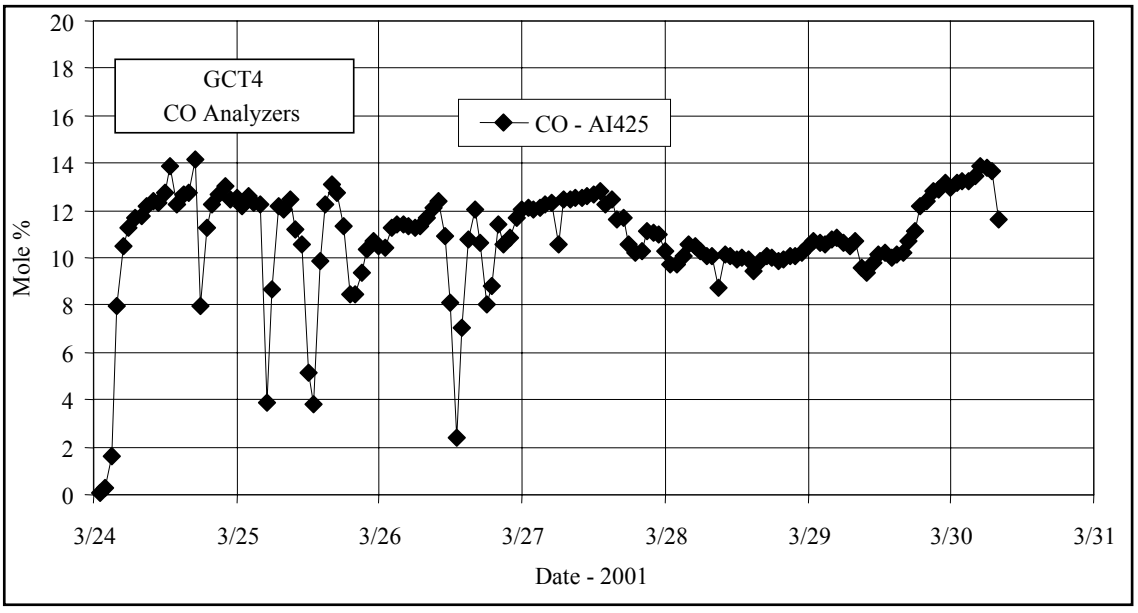

Figure 4.3-12 CO Gas Analyzer Data

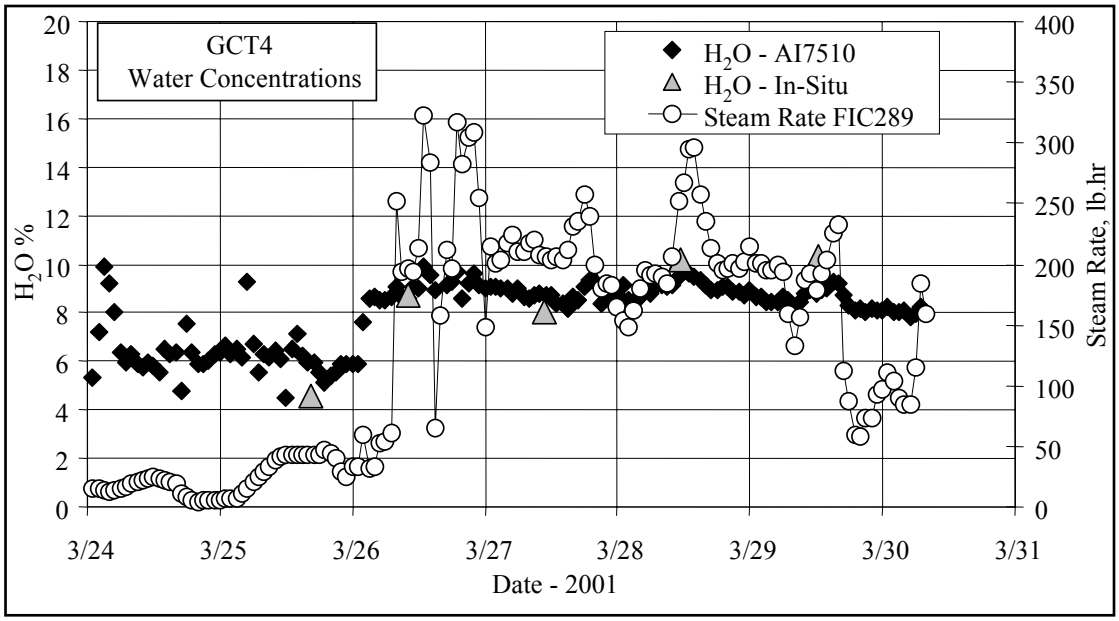

Figure 4.3-13 H_2O Gas Analyzer Data

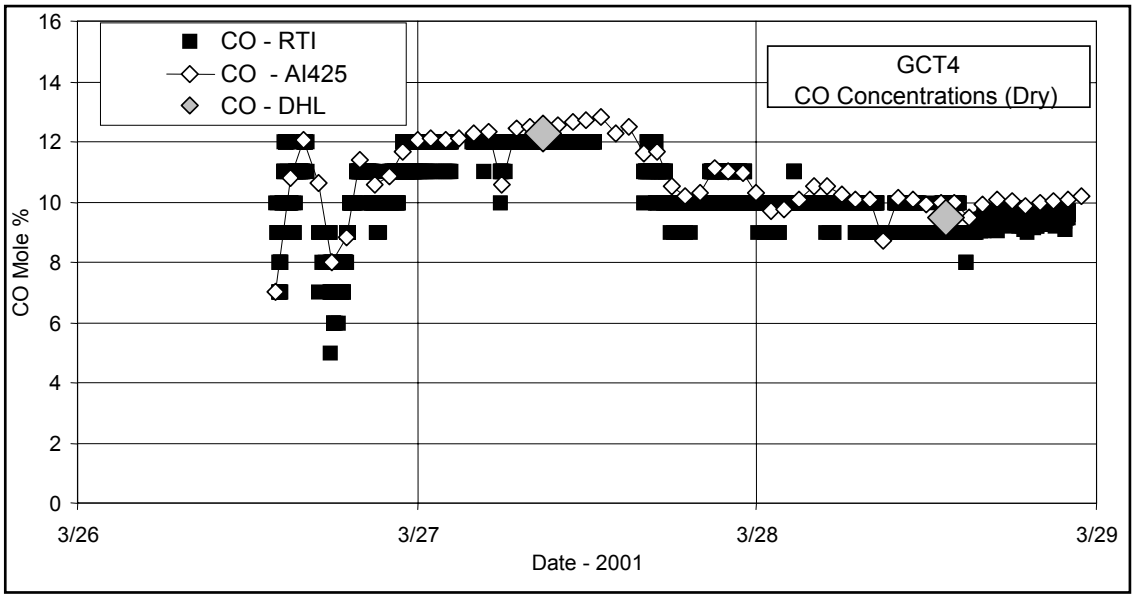

Figure 4.3-14 RTI, AI425, and DHL CO Data

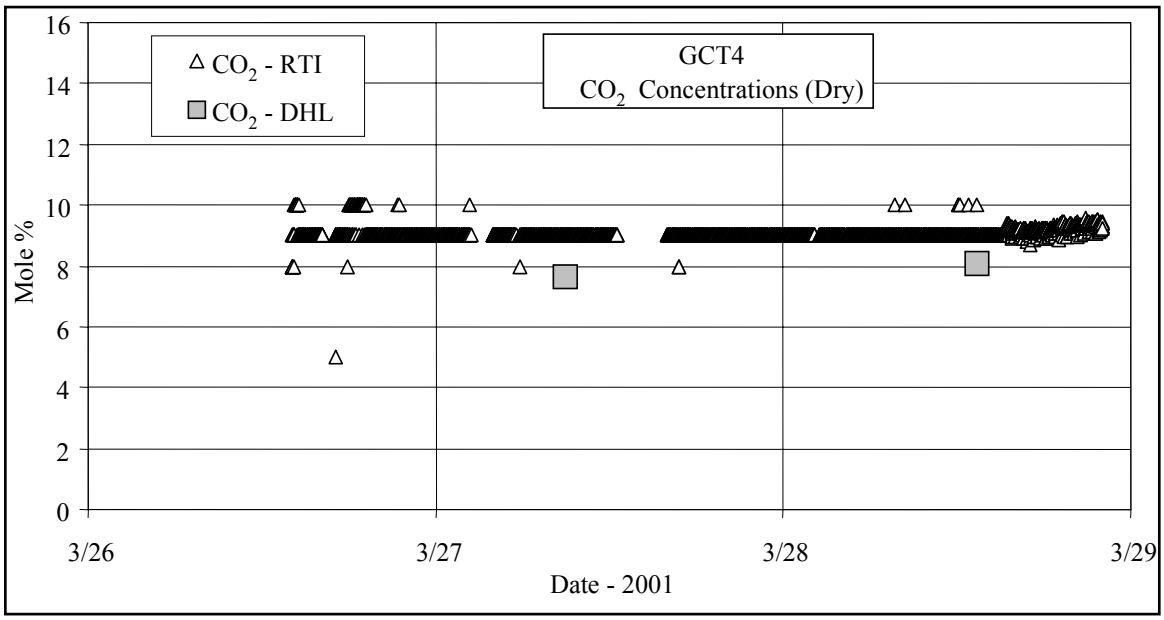

Figure 4.3-15 RTI and DHL CO_2 Data

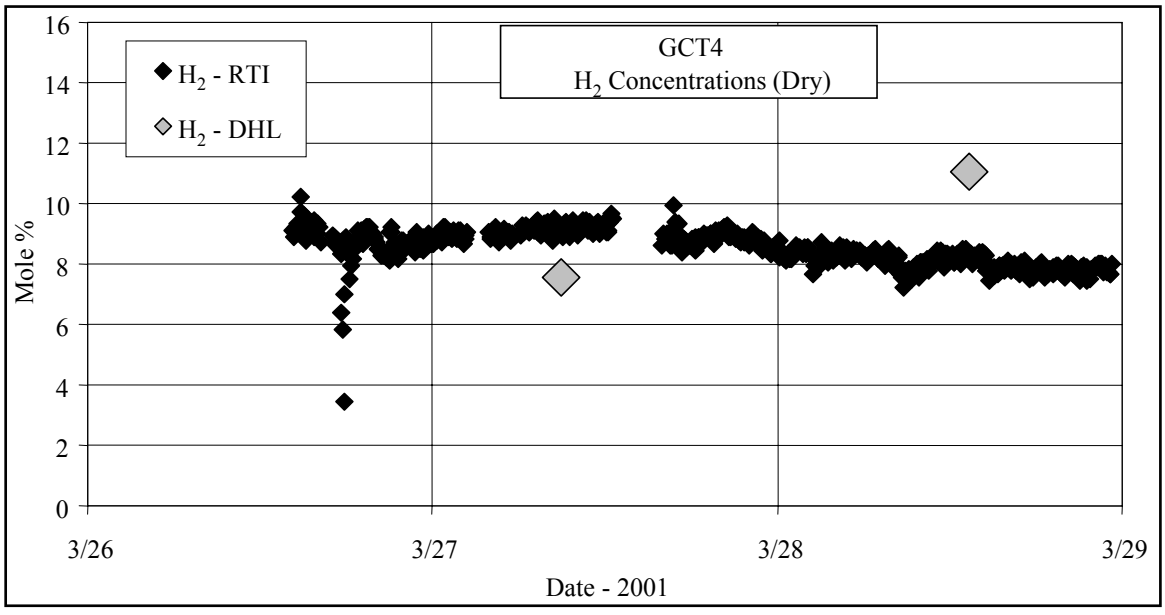

Figure 4.3-16 RTI and DHL H_2 Data

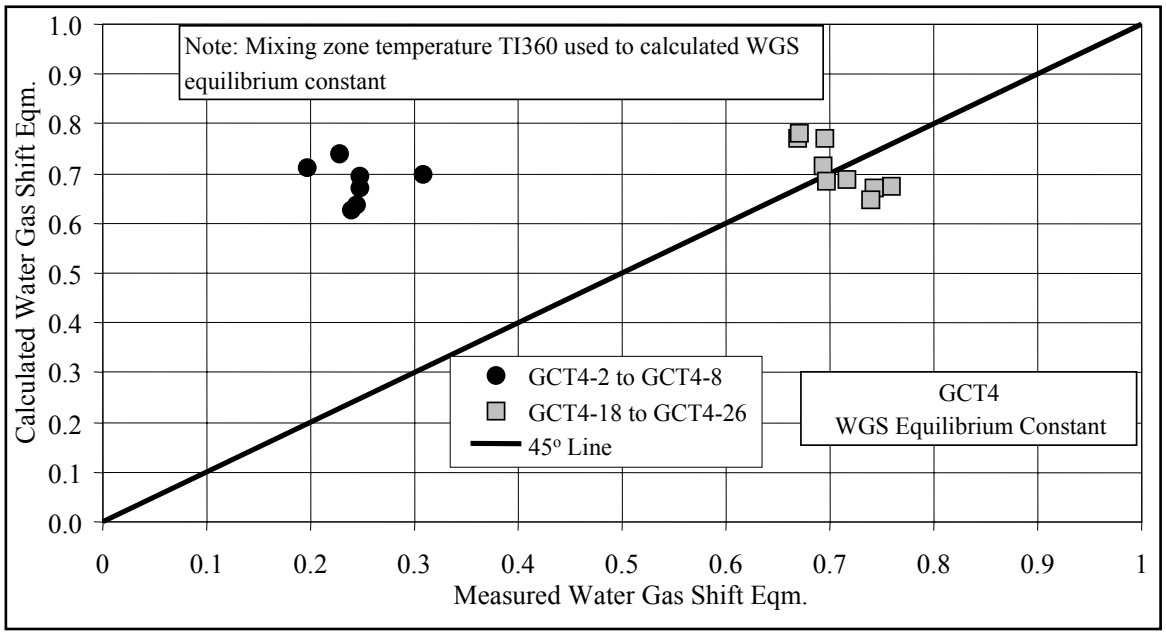

Figure 4.3-17 Water-Gas Shift Equilibrium Constants

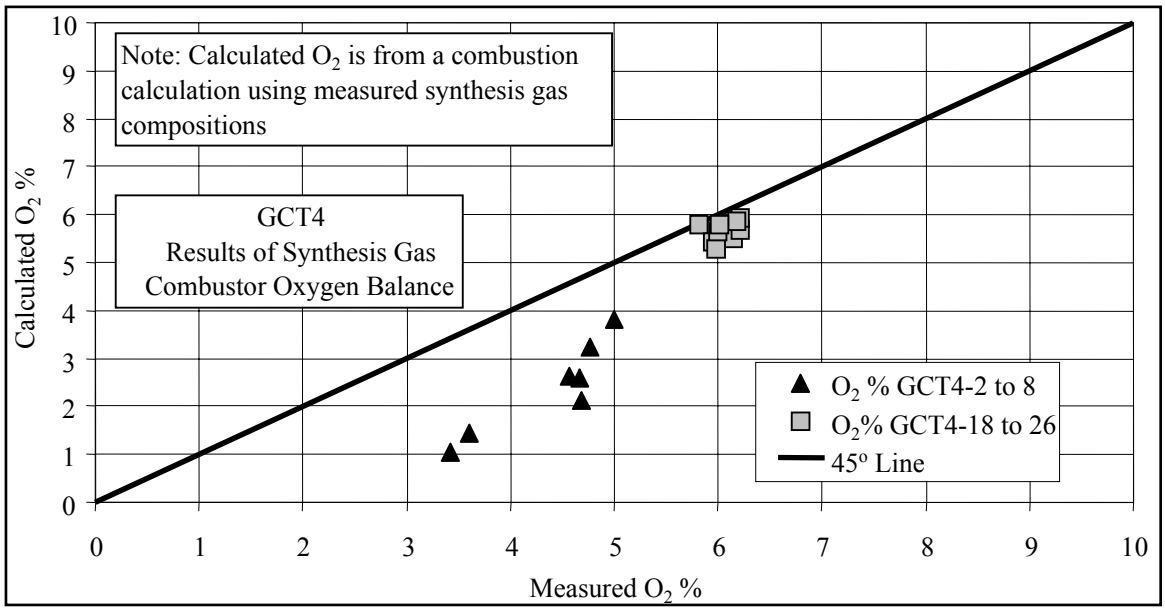

Figure 4.3-18 Calculated and Measured Synthesis Gas Combustor O_2

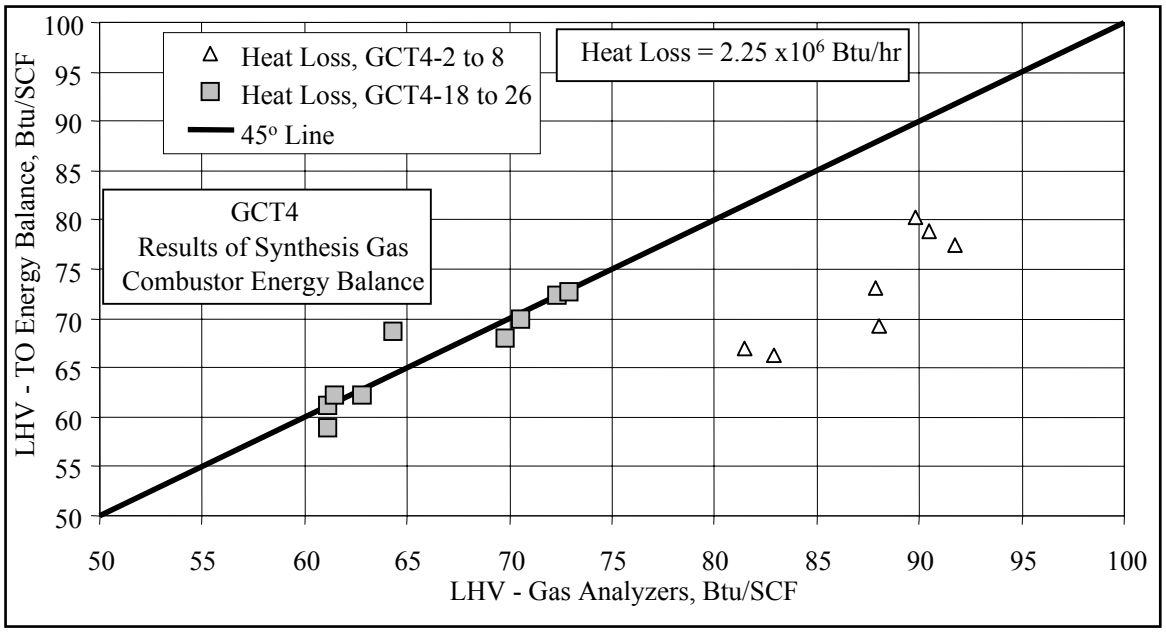

Figure 4.3-19 Calculated and Measured LHV

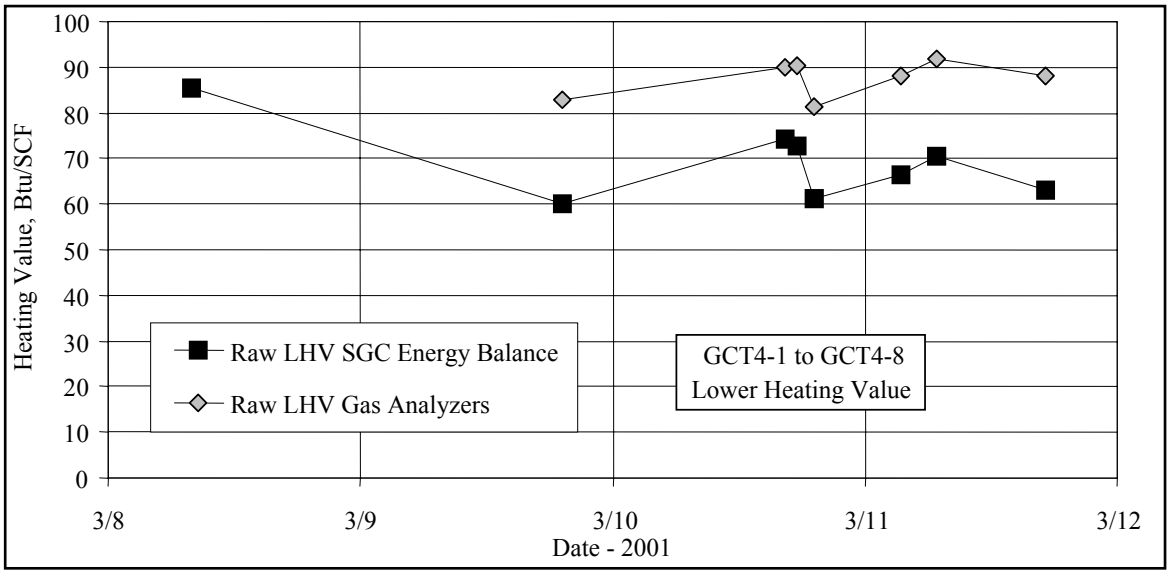

Figure 4.3-20 Calculated and Measured LHV, March 8 Through March 12, 2001

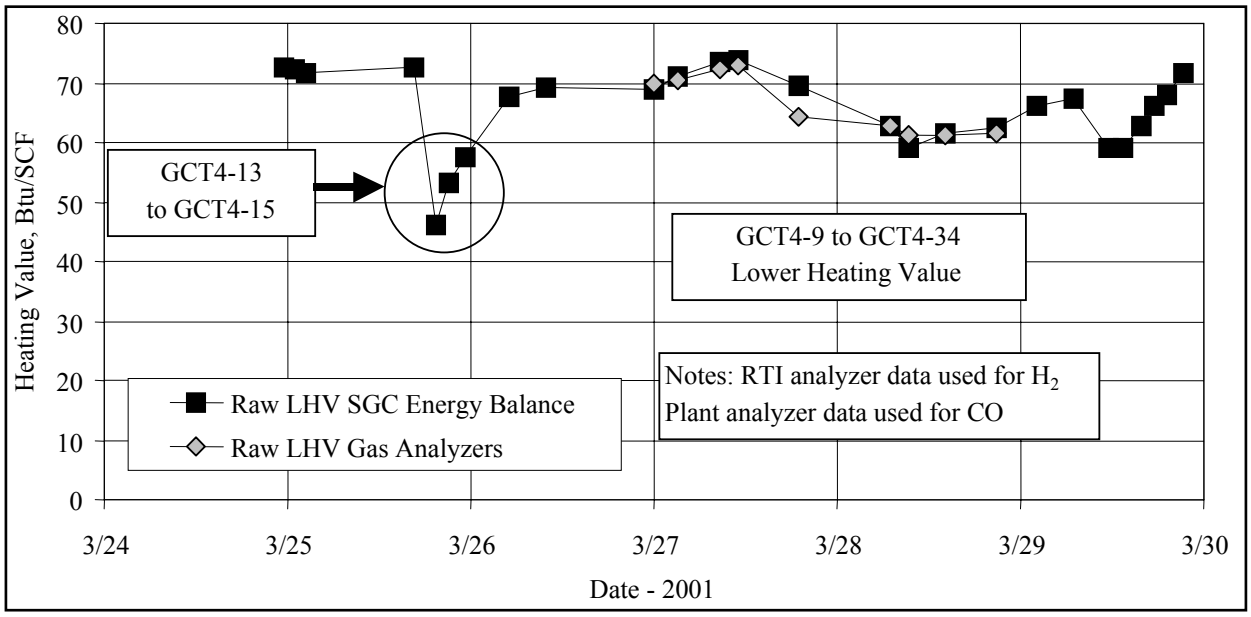

Figure 4.3-21 Calculated and Measured LHV, March 24 Through March 30, 2001

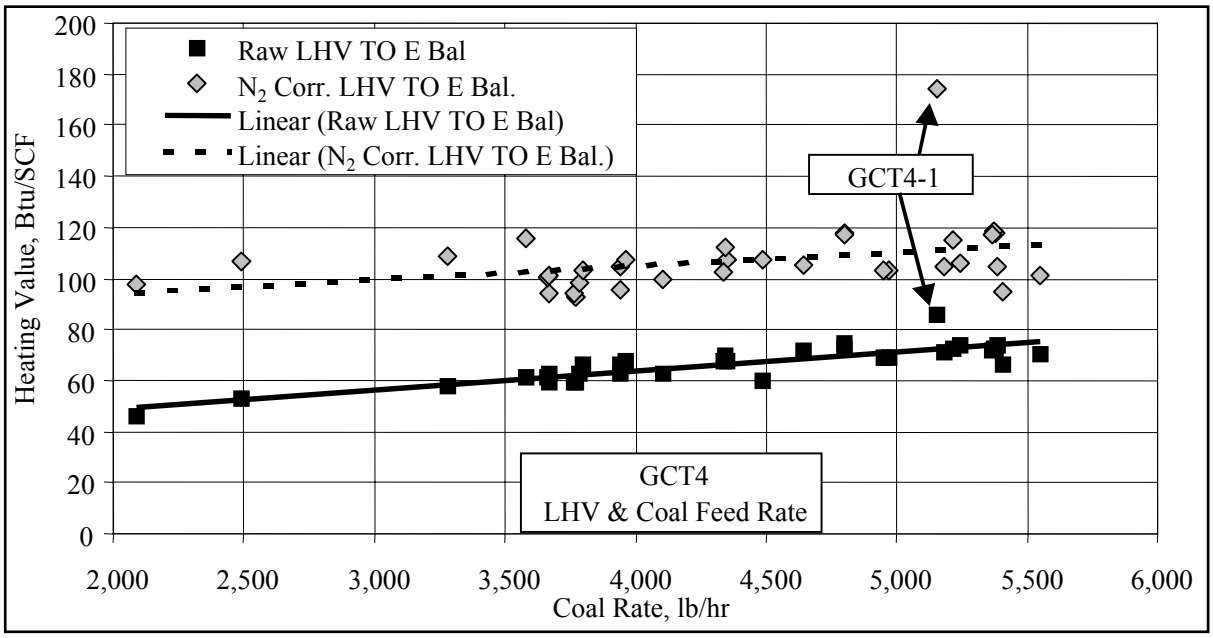

Figure 4.3-22 LHV and Coal Rate

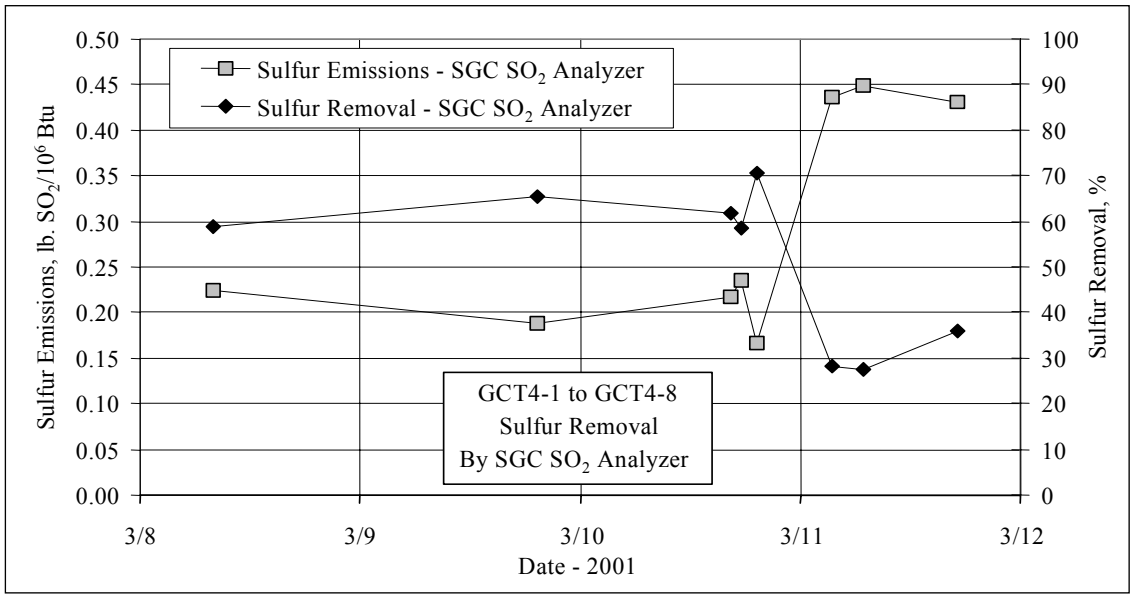

Figure 4.3-23 Sulfur Emissions & Removal, March 8 Through March 12, 2001

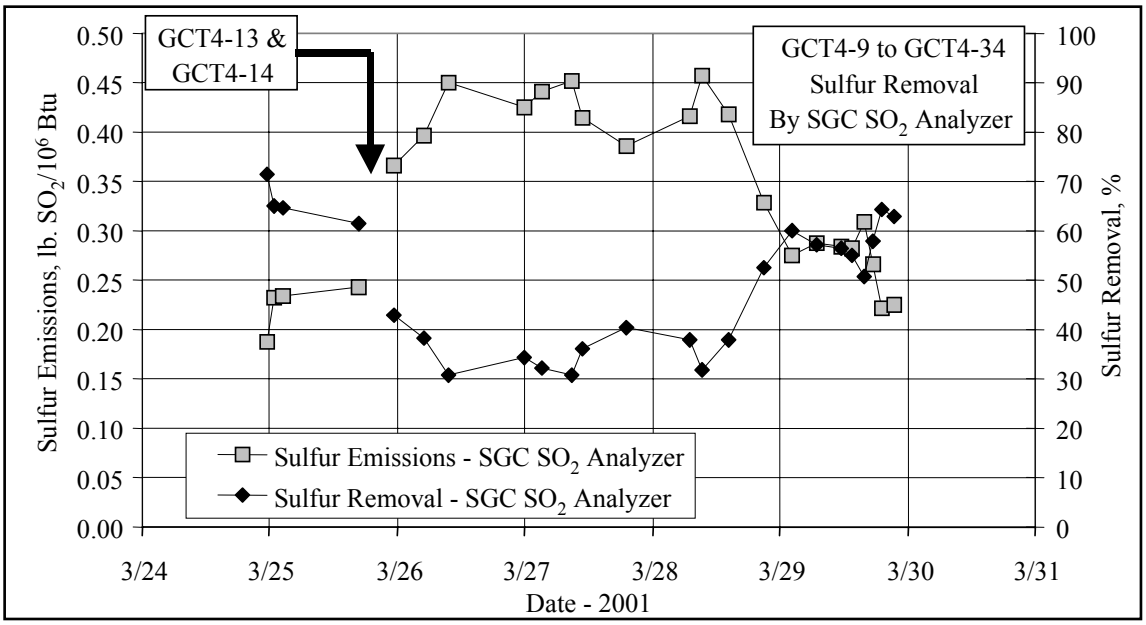

Figure 4.3-24 Sulfur Emissions and Removal, March 24 Through March 31, 2001

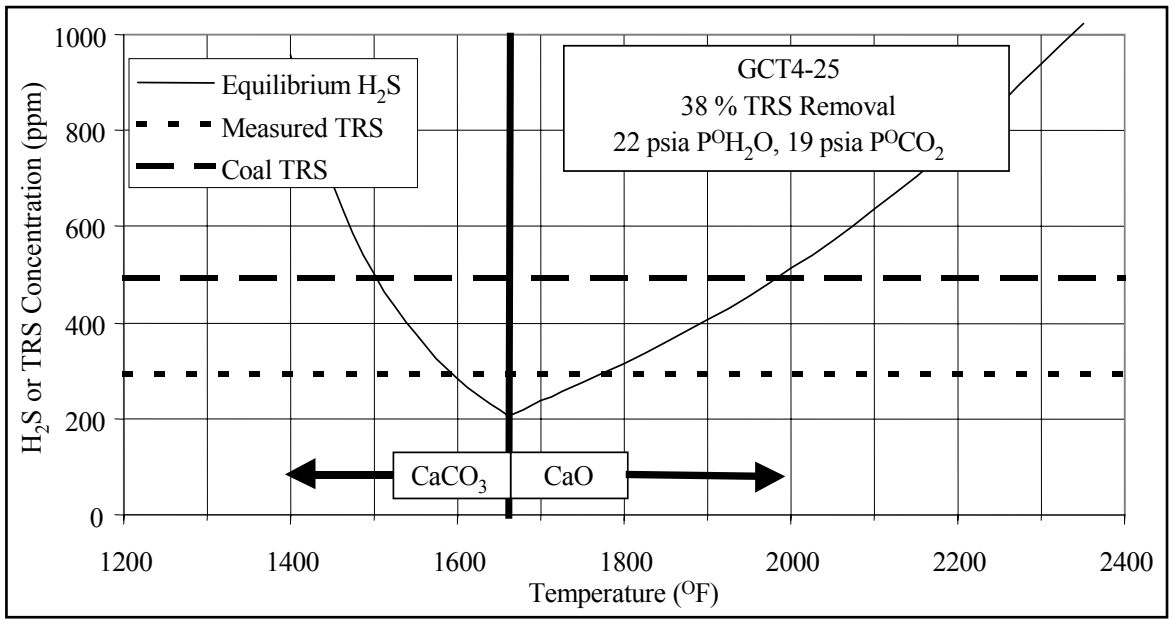

Figure 4.3-25 H_2S Equilibrium

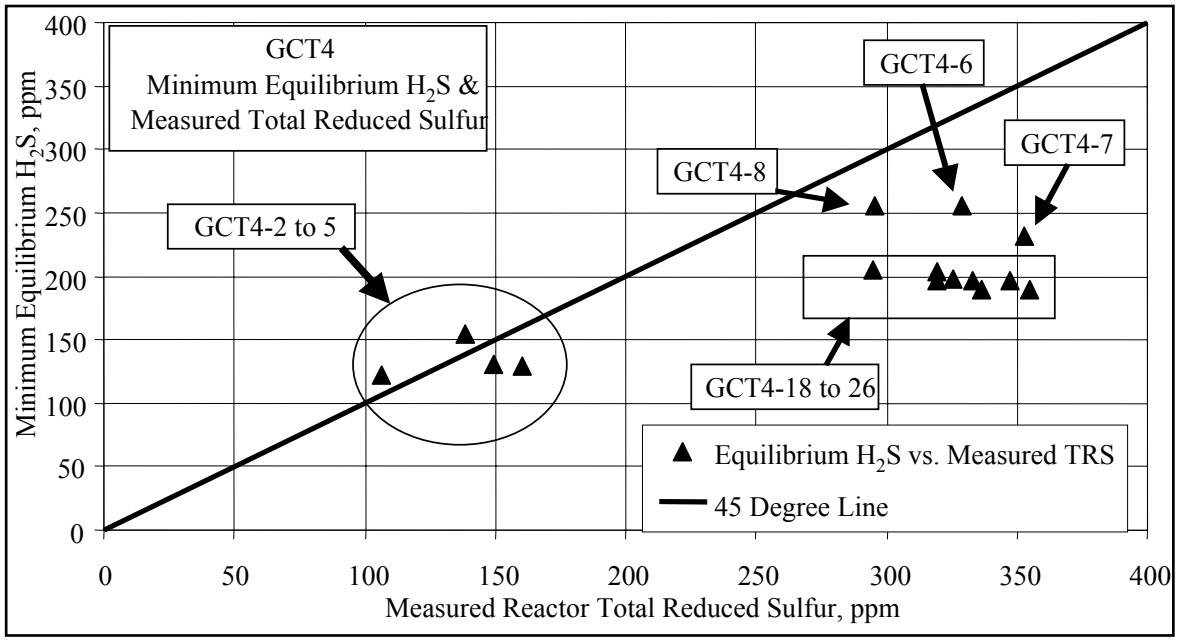

Figure 4.3-26 H_2S Equilibrium

4.4 SOLIDS ANALYSES

Solid samples were collected during GCT4 from the fuel feed system (FD0210), the sorbent feed system (FD0220), the transport reactor standpipe, the standpipe spent solids transport system (FD0510), and the PCD fine solids transport system (FD0520). In situ solids samples were also collected from the PCD inlet. These solids were analyzed for chemical composition and particle size. This section will use the chemical analysis data to show:

- Chemical composition changes.
- Particle size and bulk density changes.
- Effect of riser temperature on PCD char volatiles.

Figure 4.4-1 shows the fuel sulfur and ash as sampled from the fuel feed system during GCT4. The Powder River Basin (PRB) coal had from 0.26- to 0.34-percent sulfur and from 4.7- to 6.5-percent ash. The sulfur and ash weight percent were steadier during operating periods GCT4-9 to -34.

The coal carbon and hydrogen contents sampled from FD0210 are shown in Figure 4.4-2. The carbon was between 57- and 59-weight percent. The hydrogen content was from 3.75- to 4.25-weight percent. The hydrogen is measured dry and reported as sampled and does not include the hydrogen in the coal moisture.

The coal oxygen and moisture contents sampled from FD0210 are shown in Figure 4.4-3. The coal oxygen was constant during GCT4 at 12-weight percent. The oxygen is reported as received and does not include the oxygen in the coal free moisture. Oxygen is also not directly measured, but is the value required to make the elemental analysis add up to 100 percent. Therefore, it is the least accurate of the coal elemental analyses. The coal moisture was between 17- and 21-weight percent for GCT4.

The coal higher heating value (HHV) and lower heating value (LHV) are provided in Figure 4.4-4. The LHV was determined from HHV by reducing the heating value to account for the coal moisture and hydrogen. The LHV and HHV slightly decreased during GCT4.

The results of the 11 GCT4 coal analyses are provided in Table 4.4-1. Coal moisture, carbon, hydrogen, nitrogen, sulfur, ash, oxygen, volatiles, fixed carbon, and higher heating value are provided in Table 4.4-1, as are the GCT4 average values.

The Sauter mean diameter (SMD) and mass mean diameter (D_{50}) particle size of the coal feed to the transport reactor in GCT4 are shown in the plot in Figure 4.4-5. The coal was coarser for the first 4 days of testing, at a coal SMD diameter between 350 to 425 μm, while the D_{50} was between 340 and 380 μm. For March 22 to 24, the feed coal had SMD of 260 to 280 μm, with D_{50} of 260 to 300 μm. On March 26 at 20:00 the particle size jumped up to 320 to 370 μm with D_{50} at 300 to 360 μm.

A measure of the amount of fines would be the percent of the smallest size fraction. To show the level of fines in the coal feed, the percent of ground coal less than 45 μm is provided in Figure 4.4-6. The fines percent was 6 to 8 percent during the first 4 days of testing, around 15 percent during the March 22 to 24 testing, and around 10 percent during March 26 to March 30 testing. One of the probable causes of coal feeder trips is excessive fines in the coal. Periods of minimal coal feeder trips March 26 to March 30 show less than 10-percent fines in the coal. Periods of numerous coal feeder trips March 22 to 24 show higher fines in the coal feed.

FD0220 was used during GCT4 to feed Ohio Bucyrus limestone into the transport reactor. It was also used to feed various materials, such as coal fly ash, Cellite, and sand flour, directly to the PCD during some PCD testing on March 27. The compositions of the samples taken during GCT4 are shown in Figure 4.4-7. Most of the samples taken before March 27 and after March 29 had high-$CaCO_3$ contents, indicating that they were samples of limestone rather than the other materials fed through FD0220.

The SMD and mass mean diameter (D_{50}) of the solids sampled from the sorbent feeder FD0220 are shown in Figure 4.4-8. The SMD was between 6 to 10 μm prior to the introduction of the various materials for the PCD tests. The D_{50} was between 12 and 18 μm during this time. During the March 27 PCD tests, the SMD increased to 25 μm and the D_{50} increased to 30 μm. After the March 27 PCD testing, the SMD and D_{50} values returned to their previous values.

Figure 4.4-9 shows a plot of the SMD and D_{50} for the PCD solids sampled from FD0520. The SMD was fairly constant at 8 to 11 μm from March 9 to 11. Following a coal trip at 23:30 on March 10, the SMD increased from 10 μm to about 15 μm from 00:00 to 12:00 on March 11. The SMD then decreased, falling back down to 10 μm by the end of March 11. The D_{50} followed the same trend from March 9 to 12, increasing on March 11 and then decreasing at 12:00, March 11. The D_{50} varied between 11 and 22 μm from March 9 to 12.

The char fines SMD was constant at between 8 and 12 μm from March 24 to March 28. On the evening of March 28, the SMD spiked up to 17 μm at 18:00. The testing ended with the SMD at about 15 μm for the last day of testing. The D_{50} followed the same trend as the SMD, with the D_{50} varying between 13 and 27 μm.

The solid compounds produced by the transport reactor were determined using the solids analysis and the following assumptions:

1. All carbon dioxide measured came from $CaCO_3$, hence moles CO_2 = moles $CaCO_3$.
2. All sulfide sulfur measured came from CaS.
3. All sulfate sulfur measured came from $CaSO_4$.
4. All calcium not taken by CaS, $CaSO_4$, and $CaCO_3$ came from CaO.
5. All magnesium came from MgO.

6. Total carbon is measured, which is the sum of organic and inorganic (CO_2) carbon. The organic carbon is the total carbon minus the inorganic carbon (CO_2).

7. Inerts are the sum of the Fe_2O_3, P_2O_5, K_2O, Na_2O, and TiO_2.

FD0510 was operated during GCT4 to control the standpipe level. No FD0510 solid samples were taken during GCT4 because the standpipe samples should provide a more accurate view of the circulating solids compositions. Three FD0510 samples were taken on March 30 while the reactor was being drained of solids after GCT4 was completed. They are discussed at the end of this section.

Solids from the standpipe were sampled from March 9 to March 11. On March 11 the standpipe sampler plugged, so no more samples could be obtained from the standpipe. Table 4.4-2 shows the chemical analyses of the standpipe solids. The main component in the standpipe solids was SiO_2 at 80.1 to 86.5 percent, which is the main component of the startup sand. This is understandable since the reactor was started up on March 8 and was filled with startup sand prior to startup. The next largest compound was Al_2O_3 (5.0 to 9.2 percent), also from the startup sand. Longer term operation than the 2 days of standpipe samples available will be required to track the substitution of sand with coal ash and limestone reaction products in the reactor. Both the CO_2 (and $CaCO_3$) and sulfur (as CaS) contents were very low. This indicates that sulfur is not accumulating in the reactor. The CaO content was from 2.1 to 3.7 percent and could have come either from the feed limestone or the PRB coal ash. The organic carbon was 0.8 to 5.4 percent and was decreasing as the testing progressed. Preliminary TC06 data indicate that there is some carbon in the standpipe just after startup, but it decreases to low values once the unit is in continuous operation. An insufficient amount of the final sample, AB08025, was obtained to measure carbon and CO_2.

Figure 4.4-10 is a plot of the organic carbon (total carbon minus CO_2 carbon) for the PCD solids sampled from FD0520. Since FD0520 ran continuously during GCT4, solid samples were taken often, with a goal of one sample every 2 hours. About half of the GCT4 PCD solids that were sampled were analyzed. Solids recovered in situ during the PCD inlet particulate sampling were also analyzed. The in situ carbons are shown in Figure 4.4-10. The in situ solids organic carbon analyses compared well with the FD0520 solids except for the March 27 carbon analyses.

The organic carbon decreased from 58 percent on March 9 to 14 percent at 18:00 on March 11. The fine char carbon then increased to 40.9 percent when coal feeder problems caused the reactor temperature to decrease. Periods of low organic carbon content indicate excellent carbon conversion. The final 9 days of operation had the organic carbon content generally falling from 60 to 25 percent.

Figure 4.4-11 shows the amounts of $CaCO_3$, CaS, and CaO in the PCD solids as sampled from FD0520. Also shown in Figure 4.4-11 are the in situ solids concentrations for $CaCO_3$, CaS, and CaO. The $CaCO_3$ was constant, between 6 and 8 percent for the first 5 days of operation, except for the second, third, and final sample. The CaO started the run at 7-weight percent and then rose to 22-weight percent on March 11. The calcination increased during the first 5 days of operation. The CaS was generally decreasing during the first 5 days of operation, from about 3 to 2 percent.

The last 9 days of operation had erratic $CaCO_3$ concentrations between 4 and 22 percent with no real trend. The CaO concentration increased during the last 9 days, especially from March 28 to 30. The CaS slowly decreased from 3 to 0.5 percent.

Table 4.4-3 shows the PCD fines compositions for the samples collected in FD0520. The consistency is excellent in that the totals add up to between 96.1 and 102.8 percent. Also shown in Table 4.4-3 are the HHV, LHV, and volatiles for the PCD char fines. As expected, the trend of heating values follows the carbon content of the PCD fines.

The PCD char volatiles are shown plotted against riser temperature in Figure 4.4-12. There is a trend of decreasing char volatiles with increasing rising temperature. The volatiles were from 5 to 12 percent, while the organic carbon contents were from 14.8 to 56.8 percent.

The PCD char volatiles are shown plotted vs. the PCD char organic carbon in Figure 4.4-13. For all samples except one, the PCD char organic carbon was larger than the PCD char volatiles, which indicates that some of the PCD char carbon is not being measured as part of the PCD char volatiles. This is because the char carbonate is measured as a char volatile. This is probably fixed carbon that formed after the volatiles sat in the PCD for a while and cooked.

Table 4.4-4 provides analyses of three samples collected from FD0510 while the reactor was being drained of solids on March 30, after GCT4 was completed. The main component was SiO_2 at 60.4 percent, which indicated that some of the startup sand was replaced by coal ash and limestone reaction products since solids taken a few days after startup had over 80-percent SiO_2 (see Table 4.4-2). The Al_2O_3 was slightly higher than the startup solids, indicating that some Al_2O_3 may come from the PRB coal ash and is collected in the reactor. The CaO content of the end-of-run reactor solids was higher than the start-of-run reactor solids, indicating that some of the feed limestone was accumulated in the reactor during GCT4. The CaS content of the reactor did not change between the start and end of the run, indicating that there was no accumulation of sulfur in the reactor during GCT4. The organic carbon contents were extremely low. This could be due to low-reactor-carbon content during the run or due to carbon burnout upon shutdown.

The solids sampled first (see Table 4.4-4) are solids from the bottom of the reactor. The three samples indicate that the standpipe solids were not perfectly mixed, in that there was a slight accumulation of sand-like particles (higher in SiO_2 and larger in particle size) in the bottom of the reactor. The ash and limestone particles (higher in CaO and smaller in particles size) tended to accumulate in the top of the reactor.

Table 4.4-1

Coal Analyses

Sample ID	Date and Time	Moisture (%)	C, As Sampled (%)	H, As Sampled (%)	N, As Sampled (%)	S, As Sampled (%)	Ash, As Sampled (%)	O_2, As Sampled (%)	Volatiles, As Rcvd (%)	Fixed C, As Rcvd (%)	HHV, As Sampled Btu/lb	Sulfur %
AB07982	3/09/01 14:00	18.87	58.99	4.23	0.60	0.26	4.83	12.23	34.97	41.34	9,711	0.27
AB08026	3/10/01 20:00	19.27	58.46	4.21	0.57	0.27	5.22	12.00	35.47	40.03	9,645	0.28
AB08028	3/11/01 20:00	17.19	59.42	4.31	0.64	0.33	6.48	11.63	36.49	39.84	9,594	0.35
AB08029	3/12/01 04:00	17.41	59.21	4.21	0.59	0.34	6.49	11.74	35.76	40.34	9,734	0.35
AB08113	3/24/01 12:00	19.30	57.82	4.11	0.72	0.32	6.19	11.54	34.71	39.80	9,585	0.34
AB08115	3/25/01 12:00	20.09	57.10	3.88	0.71	0.30	5.58	12.34	34.42	39.92	9,469	0.32
AB08144	3/26/01 12:00	19.98	57.44	3.83	0.70	0.31	5.71	12.04	34.00	40.31	9,471	0.33
AB08163	3/27/01 20:00	20.47	56.70	3.96	0.69	0.31	5.39	12.48	35.74	38.40	9,473	0.33
AB08190	3/29/01 00:00	20.36	56.79	3.80	0.69	0.33	5.57	12.46	35.19	38.87	9,494	0.34
AB08215	3/29/01 20:00	20.48	56.92	3.72	0.76	0.29	5.69	12.14	34.12	39.70	9,459	0.30
AB08216	3/30/01 04:00	20.96	57.04	3.90	0.70	0.28	5.12	11.99	33.80	40.12	9,420	0.29
	Average	19.49	57.81	4.01	0.67	0.30	5.66	12.05	34.97	39.88	9,550	0.32
	Standard Dev.	1.25	1.03	0.21	0.06	0.03	0.54	0.32	0.85	0.77	109	0.03

Note: % is weight percent.

Table 4.4-2

Standpipe Solids Chemical Analyses

Sample Number	Sample Date and Time	SiO_2 (Wt %)	Al_2O_3 (Wt %)	CaO (Wt %)	MgO (Wt %)	Other Inerts (Wt %)	$CaCO_3$ (Wt %)	CaS (Wt %)	Organic Carbon (Wt %)	Total (Wt%)
AB07973	3/09/01 04:30	85.2	5.8	2.1	0.6	2.7	0.3	0.2	5.1	102.1
AB07974	3/09/01 09:30	86.5	3.7	2.8	0.6	2.4	0.5	0.2	5.4	102.1
AB07979	3/09/01 14:00	84.0	5.0	3.8	0.9	3.0	0.4	0.2	3.8	101.2
AB07980	3/09/01 16:00	80.1	9.2	3.4	0.8	3.8	0.4	0.2	1.2	99.1
AB08022	3/10/01 14:00	83.9	5.3	4.2	1.0	3.5	0.5	0.2	4.9	103.4
AB07981	3/10/01 16:00	81.9	7.2	3.5	0.9	4.1	0.5	0.2	2.1	100.3
AB08023	3/11/01 03:00	84.9	5.3	3.8	0.9	3.4	0.6	0.1	0.9	100.0
AB08024	3/11/01 12:00	81.8	7.8	3.7	1.0	4.6	0.5	0.2	0.8	100.4
AB08025	3/11/01 16:00	84.2	5.6	4.2	0.9	3.6	-	0.2	-	

Notes:
1. Sample AB08025 had insufficient sample to determine carbon and CO_2.
2. Other inerts consist of Fe_2O_3, P_2O_5, Na_2O, K_2O, and TiO_2.

Table 4.4-3

Analyses for PCD Char Fines From FD0520

Sample Number	Sample Date & Time	SiO_2 (Wt%)	Al_2O_3 (Wt%)	Other Inerts[1] (Wt%)	$CaCO_3$ (Wt%)	CaS (Wt%)	CaO (Wt%)	MgO (Wt%)	Organic C ($C-CO_2$) (Wt%)	Total (Wt%)	HHV (Btu/lb)	LHV (Btu/lb)	Volatiles[2] (Wt%)
AB07994	3/09/01 08:00	16.40	6.49	3.9	7.6	2.8	4.4	2.2	56.8	100.4	8,542	8,453	6.18
AB07996	3/09/01 12:00	16.83	6.57	4.0	6.7	2.8	5.1	2.2	56.4	100.6	8,415	8,314	6.18
AB07998	3/09/01 16:00	16.44	6.56	4.0	6.8	2.9	5.3	2.3	56.1	100.4	8,506	8,405	6.21
AB08000	3/09/01 20:00	15.61	6.54	4.1	12.1	4.0	7.2	3.6	48.8	101.9	7,286	7,203	7.37
AB08007	3/10/01 18:00	18.86	7.55	4.9	11.6	4.8	9.4	4.0	41.2	102.4	6,268	6,207	6.40
AB08008	3/10/01 20:00	18.37	6.96	5.0	0.3	4.2	17.3	4.0	40.0	96.1	6,119	5,982	7.00
AB08009	3/10/01 22:00	26.20	10.04	6.6	8.7	2.2	16.3	4.7	25.7	100.3	4,012	3,974	21.32
AB08012	3/11/01 04:00	22.58	9.19	5.9	7.7	2.4	14.0	4.2	34.8	100.8	5,343	5,287	5.98
AB08013	3/11/01 08:00	26.99	9.95	6.4	7.2	2.5	16.2	4.6	26.9	100.8	4,265	4,216	5.99
AB08014	3/11/01 12:00	26.54	9.95	6.3	7.3	1.8	16.9	4.8	29.1	102.5	4,143	4,104	5.79
AB08015 a	3/11/01 16:00	26.61	10.39	6.2	7.8	2.2	15.8	4.9	27.0	100.9	4,030	3,991	6.18
AB08016	3/11/01 18:00	29.47	11.75	8.0	5.8	1.6	21.5	5.7	13.9	97.7	2,175	2,133	4.71
AB08017	3/11/01 20:00	31.82	11.42	7.1	6.4	2.2	18.4	5.3	17.7	100.3	2,878	2,850	5.63
AB08021 a	3/12/01 04:00	17.66	7.56	4.4	17.4	0.7	7.3	3.7	40.9	99.5	6,133	6,059	13.36
AB08121	3/24/01 12:00	14.37	5.44	3.8	8.2	3.1	2.9	2.2	58.1	98.2	8,818	8,706	7.49
AB08123	3/24/01 16:00	13.21	4.94	3.0	16.2	2.3	4.2	3.3	51.4	98.7	7,758	7,633	11.07
AB08125	3/24/01 20:00	13.35	5.36	3.4	11.7	3.1	4.9	3.1	53.8	98.6	8,200	8,071	8.72
AB08127	3/25/01 00:00	19.27	7.46	4.4	6.2	2.2	6.0	2.6	49.6	97.8	7,657	7,526	6.75
AB08128	3/25/01 06:00	12.55	4.70	3.0	13.2	1.7	3.9	2.7	55.9	97.7	8,525	8,387	11.18
AB08130	3/25/01 10:00	12.40	5.03	3.1	10.8	1.9	4.7	2.6	57.0	97.5	8,669	8,535	10.40
AB08133	3/25/01 16:00	16.52	5.89	3.8	7.1	2.2	6.3	2.5	53.9	98.2	8,203	8,082	8.29
AB08134	3/26/01 02:00	29.09	8.59	5.7	5.3	2.4	8.4	2.8	38.6	100.7	5,605	5,527	5.98
AB08135	3/26/01 04:00	27.59	8.54	6.1	5.3	2.3	8.5	2.8	37.8	98.9	5,807	5,750	5.80
AB08136	3/26/01 08:00	24.47	8.78	5.9	12.4	1.7	3.9	2.6	41.5	101.3	6,341	6,218	5.66
AB08148	3/26/01 12:00	14.34	5.61	3.6	4.5	0.8	3.4	1.5	62.7	96.4	9,788	9,609	8.77
AB08150	3/26/01 16:00	26.49	8.84	6.0	6.5	1.9	7.0	2.8	38.6	98.2	6,016	5,934	6.63
AB08152	3/26/01 20:00	16.87	6.61	4.1	4.6	1.0	3.8	1.6	59.6	98.1	9,066	8,930	7.44
AB08154	3/27/01 00:00	22.06	8.60	5.0	4.2	1.4	5.1	2.0	50.9	99.1	7,712	7,608	6.78
AB08171	3/27/01 04:00	45.64	4.58	3.0	16.3	0.0	6.7	3.7	14.8	94.9	2,259	2,246	15.65
AB08155	3/27/01 08:00	36.80	13.47	8.2	4.2	0.8	13.5	4.0	18.6	99.5	2,730	2,686	5.37
AB08172	3/27/01 08:00	37.24	10.77	6.9	12.2	0.5	10.0	4.1	19.2	101.0	2,646	2,628	8.86
AB08175	3/27/01 12:00	27.79	9.16	6.4	7.3	1.3	8.0	3.0	36.7	99.6	5,498	5,436	6.66
AB08178	3/27/01 16:00	28.44	7.81	5.6	13.6	0.9	4.8	3.1	32.8	97.1	4,980	4,922	10.46
AB08180	3/27/01 20:00	27.10	7.40	5.6	12.7	0.8	5.5	2.8	37.9	99.7	5,602	5,531	10.00
AB08182	3/28/01 00:00	26.90	5.89	4.8	21.7	0.6	1.8	3.3	32.7	97.7	5,001	4,935	13.42
AB08196	3/28/01 04:00	17.26	7.14	5.8	7.5	1.7	5.9	2.6	51.1	98.9	7,688	7,587	7.27
AB08196 a	3/28/01 04:00	18.27	7.11	5.2	9.4	1.7	6.0	2.6	48.5	98.7	7,261	7,097	7.97
AB08197	3/28/01 08:00	32.24	6.81	5.0	8.6	1.0	5.7	2.5	40.9	102.8	5,466	5,350	7.74
AB08198	3/28/01 16:00	31.33	9.19	6.7	6.7	1.1	9.8	3.4	31.7	99.8	4,815	4,751	5.46
AB08200	3/28/01 20:00	29.91	8.28	6.4	9.1	1.1	11.3	4.1	28.4	98.5	4,413	4,360	7.37
AB08202	3/29/01 00:00	20.96	8.11	5.6	13.7	0.2	18.9	6.5	26.1	100.1	4,043	4,000	8.94
AB08204	3/29/01 04:00	18.69	7.61	5.8	13.2	0.6	18.2	6.5	29.0	99.6	4,639	4,591	8.61
AB08205	3/29/01 08:00	15.55	7.05	5.0	17.2	0.2	18.2	6.9	28.6	98.8	4,487	4,437	10.76
AB08221	3/29/01 18:00	17.15	7.27	5.5	13.8	0.2	28.3	10.3	17.4	100.0	2,774	2,753	8.55
AB08223	3/30/01 00:00	17.05	7.91	5.6	12.0	0.7	21.3	7.9	26.4	98.9	4,194	4,155	7.35
AB08225	3/30/01 04:00	18.08	7.84	5.9	11.4	0.6	23.6	8.1	24.2	99.8	3,963	3,923	6.74

Notes:

1. Other inerts consist of Fe_2O_3, P_2O_5, Na_2O, K_2O, and TiO_2.
2. Volatiles from ASTM procedure and include CO_2.

Table 4.4-4

End-of-Run Reactor Solids Analyses

Sample Number	Sample Date and Time	SiO_2 (Wt %)	Al_2O_3 (Wt %)	CaO (Wt %)	MgO (Wt %)	Other Inerts[1] (Wt %)	$CaCO_3$ (Wt %)	CaS (Wt %)	Organic Carbon (Wt %)	Total (Wt%)
AB08218	3/30/01 09:00	65.0	10.0	16.0	2.5	4.8	1.7	0.3	0.2	100.5
AB08219	3/30/01 10:00	59.5	9.8	21.1	3.2	4.8	1.3	0.3	0.3	100.4
AB08220	3/30/01 11:00	56.7	10.1	23.2	3.5	4.9	1.2	0.2	0.1	99.9
	Average	60.4	10.0	20.1	3.1	4.8	1.4	0.3	0.2	

Notes:
1. Other inerts consist of Fe_2O_3, P_2O_5, Na_2O, K_2O, and TiO_2.

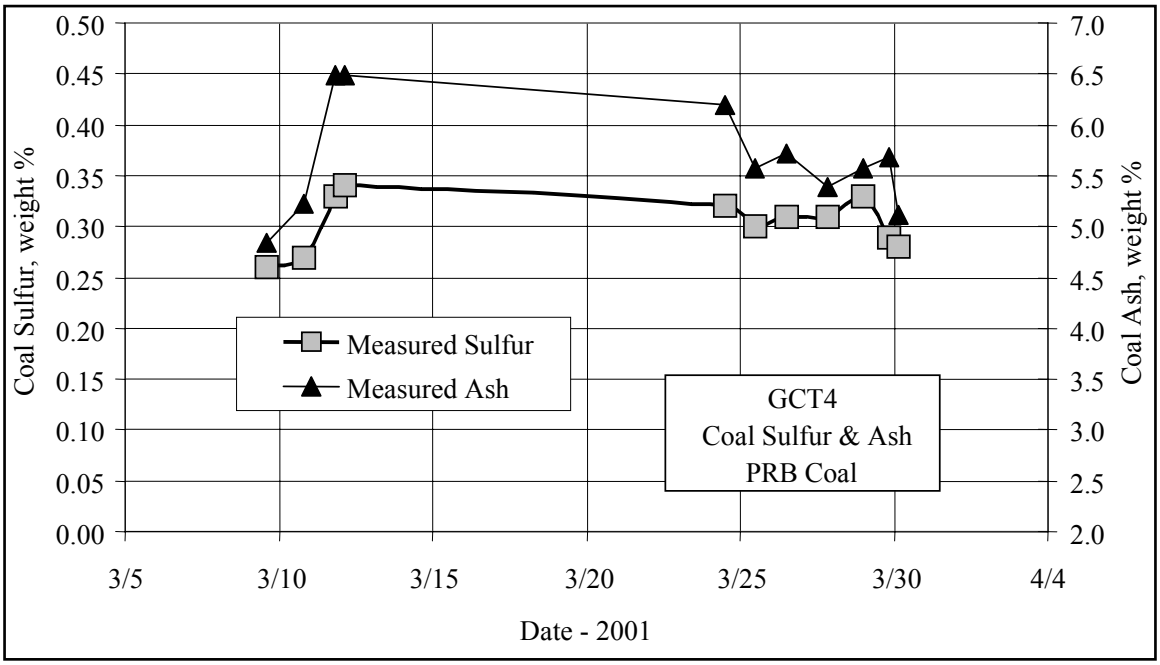

Figure 4.4-1 Coal Sulfur and Ash

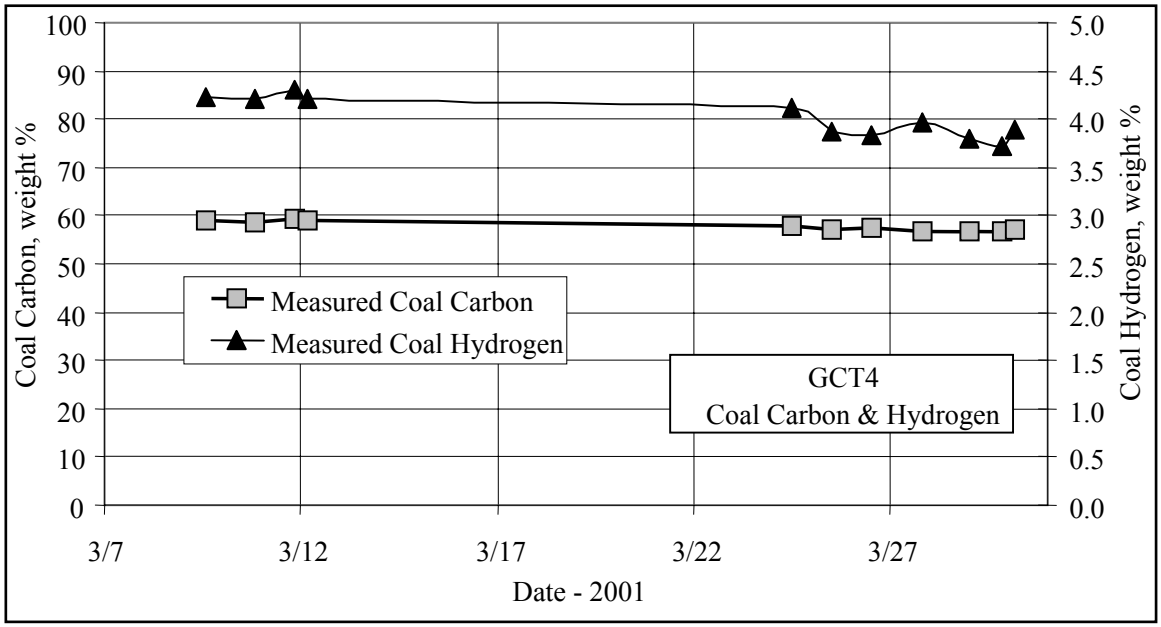

Figure 4.4-2 Coal Carbon and Hydrogen

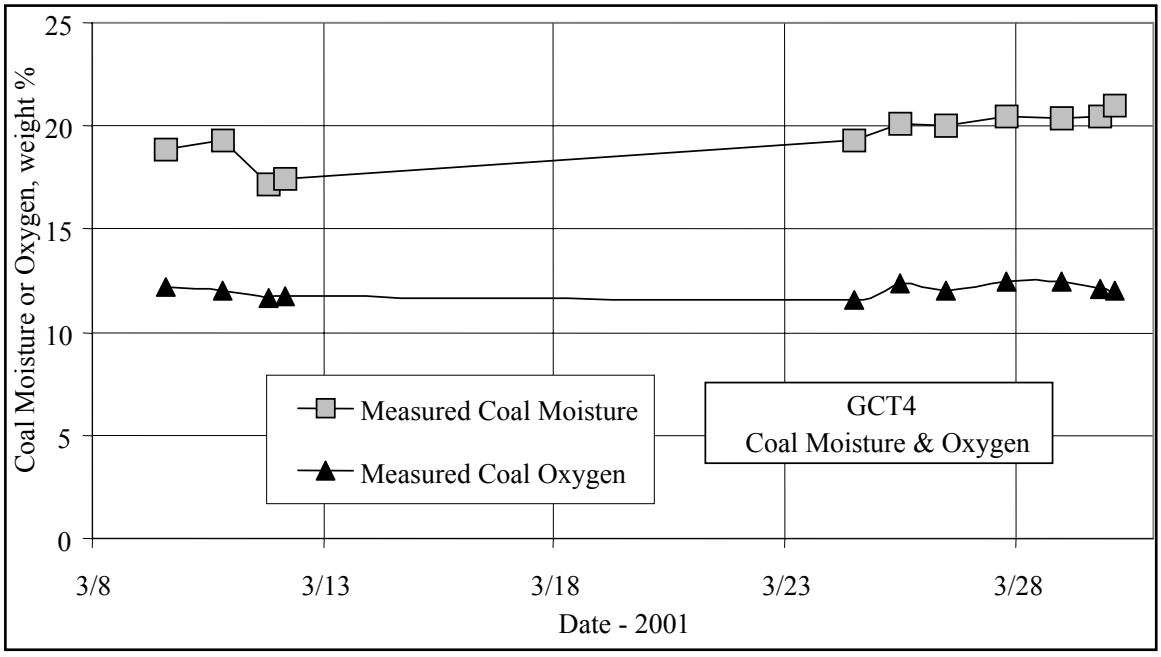

Figure 4.4-3 Coal Moisture and Oxygen

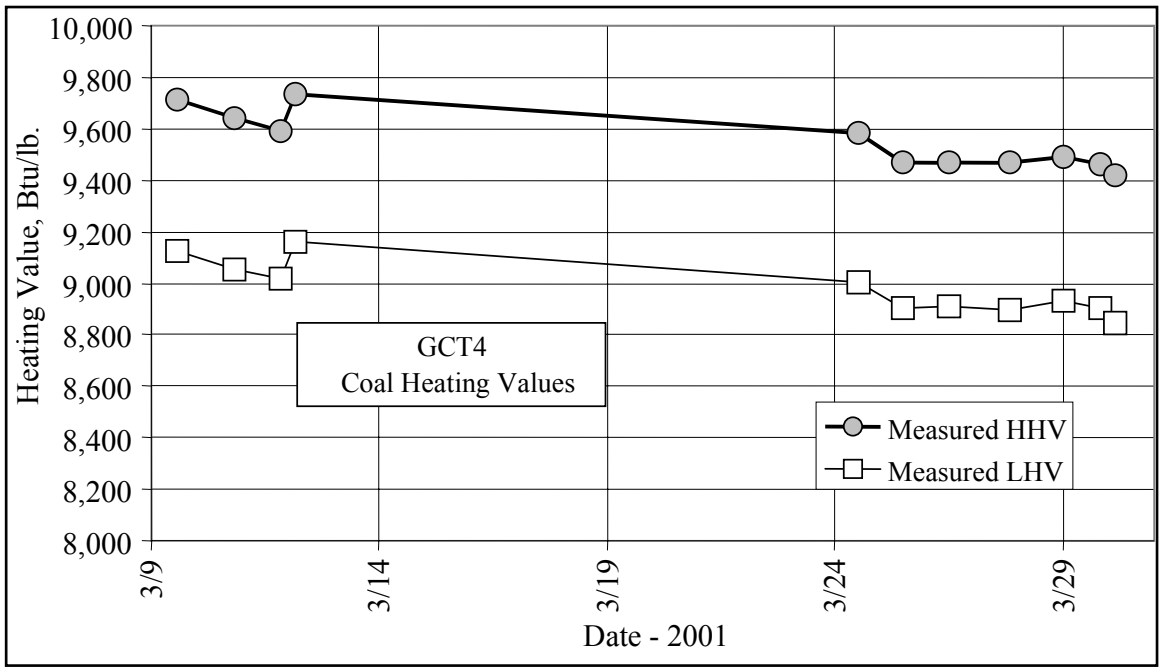

Figure 4.4-4 Coal Higher and Lower Heating Value

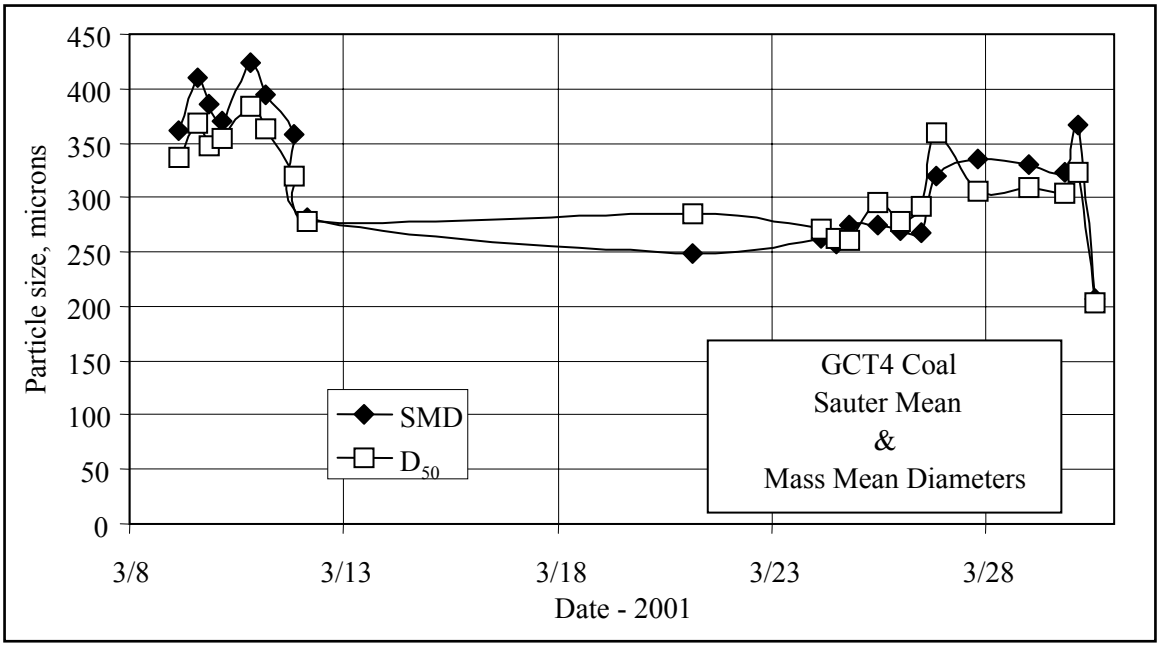

Figure 4.4-5 Coal Sauter Mean and Mass Mean Diameters

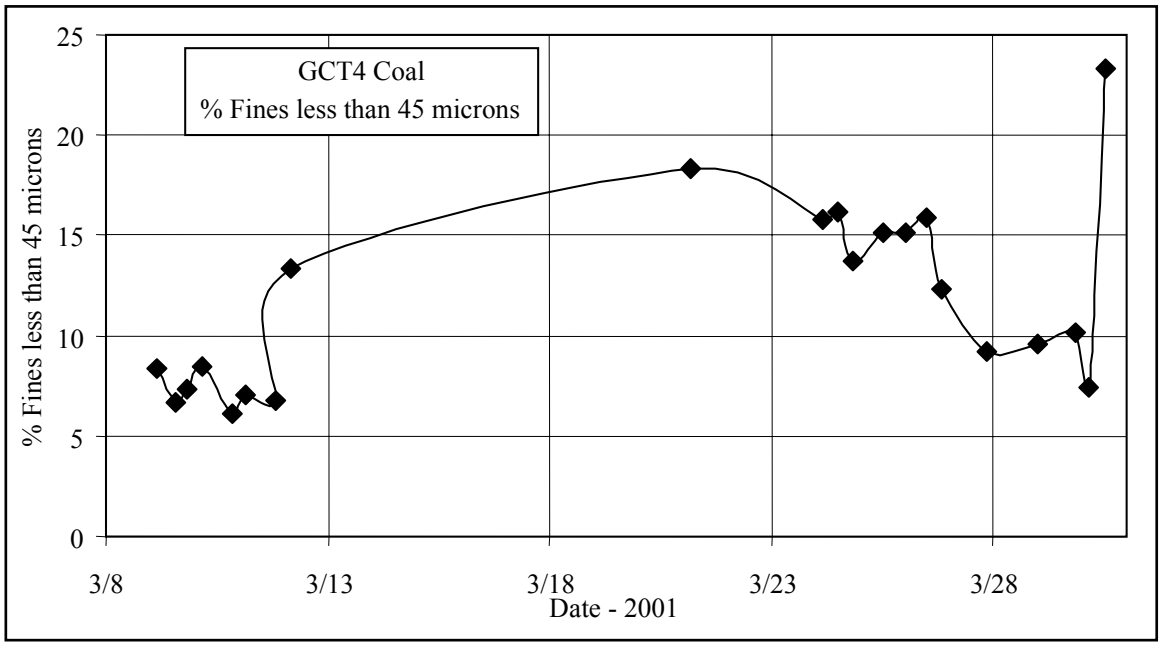

Figure 4.4-6 Percent Coal Fines

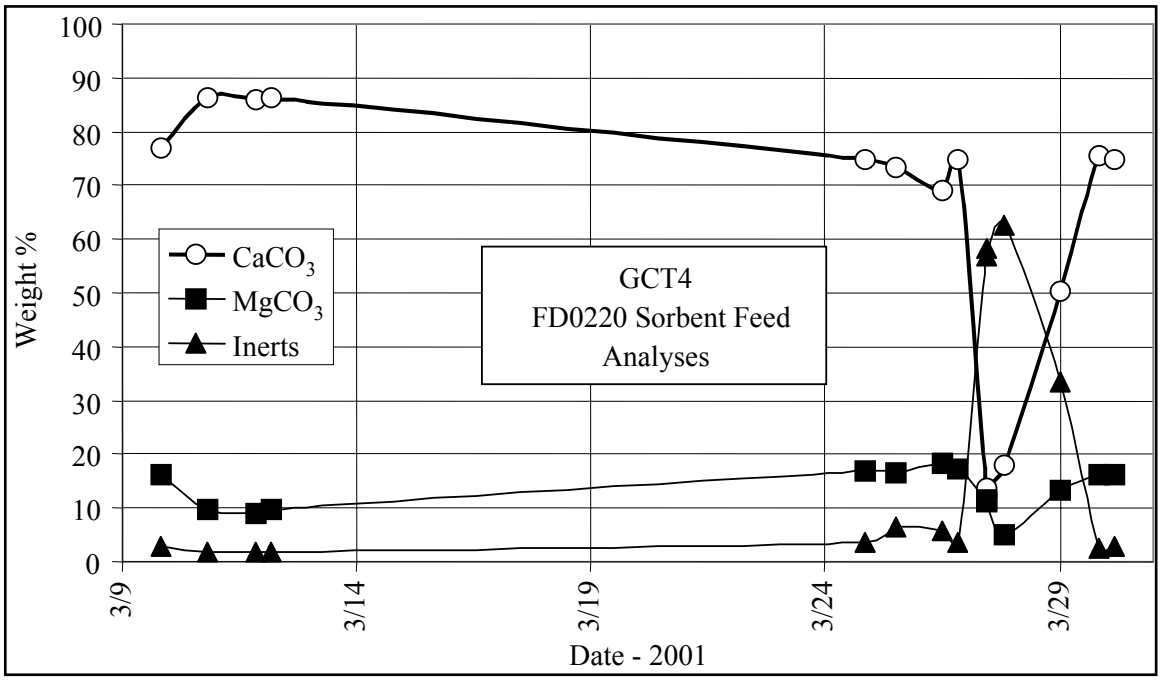

Figure 4.4-7 Sorbent Feed Analyses

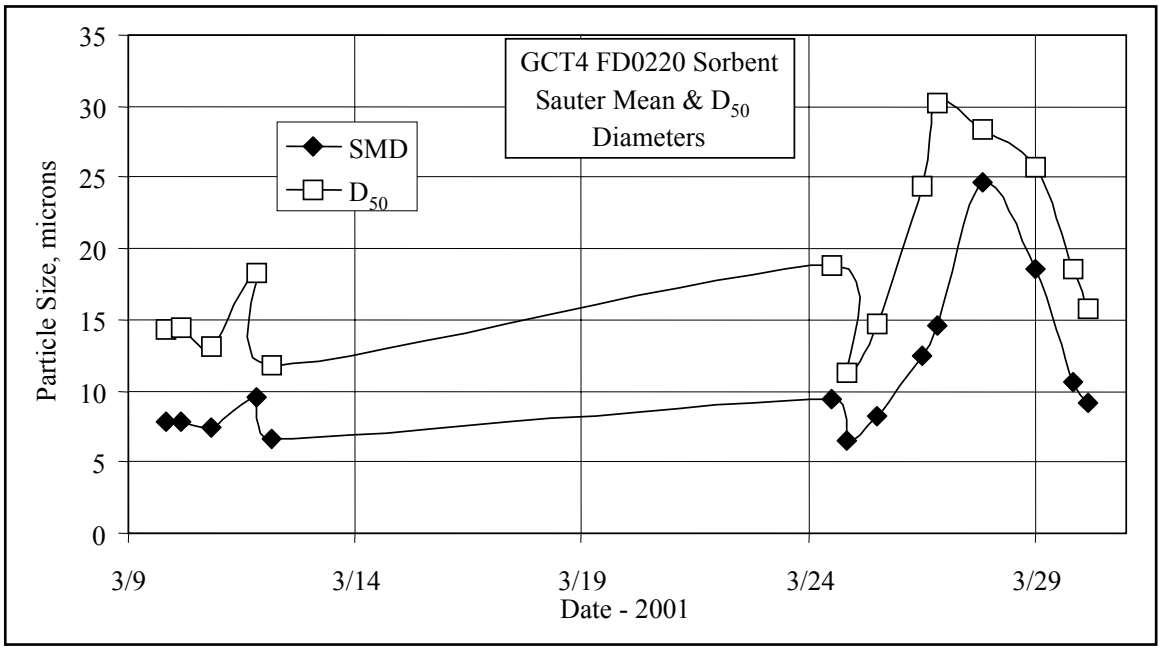

Figure 4.4-8 Sorbent Feed Particle Size

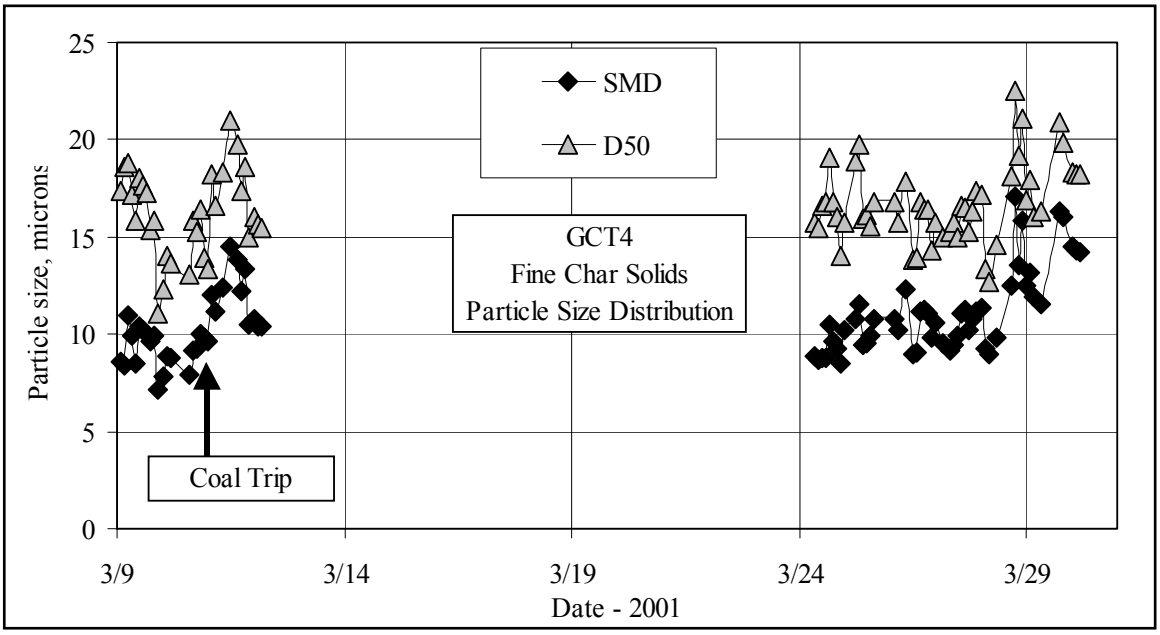

Figure 4.4-9 Fine Char Particle Size

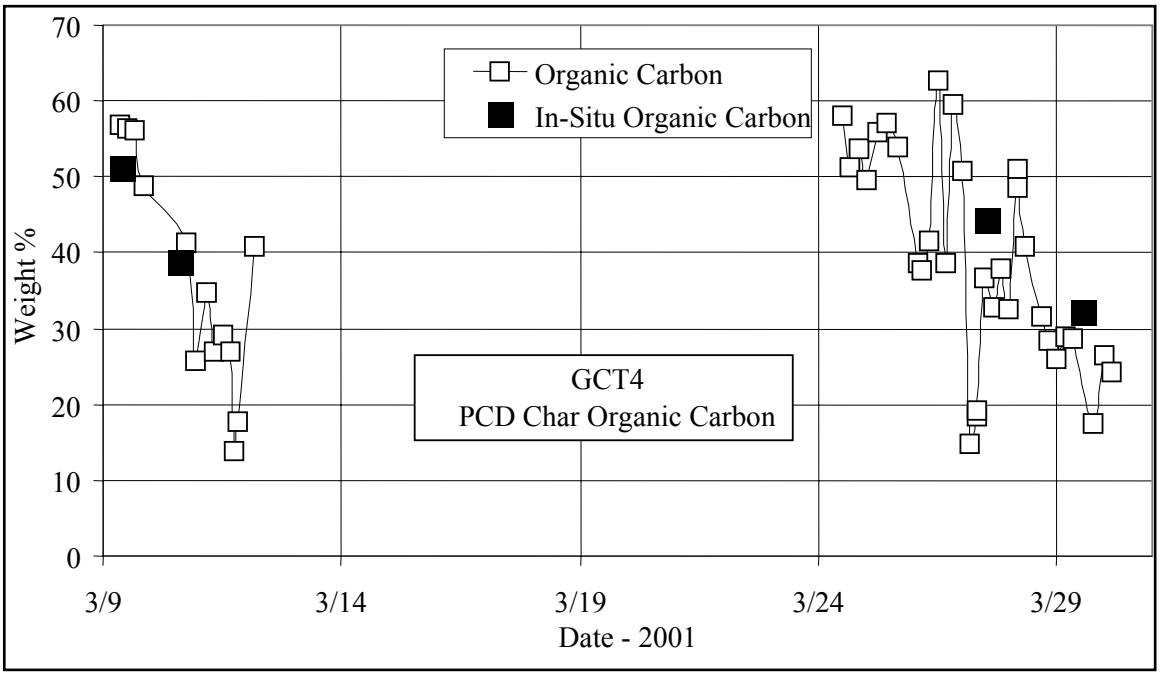

Figure 4.4-10 Fine Char Organic Carbon

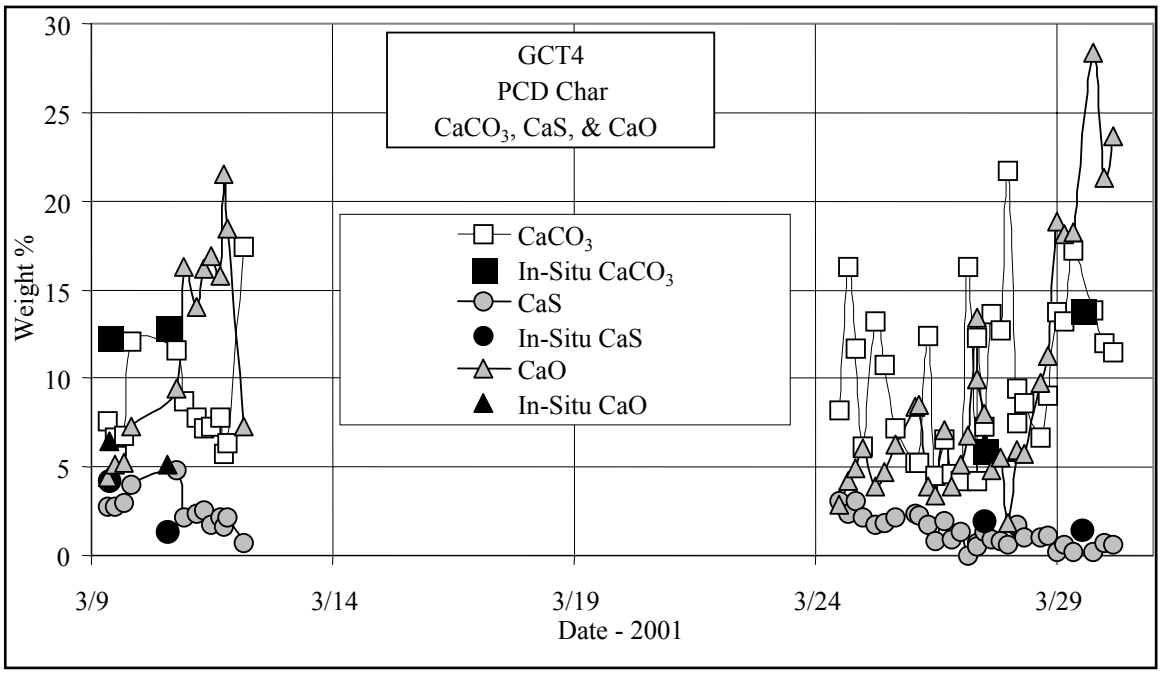

Figure 4.4-11 Fine Char $CaCO_3$, CaS, and CaO

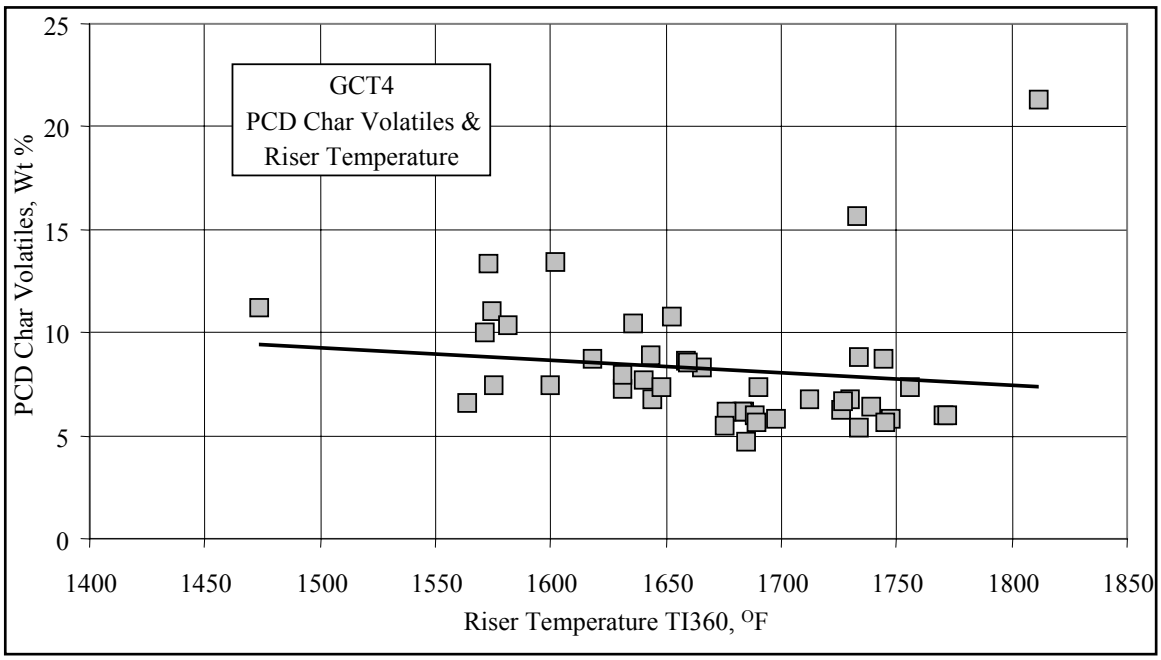

Figure 4.4-12 Fine Char Volatiles Vs. Riser Temperature

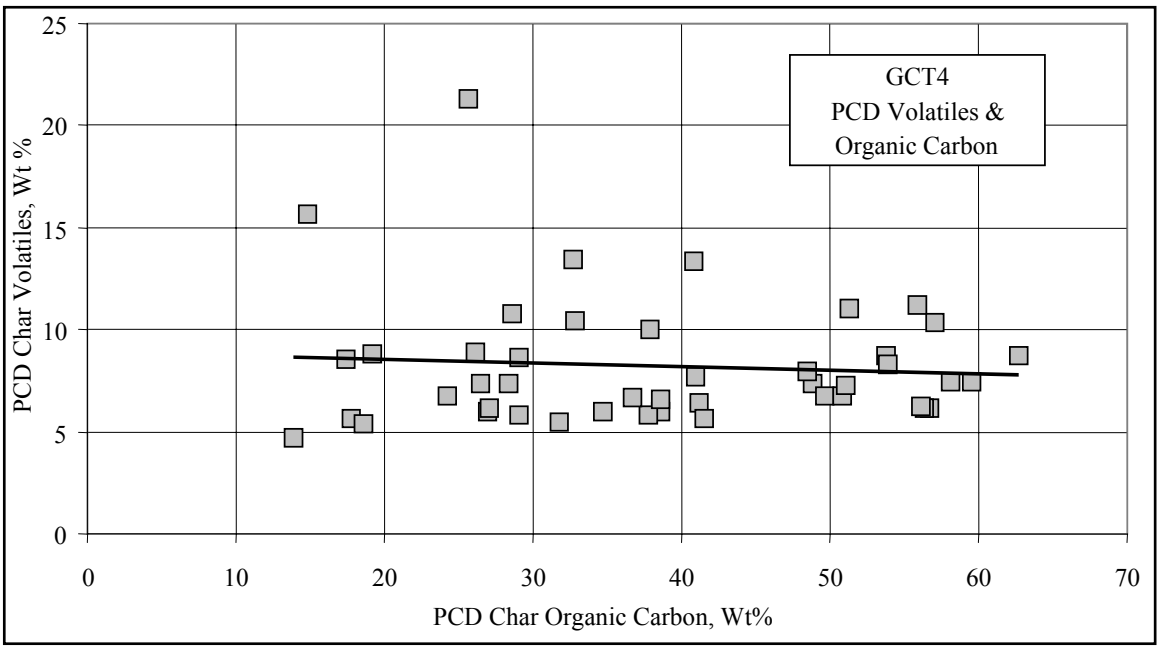

Figure 4.4-13 Fine Char Volatiles Vs. Organic Carbon

4.5 MASS AND ENERGY BALANCES

Using the gas analyses, solids analyses, and process flows entering and leaving the Halliburton KBR transport reactor, the following were determined:

- Overall mass balance.
- Nitrogen balance.
- Carbon balance.
- Carbon conversion.
- Sulfur balance.
- Sulfur removal.
- Hydrogen balance.
- Oxygen balance.
- Calcium balance.
- Sulfur capture dependence on calcium to sulfur ratio.
- Inerts balance.
- Energy balance.
- Gasification efficiencies.

The process flows into the Halliburton KBR transport reactor are:

- Coal flow through FD0210.
- Sorbent flow through FD0220.
- Air flow measured by FI205.
- Nitrogen flow measured by FI609.
- Steam flow measured by FIC204.

The process flows from the KBR transport reactor are:

- Synthesis gas-flow rate from the PCD measured by FI465.
- PCD solids flow through FD0520.
- Reactor solids flow through FD0510.

The coal flow through FD0210 was determined from a correlation between feeder speed (revolutions per minute [RPM]) and coal dumps from the FD0210 surge bin between fills. This correlation is shown in Figure 4.5-1. The correlation is:

$$\text{Coal rate} = -2.8813(\text{RPM})^2 + 291.81(\text{RPM}) - 1829 \quad (1)$$

The hourly average coal-flow rates are shown in Figures 4.3-2 and -5, in Section 4.3, Gas Analysis. Table 4.5-1 provides the coal rates for the operating periods.

The sorbent flow through FD0220 was determined from a correlation between feeder speed and sorbent dumps from the FD0220 storage bin between fills. This sorbent fill/feeder speed data and correlation is shown in Figure 4.5-2. The correlation for the sorbent feeder is:

$$\text{Sorbent rate} = 41.722\ (\text{RPM}) + 105.06 \qquad (2)$$

The operating period limestone rates are shown in Table 4.5-1.

The hourly average synthesis gas- and nitrogen-flow rates are shown in Figures 4.3-3 and 4.3-6. Table 4.5-1 provides the synthesis gas and nitrogen operating period flow rates. The synthesis gas rate was checked for all the operating periods using an oxygen balance around the synthesis gas combustor and found to be in excellent agreement with the synthesis gas combustor data for operating periods GCT4-18 to -26. The agreement was poor for operating periods GCT4-2 to -8 (see Figure 4.3-18).

It is estimated that about 1,000 lb/hr nitrogen from FI609 does not enter the process but is used to seal valves, for pressurized/depressurized feed and ash lock hopper systems, and in the seals for the screw coolers. Values shown in Table 4.5-1 assume that 1,000 lb/hr of nitrogen from FI609 does not enter the transport reactor.

The steam rate to the reactor was determined from FIC289, which measures the steam flow to the reactor J-leg rather than from FI204, which measures the total steam flow to the reactor. FI204 was not reading correctly for most of GCT4 and the mixing zone steam nozzles were plugged for most of the run. The steam nozzles to the reactor J-leg were generally less plugged during GCT4, so most of the steam entering the reactor entered through FIC289. The hourly average steam rate is shown in the plot in Figures 4.3-9 and -13. The steam rate for the operating periods is provided in Table 4.5-1.

The solids flow from the PCD can be determined from two different methods by using:

1. In situ particulate sampling data upstream of the PCD.
2. FD0530 weight cell data.

The best measurement of the solids flow to the PCD is the in situ PCD inlet particulate determination. Using the synthesis gas-flow rate, the solids flow to the PCD can be determined because the PCD captures all of the solids.

The FD0530 weight cell data can be used to determine the PCD solids flow only if both the FD0530 feeder and the FD0510 feeder (standpipe solids) are off because FD0520 and FD0510 both feed into FD0530 and FD0530 feeds the sulfator. This method assumes that the PCD solids level in the PCD and FD0502 screw cooler are constant (that is, the PCD solids level is neither increasing nor decreasing). The results for the first two methods are compared in Figure 4.5-3 for the first 5 days of operation. The estimated rates used for the test periods in mass balance and carbon conversion calculations are shown in Table 4.5-1.

There were only two in situ particulate samples taken for the first 5 days of operation. The first one compared well with the weigh cell data. The second in situ particulate sample was taken

during the startup on March 10 and was much higher than the weigh cell data. The estimated PCD solids rate was about 800 lb/hr on March 8, and then decreased to 400 lb/hr during March 9. The PCD solids rate was about 300 lb/hr on March 11. During the first 5 days of operation, solids were twice withdrawn from the reactor while FD0530 was not feeding the sulfator, so the FD0530 weigh cells measured the combined rate of solids collected by FD0520 and FD0510. The combined rates are shown in Figure 4.5-3. The FD0510 rate can be estimated by the difference between the sum of the combined rates and the FD0520 rate. During the first 5 days of operation, FD0510 was not operated during any of the steady operating periods.

The PCD solids rates from the weigh cell data and in situ data for the last 7 days of operation are compared in Figure 4.5-4. The estimated rates used for the test periods in mass balance and carbon conversion calculations are provided in Table 4.5-1.

There were four in situ particulate samples taken during the last 7 days of operation. All in situ samples compared well with the weigh cell data. The estimated PCD solids rate was about 600 lb/hr on March 24 and 25, then decreased to 350 to 500 lb/hr for the next 2 days. For the final day of operation, the PCD solids rate was estimated at about 190 to 210 lb/hr. These low PCD fines rates will produce high-carbon conversions.

Solids were often withdrawn from the reactor to control the standpipe level during the last 7 days of operation, so there were several times when the combined rates of FD0520 and FD0510 could be determined. The combined rates are shown in Figure 4.5-4. The FD0510 rate can be estimated by the difference between the sum of the combined rates and the FD0520 rate. Those rates for the steady periods are shown in Table 4.5-1. Since FD0510 was usually not operated for an entire operating period, the values shown in Table 4.5-1 and used in the mass balances have been prorated down from the FD0510 rates shown in Figure 4.5-4.

The reactor inventory change during a test period has been estimated from the change in standpipe levels and loop seal levels from the start and end of each test period. The reactor accumulation is provided in Table 4.5-1 for each operating period. The accumulation term is a measure of how steady the operating period was. True steady operation would have a zero-accumulation term. High positive or low negative accumulation terms indicate unsteady operation.

Material balances are useful in checking the accuracy and consistency of the data obtained as well as determining periods of operation where the data is suitable for model development or commercial plant design. Material balances for each operating period are provided in Figure 4.5-5 and listed in Table 4.5-1, showing the relative difference (relative error) of transport reactor feeds in minus products out divided by the feeds ({in-out}/in) and the absolute difference (absolute error) of the feeds and the products (in-out). The overall material balance was excellent, within ± 4.4 percent for the relative difference (± 1,100 lb/hr for the absolute difference), with the exception of operating period GCT4-1, which was close to the beginning of coal feed. There is a positive bias for most of the steady periods material balance at about 500 lb/hr for operating periods GCT4-9 to -22. The final 12 test periods had an excellent mass balance, with relative differences of less than 1.1 percent. The gas composition data in Section 4.3 have no effect on the overall mass balance.

Test period nitrogen balances are shown in the plot in Figure 4.5-6 and listed in Table 4.5-2. Typical nitrogen flows for GCT4-26 are shown in Table 4.5-3. No nitrogen balance can be calculated for test periods when there is no nitrogen synthesis gas analyzer data, so nitrogen balances were determined for only test periods GCT4-2 to -8 and from GCT4-18 to -26. Synthesis gas nitrogen was measured by gas analyzers for test periods GCT4-2 to -8 and determined by difference for test periods GCT4-18 to -26. The nitrogen balance is acceptable for the first seven operating periods at +5 to 8 percent relative error (745 to 1,386 lb/hr). The last nine operating periods show a negative bias of about -1.4 to -3.5 percent (-227 to -473 lb/hr), which is excellent. The same data in Figure 4.5-6 is shown in Table 4.5-2.

Test period carbon balances are shown in the plot in Figure 4.5-7 and listed in Table 4.5-4. No carbon balance can be calculated for test periods when there is no synthesis gas analyzer data, so carbon balances were determined for only test periods GCT4-2 to -8 and -18 to -26. Test periods GCT4-2 to -8 carbon balances were low by -9.1 to -23.5 percent (-243 to -663 lb/hr carbon) (more carbon leaving the unit than entering). Test periods GCT4-18 to -26 were high by 11.3 to 24.3 percent (325 to 615 lb/hr carbon) (more carbon entering the unit than leaving). The carbon balances are not very good for either period. This lack-of-carbon balance produces large errors in the carbon conversions and gasification efficiencies. The coal and synthesis gas rates dominate the carbon balance. Since standpipe solids samples were taken only during the first few days of operation, the standpipe carbon was not measured and the carbon removed from the transport reactor by FD0510 could not be accounted for. Based on preliminary TC06 data, there was minimal carbon in the standpipe solids. The carbon balance was probably low (more carbon in the products that the feeds) for the steady periods GCT4-2 to -8 due to the high C_2^+ measured by the PSDF gas analyzers. The carbon balance was high for operating periods GCT4-18 to -26, probably because the coal rates were about 10 percent too high. This appeared to also be true for GCT3 and preliminary TC06 data in that a 10-percent decrease in coal rate would produce a good carbon balance.

Carbon conversion is defined as the percent fuel carbon that is gasified to CO, CO_2, CH_4, C_2H_6, and higher hydrocarbons. The carbon conversion is important because it is the measure of how much carbon is rejected by the gasifier with the PCD and reactor solids. This rejected carbon is typically burned in a less efficient combustor and results in a less efficient use of the fuel. Carbon conversion can be calculated three ways from the available data:

- From gas analysis (using the synthesis gas rate and synthesis gas composition) and the feed carbon rate (using the coal-feed rate and coal carbon content) (gas analyses).

- From PCD solids data (using the PCD solids-flow rate and PCD solids carbon content) and the feed carbon rate (solids analyses).

- From the products analysis using the gas analysis data and the PCD solids data (product analyses).

If there was a good carbon balance, all three carbon conversion calculation methods would produce the same result, within experimental error. All three carbon conversions for the operating periods are shown in Figure 4.5-8 and Table 4.5-4. The gas compositions used are

determined using procedures described in Section 4.3. Solids compositions are provided in Section 4.4. The gas analysis and products procedures can only be used for periods when there was gas analyzer data. Since the solids carbon conversions are not dependent on the gas analyzer data, the solids carbon conversions can be determined for all the operating periods.

The carbon conversions calculated from the solids analyses for the operating periods GCT4-1 to -8 increased from 85.1 to 97.4 percent, indicating excellent carbon conversion. The carbon conversions calculated from the gas analyses for the operating periods GCT4-2 to -8 were all above 100 percent and were caused by the high C_2^+ gas analyzer data. The carbon conversions calculated from the solids analyses for the operating periods GCT4-9 to -34 increased from 90.2 to 98.2 percent, indicating excellent carbon conversion. The two operating periods with lower than 89 percent solids carbon conversions (GCT4-13 and -14) were operations during low coal-feed rates. The carbon conversions based on the products agreed well with the carbon conversions based on the solids analyses. The carbon conversions based on the gas analyses for operating periods GCT4-18 to -26 were from 81.8 to 85.1 percent, with two low conversions of less than 78 percent. GCT4 carbon conversions by the solids and products analyses should be more accurate than those by the gas analyses.

Sulfur balances for all the GCT4 operating periods are provided in Figure 4.5-9 and Table 4.5-5. Since the syngas combustor SO_2 analyzer is downstream of the syngas combustor, it did not plug with tar during GCT4 and was in operation during the entire run. Therefore, sulfur balances could be determined for all of the operating periods. The sulfur balances are not very good. The first 5 days of operation (GCT4-1 to -9) have a sulfur balance between -14.1 and +6.9 percent (-1.9 to +2.0 lb/hr). The large change in sulfur balance indicates that the unit did not reach constant conditions with respect to sulfur during the first 4 days of operation. The final 7 days of steady operation had most of the sulfur balances between +20 and +40 percent. The periods of negative sulfur balance (less than zero percent) were during periods of low coal-feed rates (GCT4-13 to -15). For the last eight operating periods the sulfur balance deteriorated to +40 to +50 percent error.

With such large errors in the sulfur balances it is difficult to determine actual sulfur removal. As with the carbon conversions with a poor carbon balance, there are three different methods to determine the sulfur removals:

1. From synthesis gas sulfur emissions (using the synthesis gas combustor flue-gas rate and synthesis gas combustor flue gas SO_2 measurement) and the feed sulfur rate (using the feed coal rate and coal sulfur content) (gas analyses).

2. From PCD solids analysis (using PCD solids-flow rate and PCD solids sulfur content) and the feed sulfur rate (solids analyses).

3. From the products analysis, using the gas analysis data and the PCD solids data (product analyses).

The three sulfur removals are shown in the plot in Figure 4.5-10 and in Table 4.5-5. The sulfur in the fuel is an inaccurate measurement due to the multiplication of a very small number (coal sulfur) by a very large number (coal-feed rate). The low coal sulfur contents (0.25- to 0.35-

weight percent sulfur) increase the error in feed sulfur. The gaseous sulfur measurement (synthesis gas-flow rate, synthesis gas combustor-flow rate, and synthesis gas combustor-exit-SO_2 concentration) should be more accurate, even though it is also the product of a small number (SGC SO_2) and a large number (SCG flue-gas rate). This is because it is more accurate to measure gas-flow rates and compositions, and these flows and compositions are measured continuously. The PCD fines sulfur rate may have inaccuracies in the very low sulfur in the PCD solids. There appeared to be no accumulation of sulfur-containing solids in the reactor during GCT4 because the standpipe and FD0510 reactor samples contain very small amounts of sulfur.

The sulfur-mass balance is difficult to close due to the low sulfur flows and compositions as a result of using low-sulfur PRB coal. The synthesis gas combustor SO_2 concentration was used for the sulfur emissions shown in Figures 4.3-23 and -24. The sulfur removals shown in Table 4.3-3 and Figures 4.3-23 and -24 are based on the feed sulfur and gaseous sulfur. The sulfur removals for the solids and products analyses are low for the last 3 days of operation due to the low levels of sulfur in the PCD fines (see Table 4.4-3). For both the early- and late-March testing, the sulfur removal seemed to drop off suddenly after a few days.

Operating period hydrogen balances are provided in Figure 4.5-11 and Table 4.5-2, with typical values provided in Table 4.5-3. Hydrogen balances could only be done for periods with gas analyzer data. The hydrogen balance was poor for operating periods GCT4-2 to -8, with a high bias from 4.6 to 17.8 percent (11 to 84 lb/hr hydrogen). The hydrogen balance was good for the operating periods GCT4-18 to -26, with a slight high bias of -1.3 to 5.0 percent (-4 to 17 lb/hr hydrogen). The coal and synthesis gas streams dominate the hydrogen balance. The hydrogen in the coal is usually larger than hydrogen in the steam added. The data indicates that the periods when the synthesis gas hydrogen was measured by the RTI analyzers had the better hydrogen balances.

Operating period oxygen balances are provided in Figure 4.5-12 and Table 4.5-2, with typical values provided in Table 4.5-3. Oxygen balances could only be done for periods with gas analyzer data. The oxygen balance was poor for the operating periods GCT4-2 to -8, with a low bias from -21.1 to -11.7 percent (-1,304 to -487 lb/hr oxygen). The oxygen balance for the operating periods GCT4-18 to -26 was good, with a slight negative bias of -3.8 to -5.2 percent (-217 to -106 lb/hr oxygen). Note the large oxygen contribution of the feed coal, since the PRB coal has a high-oxygen content (moisture plus elemental oxygen). The coal and PCD solids oxygen concentration is determined by difference, so it is typically a less accurate value than the other elemental analyses.

Operating period calcium balances are provided in Figure 4.5-13 and Table 4.5-2, with typical values provided in Table 4.5-3. The PRB operation is characterized by low sorbent-feed rates because of low sulfur in the PRB coal. Note that about half of the inlet calcium comes from fuel and half from sorbent. The calcium balances were poor during GCT4, with a positive calcium bias from 20 to 85 percent. This is probably due to the low calcium flows in the system, the inaccuracies of the sorbent and coal feeder flows, and because the calcium flow is the result of multiplying a small number (calcium in the coal) by a large number (coal-flow rate).

Figure 4.5-14 is a plot of GCT4 sulfur emissions (expressed as pounds SO_2 emitted per MBtu coal fed) and sulfur removal as a function of calcium to sulfur ratio (Ca/S) based on the coal and sorbent fed to the transport reactor. It would appear that the sulfur emissions are independent of the feed Ca/S. Due to the poor sulfur and calcium balances, the true trend might not be evident due to the errors in the data. The sulfur emissions and removals are based on the synthesis gas combustor SO_2 analyzer (see Table 4.3-3, Section 4.3). The feed Ca/S ratios are provided in Table 4.5-5 for each operating period. The emissions seemed to be grouped into two different ranges, those below 0.35 lb SO_2 per 10^6 Btu coal and those above 0.35 lb SO_2 per 10^6 Btu coal. The group below 0.35 lb SO_2 per 10^6 Btu coal were generally at the start of run, March 8 to 10 and March 25, and at the end of the run, March 29 (see Figures 4.3-24 and -25). The SO_2 removals based on the products are generally quite low, below 30 percent. The only SO_2 removals above 50 percent by products were at the start of the run on March 8 to 10 and March 25.

Figure 4.5-15 is a plot of GCT4 sulfur emissions (expressed as lb SO_2 emitted per MBtu coal fed) and sulfur removal by products as a function of calcium to sulfur ratio (Ca/S) measured in the PCD solids samples from FD0520. The measured PCD solids Ca/S ratio is much higher than the feed Ca/S because the PRB coal has a high-calcium content. There appears to be a critical solids Ca/S ratio at about 8.0. Above a solids Ca/S ratio of 8.0 the emissions are high and removals low. Below a Ca/S ratio of 8.0, the emissions are low and the SO_2 removals high.

Operating period inerts balances are provided in Figure 4.5-16, with typical values provided in Table 4.5-3. Table 4.5-2 provides the results of the inerts balances for all of the operating periods. The inerts are all the solid compounds that do not have carbon, calcium, magnesium, sulfur, oxygen, or hydrogen. The inerts balance mainly reflects the coal and PCD solids rate, since the limestone sorbent typically had 3.3 percent inerts. The inerts balance is similar to the calcium balance in that both are dominated by the coal and PCD solids rates and compositions. The inerts balance on March 9 was one period in excellent agreement. The inerts balance on March 11 was high by 35 percent. The March 25 and March 26 inerts balances were centered on the zero-percent error line, but with a high variation of ± 40 percent. The March 27 inerts balance was very high at 60 percent. The remainder of the run had inerts balances centered on zero-percent error, but with a very high variation.

The mass balances and other internal checks demonstrate that operating periods GCT4-1 to -8 had unacceptable mass balances and should not be used for further consideration. The gas-flow rates were self-consistent as shown by the good overall mass balance, which is dominated by the gas-flow rate measurements (zero to + 4.0 percent for all operating periods). The nitrogen balance was good (-1.5 to -3.8 percent) for the last 26 operating periods. The carbon balance was not good (+ 15 percent bias for the last 26 operating periods), possibly due to reporting the coal-feed rate too high. The sulfur balance was poor, with a high bias at +20 percent for the last 26 operating periods. This also might have been due to the actual coal rate being lower than reported. The hydrogen balance was good (- 1- to +5-percent bias) for GCT4-18 to -26. The oxygen balances were acceptable (-5 to -2 percent). The calcium balance was not good (+ 60-percent bias) for the last 26 operating periods, while the inerts balance had a high variation but was usually centered on zero-percent error.

The transport reactor energy balance for GCT4 is provided in Figure 4.5-17, with standard conditions chosen to be 1 atmosphere pressure and 100°F. Table 4.5-6 shows a breakdown of the individual components of the energy balance. The "energy in" consists of the coal, air, and steam fed to the transport reactor. The nitrogen and sorbent fed to the reactor were considered to be at ambient conditions and hence have zero enthalpy. The energy to calcine the sorbent limestone was neglected. At the maximum linestone rate, the heat absorbed by the limestone calcination was about 0.5 x 10^6 Btu/hr, which is only about 1 percent of the total energy of the system. "Energy out" consisted of the synthesis gas and PCD solids. The lower heating value of the coal and PCD solids were used in order to be consistent with the lower heating value of the synthesis gas. Solids taken from the reactor by FD0510 were neglected in the energy balance. The FD0510 flow was very low and the solids had no latent heat. The energy of the synthesis gas was determined at the transport reactor cyclone exit. The synthesis gas latent heat was estimated for all operating periods, using the SGC energy balance. Those values are provided in Table 4.3-3. Sensible enthalpy of the synthesis gas was determined by overall gas heat capacity from the GCT3 synthesis gas compositions and the individual gas heat capacities. The synthesis gas and PCD solids energy consists of both latent and sensible heat. The heat loss in the reactor was estimated to be 1.5 x 10^6 Btu/hr, which was measured during a previous transport reactor combustion test, done without the combustion heat exchanger, HX0204, in service. For most of the test runs, the GCT4 energy balance was biased high by 10 to 17 percent (4 to 7 MBtu/hr), which is consistent with the carbon balance being biased high by 15 percent. A reduction in coal-flow rates would put most of the operating periods in energy balance. The exceptions were GCT4-3 to -5 and -13 to -15; -13 to -15 were operating periods with low coal-flow rates.

Gasification efficiency is defined as the percent of the coal energy that is converted to potentially useful synthesis gas energy. Two types of gasification efficiencies are used: cold gas efficiency and hot gas efficiency. Cold gas efficiency is the amount of coal energy that is available to a gas turbine as latent heat of the synthesis gas. The synthesis gas sensible heat that could be used to generate steam in a heat recovery steam generator is ignored.

Similar to carbon conversion and sulfur removal, the cold gas efficiency can be calculated at least three different ways, and since the energy balance is off by 10 to 17 percent, each result could be different. If there was a good energy balance all three calculations would produce the same result. Three calculation methods were performed for cold gas efficiency consistent with the three methods of carbon conversion:

1. Based on the coal feed heat (coal latent heat) and the latent heat of the synthesis gas. This method assumes that the coal feed heat and the synthesis gas latent heat are correct (gas analyses).

2. Based on the feed heat (coal latent heat) and the latent heat of the synthesis gas as determined by a transport reactor energy balance rather than the gas analyses. This assumes that the synthesis gas latent heat is incorrect (solids analyses).

3. Based on the synthesis gas latent heat and heat lost, PCD solids sensible heat, latent heat PCD solids, and synthesis gas sensible heat. This assumes that the coal feed is in error (products analyses).

These three calculation methods are consistent with the three methods of calculating carbon conversion and each makes a choice as to which part of the energy balance is wrong.

The cold gas gasification efficiencies for the three calculation methods are shown in the plot in Figure 4.5-18 and are provided in Table 4.5-7. Synthesis gas LHV can be determined for all operating periods by using the LHV calculated by the SGC energy balance. The gas analysis cold gas gasification efficiencies were between 51 and 68 percent, except for GCT4-13 to -15. The solids analysis cold gas gasification efficiencies were between 61 and 71 percent, except for GCT4-13 to -15. The products analysis cold gas gasification efficiencies were between 56 and 66 percent, except for GCT4-13 to -15. As before with the carbon conversions, the gas analysis gasification efficiency was the highest, the solids analysis the lowest, and the products analysis was between the gas and solids analysis. Since both the synthesis gas rate and the PCD solids rates are independently checked, it is most likely that coal-feed rate errors are producing the error in the energy and carbon balances. Therefore the best estimate of the cold gas efficiency is by the products.

The hot gasification efficiency is the amount of coal energy that is available to a gas turbine plus a heat recovery steam generator. The hot gas efficiency counts both the latent and sensible heat of the synthesis gas. As in the cold gasification efficiency, carbon conversions, and sulfur removal, the hot gas efficiency can be calculated at least three different ways. Since the energy balance is off by about 10 to 17 percent, each efficiency will be different. Three calculation methods for hot gasification, which are consistent with the three methods of carbon conversion are:

1. Based on the feed heat (coal latent heat) and the latent heat and sensible heat of the synthesis gas. This assumes that the feed heat and the synthesis gas latent heat are correct (gas analyses).

2. Based on the feed heat (coal latent heat) and the sensible heat of the synthesis gas plus the latent heat of the synthesis gas as determined by transport reactor energy balance. This assumes that the synthesis gas latent heat is incorrect (solids analyses).

3. Based on the synthesis gas latent heat and sensible heat and the heat lost (reactor heat loss, PCD solids sensible heat, and latent heat PCD solids). This assumes that the coal feed is in error (products analyses).

These three calculation methods are consistent with the three methods of calculating carbon conversion and cold gasification efficiency and make a choice of which parts of the energy balance are correct.

The hot gasification efficiency assumes that the sensible heat of the synthesis gas can be recovered in a heat recovery steam generator, so the hot gasification efficiency is always higher than the cold gasification efficiency. Three gasification calculation methods are shown in the plot in Figure 4.5-19 and in Table 4.5-7. The methods are similar to the cold gasification method in that gas assumes that the heat loss is in error, the solids assumes that the synthesis gas latent heat is in error, and the products assumes that the coal heat is in error. The hot

gasification efficiency by the products increased from 80 to nearly 98.5 percent during the first three periods of operation. The last 7 days of operation had increasing products hot gasification efficiencies, from 86.6 to 96.2 percent. These high efficiencies are a result of the low PCD fines carbon content and low PCD fines rates. As with the cold gasification efficiencies, the hot gasification efficiency by products should be more accurate than the hot gasification efficiencies by the gas and solids.

Two main sources of losses in efficiency are the reactor heat loss and the latent heat of the PCD solids. The reactor heat loss of 1.5×10^6 Btu/hr is about 3 to 6 percent of the feed coal energy, while the total energy of the PCD solids was about 3 to 17 percent of the feed coal energy. The heat loss percentage will decrease as the reactor size is increased. While the transport reactor does not recover the latent heat of the PCD solids, this latent heat could be recovered in a combustor. The heat of the PCD solids can be decreased by decreasing both the PCD solids carbon content (heating value) and the PCD solids rate.

Gasification efficiencies can be calculated for the nitrogen-corrected gas heating values determined in Section 4.3. The nitrogen-corrected hot and cold gasification efficiencies are shown in the plot in Figure 4.5-20 and listed in Table 4.5-7 for all of the operating periods. Only the gasification efficiencies based on the products are provided in Figures 4.5-7 and -20 because they are the most representative of the actual gasification efficiencies. The nitrogen-corrected efficiencies increase the cold gasification efficiencies by about 8 to 10 percent for most of the operating periods. The nitrogen correction does not increase the hot gasification efficiency because the deleted nitrogen lowers the synthesis gas sensible heat, and hence lowers the hot gasification efficiency. Note that operating period GCT4-8 had N_2-corrected hot gasification efficiency at 100.3 percent, which is clearly in error.

Table 4.5-1

Feed Rates, Product Rates, and Mass Balance

	Feeds (In)						Products (Out)						
Operating Period	Coal FD0210 lb/hr	Sorbent FD0220 lb/hr	Air FI205 lb/hr	Nitrogen FI609[1] lb/hr	Steam FIC298[2] lb/hr	Total lb/hr	Syngas FI465 lb/hr	PCD Solids FD0520 lb/hr	SP Solids FD0510 lb/hr	Reactor Accumulation lb/hr	Total lb/hr	In - Out lb/hr	(In- Out)/In %
GCT4-1	5,158	181	14,299	7,123	0	26,760	19,729	800	0	210	20,740	6,020	22.5
GCT4-2	4,489	180	12,925	7,252	94	24,940	23,883	500	0	50	24,432	508	2.0
GCT4-3	4,799	181	15,730	6,984	23	27,716	27,298	402	0	-13	27,686	30	0.1
GCT4-4	4,800	181	15,760	7,221	12	27,974	27,534	381	0	-17	27,898	76	0.3
GCT4-5	3,582	181	11,431	7,147	6	22,346	21,817	351	0	-144	22,024	322	1.4
GCT4-6	5,405	179	16,130	5,838	746	28,298	28,040	300	0	17	28,358	-59	-0.2
GCT4-7	5,552	180	15,892	5,733	972	28,329	27,649	300	0	15	27,964	364	1.3
GCT4-8	3,943	142	12,205	5,323	1,075	22,687	22,489	300	0	-43	22,746	-59	-0.3
GCT4-9	5,383	264	13,231	6,551	6	25,434	24,218	600	0	37	24,855	580	2.3
GCT4-10	5,371	481	13,050	6,612	6	25,520	24,192	600	0	102	24,894	626	2.5
GCT4-11	5,367	370	13,148	6,536	7	25,428	24,068	600	0	-39	24,630	798	3.1
GCT4-12	5,217	325	13,884	6,301	82	25,809	24,362	546	58	108	25,073	736	2.8
GCT4-13	2,090	411	8,884	6,333	46	17,764	17,093	514	0	-13	17,594	171	1.0
GCT4-14	2,491	411	9,573	6,330	41	18,846	18,050	496	0	3	18,548	297	1.6
GCT4-15	3,284	362	10,490	6,472	35	20,643	19,662	473	0	29	20,164	480	2.3
GCT4-16	4,352	613	11,924	5,576	242	22,708	21,572	404	0	94	22,070	638	2.8
GCT4-17	4,970	614	13,576	5,363	384	24,906	23,458	354	0	7	23,819	1,087	4.4
GCT4-18	4,948	367	13,926	5,780	461	25,481	24,713	427	55	27	25,221	260	1.0
GCT4-19	5,182	611	14,444	5,795	485	26,517	25,607	448	0	58	26,114	403	1.5
GCT4-20	5,246	609	14,942	5,536	472	26,805	25,979	481	0	-75	26,385	419	1.6
GCT4-21	5,384	512	14,936	5,316	434	26,582	25,767	496	0	-75	26,188	394	1.5
GCT4-22	4,345	614	10,590	5,520	446	21,514	20,445	409	0	60	20,914	601	2.8
GCT4-23	4,108	106	11,242	5,537	454	21,448	20,990	250	0	-29	21,211	237	1.1
GCT4-24	3,671	105	11,064	5,343	401	20,584	20,273	206	0	102	20,581	3	0.0
GCT4-25	3,659	117	10,880	5,529	509	20,694	20,357	218	0	66	20,641	53	0.3
GCT4-26	3,670	151	11,090	5,571	446	20,927	20,599	230	13	12	20,854	73	0.4
GCT4-27	3,944	131	11,474	5,471	451	21,471	21,055	240	0	244	21,539	-67	-0.3
GCT4-28	3,965	130	11,283	5,528	381	21,287	20,877	248	0	78	21,203	84	0.4
GCT4-29	3,771	130	11,006	5,197	382	20,486	20,164	256	0	92	20,512	-26	-0.1
GCT4-30	3,766	194	11,318	5,447	394	21,119	20,753	250	157	-265	20,896	223	1.1
GCT4-31	3,787	380	11,558	5,501	443	21,669	21,321	236	0	124	21,681	-11	-0.1
GCT4-32	3,800	381	11,330	5,189	220	20,919	20,455	229	0	166	20,850	70	0.3
GCT4-33	4,337	312	12,894	5,300	188	23,031	22,496	219	159	-75	22,799	231	1.0
GCT4-34	4,645	238	13,376	5,231	183	23,674	23,230	206	0	-1	23,435	239	1.0

Notes:

1. Nitrogen-feed rate reduced by 1,000 lb/hr to account for losses in feed systems and seals.
2. Steam rate taken from FIC289. FI204 was not reading accurately during GCT4.
3. FD0510 was not always operated during an entire test period. FD0510 flow rates shown have been prorated to account for the actual time of FD0510 operation.

Table 4.5-2

Nitrogen, Hydrogen, Oxygen, and Inerts Mass Balances

Operating Period	Nitrogen[1]		Hydrogen		Oxygen		Calcium		Inerts	
	(In- Out)/In %	In - Out lb/hr	(In- Out)/In %	In - Out lb/hr	(In- Out)/In %	In - Out lb/hr	(In- Out)/In %	In - Out lb/hr	(In- Out)/In %	In - Out lb/hr
GCT4-1							34.6	34.7	-110.1	-215
GCT4-2	6.6	1,118	10.6	33	-11.7	-534	36.6	34	-4.2	-7
GCT4-3	6.6	1,249	9.7	31	-16.2	-852	45.3	47	37.1	67
GCT4-4	6.7	1,290	7.8	25	-16.1	-847	48.4	50	42.7	77
GCT4-5	5.4	856	4.6	11	-12.6	-487	48.2	45	106.4	144
GCT4-6	7.7	1,386	8.7	38	-21.1	-1304	58.6	63	34.8	70
GCT4-7	6.8	1,200	17.8	84	-13.3	-845	57.2	63	32.6	68
GCT4-8	5.1	745	8.4	32	-11.8	-600	39.5	33	33.9	50
GCT4-9							60.6	76	-2.3	-5
GCT4-10							74.3	142	-23.8	-52
GCT4-11							67.8	107	41.1	88
GCT4-12							66.6	93	-16.4	-35
GCT4-13							67.1	93	-49.3	-51
GCT4-14							68.6	97	-49.3	-58
GCT4-15							67.6	91	-47.7	-68
GCT4-16							82.4	175	-29.4	-58
GCT4-17							87.2	188	39.2	86
GCT4-18	-1.4	-229	0.5	2	-3.6	-189	81.5	114	28.7	71
GCT4-19	-2.2	-369	1.0	4	-3.0	-166	76.3	141	30.5	118
GCT4-20	-2.6	-436	0.7	3	-2.9	-164	64.3	101	60.9	304
GCT4-21	-2.8	-473	1.9	8	-3.0	-168	62.2	82	67.1	331
GCT4-22	-3.5	-469	5.0	17	-2.5	-106	62.4	64	59.1	319
GCT4-23	-3.1	-432	3.6	12	-2.8	-120	59.0	29	63.8	131
GCT4-24	-2.4	-323	-1.3	-4	-3.8	-157	62.8	29	-0.3	-1
GCT4-25	-2.2	-304	-1.3	-4	-3.7	-154	58.3	30	12.4	23
GCT4-26	-1.6	-227	-0.2	-1	-5.2	-217	46.7	28	43.2	83
GCT4-27							26.7	16	-65.5	-122
GCT4-28							24.8	16	18.2	32
GCT4-29							14.5	10	0.9	1
GCT4-30							31.4	27	206.8	338
GCT4-31							58.8	82	-4.9	-9
GCT4-32							59.3	85	-35.4	-58
GCT4-33							59.2	78	102.1	174
GCT4-34							57.9	64	66.2	120

Notes: 1. Nitrogen-feed rate reduced by 1,000 lb/hr to account for losses in feed systems and seals.

Table 4.5-3

Typical Component Mass Balances

	Nitrogen[1]	Hydrogen	Oxygen	Calcium	Inerts
Operating Period	GCT4-26	GCT4-26	GCT4-26	GCT4-26	GCT4-26
Date	1/30/01	1/30/01	1/30/01	1/30/01	1/30/01
Time Start	19:15	19:15	19:15	19:15	19:15
Time End	22:30	22:30	22:30	22:30	22:30
Fuel	PRB	PRB	PRB	PRB	PRB
Sorbent	OH LS	OH LS	OH LS	OH LS	OH LS
Mixing Zone Temperature, ^{O}F	1,683	1,683	1,683	1,683	1,683
Pressure, psig	220	220	220	220	220
In, pounds/hr					
Fuel	25	227	1,078	31	135
Sorbent			46	29	55
Air	8,350	16	2,648		
Nitrogen	5,571				
Steam		50	396		
Total	13,946	292	4,168	60	191
Out, pounds/hr					
Synthesis Gas	14,172	292	4,362		
PCD Solids		0	24	32	108
Total	14,172	293	4,386	32	108
(In-Out)/In, %	-1.6%	-0.2%	-5.2%	46.7%	43.2%
(In-Out), pounds per hour	-227	-1	-217	28	83

Note: 1. Feed nitrogen decreased by 1,000 lb/hr.

Table 4.5-4

Carbon Balances

	Carbon In (Feed)			Carbon Out (Products)			Carbon		Carbon Conversion		
Operating Period	Coal lb/hr	Sorbent lb/hr	Total lb/hr	Syngas lb/hr	PCD Solids lb/hr	Total lb/hr	In - Out lb/hr	(In- Out)/In %	Solids %	Products %	Gas %
GCT4-1	3,043	21	3,064		461				85.1		
GCT4-2	2,644	21	2,665	2,653	256	2,908	-243	-9.1	90.6	91.4	100.3
GCT4-3	2,807	21	2,828	3,313	171	3,484	-656	-23.2	94.1	95.2	118.0
GCT4-4	2,808	21	2,829	3,330	162	3,493	-663	-23.5	94.4	95.5	118.6
GCT4-5	2,095	21	2,116	2,344	127	2,471	-355	-16.8	93.7	94.7	111.9
GCT4-6	3,178	21	3,199	3,544	102	3,646	-447	-14.0	96.8	97.2	111.5
GCT4-7	3,270	21	3,291	3,534	83	3,618	-326	-9.9	97.4	97.6	108.1
GCT4-8	2,338	16	2,355	2,685	50	2,734	-379	-16.1	97.4	97.8	114.8
GCT4-9	3,095	31	3,126		306				90.2		
GCT4-10	3,085	56	3,141		309				90.1		
GCT4-11	3,081	43	3,124		320				89.8		
GCT4-12	2,984	38	3,022		295				90.3		
GCT4-13	1,196	48	1,243		254				79.1		
GCT4-14	1,426	48	1,474		233				83.9		
GCT4-15	1,881	42	1,923		204				89.3		
GCT4-16	2,496	71	2,567		161				93.4		
GCT4-17	2,853	71	2,924		169				94.3		
GCT4-18	2,827	43	2,870	2,325	219	2,545	325	11.3	92.3	91.5	82.3
GCT4-19	2,958	71	3,029	2,426	114	2,540	489	16.1	96.4	95.8	82.0
GCT4-20	2,986	71	3,057	2,509	106	2,615	442	14.5	96.6	96.1	84.0
GCT4-21	3,062	60	3,121	2,504	164	2,669	453	14.5	94.8	94.0	81.8
GCT4-22	2,463	71	2,534	1,762	156	1,919	615	24.3	93.9	92.2	71.6
GCT4-23	2,331	12	2,343	1,800	110	1,910	434	18.5	95.3	94.3	77.2
GCT4-24	2,081	12	2,093	1,717	83	1,800	294	14.0	96.1	95.5	82.5
GCT4-25	2,079	14	2,092	1,711	76	1,787	305	14.6	96.4	95.8	82.3
GCT4-26	2,084	18	2,101	1,772	67	1,839	262	12.5	96.9	96.5	85.1
GCT4-27	2,240	15	2,256		70				97.0		
GCT4-28	2,254	15	2,269		76				96.8		
GCT4-29	2,146	15	2,161		68				97.1		
GCT4-30	2,143	23	2,165		61				97.4		
GCT4-31	2,154	44	2,198		52				97.8		
GCT4-32	2,162	44	2,206		45				98.1		
GCT4-33	2,468	36	2,505		47				98.3		
GCT4-34	2,645	28	2,673		50				98.2		

Notes:

1. No carbon balance for GCT4-1, -9 to -17, and -27 to -34 due to lack of gas analyzer data.
2. For GCT4-18 to -26, CO_2 was measured by RTI analyzers.
3. For GCT4-18 to -26, CH_4 and C_2H_4 were estimated from TC06 data.
4. For GCT4-18 to -26, N_2 was estimated by difference.
5. Carbon accumulated and carbon out via FD0510 are neglected.

Table 4.5-5

Sulfur Balances

	Feeds (In)	Products (Out)					Sulfur Removal			Ca/S Ratio	
Operating Period	Coal lb/hr	Syngas lb/hr	PCD Solids lb/hr	Total lb/hr	In - Out lb/hr	(In- Out)/In %	Solids %	Products %	Gas %	Feeds	PCD Solids
GCT4-1	13.4	5.5	9.8	15.3	-1.9	-14.1	72.8	63.8	58.7	3.4	5.1
GCT4-2	11.7	4.0	8.5	12.5	-0.9	-7.4	72.8	67.8	65.4	3.8	5.5
GCT4-3	13.0	5.0	8.6	13.6	-0.7	-5.1	66.7	63.5	61.6	3.8	5.2
GCT4-4	13.0	5.4	8.2	13.6	-0.6	-4.7	63.2	60.3	58.5	3.8	5.2
GCT4-5	9.7	2.8	6.0	8.8	0.8	8.5	62.1	67.9	70.6	5.2	7.0
GCT4-6	15.7	11.3	3.2	14.4	1.2	7.8	20.3	22.0	28.1	3.2	11.1
GCT4-7	16.4	11.9	3.3	15.3	1.1	6.9	20.3	21.8	27.2	3.0	11.1
GCT4-8	12.6	8.1	2.5	10.6	2.0	15.7	20.0	23.7	35.7	3.1	16.3
GCT4-9	17.0	4.8	6.1	10.9	6.0	35.4	36.1	55.9	71.5	3.8	6.5
GCT4-10	16.9	5.9	5.6	11.6	5.3	31.5	33.3	48.7	64.9	6.9	7.0
GCT4-11	16.9	6.0	5.3	11.3	5.6	33.2	31.2	46.8	64.5	5.3	7.7
GCT4-12	15.7	6.1	5.3	11.4	4.3	27.4	33.8	46.6	61.3	4.9	7.1
GCT4-13	6.3	7.3	5.1	12.4	-6.2	-98.1	82.0	41.4	0.0	15.4	7.1
GCT4-14	7.5	7.1	5.0	12.1	-4.6	-62.2	67.0	41.3	0.0	12.9	7.1
GCT4-15	10.0	5.7	4.9	10.6	-0.6	-5.8	48.6	46.0	42.8	8.5	7.1
GCT4-16	13.3	8.2	3.9	12.1	1.1	8.5	29.5	32.3	38.1	10.6	7.6
GCT4-17	15.4	10.7	2.3	13.0	2.4	15.9	14.7	17.5	30.6	9.0	9.8
GCT4-18	15.3	10.1	2.6	12.7	2.7	17.4	17.0	20.6	34.4	5.1	8.0
GCT4-19	16.1	10.9	0.7	11.6	4.5	27.7	4.5	6.2	32.2	7.0	49.0
GCT4-20	16.3	11.3	1.6	12.9	3.4	20.8	9.8	12.3	30.5	5.6	28.4
GCT4-21	16.7	10.6	2.6	13.2	3.5	20.8	15.5	19.5	36.2	4.1	15.4
GCT4-22	13.5	8.0	1.5	9.5	3.9	29.3	11.2	15.9	40.5	3.9	20.4
GCT4-23	13.1	8.2	1.3	9.4	3.7	28.1	9.8	13.6	37.9	0.9	12.7
GCT4-24	11.7	8.0	0.9	8.9	2.8	24.0	7.9	10.4	31.9	1.1	15.1
GCT4-25	11.7	7.3	1.0	8.3	3.4	28.9	8.7	12.3	37.7	1.3	16.5
GCT4-26	12.1	5.8	0.9	6.7	5.4	44.7	7.8	14.1	52.5	1.9	27.3
GCT4-27	13.0	5.2	0.4	5.6	7.4	56.8	3.3	7.7	60.1	1.7	83.8
GCT4-28	12.7	5.4	0.3	5.8	6.9	54.4	2.7	6.0	57.2	2.0	112.3
GCT4-29	11.7	5.1	0.3	5.4	6.3	54.2	2.2	4.8	56.4	2.3	176.6
GCT4-30	11.3	5.1	0.3	5.3	6.0	52.7	2.4	5.1	55.1	3.7	169.4
GCT4-31	11.4	5.6	0.3	5.8	5.5	48.5	2.3	4.4	50.8	7.6	177.6
GCT4-32	11.4	4.8	0.3	5.1	6.3	55.5	2.2	5.0	57.7	7.8	186.1
GCT4-33	12.8	4.6	0.3	4.9	7.9	61.7	2.6	6.7	64.3	5.9	130.7
GCT4-34	13.5	5.0	0.5	5.5	8.0	59.5	3.4	8.3	62.9	4.2	82.5

Notes:

1. Synthesis gas sulfur emissions determined from synthesis gas combustor SO_2 analyzer.
2. Sulfur accumulated and sulfur out via FD0510 are neglected.

Table 4.5-6

Energy Balance

	Feeds (In)				Products (Out)					
Operating Period	Coal 10^6 Btu/hr	Air 10^6 Btu/hr	Steam 10^6 Btu/hr	Total 10^6 Btu/hr	Syngas[1] 10^6 Btu/hr	PCD Solids 10^6 Btu/hr	Heat Loss[2] 10^6 Btu/hr	Total 10^6 Btu/hr	In - Out 10^6 Btu/hr	(In- Out)/In %
GCT4-1	46.3	0.8	0.0	47.1	32.7	7.1	1.5	41.3	5.8	12.2
GCT4-2	40.3	0.7	0.0	41.0	31.7	3.9	1.5	37.1	3.9	9.5
GCT4-3	43.1	0.8	0.0	43.9	41.9	2.7	1.5	46.1	-2.2	-5.0
GCT4-4	43.1	0.8	0.0	43.9	41.9	2.5	1.5	45.9	-2.0	-4.4
GCT4-5	32.2	0.6	0.0	32.8	29.2	2.0	1.5	32.7	0.1	0.2
GCT4-6	48.5	0.9	1.0	50.3	40.2	1.7	1.5	43.4	7.0	13.8
GCT4-7	49.8	0.8	1.3	52.0	41.6	1.5	1.5	44.6	7.4	14.2
GCT4-8	35.4	0.6	1.4	37.4	31.0	1.1	1.5	33.5	3.9	10.4
GCT4-9	48.3	0.7	0.0	49.0	36.2	4.8	1.5	42.5	6.5	13.4
GCT4-10	48.2	0.7	0.0	48.9	36.1	4.9	1.5	42.5	6.4	13.2
GCT4-11	48.2	0.7	0.0	48.9	35.8	5.0	1.5	42.3	6.6	13.6
GCT4-12	46.8	0.7	0.0	47.6	36.8	4.6	1.5	42.9	4.7	9.9
GCT4-13	18.8	0.5	0.0	19.2	19.2	3.9	1.5	24.6	-5.4	-28.0
GCT4-14	22.4	0.5	0.0	22.9	22.2	3.6	1.5	27.3	-4.5	-19.5
GCT4-15	29.5	0.5	0.0	30.0	25.4	3.1	1.5	30.1	0.0	-0.1
GCT4-16	39.1	0.6	0.3	40.0	31.2	2.7	1.5	35.3	4.6	11.6
GCT4-17	44.6	0.7	0.5	45.8	34.8	2.6	1.5	38.9	6.9	15.0
GCT4-18	44.4	0.7	0.6	45.7	36.4	3.5	1.5	41.3	4.4	9.7
GCT4-19	46.5	0.7	0.6	47.9	38.4	1.9	1.5	41.8	6.1	12.6
GCT4-20	47.1	0.8	0.6	48.5	39.9	1.7	1.5	43.1	5.4	11.1
GCT4-21	48.3	0.8	0.6	49.7	39.9	2.6	1.5	44.0	5.7	11.5
GCT4-22	39.0	0.6	0.6	40.1	29.6	2.4	1.5	33.5	6.7	16.6
GCT4-23	36.9	0.6	0.6	38.1	28.4	1.6	1.5	31.5	6.6	17.3
GCT4-24	33.0	0.6	0.5	34.1	26.6	1.2	1.5	29.3	4.8	14.0
GCT4-25	32.9	0.6	0.7	34.1	27.5	1.2	1.5	30.1	3.9	11.6
GCT4-26	32.9	0.6	0.6	34.1	27.9	1.1	1.5	30.5	3.6	10.6
GCT4-27	35.4	0.6	0.6	36.6	29.7	1.1	1.5	32.3	4.3	11.8
GCT4-28	35.6	0.6	0.6	36.8	29.7	1.2	1.5	32.5	4.3	11.7
GCT4-29	33.9	0.6	0.5	35.0	26.6	1.1	1.5	29.2	5.8	16.7
GCT4-30	33.8	0.6	0.5	34.9	27.3	1.0	1.5	29.8	5.2	14.8
GCT4-31	34.0	0.6	0.6	35.2	28.9	0.9	1.5	31.3	3.9	11.1
GCT4-32	34.1	0.6	0.3	35.0	28.8	0.8	1.5	31.1	3.9	11.2
GCT4-33	38.9	0.7	0.2	39.9	32.6	0.8	1.5	34.9	5.0	12.4
GCT4-34	41.7	0.7	0.2	42.7	34.9	0.8	1.5	37.3	5.4	12.6

Notes:

1. Synthesis gas latent heat estimated by synthesis gas combustor energy balance.
2. Reactor heat loss estimated from combustion test run data.
3. Standard state assumed to be 100°F.
4. Fluidization and instrument nitrogen inlet temperature assumed to be at 100°F and to have zero standard-state enthalpy.
5. Limestone sorbent inlet temperature assumed to be at 100°F and to have zero standard-state-enthalpy.

Table 4.5-7

Gasification Efficiencies

Operating Period	Raw Cold Gas Efficiency			Raw Hot Gas Efficiency			N_2 Corrected Gas Efficiency	
	Gas %	Solids %	Products %	Gas %	Solids %	Products %	Cold Products %	Hot Products %
GCT4-1	52.8	65.3	60.3	70.6	83.1	80.7	67.1	79.9
GCT4-2	51.7	61.3	57.2	78.7	88.4	87.1	65.6	87.0
GCT4-3	68.2	63.1	64.9	97.3	92.3	92.6	72.0	93.5
GCT4-4	67.3	62.8	64.4	97.1	92.6	92.9	71.9	93.8
GCT4-5	60.3	60.5	60.4	90.7	90.9	90.9	70.1	91.1
GCT4-6	55.5	69.8	64.8	82.9	97.2	96.7	71.4	98.6
GCT4-7	56.8	71.6	66.7	83.4	98.3	98.0	73.2	99.7
GCT4-8	58.0	69.0	65.2	87.5	98.5	98.4	73.0	100.3
GCT4-9	52.6	66.2	60.9	74.8	88.4	86.6	67.3	86.7
GCT4-10	52.6	66.0	60.7	74.9	88.2	86.4	67.2	86.4
GCT4-11	52.0	65.7	60.3	74.2	88.0	86.1	66.6	86.0
GCT4-12	54.8	64.9	61.0	78.5	88.6	87.3	67.2	87.4
GCT4-13	60.8	32.1	47.3	102.2	73.6	79.5	56.4	76.9
GCT4-14	62.3	42.3	51.9	99.4	79.4	82.8	61.0	81.3
GCT4-15	55.6	55.4	55.5	86.3	86.1	86.1	64.4	85.4
GCT4-16	54.2	66.0	61.5	79.8	91.6	90.5	68.5	91.0
GCT4-17	52.8	68.2	62.4	78.0	93.4	92.2	68.7	92.8
GCT4-18	55.5	65.5	61.6	81.9	91.8	90.9	67.8	91.5
GCT4-19	56.6	69.6	65.0	82.5	95.5	94.9	71.5	96.0
GCT4-20	58.8	70.3	66.4	84.8	96.3	95.8	72.5	97.0
GCT4-21	57.1	69.0	64.8	82.5	94.4	93.6	70.3	94.4
GCT4-22	52.9	70.0	63.8	75.9	93.0	91.5	70.8	92.1
GCT4-23	51.6	69.5	62.9	77.1	95.0	93.9	70.5	94.9
GCT4-24	52.6	67.1	61.5	80.8	95.3	94.5	69.5	95.4
GCT4-25	55.3	67.3	62.8	83.6	95.6	95.0	71.1	95.9
GCT4-26	56.6	67.6	63.6	84.7	95.7	95.2	71.7	96.2
GCT4-27	56.9	69.1	64.8	83.8	96.0	95.4	72.4	96.5
GCT4-28	57.2	69.3	65.1	83.5	95.6	95.0	72.7	96.0
GCT4-29	51.0	68.2	61.6	78.4	95.6	94.7	69.4	95.4
GCT4-30	52.6	67.9	62.1	80.6	95.9	95.2	70.1	96.0
GCT4-31	56.9	68.4	64.3	85.1	96.6	96.1	72.2	97.4
GCT4-32	57.4	68.9	64.8	84.5	96.0	95.5	72.2	96.5
GCT4-33	56.8	69.6	65.1	83.7	96.5	96.0	72.1	97.1
GCT4-34	57.9	70.8	66.5	83.8	96.7	96.2	73.0	97.5

Notes:

1. Synthesis gas latent heat estimated by synthesis gas combustor energy balance.
2. Reactor heat loss (1.5×10^6 Btu/hr) estimated from combustion test run data.
3. Standard state assumed to be 100°F.
4. Fluidization and instrument nitrogen inlet temperature assumed to be at 100°F and to have zero standard-state enthalpy.

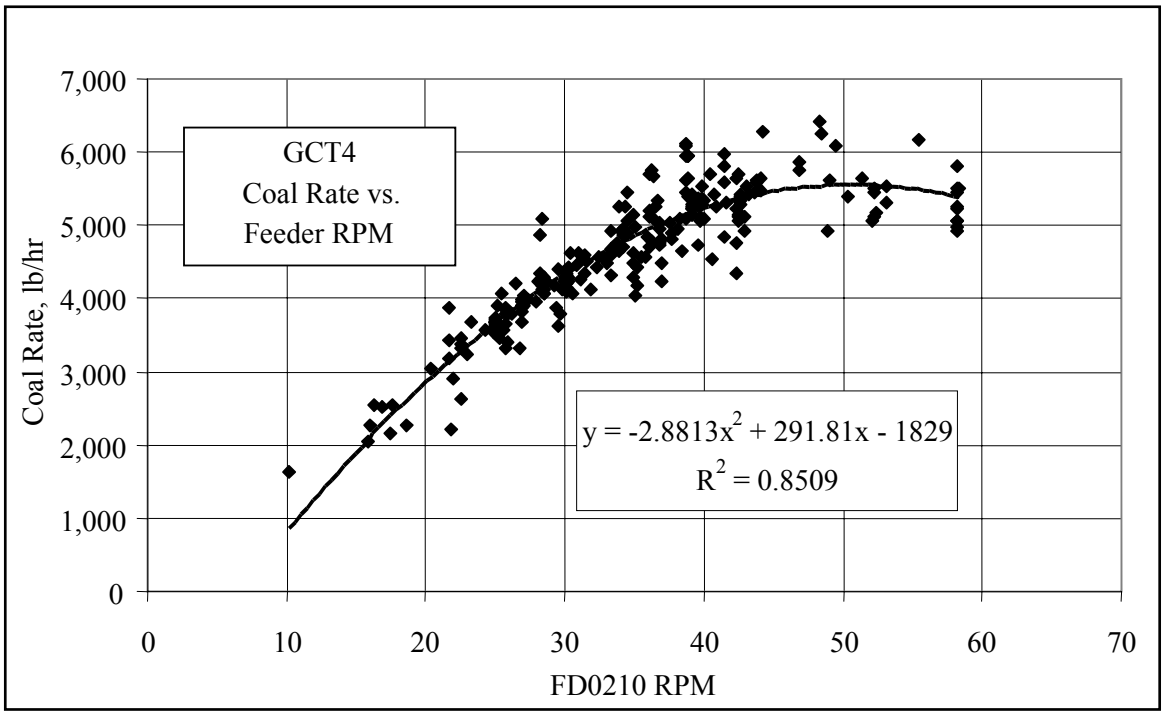

Figure 4.5-1 Coal Feeder Correlation

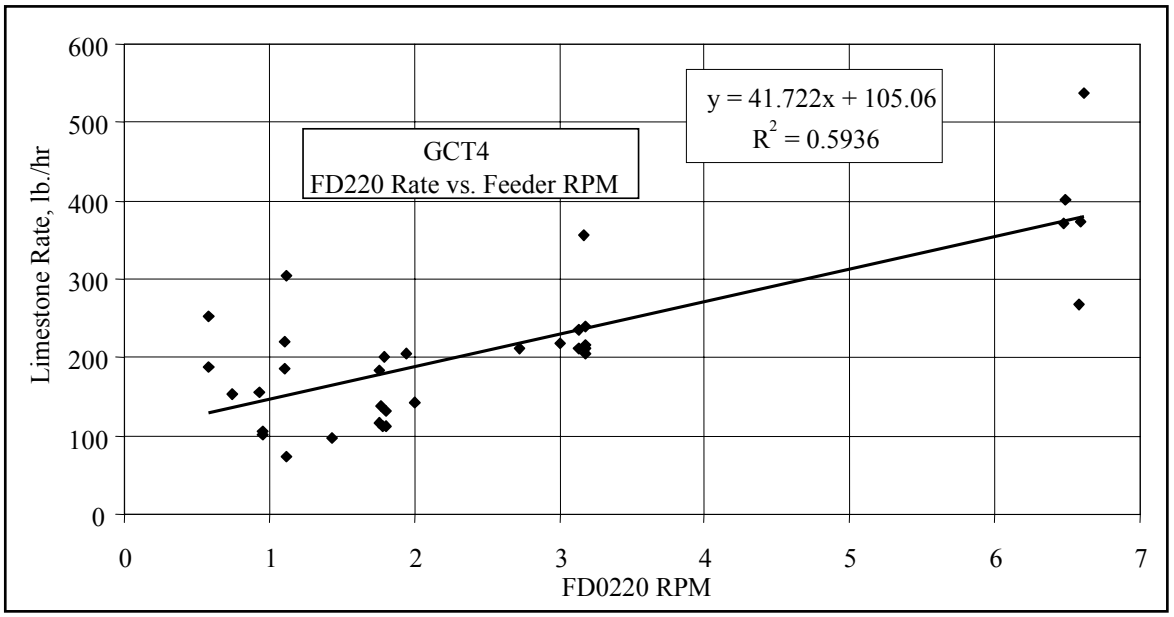

Figure 4.5-2 Sorbent Feeder Correlation

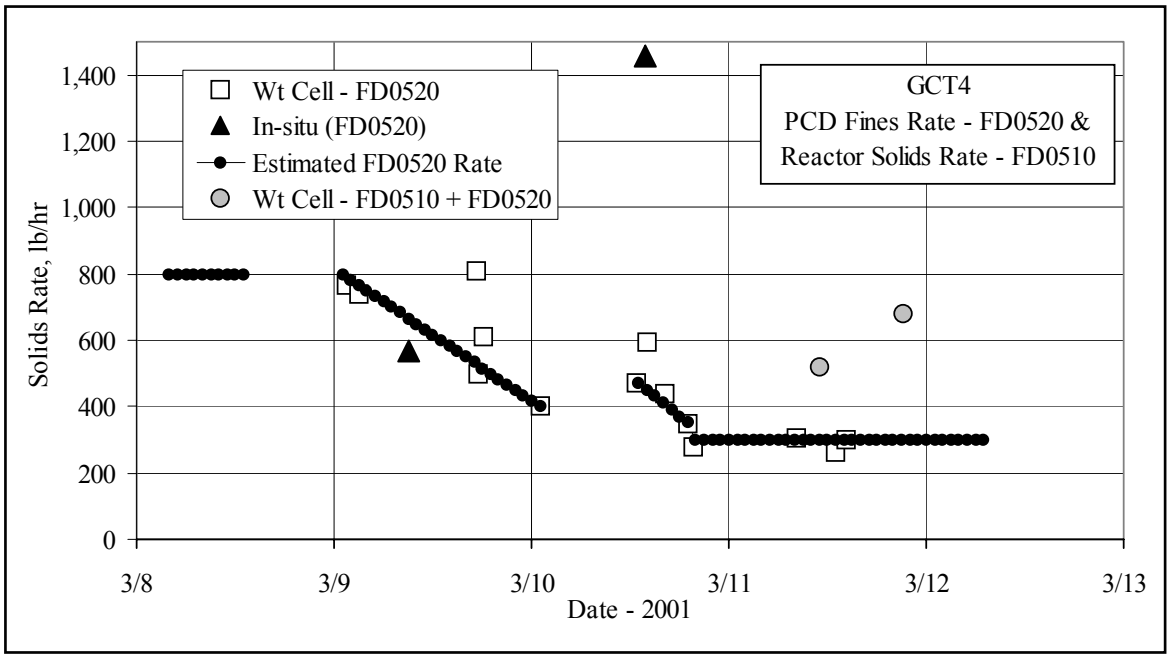

Figure 4.5-3 PCD Fines Rate, March 8 Through March 13, 2001

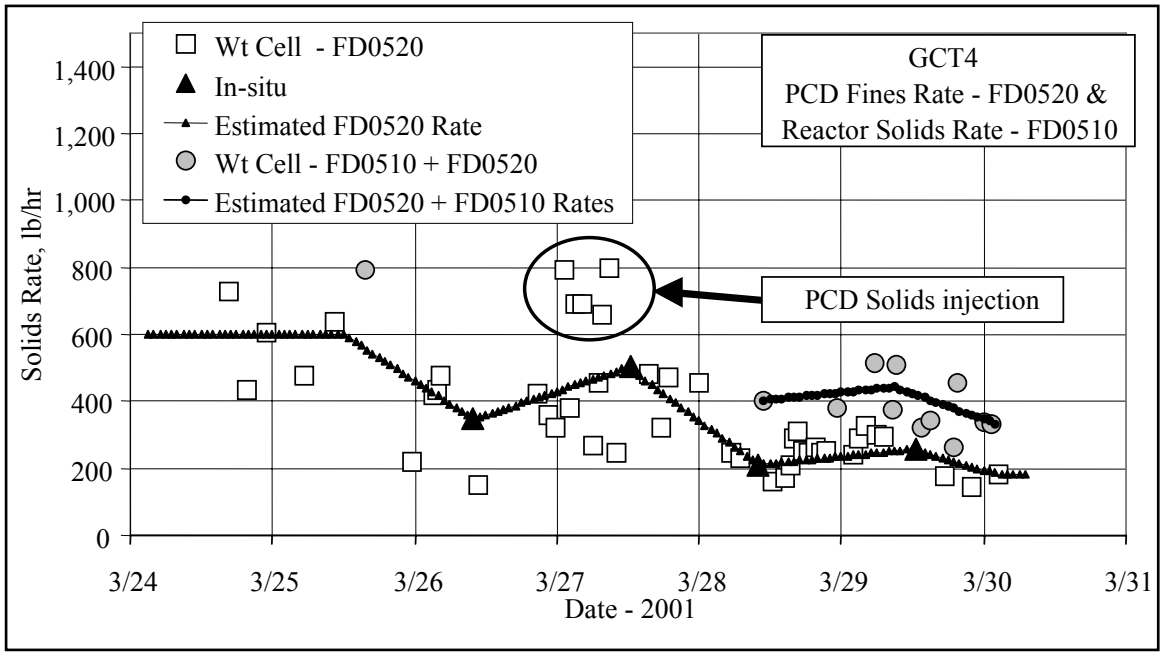

Figure 4.5-4 PCD Fines Rate, March 24 Through March 31, 2001

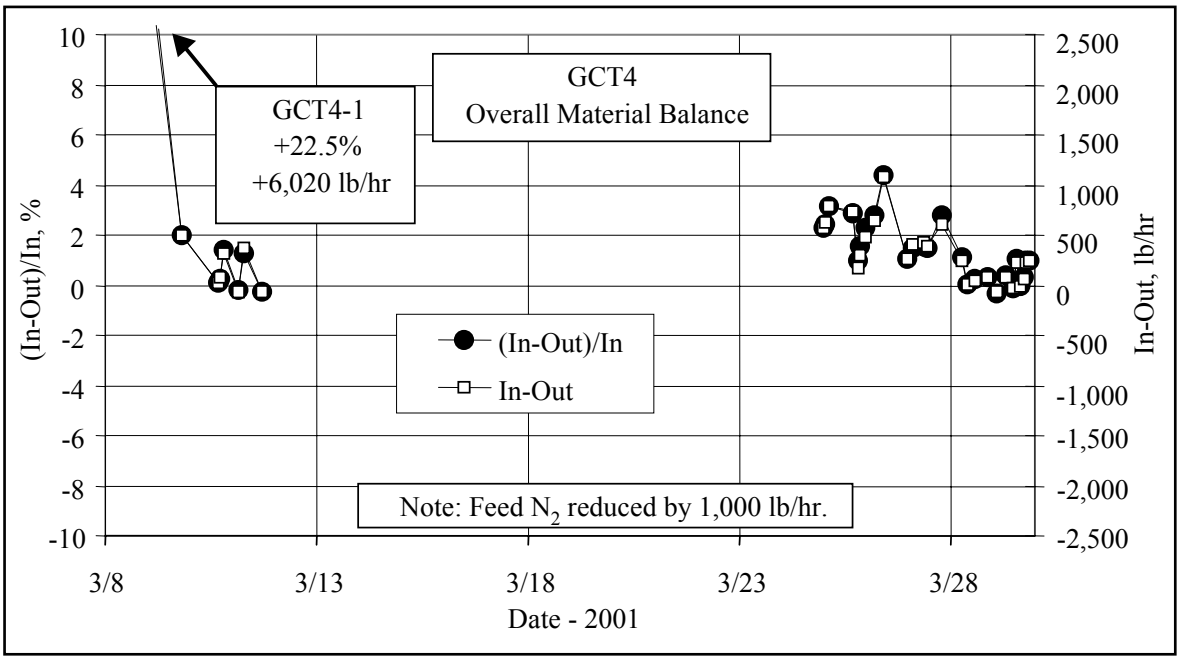

Figure 4.5-5 Overall Material Balance, March 8 Through March 28, 2001

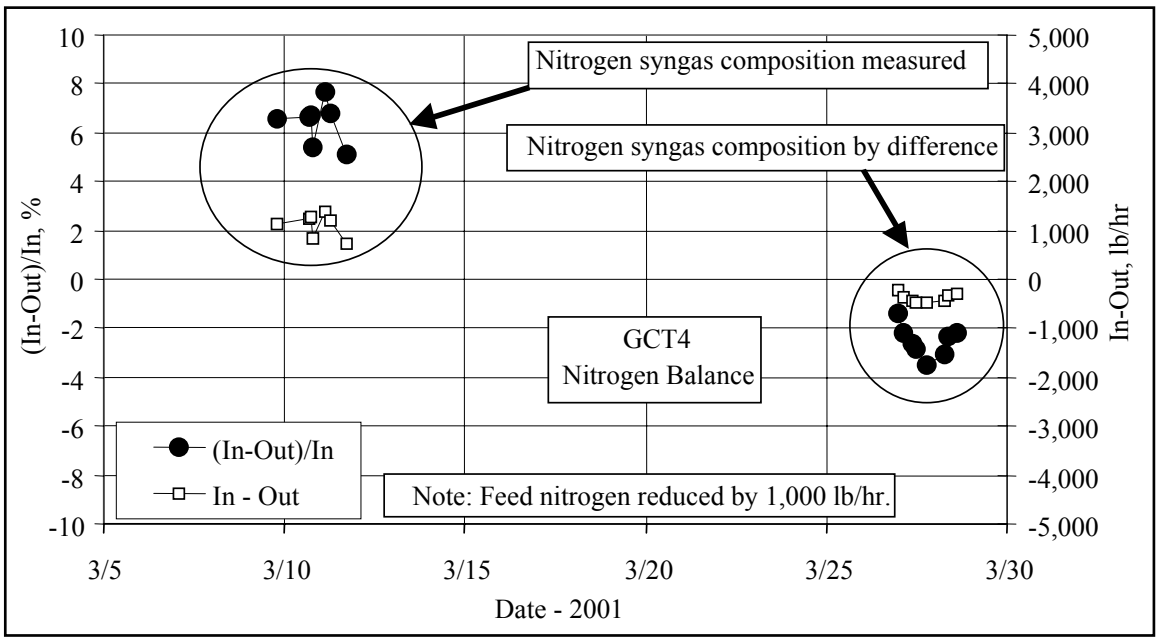

Figure 4.5-6 Nitrogen Balance, March 5 Through March 30, 2001

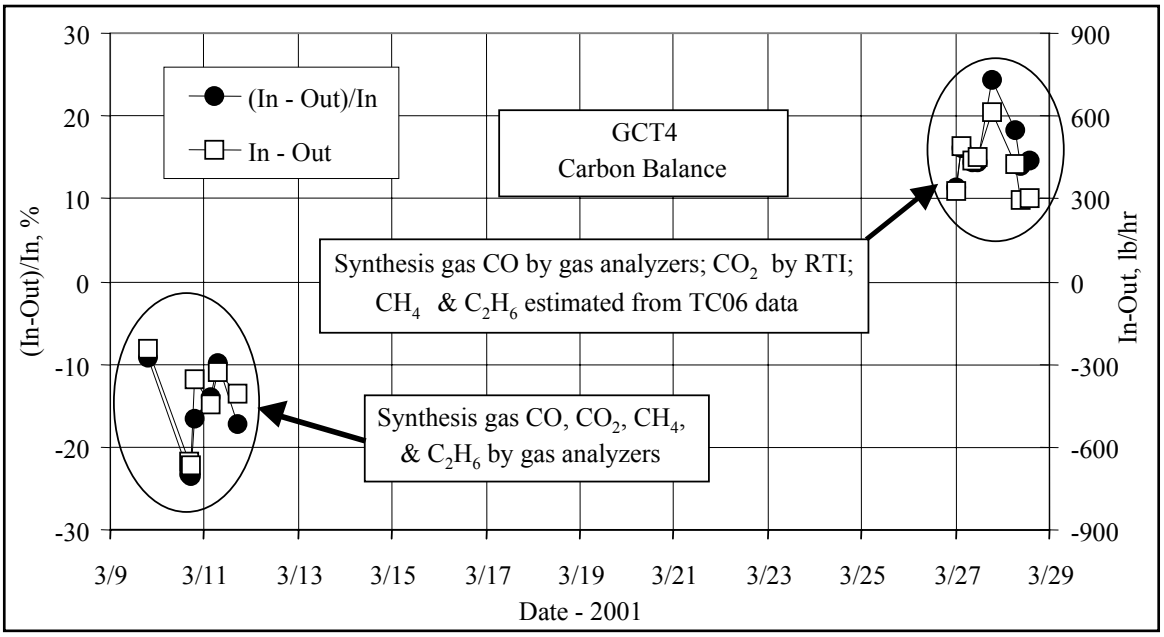

Figure 4.5-7 Carbon Balance, March 9 Through March 29, 2001

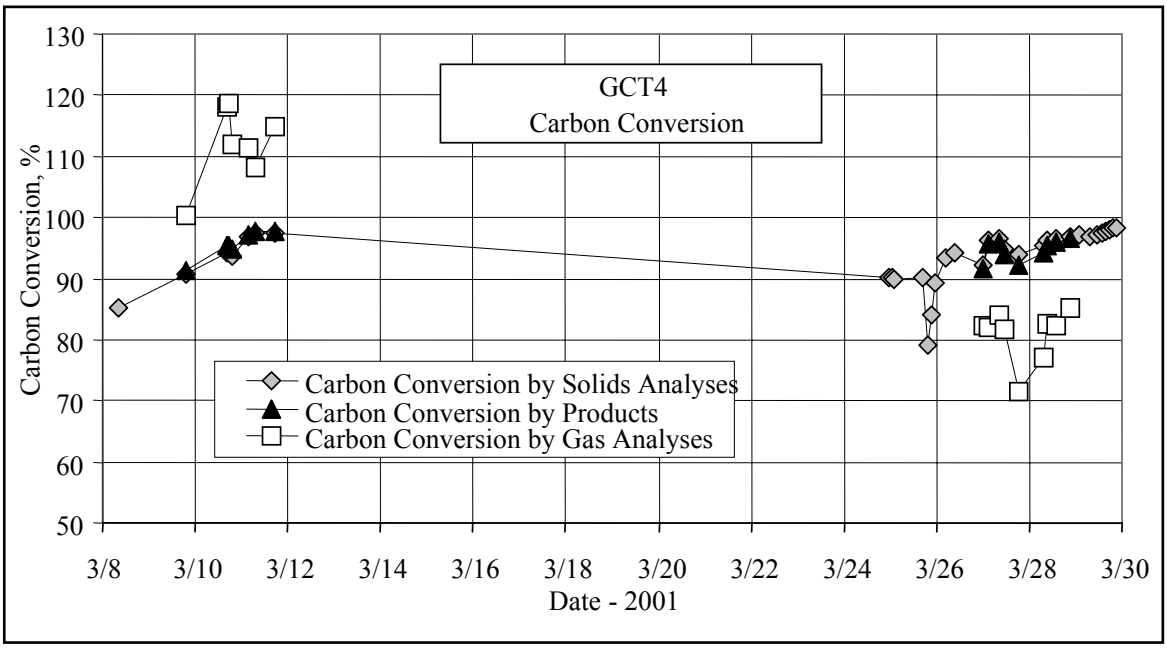

Figure 4.5-8 Carbon Conversion, March 8 Through March 30, 2001

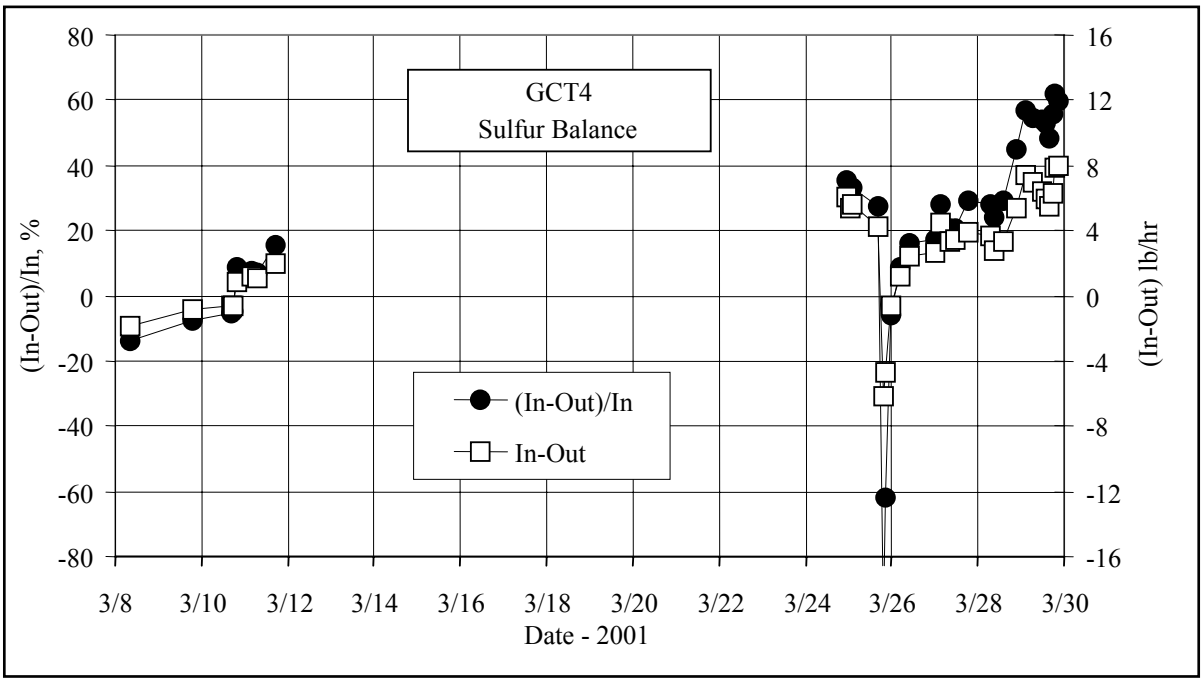

Figure 4.5-9 Sulfur Balance, March 8 Through March 30, 2001

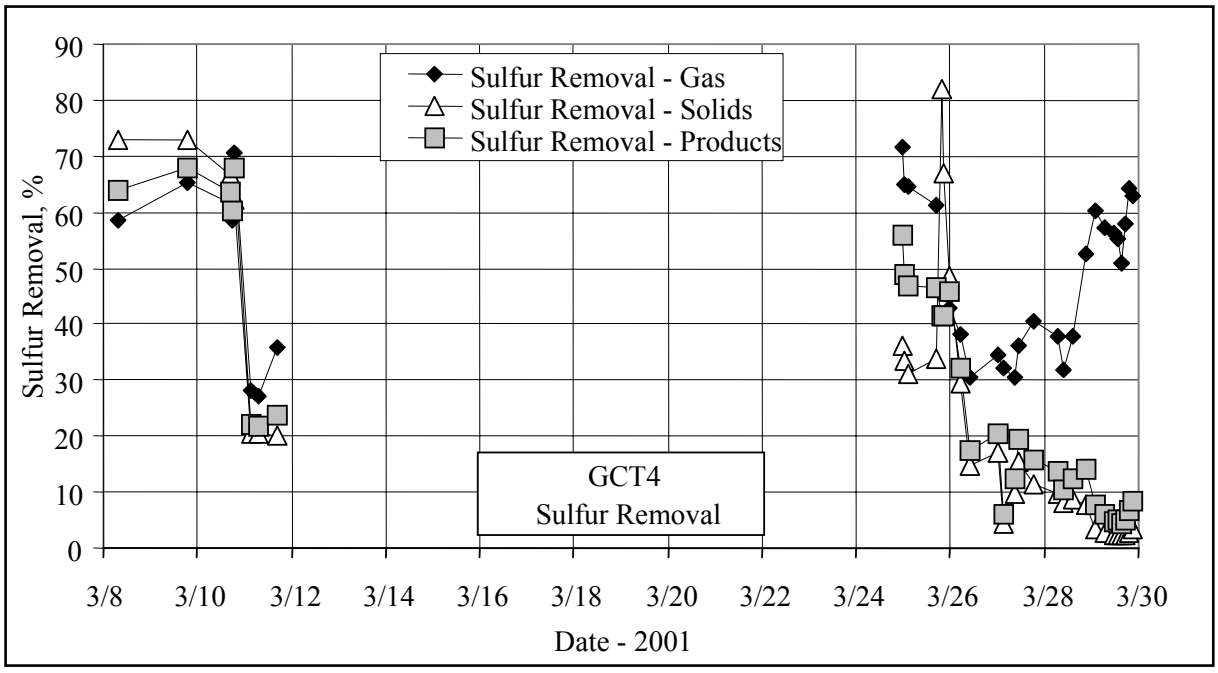

Figure 4.5-10 Sulfur Removal, March 8 Through March 30, 2001

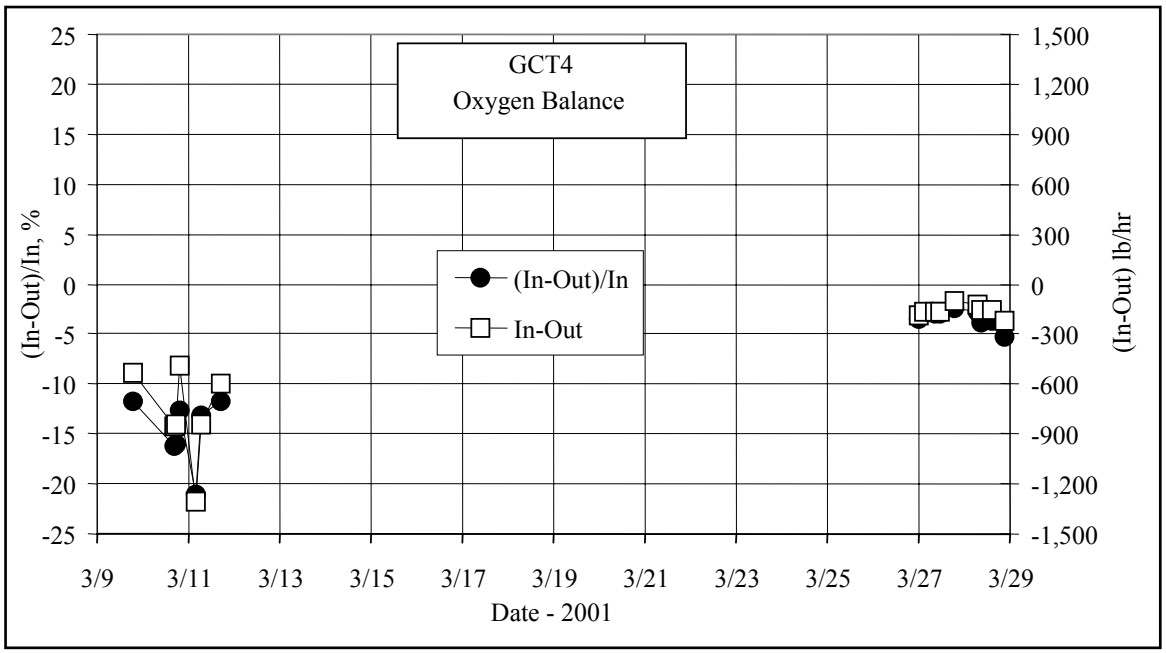

Figure 4.5-11 Hydrogen Balance, March 11 Through March 29, 2001

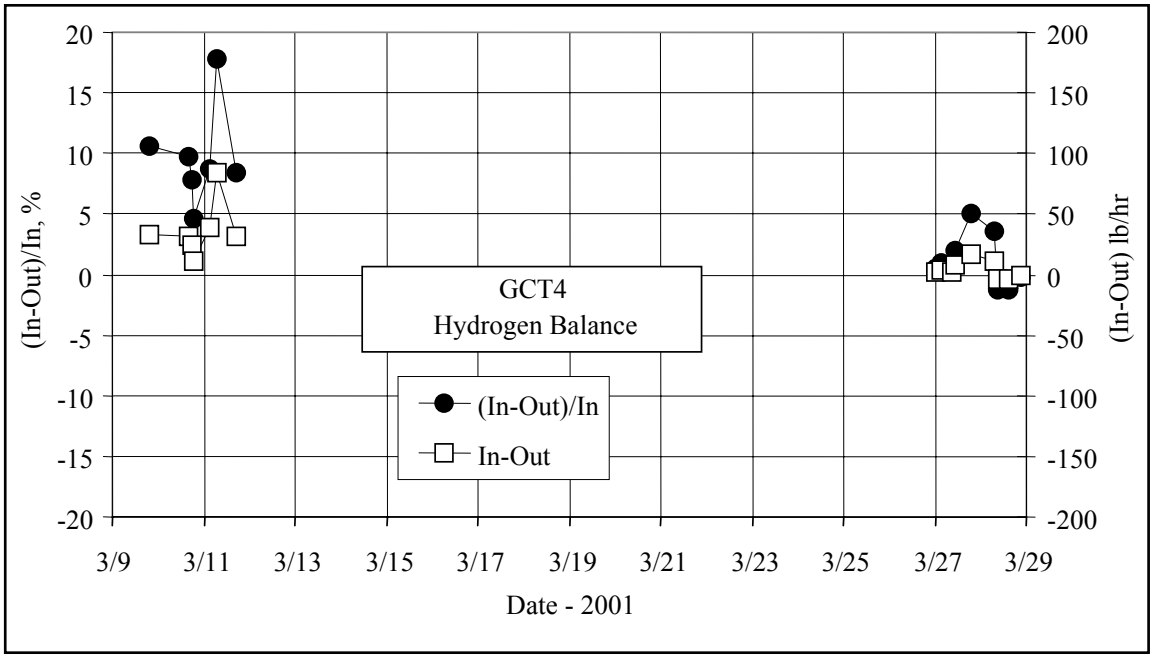

Figure 4.5-12 Oxygen Balance, March 9 Through March 29, 2001

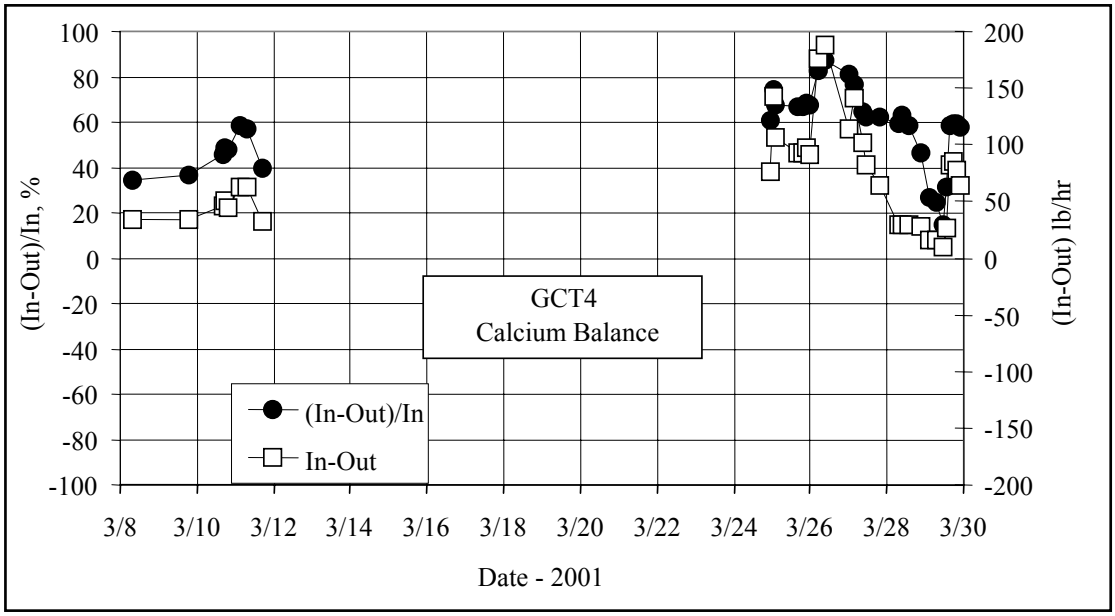

Figure 4.5-13 Calcium Balance, March 8 Through March 30, 2001

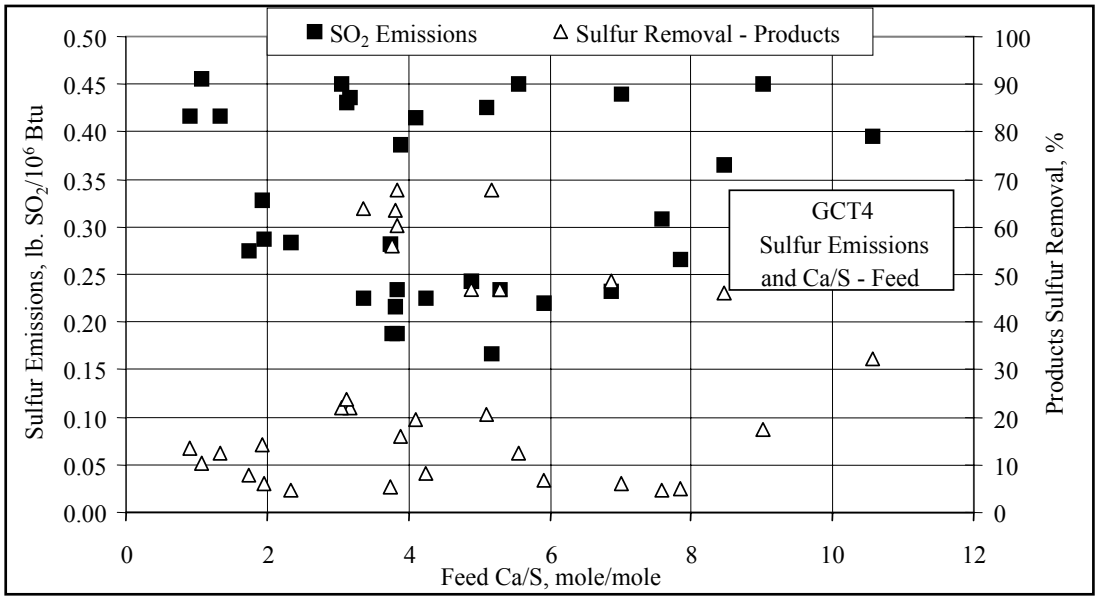

Figure 4.5-14 Sulfur Emissions and Feeds Ca/S Ratio

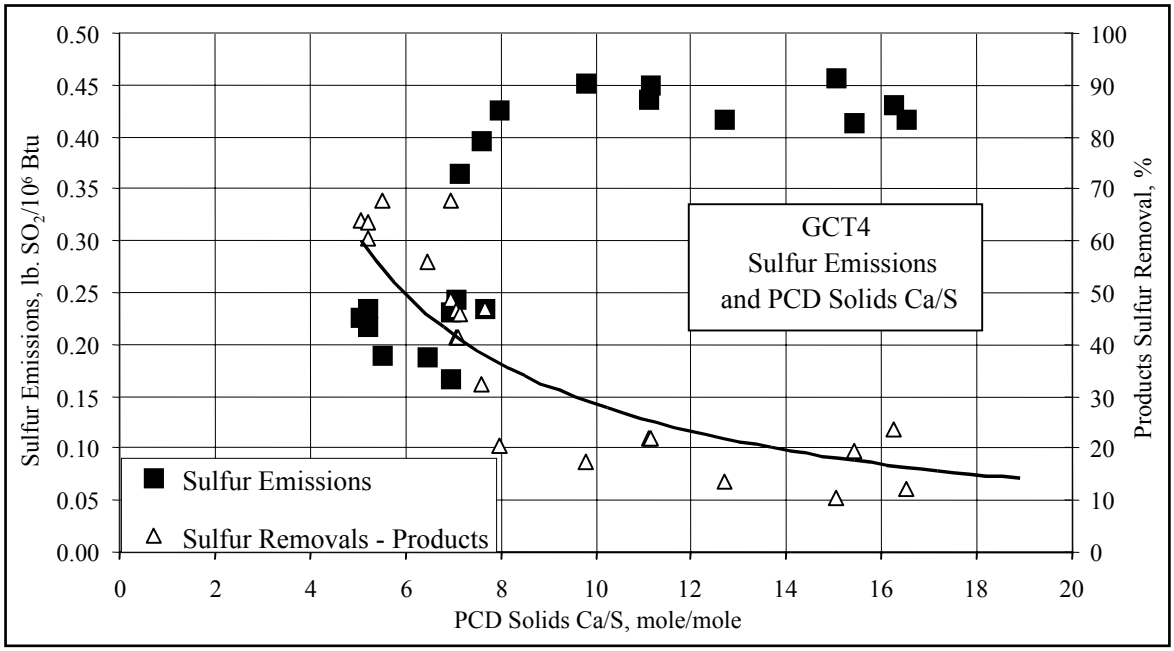

Figure 4.5-15 Sulfur Emissions and PCD Solids Ca/S Ratio

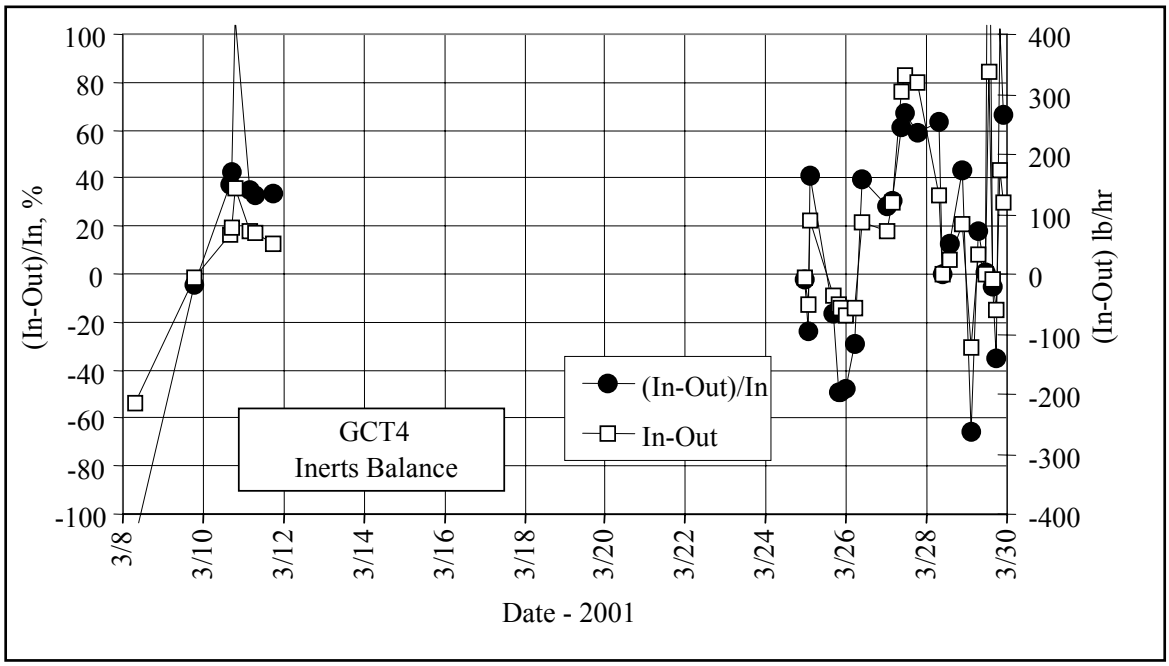

Figure 4.5-16 Inerts Balance, March 8 Through March 30, 2001

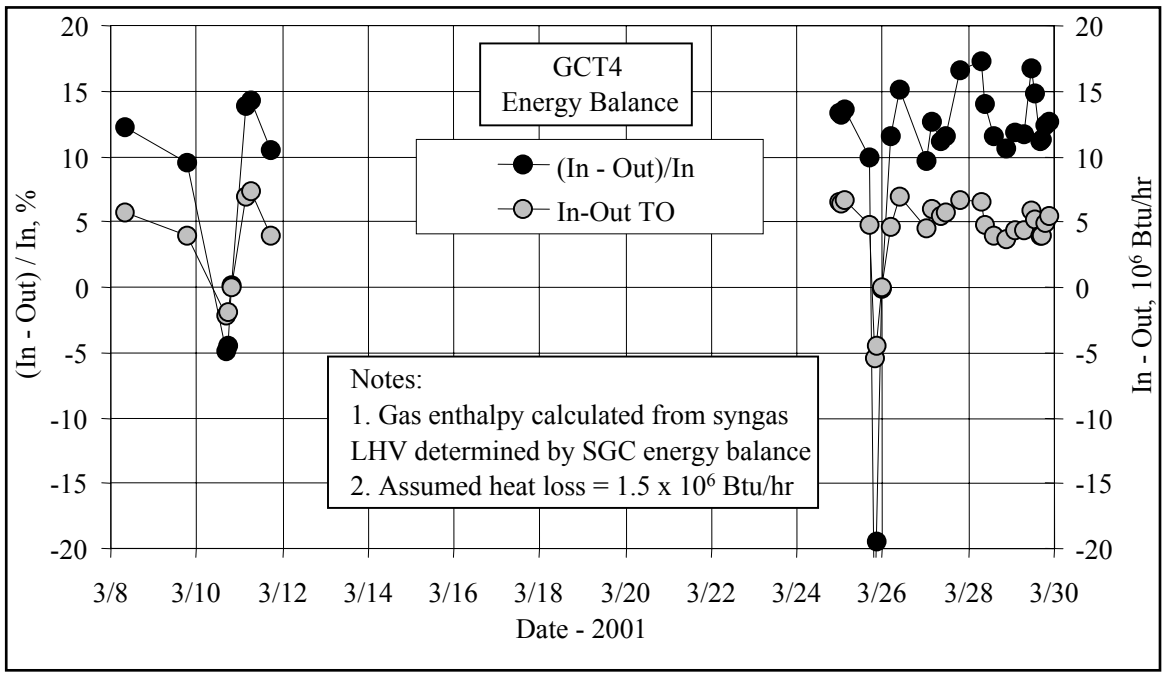

Figure 4.5-17 Energy Balance, March 8 Through March 30, 2001

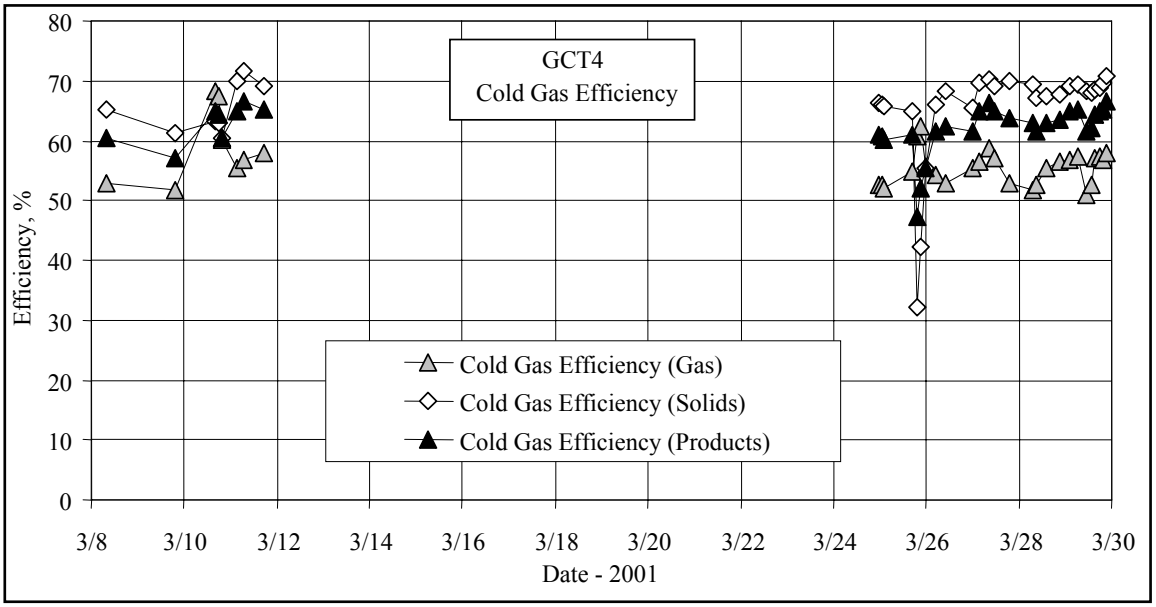

Figure 4.5-18 Gasification Efficiency — Cold, March 8 Through March 30, 2001

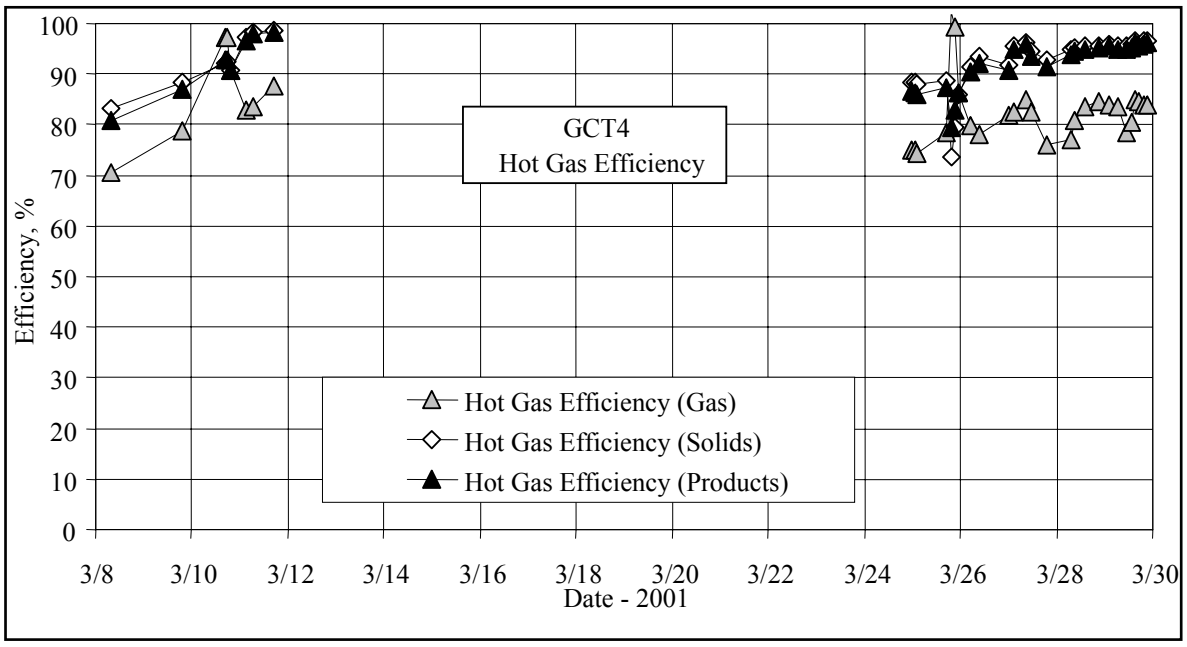

Figure 4.5-19 Gasification Efficiency — Hot, March 8 Through March 30, 2001

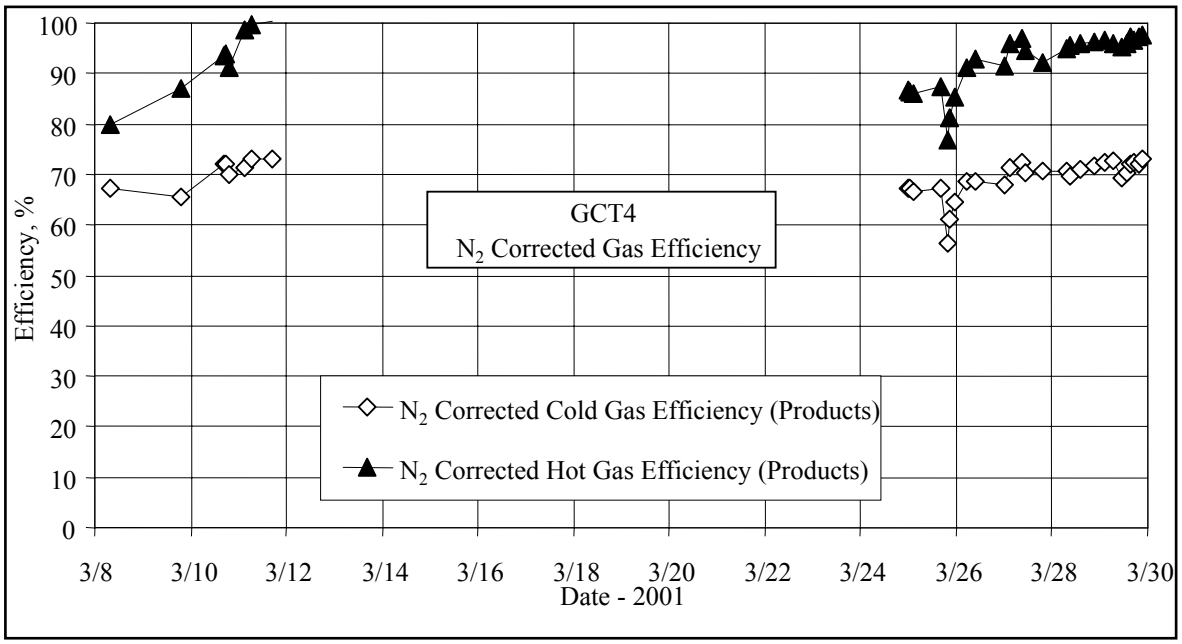

Figure 4.5-20 Nitrogen-Corrected Gasification Efficiency, March 8 Through March 30, 2001

4.6 SULFATOR OPERATIONS

During GCT4 the sulfator was operated for almost 700 hours. During this time the sulfator burned char from the gasifier for a total of 146 hours and used diesel fuel to maintain temperature for another 140 hours. The average bed temperature during fuel feed was about 1,250°F and only about 10 percent of the time was spent above 1,500°F. The lower temperature operation was due to insufficient feed char and to conserve fuel oil. The designed operating temperature is 1,600 to 1,650°F; however, the low temperatures were sufficient to achieve sulfation and complete carbon burnout.

Since the start of the gasification testing, the solids carryover rate from the sulfator to the baghouse has been high due to difficulty in properly operating the cyclone dipleg. This problems makes it difficult to build the sulfator bed levels up to normal operating levels and can result in high exit temperatures from the sulfator heat recovery exchanger. During GCT4 this carryover also resulted in high sulfator operating pressure, the solids salt out in the sulfator flue gas lines restricting the cross sectional area and resulting in higher pressure drop through the system. Figure 4.6-1 shows the dust in the flue gas line immediately downstream of the sulfator heat recovery exchanger.

The sulfator steam system was modified to provide superheated steam to the transport gasifier. This new arrangement worked well during GCT4 and provided steam at 550 to 700°F as measured near the gasifier. Due to low steam consumption in the gasifier there was on average about 100°F temperature loss from the steam source exiting the sulfator to the gasifier.

A consistent problem during sulfator operations has been a decline in bed mixing as the run continues. At the start of a test run, all bed thermocouples will read within about 100°F of one another. In general, near the end of a run one or more thermocouples will have deviated by as much as 1,000°F from the other bed temperatures. The lowest level thermocouple in the bed is always the first affected and as the problem worsens, higher thermocouples deviate in succession. The temperature profile from GCT4 is shown in Figure 4.6-2. The thermocouples are arranged with the lowest in the bed listed first. It is apparent that by the end of the test the bed is not well mixed in the vicinity of two of the thermocouples. The most likely explanation is that refractory has fallen from the vessel wall and is obstructing some of the nozzles of the air distribution grid.

The lower 10 feet of the sulfator refractory was replaced prior to GCT3. In an inspection after GCT4, the sulfator refractory showed signs of cracking and spalling. Several large pieces of refractory had fallen from the wall and were lying in the bottom of the vessel. Less than an inch (thickness) of refractory was missing because there were no refractory anchors visible.

Figure 4.6-1 Solids Salted in Sulfator Flue Gas Line

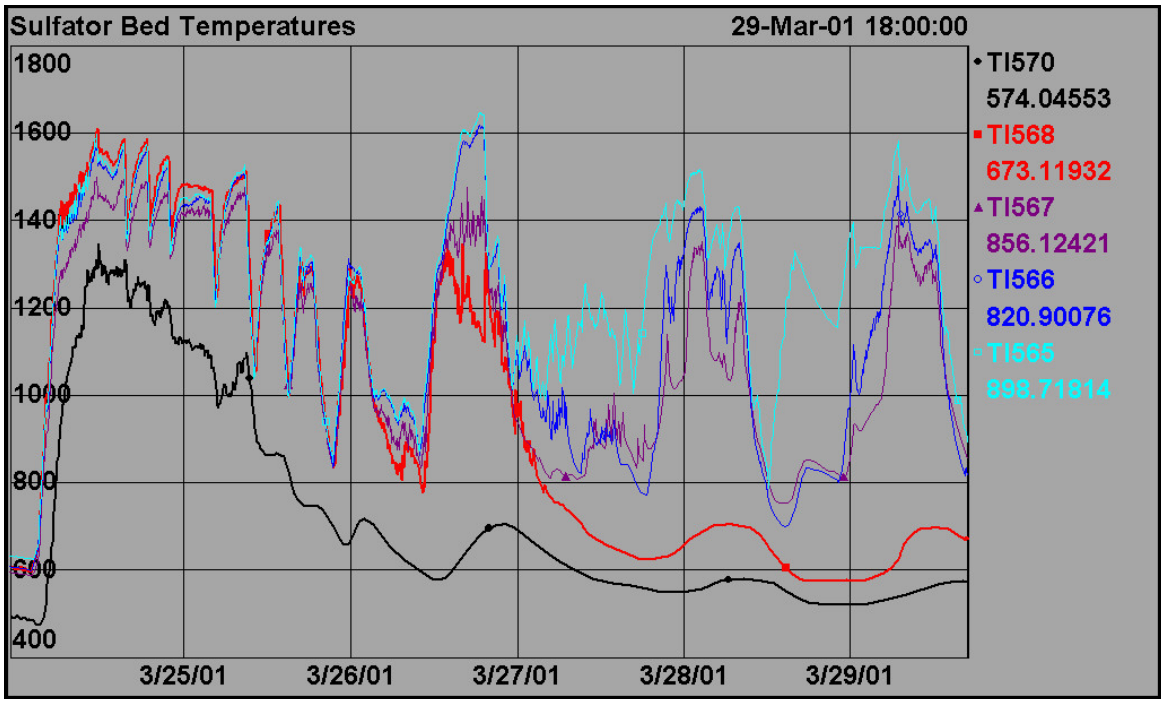

Figure 4.6-2 Sulfator Temperature Profile in GCT4

4.7 PROCESS GAS COOLERS

Heat transfer calculations were done on the primary gas cooler (HX0202) and the secondary gas cooler (HX0402) to determine if their performance had deteriorated during GCT4 due to tar or other compounds depositing on the tubes.

The primary gas cooler is between the transport reactor cyclone (CY0201) and the Siemens Westinghouse PCD (FL0301). During GCT4, HX0202 was not bypassed and took the full gas flow from the transport reactor. The primary gas cooler is a single-flow heat exchanger with hot gas from the transport reactor flowing through the tubes and the shell side operating with the plant steam system. The pertinent equations are:

$$Q = UA\Delta T_{LM} \tag{1}$$

$$Q = c_p M(T_1 - T_2) \tag{2}$$

$$\Delta T_{LM} = \frac{(T_1 - t_2) - (T_2 - t_1)}{\ln \frac{(T_1 - t_2)}{(T_2 - t_1)}} \tag{3}$$

Q = Heat transferred, Btu/hour
U = Heat transfer coefficient, Btu/hr/ft^2/°F
A = Heat exchanger area, ft^2
ΔT_{LM} = Log mean temperature difference, °F
c_p = Gas heat capacity, Btu/lb/°F
M = Mass flow of gas through heat exchanger, lb/hr
T_1 = Gas inlet temperature, °F
T_2 = Gas outlet temperature, °F
$t_1 = t_2$ = Steam temperature, °F

Using equations (1) through (3) and the process data, the product of the heat transfer coefficient and the heat exchanger area (UA) can be calculated. The GCT4 HX0202 UA is shown in Figures 4.7-1 and -2 as hourly averages along with the design UA of 5,200 Btu/hr/°F and the pressure drop across HX0202. If HX0202 is plugging, the UA should decrease and the pressure drop should increase. The UA deterioration is a better indication of heat exchanger plugging because the pressure drop is calculated by the difference of two numbers of about the same size, usually from 150 to 240 psig, resulting in pressure drops of 1 to 3 psi.

The UA for the first 5 days of operation started all three periods of operation below the design UA of 5,200 Btu/hr/°F and then rose to above the design UA. All three periods of operation had the pressure drop decrease. The UA decrease on March 12 occurred at the same time as the

coal and synthesis gas rates were decreased. There appeared to be no plugging during these three periods of operation.

The UA and pressure drop for the final 7 days of operation are shown in the plot in Figure 4.7-2. The UA increased to the design UA after 1 day of operation and then varied around the design UA during the period when there were a few coal trips. Once the coal rate was constant on March 26 the UA increased to 8,000 Btu/hr/°F for about 12 hours on March 27. At 15:00 on March 27, the UA began a decrease to 7,000 Btu/hr/°F, after the coal and synthesis gas rates were decreased, and remained constant at 7,000 Btu/hr/°F until 18:00 on March 29. After an increase in coal-feed rate on March 29 the UA gradually increased to 8,000 Btu/hr/°F by the end of GCT4. The pressure drop varied from 1 to 2 psi from March 24 to March 26. When the UA increased on March 26 the pressure drop was constant at about 2.0 psi when the UA increased to 8,000 Btu/hr/°F. When the UA was constant at 7,000 Btu/hr/°F, the pressure drop was constant at 1.3 psi. For the last 12 hours of the run the pressure drop increased to 2.0 psi. There appeared to be no HX0202 plugging during GCT4.

The GCT3 test run had HX0202 UAs in the same range as GCT4 at 8,000 to 9,000 Btu/hr/°F. The pressure drops for GCT3 HX0202 were also comparable with GCT4, with pressure drops of 1 to 2 psi.

The secondary gas cooler, HX0402, is a single-flow heat exchanger with hot gas from the PCD flowing through the tubes and the shell side operating with plant steam system. Some heat transfer and pressure drop calculations were done around HX0402 to determine if any plugging or heat exchanger performance deterioration occurred during GCT4. HX0402 is not part of the combustion gas turbine commercial flow sheet. In the commercial gas turbine flow sheet, the hot synthesis gas from the PCD would be sent directly to a combustion gas turbine. HX0402 would be used commercially if the synthesis gas was to be used in a fuel cell or as a chemical plant feedstock.

Using equations (1) through (3) and the process data, the product of the heat transfer coefficient and the UA can be calculated. The UA for the first 5 days of GCT4 testing is shown in Figure 4.7-3 as hourly averages, along with the design UA of 13,100 Btu/hr/°F and the pressure drop across HX0402. If HX0402 is plugging, the UA should decrease and the pressure drop should increase.

The UA was generally above the design UA of 13,100 Btu/hr/°F for the first 5 days of GCT4. During March 9 the UA was constant at 16,600 Btu/hr/°F. In the last 12 hours of March 11 and first 12 hours of March 12 the UA was between 16,000 and 17,000 Btu/hr/°F. Late on March 11 the UA dropped to just below the design UA of 13,100 Btu/hr/°F, when the coal and synthesis gas rates were decreased.

The pressure drop was between at 1.0 and 4.0 psi for the first 5 days of GCT4 operation. The pressure dropped decreased during March 9 and from March 10 to March 12. There was no evidence of HX0402 plugging during the first 5 days of operation.

The HX0402 UA and pressure drop for last 7 days of GCT4 are provided in Figure 4.7-4. The UA was above the design UA for nearly the entire 7 days. During the period of steady coal operation from March 28 and March 29, the UA was at 14,000 Btu/hr/°F. At the end of the run the UA increased to above 16,000 Btu/hr/°F while the coal and synthesis gas rates were increased. The pressure drop was between 1.0 and 3.5 psi for the last 7 days of operation. The pressure was steady for March 28 and 29 at 2.0 psi. At the end of the run, the pressure drop increased to 3.0 psi. Again there was no indication of HX0402 plugging during the last 7 days of GCT4 operation.

The GCT3 test run had HX0402 UAs in the same range as GCT4 at 14,000 to 16,000 Btu/hr/°F. The pressure drops for GCT3 HX0402 were also comparable to GCT4 with pressure drops of 1 to 3.5 psi.

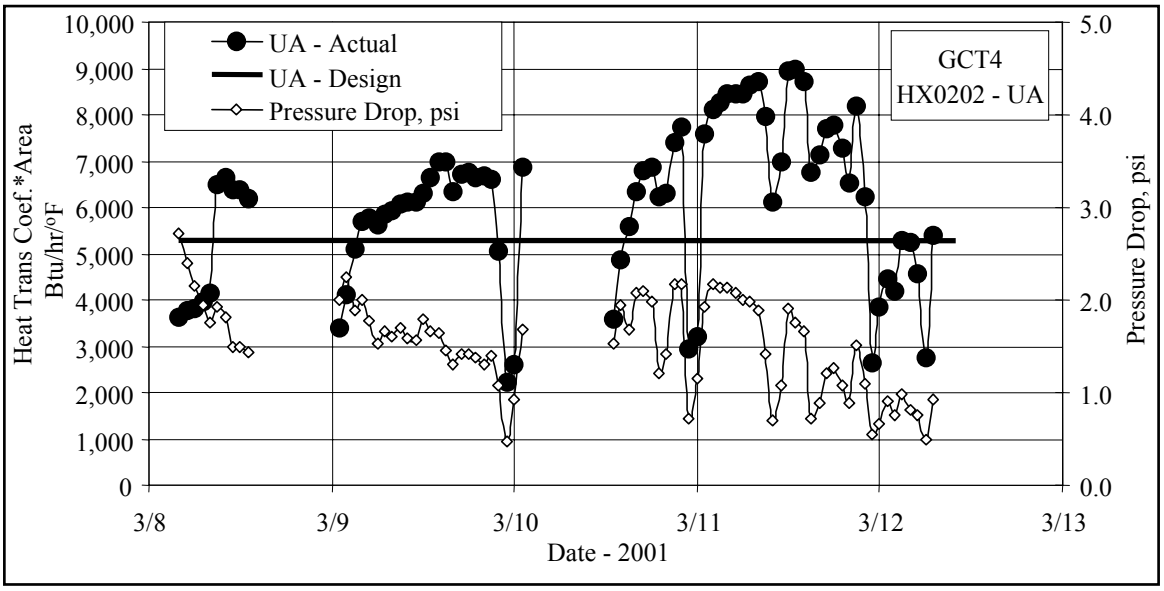

Figure 4.7-1 HX0202 Heat Transfer Coefficient and Pressure Drop — March 8 Through 13, 2001

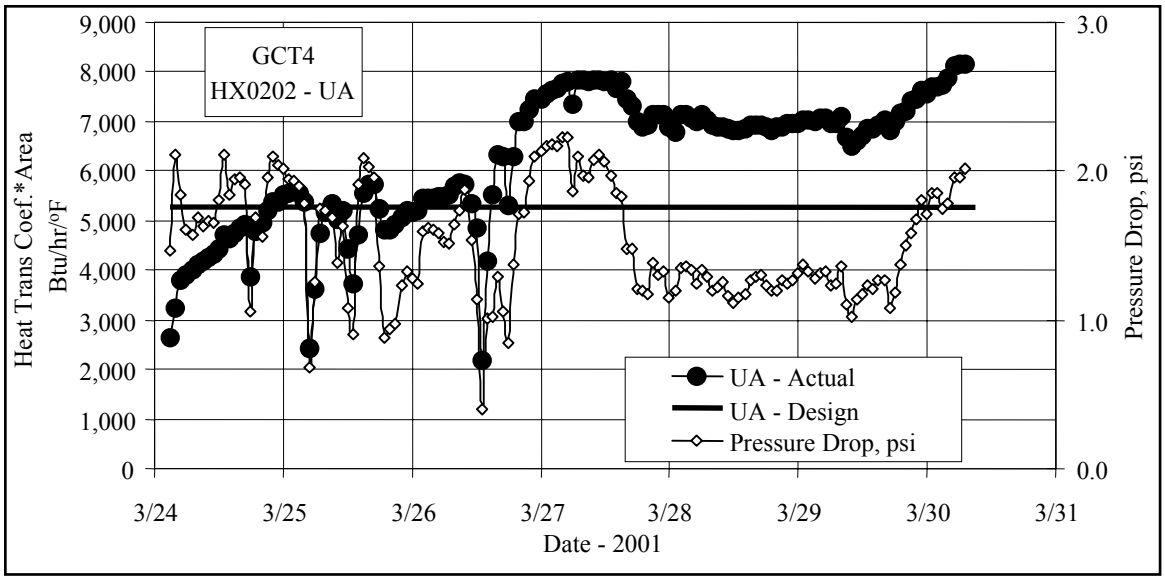

Figure 4.7-2 HX0202 Heat Transfer Coefficient and Pressure Drop — March 24 Through 31, 2001

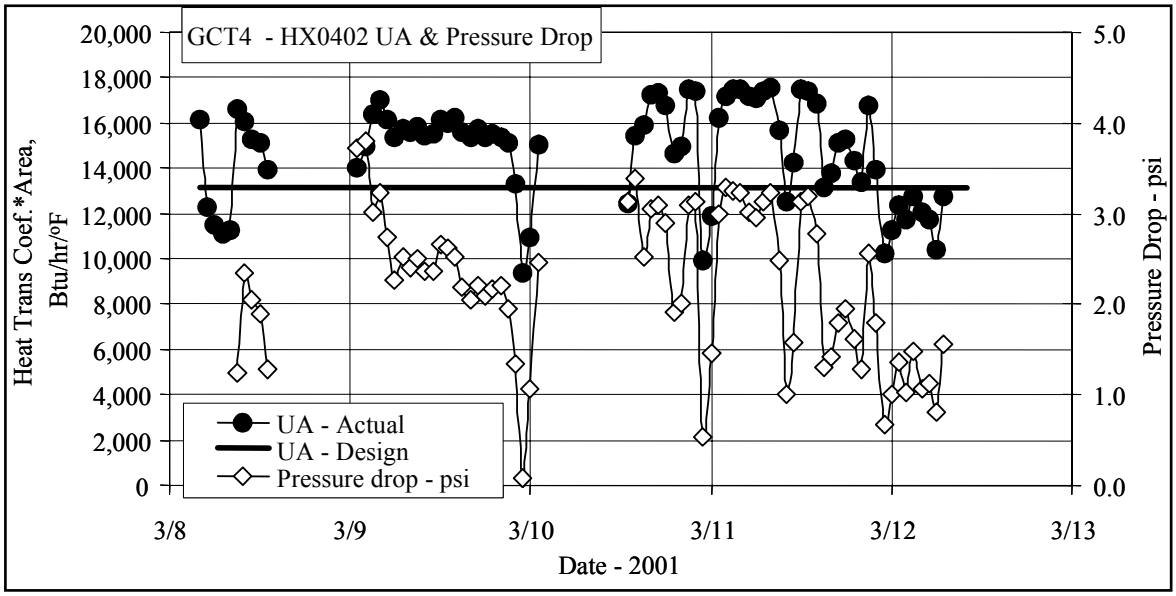

Figure 4.7-3 HX0402 Heat Transfer Coefficient and Pressure Drop — March 8 Through 13

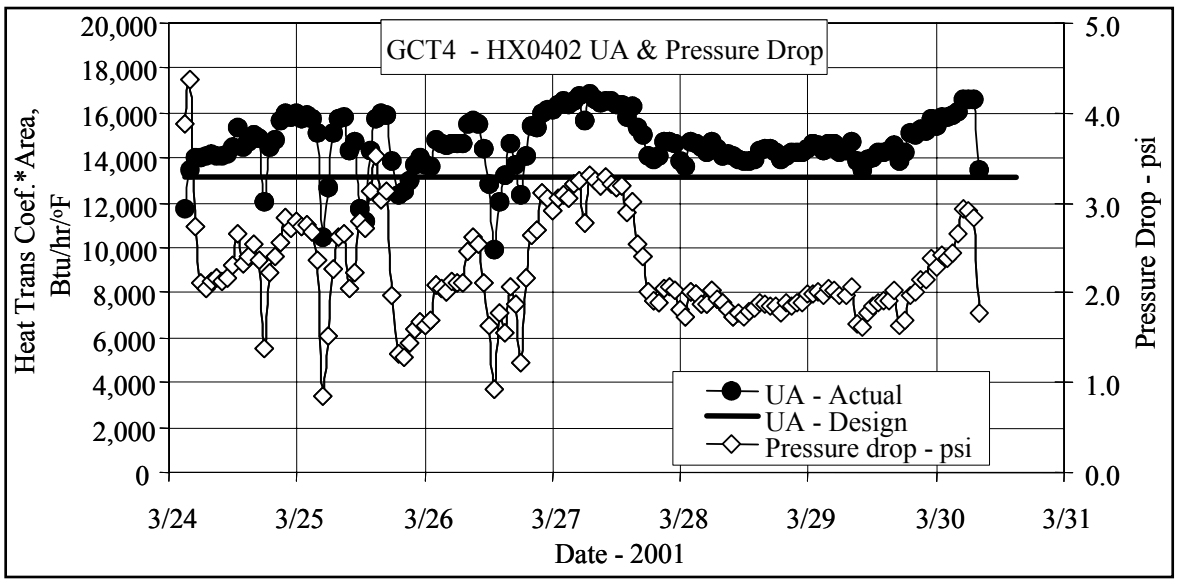

Figure 4.7-4 HX0402 Heat Transfer Coefficient and Pressure Drop — March 24 Through 31

TERMS

Listing of Abbreviations

AAS	Automated Analytical Solutions
ADEM	Alabama Department of Environmental Management
APC	Alabama Power Company
APFBC	Advance Pressurized Fluidized-Bed Combustion
ASME	American Society of Mechanical Engineers
AW	Application Workstation
BET	Brunauer-Emmett-Teller (nitrogen-adsorption specific surface technique)
BFI	Browning-Ferris Industries
BFW	Boiler Feed Water
BMS	Burner Management System
BOC	BOC Gases
BOP	Balance-of-Plant
BPIR	Ball Pass Inner Race, Frequencies
BPOR	Ball Pass Outer Race, Frequencies
BSF	Ball Spin Frequency
CAD	Computer-Aided Design
CAPTOR	Compressed Ash Permeability Tester
CEM	Continuous Emissions Monitor
CFB	Circulating Fluidized Bed
CFR	Code of Federal Regulations
CHE	Combustor Heat Exchanger
COV	Coefficient of Variation (Standard Deviation/Average)
CPC	Combustion Power Compay
CPR	Cardiopulmonary Resuscitation
CTE	Coefficient of Thermal Expansion
DC	Direct Current
DCS	Distributed Control System
DHL	DHL Analytical Laboratory, Inc.
DOE	U.S. Department of Energy
DSRP	Direct Sulfur Recovery Process
E & I	Electrical and Instrumentation
EERC	Energy and Environmental Research Center
EPRI	Electric Power Research Institute
EDX	Energy-Dispersive X-Ray
ESCA	Electron Spectroscopy for Chemical Analysis
FCC	Fluidized Catalytic Cracker
FCP	Flow-Compacted Porosity
FETC	Federal Energy Technology Center
FFG	Flame Front Generator
FI	Flow Indicator
FIC	Flow Indicator Controller
FOAK	First-of-a-Kind
FTF	Fundamental Train Frequency

FW	Foster Wheeler
GBF	Granular Bed Filter
GC	Gas Chromatograph
GEESI	General Electric Environmental Services, Inc.
HHV	Higher Heating Valve
HP	High Pressure
HRSG	Heat Recovery Steam Generator
HTF	Heat Transfer Fluid
HTHP	High-Temperature, High-Pressure
I/O	Inputs/Outputs
ID	Inside Diameter
IF&P	Industrial Filter & Pump
IGV	Inlet Guide Vanes
IR	Infrared
KBR	Kellogg Brown & Root
LAN	Local Area Network
LHV	Lower Heating Valve
LIMS	Laboratory Information Management System
LMZ	Lower Mixing Zone
LOC	Limiting Oxygen Concentration
LOI	Loss on Ignition
LPG	Liquefied Propane Gas
LSLL	Level Switch, Low Level
MAC	Main Air Compressor
MCC	Motor Control Center
MMD	Mass Median Diameter
MS	Microsoft Corporation
NDIR	Nondestructive Infrared
NETL	National Energy Technology Laboratory
NFPA	National Fire Protection Association
NOx	Nitrogen Oxides
NPDES	National Pollutant Discharge Elimination System
NPS	Nominal Pipe Size
OD	Outside Diameter
ORNL	Oak Ridge National Laboratory
OSHA	Occupational Safety Health Administration
OSI	OSI Software, Inc.
P&IDs	Piping and Instrumentation Diagrams
PC	Pulverized Coal
PCD	Particulate Control Device
PCME	Pollution Control & Measurement (Europe)
PDI	Pressure Differential Indicator
PDT	Pressure Differential Transmitter
PFBC	Pressurized Fluidized-Bed Combustion
PI	Plant Information
PLC	Programmable Logic Controller
PPE	Personal Protection Equipment

PRB	Powder River Basin
PSD	Particle Size Distribution
PSDF	Power Systems Development Facility
ΔP or DP or dP	Pressure Drop or Differential Pressure
PT	Pressure Transmitter
RAPTOR	Resuspended Ash Permeability Tester
RFQ	Request for Quotation
RO	Restriction Orifice
RPM	Revolutions Per Minute
RSSE	Reactor Solid Separation Efficiency
RT	Room Temperature
RTI	Research Triangle Institute
SCS	Southern Company Services, Inc.
SEM	Scanning Electron Microscopy
SGC	Synthesis Gas Combustor
SMD	Sauter Mean Diameter
SRI	Southern Research Institute
SUB	Start-up Burner
TCLP	Toxicity Characteristic Leaching Procedure
TR	Transport Reactor
TRDU	Transport Reactor Demonstration Unit
TRS	Total Reduced Sulfur
TSS	Total Suspended Solids
UBP	Uncompacted Bulk Porosity
UND	University of North Dakota
UPS	Uninterruptible Power Supply
UV	Ultraviolet
VFD	Variable Frequency Drive
VOCs	Volatile Organic Compounds
WGS	Water-Gas Shift
WPC	William's Patent Crusher
XRD	X-Ray Diffraction
XXS	Extra, Extra Strong

Listing of Units

acfm	actual cubic feet per minute
Btu	British thermal units
°C	degrees celsius or centigrade
°F	degrees fahrenheit
ft	feet
FPS	feet per second
gpm	gallons per minute
g/cm^3 or g/cc	grams per cubic centimeter
g	grams
GPa	gigapascals
hp	horsepower
hr	hour
in.	inches
inWg (or inWc)	inches, water gauge (inches, water column)
in.-lb	inch pounds
°K	degrees kelvin
kg	kilograms
kJ	kilojoules
kPa	kilopascals
ksi	thousand pounds per square inch
m	meters
MB	megabytes
min	minute
mm	millimeters
MPa	megapascals
msi	million pounds per square inch
MW	megawatts
m/s	meters per second
MBtu	Million British thermal units
m^2/g	square meters per gram
μ or μm	microns or micrometers
dp_{50}	particle size distribution at 50 percentile
ppm	parts per million
ppm (v)	parts per million (volume)
ppm (w)	parts per million (weight)
lb	pounds
pph	pounds per hour
psia	pounds per square inch
psig	pounds per square inch gauge
ΔP	pressure drop
rpm	revolutions per minute
s or sec	seconds
scf	standard cubic feet
scfh	Standard cubic feet per hour
scfm	standard cubic feet per minute

V	volts
W	watts